

**THE ROLE OF NADPH OXIDASE 2 IN AXON GUIDANCE DURING
ZEBRAFISH VISUAL SYSTEM DEVELOPMENT**

by
Aslihan Terzi

A Dissertation

*Submitted to the Faculty of Purdue University
In Partial Fulfillment of the Requirements for the degree of*

Doctor of Philosophy



Department of Biological Sciences

West Lafayette, Indiana

August 2020

**THE PURDUE UNIVERSITY GRADUATE SCHOOL
STATEMENT OF COMMITTEE APPROVAL**

Dr. Daniel M. Suter, Chair

Biological Sciences

Dr. Qing Deng

Biological Sciences

Dr. Yuk Fai Leung

Biological Sciences

Dr. Chris Rochet

Medicinal Chemistry and Molecular Pharmacology

Approved by:

Dr. Janice P. Evans

This work is dedicated to Sevim, Zeynep and Duru Terzi.

ACKNOWLEDGMENTS

First and foremost, I would like to thank my mentor Dr. Daniel M. Suter. He has been a great mentor, always very supportive. He always pushed me hard to become a better scientist. While helping me to improve my weaknesses, he has never forgotten to praise my strengths. I learned not only to be a good scientist, but also to be a good mentor and teacher from him. He always supported my professional development, encouraging me to seek every help that I can get. He always asked me how I feel and how I do and did his best to support me mentally. That is something I appreciate a lot and I could not ask for a better mentor.

I would like to thank my committee members Dr. Qing Deng, Dr. Yuk Fai Leung, Dr. Chris Rochet, and a previous member Dr. Matthew Tantama for helping me to develop my project in a better direction. Throughout my Ph.D., their guidance and support always helped me to learn looking at different perspectives. They were always more than supportive and encouraging to pursue the best ways to get answers efficiently.

I would like to thank my past and present lab members, Dr. Cory Weaver, Haley Roeder, Dr. Yuan Ren and Sabbir Alam. I thank Dr. Kristi McElmurry, she has been a great lab mate and a friend. I appreciate her support and kindness and friendship during these very hard years in graduate program. I had a chance to mentor great undergraduate researchers in our group, Tenazious Woods, Leah Biasi, Saroon Bhoopathy and Perapa Chotiprasidhi. I appreciate their help with maintaining zebrafish and helping me to be a better mentor. I also want to thank all lab members of Dr. Deng's, Dr. Leung's and Dr. Donna Fekete's lab. They always helped me with anything I was in need of, always sparing time to answer my questions. I would like to thank Deborah Biesemeier, Skye Brown, and George Stoner for their help with fish room maintenance. I thank a dearest friend and a colleague, Dr. Aktan Alpsoy, for his friendship, and all the technical advice that helped me to troubleshoot my experiments.

I also want to thank my teaching mentors Dr. Stephanie Gardner and Dr. Elwood Walls. I had privilege to work with both of them in several classes during which I learned how to teach and what the effective ways of teaching are. I received a prestigious teaching award from Purdue Teaching Academy by learning how to be a good teaching assistant from them. The skills I gained with them are very essential and will help me to become a better teacher in the future.

Finally, I would like to thank my family. I could not have succeeded without their help and support along the way. They always encouraged my quest to be a scientist even if that meant drifting me far away from them. My father, Seref, always did his best for me to have the best education I could get. My mother, Sevim, taught me to be the best in what I do. My little brother, Dogukan, always made me laugh with this weird sense of humor and taught me to take responsibility. Finally, my big brother, Evren; all of these would not be possible without him. He always believed in me, even in the times I lost my drive, he encouraged me to move on. He helped me in every way he can to support my success and happiness. I feel very lucky to have such a big brother, I will make sure his efforts and sacrifices will not be wasted. Lastly, I want to thank Burak Bal, who made everything meaningful with his endless love and support.

TABLE OF CONTENTS

LIST OF TABLES.....	10
LIST OF FIGURES	11
LIST OF ABBREVIATIONS.....	13
ABSTRACT.....	16
CHAPTER 1. INTRODUCTION	17
1.1 ROS and cellular signaling.....	17
1.2 NADPH Oxidases.....	18
1.3 NOX enzymes in the nervous system.....	22
1.4 NOX enzymes in neurogenesis	27
1.4.1 NOX1 and NOX3.....	33
1.4.2 NOX2	33
1.4.3 NOX4	35
1.4.4 DUOX	36
1.5 NOX enzymes in neurite growth and the neuronal cytoskeleton.....	36
1.5.1 Bidirectional interaction between NOX2 and actin cytoskeleton	38
1.5.2 The role of NOX in axonal regeneration.....	39
1.6 Cellular antioxidant systems.....	41
1.7 Retinal development in zebrafish	42
1.7.1 RGC neurogenesis.....	44
1.7.2 RGC axonal guidance.....	45
1.8 Introduction to the project	47
CHAPTER 2. METHODS.....	48
2.1 General Methods	48
2.1.1 Zebrafish housing and breeding	48
2.1.2 Genotyping	48
2.1.3 Microinjection	49
2.1.4 Statistical analysis	50
2.2 Methods for Chapter 3.....	50
2.2.1 Whole-mount immunohistochemistry.....	50

2.2.2	Whole mount <i>in situ</i> hybridization.....	51
2.2.3	H ₂ O ₂ imaging <i>in vivo</i>	52
2.2.4	Optokinetic response (OKR) assay	53
2.2.5	Quantitative PCR.....	54
2.3	Methods for Chapter 4.....	55
2.3.1	Dissociated RGC neuronal culture	55
2.3.2	Growth cone collapse quantification.....	56
2.3.3	H ₂ O ₂ imaging <i>in vitro</i>	56
2.3.4	Whole-mount immunohistochemistry.....	57
2.3.5	Imaging sparsely labeled RGCs	58
2.4	Methods for Chapter 5.....	58
2.4.1	Cloning full length Zebrafish <i>nox2</i> gene.....	58
2.4.2	Cloning roGFP2-orp1 in Gateway middle entry vector	59
2.4.3	Generating constructs for tissue-specific knockout	60
2.4.4	Zebrafish blastula stage cell transplantations.....	62
2.4.5	Zebrafish embryo dissociation	64
2.4.6	NADPH Oxidase assay	65
CHAPTER 3. CHARACTERIZATION OF NOX2 <i>-/-</i> MUTANT ZEBRAFISH DURING DEVELOPMENT.....		67
3.1	Introduction	67
3.2	Results	69
3.2.1	Nox2 mutant zebrafish exhibit aberrant axon projections along CNS.....	69
3.2.2	<i>nox2</i> mutant zebrafish exhibit normal brain development	71
3.2.3	<i>nox2 -/-</i> mutants have impaired vision	73
3.2.4	H ₂ O ₂ levels in homozygous <i>nox2 -/-</i> mutants	73
3.2.5	The <i>nox2</i> mutation exhibits incomplete penetrance.....	75
3.2.6	Loss of functional Nox2 is compensated by other Nox isoforms	82
3.3	Discussion.....	84
3.3.1	The role of Nox2 in zebrafish CNS development.....	84
3.3.2	The role of Nox2 in neurogenesis	85
3.3.3	Analysis of incomplete penetrance in <i>nox2</i> mutants.....	88

3.3.4	The function of H ₂ O ₂ in <i>nox2</i> mutants	90
CHAPTER 4.	NOX2 AND SLIT2/ROBO2 SIGNALING DURING RGC GUIDANCE	92
4.1	Introduction	92
4.2	Results	93
4.2.1	Nox inhibition abolishes slit2-mediated growth cone collapse <i>in vitro</i>	93
4.2.2	Nox2 is required for slit-2 mediated H ₂ O ₂ production.....	95
4.2.3	Partial loss of Nox2 and Robo2 combined does not affect formation of optic chiasm	97
4.2.4	Partial loss of Nox2 and Robo2 combined alters tectal innervation <i>in vivo</i>	98
4.3	Discussion.....	100
4.3.1	Nox2-slit2/Robo2 interaction <i>in vitro</i>	100
4.3.2	Nox2-Slit2/Robo2 interaction <i>in vivo</i>	100
4.3.3	Analysis of individual RGC growth cone guidance.....	102
4.3.4	The role of Slit/Robo during midline crossing.....	104
CHAPTER 5.	TOOLS TO INVESTIGATE NOX2 IN RGC DEVELOPMENT	106
5.1	Studying cell-autonomous effects of Nox2 in RGC guidance	106
5.1.1	Introduction	106
5.1.2	Generating RGC-specific <i>nox2</i> mutant zebrafish.....	106
5.1.3	Cell Transplantation	109
5.1.4	RGC-specific Nox2 rescue in general <i>nox2</i> ^{-/-} mutants.....	111
5.1.5	Conclusion.....	111
5.2	Alternative Ways for Measuring Nox activity in Zebrafish Cells.....	112
5.2.1	Introduction	112
5.2.2	RGC-specific expression of roGFP2-orp1 biosensor.....	112
5.2.3	NADPH Oxidase Assay	113
CHAPTER 6.	GENERAL DISCUSSION	116
6.1	The signaling downstream of Slit/Robo interaction.....	118
6.1.1	Slit-Robo GTPase activating proteins (srGAPs).....	118
6.1.2	Cofilin.....	119
6.1.3	microRNAs.....	120
6.2	The role of Nox2-derived H ₂ O ₂ in cellular signaling during axonal guidance	121

6.2.1	Redox regulation of actin cytoskeleton	123
6.2.2	Redox regulation of actin binding proteins	123
6.2.3	Redox regulation of actin regulatory proteins.....	124
6.2.4	Redox regulation of signaling proteins	125
6.3	Conclusion.....	125
REFERENCES		127
PUBLICATIONS.....		168

LIST OF TABLES

Table 1: Localization of NOX subunits in neurons.	25
Table 2: Summary of the role of different NOX isoforms in neurogenesis.....	30
Table 3: Genotyping Primers for PCR.....	49
Table 4: qPCR primers.....	55
Table 5: Primers for Gateway entry vector cloning.....	60

LIST OF FIGURES

Figure 1: Composition of NADPH oxidases.	21
Figure 2: NOX-mediated ROS in neuronal development.	32
Figure 3: Structure of the zebrafish visual system.	43
Figure 4: Gateway Cloning Principle.	62
Figure 5: The setup of the transplantation rig.	63
Figure 6: Schematic of transplantation micropipette and plate setup.	64
Figure 7: The principle of NADP/NADPH Glo Assay.	66
Figure 8: Characterization of zebrafish <i>nox2</i> mutant lines that were generated by CRISPR/Cas9 genome editing.	68
Figure 9: Axons are mistargeted in the CNS of homozygous <i>nox2</i> mutants.	70
Figure 10: Early development of CNS is normal in homozygous <i>nox2</i> mutants.	72
Figure 11: H ₂ O ₂ levels in retinas of homozygous <i>nox2</i> <i>-/-</i> mutants.	74
Figure 12: The phenotypic characterization of <i>nox2</i> <i>-/-</i> mutants.	76
Figure 13: The overall phenotypic difference coincides with the RGC phenotypes in <i>nox2</i> <i>-/-</i> mutants.	78
Figure 14: Phenotypes in <i>nox2</i> <i>-/-</i> (<i>II</i>) mutants are comparable to <i>nox2</i> <i>-/-</i> (<i>I</i>) mutants.	79
Figure 15: The validation of the genotypes of <i>nox2</i> <i>-/-</i> fish.	81
Figure 16: Loss of Nox2 is compensated by other Nox isoforms.	83
Figure 17: Aberrant axon projections in <i>nox2</i> <i>-/-</i> hindbrain area.	84
Figure 18: Schematic representation of zebrafish neuroanatomy.	85
Figure 19. RGC specification seems unaffected in <i>nox2</i> <i>-/-</i> mutants.	87
Figure 20: <i>nox2</i> mRNA expression fold-changes in 2 dpf old embryos.	90
Figure 21: Nox inhibition abolishes slit2 mediated growth cone collapse.	94
Figure 22: Slit2 causes an increase in intracellular H ₂ O ₂ levels in wild-type RGCs, but not in <i>nox2</i> <i>-/-</i> or <i>astray</i> <i>-/-</i> RGCs.	96
Figure 23: Partial loss of Nox2 and Robo2 together alters RGC pathfinding <i>in vivo</i>	99
Figure 24: Imaging of individual RGCs in wild-type and <i>nox2</i> <i>-/-</i> larvae.	103
Figure 25: Construct design for tissue-specific knock-out approach.	108

Figure 26: Alternative approach for tissue-specific knockout construct design.....	109
Figure 27: RGC-specific full length Nox2 expression.	111
Figure 28: Construct design for RGC-specific roGFP2-orp1 expression.....	113
Figure 29: NADP/NADPH Glo assay validation in zebrafish cells.	115
Figure 30: Proposed mechanism for Slit/Robo mediated Nox2 activation at growth cones.	117
Figure 31: Nox-mediated ROS affects neuronal cytoskeleton during neurite growth.....	122

LIST OF ABBREVIATIONS

AC: Anterior commissure
Akt: Protein kinase B
Ang II: Angiotensin II
BDBF: Brain-derived neurotrophic factor
BMP2: Bone morphogenic protein 2
BrdU: Bromo-deoxyuridine
CG: Celiac ganglion
CGD: Chronic granulomatous disease
CNS: Central nervous system
CRISPR: Clustered regularly interspaced short palindromic repeats
CRMP2: Collapsin response mediator protein 2
DAPI: 4',6-diamidino-2-phenylindole
DCC: Deleted in colorectal cancer
DG: Dentate gyrus
DMAMQ: 2-[(dimethylamino)methyl]-8-hydroxyquinoline
DRG: Dorsal root ganglion
DTT: Dithiothreitol
DUOX: Dual oxidase
ECCs: Embryonic carcinoma cells
EDTA: Ethylenediaminetetraacetic acid
ER: Endoplasmic reticulum
Erk1/2: Extracellular-signal-regulated kinase 1/2
ESC: Embryonic stem cells
FACS: Fluorescent activated cell sorting
FAD: Flavin adenine dinucleotide
FGF2: Fibroblast growth factor 2
GCL: Ganglion cell layer
gRNA: Guide RNA
GTP: Guanosine-5'-triphosphate

HB: Hindbrain
HEK293: Human embryonic kidney cells
HIF1 α : Hypoxia-inducible factor 1 α
IL-1 β : Interleukin 1 β
INL: Inner nuclear layer
IPL: Inner plexiform layer
iPSC: Induced pluripotent stem cells
LA: α -lipoic acid
LTD: Long term depression
LTP: Long term potentiation
MAPK: Mitogen-activated protein kinase
Mef2ca: myocyte enhancer factor 2ca
MB: Midbrain
MG: Müller glia
MHB: Midbrain hindbrain boundary
MICAL: Molecule interacting with CasL
miR: microRNA
mNTS: Medial nucleus of solitary tract
NADP(H): Nicotinamide adenine dinucleotide phosphate
NGF: Nerve growth factor
NMDA: N-methyl-D-aspartate
NPC: Neural progenitor cells
NSC: Neural stem cells
Nox: NADPH Oxidase
PAGE: Polyacrylamide gel
PDGF: Platelet-derived growth factor
PI3K/Akt: Phosphoinositide 3-kinase/protein kinase B
PIP3: Phosphatidylinositol (3,4,5)-trisphosphate
PKC: Protein kinase C
PKG1: cyclic GMP-dependent protein kinase 1
PrP: Prion protein

PRR: Proline-rich region
PTEN: Phosphatase and tensin homolog
PTU: N-Phenylthiourea
PVN: paraventricular nucleus
RA: Retinoic acid
RGC: Retinal ganglion cell
ROI: Region of interest
ROS: Reactive oxygen species
RyR: Ryanodine receptors
OC: Optic chiasm
ON: Optic nerve
ONL: Outer nuclear layer
OPL: Outer plexiform layer
OT: Optic tectum
SAC: Stratum album centrale
Sema: Semaphorin
SCI: Spinal cord injury
SFGS: Stratum fibrosum griseum et superficiale
SGC: Stratum griseum centrale
SHH: Sonic Hedgehog
SH3: Src Homology Domain 3
SO: Stratum opticum
SOD3: Extracellular superoxide dismutase
SPV: Stratum periventriculare
srGAP: Slit-Robo GTPase activating proteins
SVZ: Subventricular zone
TBI: Traumatic brain injury
TC: Telencephalon
TPR: Tetratricopeptide repeat
TrkB: Tropomyosin receptor kinase B
UV: ultraviolet

ABSTRACT

Reactive oxygen species (ROS) are critical for maintaining cellular homeostasis and function when produced in physiological ranges. Important sources of cellular ROS include NADPH oxidases (Nox), which are evolutionarily conserved multi-subunit transmembrane proteins. Nox-mediated ROS regulate a variety of biological processes including stem cell proliferation and differentiation, calcium signaling, cell migration, and immunity. ROS participate in intracellular signaling by introducing post-translational modifications to proteins and thereby altering their functions. The central nervous system (CNS) expresses different Nox isoforms during both development and adulthood. There is now emerging evidence that Nox-derived ROS also control neuronal development and pathfinding. Our lab has recently shown that retinal ganglion cells (RGCs) from *nox2* mutant zebrafish exhibit pathfinding errors. However, whether Nox could act downstream of receptors for axonal growth and guidance cues is presently unknown. To investigate this question, we conducted a detailed characterization of the zebrafish *nox2* mutants that were previously established in our group. Abnormal axon projections were found throughout the CNS of the *nox2* mutant zebrafish. Anterior commissural axons failed proper fasciculation, and aberrant axon projections were detected in the dorsal longitudinal fascicle of the spinal cord. We showed that the major brain regions are intact and that the early development of CNS is not significantly altered in *nox2* mutants. Hence, the axonal deficits in *nox2* mutants are not due to general developmental problems, and Nox2 plays a role in axonal pathfinding and targeting. Next, we investigated whether Nox2 could act downstream of slit2/Robo2-mediated guidance during RGC pathfinding. We found that slit2-mediated RGC growth cone collapse was abolished in *nox2* mutants *in vitro*. Further, ROS biosensor imaging showed that slit2 treatment increased growth cone hydrogen peroxide levels via mechanisms through Nox2 activation. Finally, we investigated the possible relationship between slit2/Robo2 and Nox2 signaling *in vivo*. *Astray/nox2* double heterozygous mutant larvae exhibited decreased tectal area as opposed to individual heterozygous mutants, suggesting both Nox2 and Robo2 are required for the establishment of retinotectal connections. Our results suggest that Nox2 is part of a signal transduction pathway downstream of slit2/Robo2 interaction regulating axonal guidance cell-autonomously in developing zebrafish retinal neurons.

CHAPTER 1. INTRODUCTION

Part of the literature review described in this chapter was previously published. The text presented here is adapted, with permission, from the original publication (Terzi & Suter, 2020).

1.1 ROS and cellular signaling

Reactive oxygen species (ROS) are not only damaging when in abundance but can also act as signaling molecules at physiological concentrations to regulate cell homeostasis and physiology (Aviello & Knaus, 2018; Holmström & Finkel, 2014; Nathan & Cunningham-Bussel, 2013; Ying Wang, Branicky, Noë, & Hekimi, 2018). ROS are derivatives of oxygen, some of which are radicals containing a free electron rendering these molecules highly reactive. Intracellular levels of ROS are tightly controlled by cellular antioxidant mechanisms to maintain a proper intracellular redox balance (Birben, Sahiner, Sackesen, Erzurum, & Kalayci, 2012; He et al., 2017). High ROS levels are associated with oxidative stress, aging, cardiovascular and respiratory dysfunction, and cancer (Al Ghouleh et al., 2011; Davalli, Mitic, Caporali, Lauriola, & D'Arca, 2016; Taniyama & Griendling, 2003; Weinberg, Ramnath, & Nagrath, 2019). Low ROS levels on the other hand impair learning and memory, cell proliferation, migration and microglial chemotaxis (Kishida et al., 2006; Kishida, Pao, Holland, & Klann, 2005; Lelli et al., 2013; Mofarrahi et al., 2008; Somanna et al., 2016). Thus, intermediate ROS levels appear to be optimal for normal cellular development and function. Elucidating the precise control of intracellular ROS levels is therefore crucial to understand the mechanisms behind cellular redox balance.

Among the different ROS, hydrogen peroxide (H_2O_2) is likely the most important signaling molecule for several reasons. First, it does not harbor an unpaired electron and is therefore less reactive compared to other ROS; second, H_2O_2 exhibits a higher cell permeability than other ROS and can cross cell membranes through aquaporins or by simple diffusion; third, the half-life of H_2O_2 is longer than that of other ROS (10^{-5} sec), and lastly, it can oxidize cysteine residues of redox-sensitive proteins to modify their activity (Bienert et al., 2007; Bienert, Schjoerring, & Jahn, 2006; Dickinson & Chang, 2011; Giorgio, Trinei, Migliaccio, & Pelicci, 2007; Miller, Dickinson, & Chang, 2010; Reczek & Chandel, 2015). Another ROS, superoxide ($\text{O}_2^{\cdot-}$), undergoes dismutation into H_2O_2 and exhibits low rate constants for oxidation to be able to modify signaling. Hydroxyl radical does not exhibit enough target specificity to be a second messenger (Forman,

Maiorino, & Ursini, 2010). Taken together, although it is not easy to unambiguously determine the specific ROS involved in cellular signaling, based on the kinetic properties and substrate specificity of different ROS, H₂O₂ is likely the key signaling molecule. Indeed, H₂O₂ contributes to variety of cellular activities such as cell proliferation, differentiation, migration, survival, and autophagy (Coant et al., 2010; Dvorianchikova, Grant, Santos, Hernandez, & Ivanov, 2012; Mofarrahi et al., 2008; Niethammer, Grabher, Look, & Mitchison, 2009; Scherz-Shouval et al., 2007; Somanna et al., 2016; Torrecillas et al., 2001; Zimmerman et al., 2011).

1.2 NADPH Oxidases

The two major cellular sources for ROS are the mitochondrial electron transport chain and an enzyme family termed NADPH oxidases (NOX). NOXes generate ROS in various immune cells and tissues including colon, inner ear, kidney, spleen, testis, and thyroid glands, suggesting biological significance of NOX-mediated ROS production (Borregaard, Heiple, Simons, & Clark, 1983; Caillou et al., 2001; Cheng, Cao, Xu, van Meir, & Lambeth, 2001; Miklós Geiszt, Lekstrom, Witta, & Leto, 2003; Shiose et al., 2001). NOX enzymes are transmembrane proteins that transport an electron from NADPH, through FAD, across the plasma membrane to molecular oxygen (O₂) to generate O₂^{•-} (Figure 1). Superoxide can be converted to H₂O₂ either by spontaneous dismutation or via extracellular superoxide dismutase (SOD3) (Wang et al., 2018). The catalytic core of NOX enzymes is composed of six α -helical transmembrane domains. The sixth transmembrane domain is linked to an intracellular FAD-binding domain via a segment, and the FAD-binding domain is linked to an NADPH binding domain at the C-terminus. There are four critical histidine (His) residues in the transmembrane domains three and five, which bind heme and are required for electron transport. Throughout evolution, *NOX* genes are found in most eukaryotes including vertebrates, plants, insects, nematodes, and fungi, while there is no evidence for *nox* genes in prokaryotes thus far (Kawahara, Quinn, & Lambeth, 2007). However, a common heme motif exists in both organelle and b-type cytochromes found in prokaryotes, suggesting a common ancestor of flavocytochrome superfamilies between prokaryotes and eukaryotes (Sumimoto, 2008). *NOX* genes are proposed to be important for multicellular functions, since unicellular organisms generally lack these genes (Lalucque & Silar, 2003). However, this idea is controversial because there is evidence for *nox*-like genes in unicellular organisms (Bedard, Lardy, & Krause, 2007).

A molecular taxonomy study assessing 101 *NOX/DUOX* genes identified seven subfamilies of NOX enzymes (Kawahara et al., 2007). Humans express all seven isoforms in variety of tissues (Sirokmány, Donkó, & Geiszt, 2016). NOX1-4 require association with the membrane-bound subunit p22^{phox} for their enzymatic activity (Ambasta et al., 2004; Ueno, Takeya, Miyano, Kikuchi, & Sumimoto, 2005). NOX1-3 are also associated with cytosolic subunits for their full enzymatic activation. The genomes of green plants, fungi, and nematodes are devoid of these subgroups (Kawahara et al., 2007). The *NOX2* gene is the earliest isoform that evolved among *NOX1-4*, being the closest to the ancestral *nox* gene. NOX2 requires an organizer subunit p47^{phox}, an activator subunit p67^{phox}, a mediator subunit p40^{phox}, and small GTPase Rac to achieve full enzymatic activity. While the catalytic core NOX2 (gp91^{phox}) and membrane bound partner p22^{phox} reside on the plasma membrane, subunits are found in the cytosol. Upon activation signal, p47^{phox} is phosphorylated in its autoinhibitory domain. This changes the conformation and allows SH3 domain of p67^{phox} to bind proline rich region (PRR) of p47^{phox} (Brandes, Weissmann, & Schroder, 2014). Additionally, the SH3 domains of p47^{phox} bind to PRR domains of p22^{phox} to facilitate transporting p67^{phox} to plasma membrane where it activates the catalytic core NOX2 by activating the electron flow (Han, Freeman, Lee, Motalebi, & Lambeth, 1998; Nisimoto, Motalebi, Han, & Lambeth, 1999). p47^{phox} harbors a PX domain that will also be free to bind phosphatidylinositol (3,4,5)-trisphosphate (PtdIns (3,4,5) P3), or PIP3, on the plasma membrane. Small GTPase Rac binds to tetratricopeptide repeat (TPR) at the N-terminus of p67^{phox} when it is GFP bound and Rac-GTP is membrane tethered by itself to further facilitate association with plasma membrane. Phylogenic tree analysis suggests that NOX1 and its regulatory subunits emerged with the appearance of vertebrates, when p47^{phox} and p67^{phox} genes duplicated and evolved as *NOXO1* and *NOXA1* genes, respectively (Kawahara & Lambeth, 2007). *NOX3* is the last *NOX*-gene that appeared in evolution. The *NOX3* gene is not found in teleost fish, and its appearance in evolution correlates with the transition from water to land. *NOX3* gene functions in gravity perception and balance as it is mainly expressed in inner ear, where it is involved in the formation of otoconia (Bánfi et al., 2004; Paffenholz et al., 2004). NOX3 activity seems to be independent of Rac1, however, NOXO1 can activate NOX2 in the absence of NOXA1 and p67^{phox} (Cheng, Ritsick, & Lambeth, 2004; Ueno et al., 2005). Although *NOX4* originated from a common branch with *NOX1-3*, it branched off from a close root and lacks the requirement of cytosolic subunits for its activation (Kawahara et al., 2007; Serrander, Cartier, et al., 2007). Additionally,

different from NOX1-3, NOX4 isoform directly generates H₂O₂ and not superoxide due to its longer third extracytosolic loop, which could provide a proton source for the formation of H₂O₂ (Takac et al., 2011).

The most abundant NOX enzymes are calcium (Ca⁺²)-regulated NOXes, which emerged earliest in the eukaryote evolution (Kawahara et al., 2007). NOX5 and DUOX1-2 require Ca⁺² binding through EF-hand motifs for activation as opposed to cytosolic subunits. However, DUOX1 and DUOX2 require activator subunits DUOXA1 and DUOXA2 in order to be transported to plasma membrane to form an active oxidase complex (Morand et al., 2009). In contrast to all other NOXes, DUOX1-2 harbor an additional “peroxidase-like” transmembrane domain. NOX5 can produce both superoxide and H₂O₂, while DUOX generates only H₂O₂ (Bánfi et al., 2001; Donkó, Péterfi, Sum, Leto, & Geiszt, 2005; Serrander, Jaquet, et al., 2007). Mouse and rat genomes lack *Nox5* gene, and zebrafish lacks one *duox* paralog, suggesting that the activities of these isoforms are not essential and could be compensated. Amino acid substitution rates per site per 10⁹ years indicate that NOX2 and DUOX1-2 have the lowest evolution rate compared to other NOXes (Kawahara et al., 2007). These NOX enzymes are involved in host-defense, and their lack of tolerance to evolutionary changes could be explained by their crucial role in the innate immunity. Indeed, *NOX2* is the first *NOX* gene that was discovered through its role in phagocytes, and *Duox* is shown to modulate gut immunity in zebrafish larvae (Cross & Segal, 2004; Flores et al., 2010). Knocking out *Nox2* in mice resulted in a similar phenotype as in chronic granulomatous disease (CGD) patients including higher susceptibility to fungal infections (Pollock et al., 1995); however, mice lacking NOX2 do not exhibit significant other phenotypes. Similarly, the results derived from NOX4 knockout mice have been inconclusive thus far. NOX4 is expressed in kidney and neural crest stem cells, but NOX4 knockout mice have no obvious phenotypes in either kidney or neural crest cell-derived tissues (Buvelot, Jaquet, & Krause, 2019; Lee, Cho, Lee, Kim, & Bae, 2014). NOX1 and NOX2 activators NOXO1, NOXA1 and p47^{phox} can activate NOX3 as well (Ueno et al., 2005). In vitro, co-transfection of p47^{phox}, p67^{phox} and NOX1 lead to ROS production in HEK293 cells; suggesting that NOX2 cytosolic subunits are capable of activating NOX1 when NOXO1 and NOXA1 are not present (Bánfi, Clark, Steger, & Krause, 2003). Likewise, NOXA1 can activate NOX2 and loss of NOX2 can be compensated by NOX1 (Geiszt et al., 2003; Kawano, Miyamoto, Kaito, Sumimoto, & Tamura, 2012). In conclusion, knock-out of one NOX isoform can lead to compensatory activation of another isoforms.

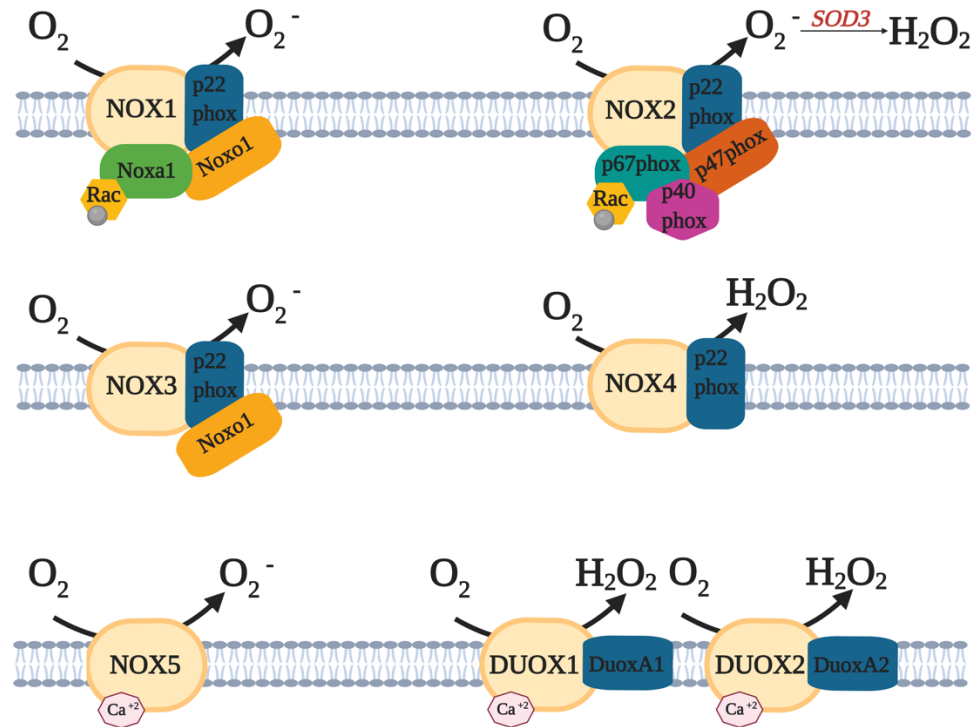


Figure 1: Composition of NADPH oxidases.

NOX isoforms are shown in their active state. The catalytic core of the NOX complex resides in the membrane where it interacts with membrane binding partners and cytosolic subunits. NOX1 and NOX2 depend on subunit assembly for activation. NOX3 requires only p22^{phox}, but NOXO1 can enhance its activity. NOX4 is constitutively active. NOX5 requires Ca⁺² binding. DUOX1 and DUOX2 require activator subunits for membrane localization and Ca⁺² binding for activation.

NOX enzyme subunits exhibit diverse patterns of subcellular localizations based on the cell type and activation state. NOX subunits can be found in both plasma membrane and intracellularly in organellar membranes depending on the function of the NOX complex. Localizing the NOX complex to intracellular organelles might favor an intracellular signaling mechanism, while plasma membrane associated NOX complex could engage in both autocrine and paracrine signaling. For instance, in resting neutrophils NOX2 is mainly associated with granular membranes, while subunits p47^{phox} and p67^{phox} are found in the cytosol, whereas upon stimulation all subunits translocate to plasma membrane, where they form an active NOX2 complex to produce extracellular superoxide (Borregaard et al., 1983; Clark, Volpp, Leidal, & Nauseef, 1990). Similarly, in unstimulated endothelial cells NOX2 complex subunits are found mainly intracellularly, associated with perinuclear compartments as well as membrane fractions in a pre-

assembled form, possibly contributing to constitutive production of low-level ROS in these cells (Li & Shah, 2002, 2003). Unlike in the case of the NOX2 complex, NOX1 organizer NOXO1 localizes to plasma membrane in unstimulated cells, while NOXA1 is mainly in the cytosol (Cheng, Diebold, Hughes, & Lambeth, 2006; Ueyama, Geiszt, & Leto, 2006). In microglia, the NOX1-p22^{phox} complex translocate to the phagosome membrane from intracellular compartments upon activation, similar to the NOX2 activation in neutrophils (Chéret et al., 2008). Thus, different NOX isoforms could be modulated similarly for the same function. In vascular smooth muscle cells, NOX1 localizes to caveolin near cell surface and NOX4 localizes to focal adhesion points and nuclei, indicating diverse actions based on isoform type and intracellular localization (Hilenski, Clempus, Quinn, Lambeth, & Griending, 2004). NOX4 is present on mitochondria in endothelial and mesangial cells, while it preferentially localizes to nucleus in endothelial cells based on another study (Block, Gorin, & Abboud, 2009; Chen, Kirber, Xiao, Yang, & Keaney, 2008; Kuroda et al., 2005; Van Buul, Fernandez-Borja, & Hordijk, 2005). NOX5 mainly localizes to perinuclear compartments and endoplasmic reticulum (ER), although it has also been found in Golgi complex, mitochondria, and caveolae (BelAiba et al., 2007; Fulton, 2009; Jagnandan et al., 2007; Serrander, Jaquet, et al., 2007). DUOX enzymes and their activator subunits exhibit distinct subcellular localizations. DUOXA protein is found on ER membranes, when DUOX is not present (Morand et al., 2009). In lung cells, DUOX1 and DUOX1A co-localize at the plasma membrane, while DUOX2 and DUOX2A co-localize primarily at intracellular membranes including ER (Luxen et al., 2009). In the same study, authors showed that DUOX1 and DUOX2 changed their localization to leading edge of migrating cells upon wound formation. Hence, differential localization of NOX enzymes seems to provide functional specificity. Knowledge of the subcellular location of the different NOX subunits with or without activation signals provides a better understanding of the control mechanism and physiological roles of different NOX complexes in specific cell types.

1.3 NOX enzymes in the nervous system

NOX complex expression has been detected in adult human and rodent brain homogenates, hippocampus and spinal cord, cerebellum and in central nervous system (CNS) of developing zebrafish embryos (Cheng et al., 2001; Angelica Coyoy, Olguin-Albuerne, Martinez-Briseno, & Moran, 2013; Infanger, Sharma, & Davisson, 2006; Sorce & Krause, 2009; Weaver, Leung, &

Suter, 2016). The expression of different *Nox* genes expression has been found in microglia, astrocytes, oligodendrocytes, and neurons (Abramov et al., 2005; Accetta et al., 2016; Nayernia, Jaquet, & Krause, 2014). NOX1-4 isoforms are found in neurons, and their presence in subcellular compartments is summarized in Table 1. *Nox1* and *Nox3* expression has been demonstrated in neurons but their specific subcellular locations were not investigated (Cooney, Bermudez-Sabogal, & Byrnes, 2013; Rama Rao et al., 2018). To our knowledge, NOX5 has not been localized to neurons thus far, although its expression was detected in CNS (Weaver et al., 2016). In neuronal cells, NOX2 subunits gp91^{phox}, p22^{phox}, p67^{phox}, and p47^{phox} were localized to the cell body and dendritic arbors; gp91^{phox} and p22^{phox} were localized to axonal arbors, dendrites, growth cones and at synaptic sites in hippocampal neuronal cultures (Tejada-Simon et al., 2005; Wilson, Nunez, & González-Billault, 2015). gp91^{phox}, p22^{phox}, p47^{phox} and p67^{phox} were also found in cytosol and associated with intracellular compartments such as ER and Golgi complex (Glass et al., 2006; Zawada et al., 2011). p47^{phox} and p22^{phox} subunits were found in sympathetic and sensory neurons and perivascular nerve fibers (Cao, Demel, Quinn, Galligan, & Kreulen, 2009). Cultured rat cerebellar granule neurons exhibit NOX2 localization in developing neurites, in axons, and at growth cones along with filopodia, where they can modulate protrusion efficiency (Olguín-Albuerne & Morán, 2015). NOX2 and p40^{phox} expression have also been detected in the growth cones of *Aplysia* bag cell neurons (Munnamalai et al., 2014). p40^{phox} is partially associated with filopodial F-actin bundles in the growth cone periphery, whereas NOX2 displays plasma membrane association in the peripheral domain and vesicular plasma membrane association in the central domain (Munnamalai et al., 2014). Such cytoskeletal association of cytosolic NOX subunits could keep them away from the main membrane-bound subunits when cells are not activated and has been found in other cell types as well (Ushio-Fukai, 2009). Overall, subcellular localization of NOX subunits in neurons is similar to what has been found in other cell types. NOX subunits have been found in cytosolic regions as well as plasma membrane and intracellular membranes, occasionally found in specialized compartments such as growth cones and axons, as well as actin-rich regions associating with cytoskeletal elements. With respect to NOX isoform-specific subcellular localization, most information is available for NOX2. However, much less is known about the functional relevance of the different subcellular localizations in neurons. For instance, clear evidence that NOX subunits translocate to plasma membrane upon cellular stimulation is still largely unknown. In paraventricular hypothalamic neurons, p47^{phox} was found

mainly at post-synaptic dendrites, and Angiotensin II (AngII) stimulation promoted p47^{phox} translocation to endomembranes near plasma membrane suggesting that activation signals can change subcellular localizations in neurons as well (Coleman et al., 2013). In future studies, more detailed dynamic analysis of the specific localization of different Nox subunits during cellular activation will help to improve our understanding of the functions and down-stream effectors of NOX enzymes in neurons.

Table 1: Localization of NOX subunits in neurons.

NOX Subunit	Cell Type	Cellular Localization	Reference
NOX1	Neurons in frontal cortex, striatum, hippocampus and thalamus	N/A	(Rama Rao et al., 2018)
gp91^{phox}	Aplysia bag cell neurons, cerebellar granule neurons, cortical neurons, dopaminergic neurons, hippocampal neurons, mNTS neurons	Cell body, dendrites, axons, growth cones, plasma membrane of cell body, plasma membrane of growth cone, cytosol, endomembranes, Golgi complex, rough ER	(Glass et al., 2006; Munnamalai et al., 2014; Olguín-Albuerne & Morán, 2015; Tejada-Simon et al., 2005; Wilson et al., 2015; Zawada et al., 2011)
p22^{phox}	cortical neurons, hippocampal neurons, mNTS neurons	Cell body, dendrites, axons, axon tip, Golgi complex, mitochondria, synaptic sites	(Glass et al., 2006; Tejada-Simon et al., 2005; Wilson et al., 2015)
p40^{phox}	Aplysia bag cell neurons	Cell body, plasma membrane, growth cone, cytosol	(Munnamalai et al., 2014)
p47^{phox}	CG and DRG neurons, cortical neurons, dopaminergic neurons, hippocampal neurons, mNTS neurons, PVN neurons	Cell body, dendrites, axons, cytoplasm, plasma membrane, rough ER, smooth ER, endomembranes	(Cao, Dai, Parker, & Kreulen, 2007; Coleman et al., 2013; Glass et al., 2006; Tejada-Simon et al., 2005; Wilson et al., 2015; Zawada et al., 2011)
p67^{phox}	cortical neurons, dopaminergic neurons, hippocampal neurons	Cell body, dendrites, synaptic sites	(Tejada-Simon et al., 2005; Wilson et al., 2015; Zawada et al., 2011)
NOX3	Cortical neurons	N/A	(Cooney et al., 2013)
NOX4	Catecholaminergic neurons, hippocampal pyramidal cells, Purkinje cells	Mitochondria	(Case, Li, Basu, Tian, & Zimmerman, 2013; Vallet et al., 2005)
DUOX1-2	Cortical neurons	Cell body, dendrites	(Damiano et al., 2012)

Uncontrolled ROS production by NOX enzymes has been noted in several CNS pathologies including adult neurodegenerative diseases and traumatic injuries. Inhibiting NOX2 enzyme alleviated symptoms of multiple sclerosis, Alzheimer's Disease and Amyotrophic Lateral Sclerosis (ALS) in mice (Park et al., 2008; Ravelli et al., 2019; Wu, Berangere Re, Nagai, Ischiropoulos, & Przedborski, 2006). Accordingly, human subjects of ALS with lower NOX2 activity showed increased survival from the disease onset (Marrali et al., 2014). NOX-derived ROS was implicated in the dopaminergic neuronal degeneration, which is a hallmark of Parkinson's Disease (Cheng et al., 2018; Sharma & Nehru, 2016). Increased NOX2 expression was detected in the post-mortem brains of patients who died from traumatic brain injury (TBI) and secondary effects of TBI on motor neuron dysfunctions were abolished with decreasing ROS levels (Chandran et al., 2018; Schiavone, Neri, Trabace, & Turillazzi, 2017). In addition, *NOX* expression was increased upon spinal cord injury (SCI) and pharmacological inhibition of NOXes reduced oxidative stress and inflammation (Cooney, Zhao, & Byrnes, 2014). On the other hand, controlled ROS production is required for maintaining cellular homeostasis and regulating several cellular activities in the nervous system. Physiological and developmental roles of ROS in the CNS have been reviewed previously (Bórquez et al., 2016; Wilson, Muñoz-Palma, & González-Billault, 2018). For instance, H₂O₂ application to cultured rat hippocampal neurons resulted in Ca⁺² release from ER, that could potentially interfere with Ca-related signaling events (Gerich, Funke, Hildebrandt, Faßhauer, & Müller, 2009). Learning and memory were both affected by cellular H₂O₂ levels. In rat hippocampal slices, low H₂O₂ increased N-methyl-D-aspartate (NMDA)-independent long-term potentiation (LTP) and decreased long-term depression (LTD), while higher concentrations had opposite effects (Kamsler & Segal, 2003; Kishida & Klann, 2007). NMDA-dependent LTP and synaptic plasticity involved NOX-derived superoxide and NOX inhibition resulted in impaired memory formation (Francis-Oliveira, Vilar Higa, Dati, Shieh, & De Pasquale, 2018; Kishida et al., 2006, 2005). Moreover, during development H₂O₂ accumulates in *C. elegans* and zebrafish larvae, suggesting an involvement of ROS-mediated signaling in embryonic development (Gauron et al., 2016; Knoefler et al., 2012). Given the role of ROS signaling in various neuronal functions, Nox-derived ROS have also been implicated in neuronal development.

1.4 NOX enzymes in neurogenesis

Multipotent neural stem cells (NSCs) can self-renew and differentiate like other stem cells. ROS are important in regulating the stemness of NSCs (Figure 2). Perez Estrada et al. showed that H₂O₂ treatment increased neurogenesis and oligodendrocyte differentiation in adult rat primary neural progenitor cell (NPC) cultures through altering gene expression (Perez Estrada, Covacu, Sankavaram, Svensson, & Brundin, 2014). Tsatmali et al. found two distinct cell populations in rat cortical cultures: low- and high-ROS exhibiting cells. Low-ROS exhibiting cells were positive for the neural progenitor marker nestin and incorporated bromo-deoxyuridine (BrdU), whereas high-ROS cell populations were positive for differentiated neuronal markers β -tubulin and tau (Tsatmali, Walcott, & Crossin, 2005). Examination of different developmental stages of the rat brain *in vivo* validated that higher ROS levels were acquired in newborn neurons and persisted only in neurogenic zones in the adult brain (Tsatmali, Walcott, Makarenkova, & Crossin, 2006). What could be the source of this differentially produced ROS in progenitor and newly differentiated neurons? Recent evidence shows that NOX enzymes are likely the main source of ROS in NSCs *in vivo*. Nerve growth factor (NGF) promoted differentiation and neurite outgrowth as well as increased ROS levels, possibly H₂O₂, in cells derived from rat adrenal medulla (PC12 cells). Treating PC12 cells with the NOX-inhibitor DPI or transfecting cells with dominant negative form of Rac1 inhibited NGF-induced ROS increase and neurite outgrowth, suggesting a role for active NOX complex in the neuronal differentiation process (Suzukawa et al., 2000). NOX inhibition abolished BrdU incorporation in neurospheres formed by neural progenitor cells (NPCs) from embryonic mouse hippocampal cultures, providing evidence for the role of NOX-derived ROS in NPC stemness (Yoneyama, Kawada, Gotoh, Shiba, & Ogita, 2010). Besides embryonic cells, NSCs derived from the adult neurogenic zone were shown to require NOX-mediated H₂O₂ production for proliferative self-renewal capacity and neurogenesis (Haigh, Tumpach, Collins, & Drew, 2016; Le Belle et al., 2011). NSCs were treated with 2-[(dimethylamino)methyl]-8-hydroxyquinoline (DMAMQ), a compound that is related to drugs for neurodegenerative disease therapy. Proliferative activities of NSCs from the subventricular zone (SVZ) along with neurite outgrowth of differentiated neurons and intracellular ROS levels were increased upon DMAMQ treatment, and the effects were abolished with the inhibition of NOX enzymes with DPI (Haigh et al., 2016). Since this study was based solely on DPI-mediated inhibition of NOX, the possibility of other flavoenzymes in the process cannot be excluded. In summary, all of these studies

demonstrate that NOX-mediated ROS production is required for proper neurogenesis; however, the underlying molecular mechanisms have largely remained unknown until recently.

Current evidence suggests that ROS-mediated proliferation of NSCs involve the phosphoinositide 3-kinase/protein kinase B (PI3K/Akt) and mitogen-activated protein kinase/extracellular-signal-regulated kinase 1/2 (MAPK/ERK1/2) pathways (Figure 2). The PI3K/Akt pathway modulates cell survival and proliferation, and phosphatase and tensin homolog (PTEN) negatively regulates this signaling cascade (Hemmings & Restuccia, 2012; Yu & Cui, 2016). PTEN deletion enhances NSC self-renewal and neurogenesis (Gregorian et al., 2009; Groszer et al., 2006) and PTEN can be oxidized by H₂O₂ after which PTEN activity is abolished (Le Belle et al., 2011). NOX inhibition decreased proliferation of wild-type NSCs, whereas NSCs derived from PTEN heterozygous mice exhibited increased proliferation upon NOX inhibition (Le Belle et al., 2011). Later studies with *in vivo* mouse models of autism spectrum disorders showed that changes in ROS levels in the NSCs can alter the CNS development (Le Belle et al., 2014). Pregnant mice were injected with lipopolysaccharide (LPS) to induce maternal inflammation. The pups born from these mice exhibited mild brain overgrowth, thickened cortex, increased SVZ proliferation, and self-renewal along with elevated endogenous ROS levels. Inhibiting intracellular ROS with apocynin *in vivo*, attenuated the brain overgrowth and NSC self-renewal in pups that are born to LPS-treated mothers. Some of the progeny exhibited smaller brains upon apocynin treatment, suggesting that optimal ROS levels are required for normal neurogenesis. Although not studied in detail, activation of MAPK/ ERK1/2 pathway has also been implicated in ROS-mediated neuronal differentiation from human embryonic stem cells in response to oxidative stress (Hu et al., 2018). Moreover, *Sod3*-expression was detected in hippocampus, where it can contribute to ROS-mediated neurogenesis through converting NOX-generated superoxide to hydrogen peroxide (Oury, Card, & Klann, 1999). SOD3 function is required for long-term survival of newborn neurons, possibly acting through activation of Akt pathway, supporting the involvement of NOX enzymes in the PI3K/AKT pathway (Kemp et al., 2010; Rola et al., 2007; Zou et al., 2012). Lastly, there is also evidence for interaction of NOX- and neurotrophin-mediated signaling involving PI3K/MAPK pathways. PI3K/MAPK pathways are activated by brain-derived neurotrophic factor (BDNF)-tropomyosin receptor kinase B (TrkB) interaction, and BDNF-driven NPC self-renewal capacity was attenuated in Nox2 knockout mice (Le Belle et al., 2011; Yoshii & Constantine-Paton, 2010). This suggests two plausible explanations how NOX2 and BDNF-TrkB signaling

could cooperate: (1) BDNF-TrkB activates Nox2 complex, which in turn modulates PI3K/MAPK pathways; (2) NOX2 acts on BDNF-TrkB activation by oxidizing and modulating activity of TrkB. The oxidation of TrkB has not been shown yet to our knowledge; however, receptor tyrosine kinases are known to be redox-sensitive, such as epidermal growth factor receptor and platelet-derived growth factor receptor (Corcoran & Cotter, 2013). Thus, in summary, NOX-mediated ROS production appears to be important in maintaining self-renewal and differentiation of NSCs in both embryonic development and adult stages, and the controlled production of ROS is critical for normal nervous system development.

Individual NOX isoforms in regulating stemness of NSCs (NOX1, NOX2, NOX3, NOX4 and DUOX1) have been implicated in NSC maintenance, proliferation and differentiation, and will be discussed next (See Table 2 for summary; Figure 2). As *Nox5* is not expressed in rodents, there is no evidence for its involvement in neural development thus far.

Table 2: Summary of the role of different NOX isoforms in neurogenesis.

Isoform(s)	Model	Effect on neurogenesis	References
NOX1-3	PC12 cells	Promotes NGF-induced differentiation	(Suzukawa et al., 2000b)
NOX1-3	Embryonic hippocampal NSCs	Modulates proliferation	(Yoneyama et al., 2010)
NOX1-5, DUOX1-2	Adult hippocampal NSCs	Maintains self-renewal capacity and enhances proliferation	(Haigh et al., 2016)
NOX1-3	Embryonic and adult hippocampal NSCs	Modulates self-renewal and proliferation through PI3K/Akt pathway	(Le Belle et al., 2011, 2014)
NOX1	PC12 cells	Negatively regulates NGF-induced differentiation	(Ibi et al., 2006)
NOX2	SH-SY5Y neuroblastoma cells	Induces RA-mediated neuroblastoma cell differentiation	(Nitti et al., 2010, 2007)
NOX2	Adult hippocampal NSCs	Induces NMDA-mediated oligodendrocyte differentiation; prevents lineage progression and supports NSC maintenance in response to IL-1 β	(Cavaliere, Urra, Alberdi, & Matute, 2012; Cavaliere, Benito-Muñoz, Panicker, & Matute, 2013; Kokovay et al., 2012)
NOX2	Adult hippocampal NPCs	Induces FGF2-mediated PI3K/Akt pathway activation, maintains proliferative NPC pool and promotes neurogenesis	(Dickinson, Peltier, Stone, Schaffer, & Chang, 2011)
NOX2	Adult hippocampal NPCs & CGD patient-derived iPSCs	Maintains the NPC pool in adult mice brain and is required for proliferation and differentiation	(Nayernia et al., 2017)
NOX2	Adult hippocampal NSCs	Promotes switch from quiescence to proliferation stage by modulating intracellular redox balance	(Collins, Tumpach, Groveman, Drew, & Haigh, 2018)
NOX3	Cerebellar granule cell precursors	Modulates SHH-driven proliferation, possibly through PI3K/Akt pathway	(Mazzonetto et al., 2019)
NOX4	Neonatal cerebellum NSCs	Induces Ang II-driven proliferation	(Topchiy et al., 2013)

Table 2 continued

NOX4	Embryonic neural crest stem cells	Drives BMP2-induced differentiation	(Lee et al., 2014)
NOX4	ESCs, P19 ECCs	Promotes neurogenesis through ERK1/2 phosphorylation	(Choi et al., 2019)
NOX4	Embryonic hippocampal NCSs	Promotes proliferation and neurogenesis through Akt phosphorylation	(Yoshikawa et al., 2019)
NOX4	Neonatal cerebellar granule cell precursors	Modulates SHH-driven proliferation by stabilizing HIF1 α	(Eyrich, Potts, Robinson, Maximov, & Kenney, 2019)
DUOX1	P19 ESCs	Modulates RA-induced differentiation	(Kennedy et al., 2010; Ostrakhovitch & Semenikhin, 2011)

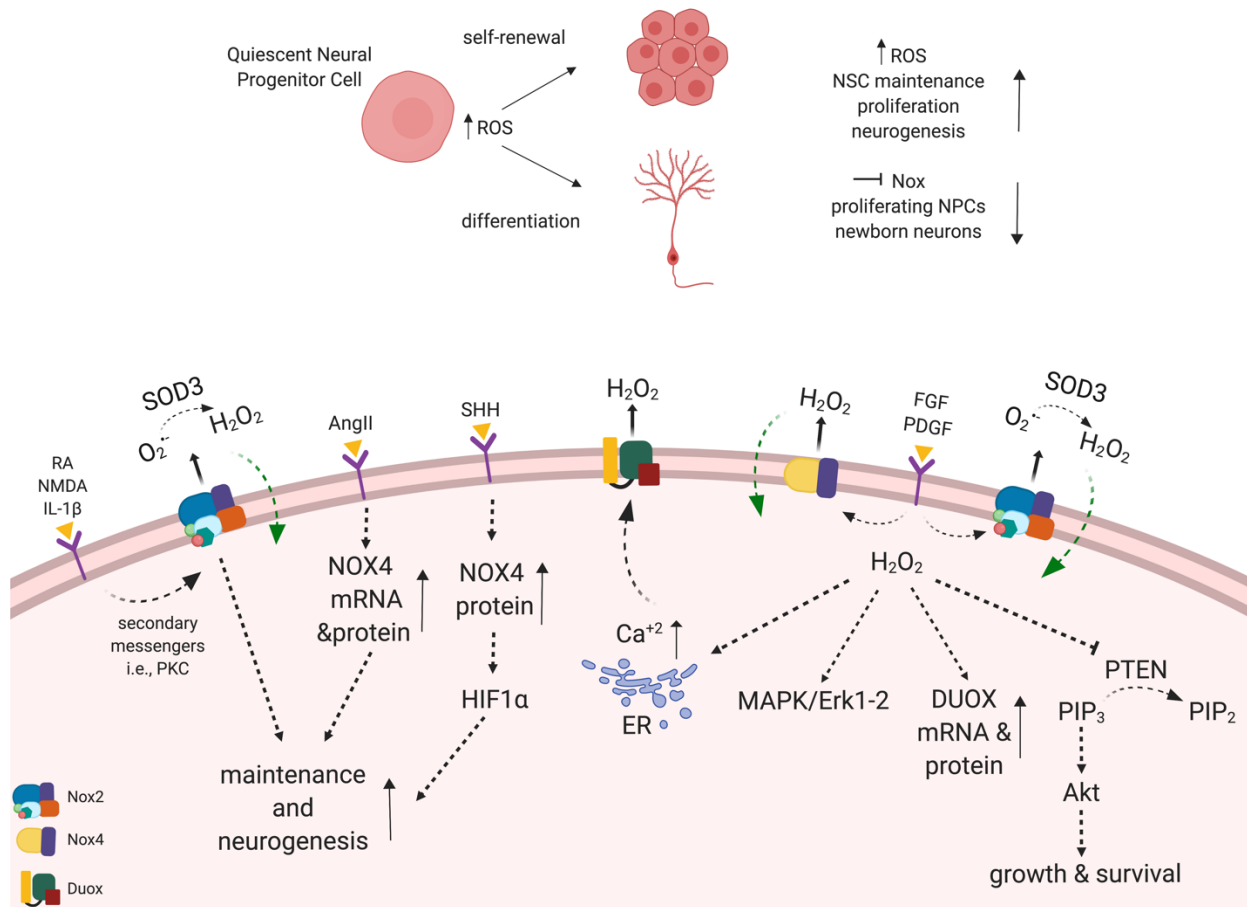


Figure 2: NOX-mediated ROS in neuronal development.

The self-renewal and differentiation phases of NPCs are regulated by ROS production. NPCs can stay in proliferative state to produce more of NPCs or undergo asymmetric division and differentiate into neurons. Inhibition of Nox decreases both the number of proliferative progenitors and differentiated neurons. Nox2 and Nox4 are under control of upstream signaling cascades. Several receptor-ligand interactions result in either activation of NOX2 complex by activation and translocation of cytosolic subunits, or activation of Nox4 by increasing transcription and translation of the gene. Resulting active Nox complexes either produce $O_2^{\cdot-}$ prior to H_2O_2 conversion by SOD3, or directly H_2O_2 , which oxidizes cellular proteins, such as PTEN. PTEN oxidation inhibits PTEN, thereby shifting the phosphoinositide-phosphate balance toward phosphatidylinositol (3,4,5)-trisphosphate (PIP_3). This results in activation of Akt to induce NPC growth and survival. Intracellular H_2O_2 can promote Ca^{+2} release from endoplasmic reticulum, that in turn can activate Ca^{+2} -signaling and Duox enzymes. Nox4 can stabilize HIF1 α to modulate neurogenesis. In the lower panel, black dashed arrows indicate the direction of the signaling pathway, green dashed arrows indicate the transport of H_2O_2 intracellularly and solid arrows indicate the end-product of signaling. Akt: protein kinase B; Ang II: Angiotensin II, BMP2: Bone morphogenic protein 2; FGF2: Fibroblast growth factor 2; HIF1 α : Hypoxia-inducible factor 1 α ; IL-1 β : Interleukin 1 β ; NMDA: N-methyl-D-aspartate; NPC: Neural progenitor cells; NSC: Neural stem cells; PDGF: Platelet-derived growth factor; PIP_2 : Phosphoinositide 2; PIP_3 : Phosphoinositide 3; PKC: Protein kinase C; PTEN: Phosphatase and tensin homolog; RA: Retinoic acid; SHH: Sonic Hedgehog

1.4.1 NOX1 and NOX3

NOX1 negatively regulates NGF-induced differentiation of PC12 cells *in vitro* (Ibi et al., 2006). Upon NGF-treatment, transcript levels of *Nox1* gene and intracellular superoxide levels were increased, while *Nox2* mRNA levels were decreased. NGF-induced neurite outgrowth and neuronal differentiation were enhanced when the cells were treated with two different NOX inhibitors, DPI and apocynin, or when *nox1* mRNAs were silenced. PI3K inhibitors increased the neurite outgrowth in control cells but did not influence the *Nox1* silenced cells, linking the PI3K/AKT pathway to Nox1 in regulating neuronal differentiation. Contradictory with this observation, in the previous study by *Suzukawa et al.* (Suzukawa et al., 2000), NGF-induced differentiation was abolished by NOX inhibition as well as by loss of Rac1 activity suggesting the requirement of NOX-mediated ROS generation in neuronal differentiation and outgrowth. The discrepancies between these two studies might be due to the differences in treatment time with NGF and NOX inhibitors. In addition, expression of other *Nox* isoforms or ROS-producing enzymes were not investigated upon *Nox1* silencing. Therefore, it is unclear whether the phenotypes are due to decreased superoxide in this model. On the other hand, mice with non-functional NOX3 protein exhibited increased *Nox1* expression in mutant cerebellum and culturing cerebellar granule cell precursors from *Nox3* mutant mice exhibited increased ROS production and sonic-hedgehog (SHH)-mediated proliferation in the progenitor cells *in vitro* (Mazzonetto et al., 2019). Authors focused on NOX3 isoform, but the effects on proliferation correlate with the increased ROS levels, which is linked to increased *Nox1* expression in these mutants. *Nox3* expression is mainly restricted to inner ear, and in line with this, expression of *Nox3* gene in cerebellum was not found different between *Nox3* mutants and wild-types. This implies the main isoform responsible for proliferation of cerebellar granule cell precursors is NOX1. Furthermore, *Akt* gene expression was upregulated in *Nox3* mutant mice, suggesting the involvement of PI3K/Akt pathway in regulating NOX-mediated neurogenesis.

1.4.2 NOX2

NOX2 is the best characterized NOX isoform in neural development. It was originally identified in phagocytes, where it generates bursts of superoxide to fight invading pathogens. Patients with chronic granulomatous disease (CGD) carry mutations in one of the NOX2 complex

subunits and struggle to fight infections (Dinauer, Orkin, Brown, Jesaitis, & Parkos, 1987; Grandvaux, Soucy-Faulkner, & Fink, 2007; Hohn & Lehrer, 1975; Mcphail, Henson, & Johnston, 1981; Rada & Leto, 2008). Human CGD patients exhibit cognitive impairment (Pao et al., 2004), and *Nox2* knockout mice display deficiencies in synaptic plasticity and memory (Kishida et al., 2006), which suggests that NOX2 is essential for proper development of the nervous system. In line with this, NOX2-mediated ROS is required for neuronal differentiation (Figure 2). *In vitro*, retinoic acid (RA)-induced neuroblastoma cell differentiation is mediated by protein kinase C delta (PKC Δ) activation that promotes the translocation of the activator subunit of NOX2 complex, p67^{phox}, to the plasma membrane, where it activates NOX2 (Nitti et al., 2010, 2007). NMDA receptor stimulation drives oligodendrocyte differentiation (Cavaliere et al., 2012), and NMDA-stimulated differentiation involves ROS production through PKC activation that mediates p67^{phox} translocation to oligodendrocyte plasma membrane (Cavaliere et al., 2013). Several studies provided evidence that NOX2-mediated ROS production is involved in NSC maintenance and proliferation *in vitro* and *in vivo* (Dickinson et al., 2011; Kokovay et al., 2012). For instance, the interleukin IL-1 β supports maintenance of NSCs from adult mice SVZ via production of ROS through NOX2 by preventing lineage progression (Kokovay et al., 2012). Furthermore, *Nox2* knockout mice exhibited decreased numbers of proliferating adult progenitors in dentate gyrus (DG) and SVZ, and newborn neurons *in vivo*. Supporting the NOX inhibition studies, NOX2-mediated H₂O₂ production in response to FGF2 required PI3K/Akt pathway activation *in vitro* (Dickinson et al., 2011; Nayernia et al., 2017). Interestingly, neurogenesis was found to be increased in prion disease (Gomez-Nicola et al., 2014), when the disease-causing prion protein (PrP^{Sc}) is accumulated. This is due to increased ROS, since healthy prion protein (PrP^C) normally decreases intracellular ROS levels generated by NOX2 activity to keep adult mice NSCs in quiescent state (Collins et al., 2018). Overall, the activation of NOX2 depends on stimulation of upstream signals that are precisely controlling the state of neural progenitors. The tight control of NOX2 activation regulates the balance between maintenance of NSCs and differentiation into neuronal cells.

CNS also contains glial cells as microglial cells that clear apoptotic cells, protein aggregates, and cellular debris (Janda, Boi, & Carta, 2018). When activated, microglia represent a major source of NOX2-derived ROS in the CNS, contributing to ROS signaling (Ma et al., 2017). So far, most studies suggest that ROS production promotes neurogenesis; however, a study on

neurogenesis and microglia showed the opposite. Microglia populate the neurogenic niche in the macaque cerebral cortex and deactivation of microglia, which results in loss of the NOX2-mediated ROS production, increased the neural precursor cells significantly (Cunningham, Martinez-Cerdeno, & Noctor, 2013). The NOX-mediated ROS that are produced by non-neuronal cells could potentially affect the fate of the neuronal development, as in the case of microglia. Although the exact role of microglia derived NOX-ROS signaling has not been established yet, it definitely has the potential to modulate the neuronal development (Haslund-Vinding, McBean, Jaquet, & Vilhardt, 2017).

1.4.3 NOX4

NOX4 isoform is localized to the mitochondrial membrane besides the plasma and intracellular vesicle membranes (Bernard et al., 2017; Case et al., 2013; Shanmugasundaram et al., 2017). Ang II is a peptide hormone that is involved in maintaining NPCs (Chao, Yang, Buch, & Gao, 2013). Furthermore, Ang II to NOX4 signaling has been implicated in different cellular processes such as angiogenesis, protein synthesis in mesangial cells, proliferation and migration of mouse cardiac fibroblasts (Gorin et al., 2003; Schröder et al., 2012; Somanna et al., 2016). In neuronal mitochondria, Ang II mediates superoxide formation via NOX4 enzyme (Case et al., 2013). The direct relationship between Ang II and ROS production by NOX4 in NSCs was shown *in vitro*. Ang II increased NSC proliferation and superoxide production as well as NOX4 protein translation (Figure 2) (Topchiy et al., 2013). In cultured neural crest stem cells, bone morphogenic protein 2 (BMP2) induced ROS production via NOX4 to drive neuronal differentiation; however, *Nox4* knockout mice did not exhibit abnormalities in neural crest-derived peripheral nervous system or major dysfunction, suggesting that a compensation mechanism by other isoforms could rescue the loss of *Nox4* enzyme (Lee et al., 2014). Furthermore, NOX4 was recently implicated in two different signaling cascades involving ERK1/2 and PI3K/Akt in the regulation of neurogenesis (Choi et al., 2019; Yoshikawa et al., 2019). During neuronal differentiation, *Nox4* mRNA transcript levels were increased, and, NOX inhibitors decreased ERK1/2 phosphorylation, while inhibition of ERK1/2 phosphorylation decreased NOX4-mediated H₂O₂ production. This reciprocal interaction suggests that there is a cooperation between NOX4-ROS and ERK1/2 in neurogenesis (Choi et al., 2019; Yoshikawa et al., 2019). In another model, *Nox4* expression was detected in cultured NSCs, and *nox4* overexpression augmented the NSC proliferation along with

Akt phosphorylation (Yoshikawa et al., 2019). Upon inducing hippocampal neuronal injury with a neurotoxin, proliferation and neurogenesis in hippocampal progenitors were abolished in *Nox4* knockout mice. NOX4-mediated H₂O₂ stabilized the hypoxia-inducible factor 1 α (HIF1 α) during SHH-induced proliferation of cerebellar granule neuron precursors, suggesting involvement of other signaling pathways in which Nox can mediate neurogenesis (Eyrich et al., 2019). In summary, NOX4, similar to NOX2, can be activated by different signals in order to promote neurogenesis (Figure 2).

1.4.4 DUOX

Experimental evidence supporting a role of DUOX enzymes in neurogenesis is limited to *in vitro* studies and has not provided insights into a specific signaling pathway so far. Expression of the cytosolic subunit *DuoxA1* has been detected in neurogenic regions in mice brain (Kennedy et al., 2010). *Duoxa1* mRNA levels exhibited transient increase during differentiation of pluripotent P19 ESCs in response to retinoic acid (RA)-treatment. This was accompanied by an increase in DUOX-mediated H₂O₂ levels and acquisition of neuronal fate. Cytoskeletal reorganization appears to be involved in fate determination upon ROS-mediated neuronal differentiation, as *duoxal* expression was accompanied by an increase in *Lamin A/C* expression. Another study showed that there is a robust expression of both *Duox1* and *Duoxal* in these neural stem cells, and that levels of *Duoxal* increase with differentiation (Ostrakhovitch & Semenikhin, 2011). Furthermore, the transcription and translation of DUOX1 and 2 in human neuroblastoma cells and human oligodendrocyte cell line required platelet derived growth factor (PDGF)-mediated H₂O₂ production by other NOX isoforms (Damiano et al., 2012). It is possible that individual NOX isoforms can modulate activation of other isoforms; for example, H₂O₂ can increase intracellular Ca⁺² levels, which in turn is capable of activating Ca⁺²-dependent NOX isoforms including DUOX1-2. These results suggest that the role of DUOX in neurogenesis could be a downstream effect of activation of other NOX enzymes in order to generate additional intracellular ROS.

1.5 NOX enzymes in neurite growth and the neuronal cytoskeleton

Neurite growth is regulated by cellular signaling that allows precise pathfinding of developing and regenerating neurons (Bashaw & Klein, 2010; Omotade, Pollitt, & Zheng, 2017;

Ye, Qiu, Gao, Wan, & Zhu, 2019). Neurons respond to chemical and physical cues in their microenvironment in order to follow the correct path and reach their synaptic targets (Berman, Moss, Bursztajn, 1993; Miller & Suter, 2018; Muller, Stahl, & Bonhoeffer, 1990; Sretavan & Reichardt, 1993). Developing axons and dendrites have a highly motile structure at their growing tip referred to as growth cones. Growth cones contain highly dynamic actin and microtubule cytoskeleton, which is regulated by guidance cues during pathfinding (Bentley & Toroian-Raymond, 1986; Challacombe, Snow, & Letourneau, 1997; Forscher, Lin, & Thompson, 1992; Gallo, 1998; Lin, Espreafico, Mooseker, & Forscher, 1996; Lowery & Vactor, 2009). Signaling cascades activated by various guidance cue/receptor pairs result in reorganization of the actin cytoskeleton allowing the growth cones to guide the developing axons to the proper target (Dent, Gupton, & Gertler, 2011; Gomez & Letourneau, 2014; Lin & Forscher, 1993; Suter & Forscher, 1998; Tanaka & Sabry, 1995). Evidence suggests that ROS take a part in axonal growth and guidance signaling. In one of the earliest studies, Suzukawa et al. showed that ROS production increased neurite outgrowth in PC12 cells (Suzukawa et al., 2000). In hippocampal cells, both H₂O₂ addition and staurosporin-mediated H₂O₂ generation increased neurite growth (Min et al., 2006). Also, NOX-mediated ROS triggered α -lipoic acid (LA)- mediated neurite outgrowth via ERK phosphorylation (Wang et al., 2011). Moreover, dendritic growth mediated by BMP requires NOX2 to form functional synapses and dendritic networks (Chandrasekaran, Lea, Sosa, Higgins, & Lein, 2015). In conclusion, NOX-mediated ROS production is important to guide the proper neuronal growth.

Important insights into the role of Nox-mediated ROS for proper arrangement of growth cone actin cytoskeleton came from studies using large *Aplysia* growth cones (Munnamalai & Suter, 2009; Munnamalai et al., 2014). Reducing ROS levels with NOX inhibitors decreased actin network assembly, filopodial bundles, lamellipodia, retrograde actin flow in the growth cones as well as neurite outgrowth (Munnamalai & Suter, 2009; Munnamalai et al., 2014). Furthermore, Munnamalai et al. provided the first immunocytochemical evidence for functional NOX2 complex in the growth cone as well as co-localization of p40^{phox} subunit and F-actin bundles in the periphery (Munnamalai et al., 2014). Actin regulatory proteins Cdc42 and Rac1 are required for NOX-mediated ROS signaling in the growth cone to modulate filopodial dynamics as well as establishing neuronal polarity (Wilson et al., 2015). On the other hand, high levels of NOX-produced H₂O₂ in response to cytokines reorganize the actin in the growth cone area and mediate

growth cone collapse (Barth, Stewart-Smeets, & Kuhn, 2009; Kuhn, 2014). In addition to NOX there is another enzyme, Molecule interacting with CasL (MICAL), involved in ROS signaling during axon guidance. MICAL is a flavoenzyme that links ROS signaling to growth cone guidance, regulating semaphorin 3A (Sema3A)-induced growth cone collapse by oxidizing actin to favor F-actin depolymerization and modifying collapsin response mediator protein 2 (CRMP2) to promote microtubule disassembly (Hung, Pak, & Terman, 2011; Hung et al., 2010; Morinaka et al., 2011; Siebold et al., 2005). Hence, axonal guidance could be a target of redox proteins.

1.5.1 Bidirectional interaction between NOX2 and actin cytoskeleton

The interaction between NOX enzymes and the actin cytoskeleton is bidirectional because F-actin can serve as binding site for cytosolic NOX subunits including p40^{phox}, p47^{phox} and p67^{phox} in unstimulated cells. For example, p40^{phox} localizes to filopodial F-actin bundles in *Aplysia* growth cones (Munnamalai et al., 2014). The exact functional role of p40^{phox} subunit in NOX activation is less understood when compared to p47^{phox} and p67^{phox}. p40^{phox} binds p67^{phox} and enhances membrane translocation of p67^{phox}-p47^{phox} for Nox2 activation (Kuribayashi et al., 2002; Wientjes, Hsuan, Totty, & Segal, 1993). p40^{phox} has a high sequence similarity with p47^{phox} at its N-terminus, can bind to p47^{phox} and increase its affinity to NOX2 (Cross, 2000; Wientjes et al., 1993; Wientjes, Panayotou, Reeves, & Segal, 1996). p40^{phox} is not necessary for enzyme activity in cell-free systems; however, it is required for phagocytic NOX2 activation (Suh et al., 2006; Wientjes et al., 1993). Furthermore, p40^{phox} activates NOX2 without p47^{phox} in cell-free system, possibly due to the function of shared domains. Very little is known about the functional role of p40^{phox} in neuronal cells; however, its expression was detected in pyramidal cells of CA1 and CA3 regions, granule cells of the dentate gyrus, Purkinje cells and granule cells of the cerebellum (Coyoy, Valencia, Guemez-Gamboa, & Morán, 2008; Mizuki et al., 1998; Serrano, Kolluri, Wientjes, Card, & Klann, 2003). p40^{phox} binds to actin in neutrophils, leukocytes, COS7 endothelial cells, and *Aplysia* bag cell neurons via the phox homology (PX) domain (Benna et al., 1999; Chen, He, Minshall, Dinauer, & Ye, 2007; Munnamalai et al., 2014; Shao, Segal, & Dekker, 2010; Tsunawaki & Yoshikawa, 2000). The PX domain is required for membrane targeting, as it serves as a binding site for phosphatidylinositol 3-phosphate (PtdIns(3)P) on the plasma membrane, whereas the actin interaction surface does not affect membrane targeting (Shao et al., 2010). However, when the PtdIns(3)P binding is blocked in p40^{phox}, the binding profile shifts to

actin association while decreasing the membrane translocation of p40-p67-p47^{phox} along with superoxide production (Chen et al., 2007). Furthermore, p40^{phox} is also associated with the actin-binding proteins moesin and coronin (Grogan et al., 1997; Munnamalai et al., 2014; Shao et al., 2010; Wientjes, Reeves, Soskic, Furthmayr, & Segal, 2001).

Promoting actin depolymerization increases superoxide production possibly by increasing the pool of p40^{phox} available for NOX activation at the membrane; however, decreased NOX activity has been reported upon actin depolymerization as well (Tamura, Kanno, & Endo, 2000; Touyz, Yao, Quinn, Pagano, & Schiffrin, 2005; Usatyuk et al., 2007). p47^{phox} interaction with cortactin was required for superoxide production in response to stimuli whereas the possible involvement of p40^{phox} was not investigated (Touyz et al., 2005; Usatyuk et al., 2007). Additionally, phosphorylated p40^{phox} negatively regulated NOX2 activation by inhibiting PKC-mediated p47^{phox} phosphorylation in cell-free system, while the same phosphorylation on p40^{phox} promoted full NOX2 activation in response to fMLP in neutrophils (Chessa et al., 2010; Lopes et al., 2004). Moreover, p40^{phox} is indispensable for enzyme activation when p47^{phox} is inadequately phosphorylated, but its activity is less critical when p47^{phox} is properly phosphorylated (Ueyama et al., 2011). CGD patients deficient with p40^{phox} exhibits higher residual NOX activity and better clinical outcome compared to CGD patients deficient in other subunits (Geer et al., 2018). Thus, the current evidence suggests that the role of p40^{phox} is multifaceted and context dependent. Association with F-actin and actin-binding proteins could act as a negative regulator for NOX activity by keeping cytosolic subunits away from the membrane in resting state, or act as a positive regulator by forming a scaffold on which NOX complex can be activated locally.

1.5.2 The role of NOX in axonal regeneration

Immediate injury responses include wound healing and inflammation to protect the injured site. Both processes mediate and are regulated by ROS production. Due to their high regeneration capacity, zebrafish are a well-established model to study tissue injury and regeneration. Following tail wounding, rapid accumulation of Duox-mediated H₂O₂ lead to recruitment of leukocytes (Niethammer et al., 2009). Lyn, a Src family kinase, was shown to be oxidized by wound-mediated H₂O₂, subsequently, recruiting neutrophils to the wound site (Yoo, Freisinger, LeBert, & Huttenlocher, 2012; Yoo, Starnes, Deng, & Huttenlocher, 2011). Given the involvement of ROS in normal neurite outgrowth, it is not surprising that ROS are also taking active part in axonal

regeneration after injury. In zebrafish larvae, fin amputation disrupted the axons, causing denervation and prominent H₂O₂ production at wound sites (Rieger & Sagasti, 2011). H₂O₂ addition could induce axon growth and help with re-innervation of axons at the injury site while axon regeneration capacity was blocked with *duox1*-morpholino treatment. In adult zebrafish, caudal fin amputation resulted in H₂O₂ production via Shh signaling to induce nerve growth in wound site (Meda et al., 2016). Shh and H₂O₂ work in a positive feedback loop until regeneration is complete (Meda et al., 2018). After injury, the severed axons that form growth cones were able to regrow under the direction of guidance cues and actin-microtubule cytoskeletal network modulation (Giger, Hollis, & Tuszynski, 2010; Hur, Saijilafu, & Zhou, 2012). Sciatic nerve injury in mice results in increased H₂O₂ levels followed by growth cone collapse. PKG1, cyclic GMP-dependent protein kinase 1, is activated through oxidation by H₂O₂ upon injury to phosphorylate cofilin and mediate growth cone collapse, which is a proper response to nerve injury (Valek et al., 2017). In wild type mice, injury caused growth cone collapse prior to regeneration. PKG redox-dead mutants were unable to cause growth cone collapse and exhibited increased outgrowth compared to wild type controls, suggesting the role of ROS-dependent oxidation of PKG1 in the axon regeneration and guidance. Indeed, authors proposed a functional model in which PKG1 modulates growth cone collapse. Based on the known activities of PKG1, it is likely that PKG1 and MICAL work in cohort to regulate growth cone collapse in response to Sema3A by changing the polymerization status of F-actin through cofilin and tubulin dynamics, respectively.

A recent comprehensive injury study showed that the NOX2 complex is responsible for axon regeneration in mouse dorsal root ganglion (DRG) neurons. Hervera and colleagues showed that in both sciatic nerve injury in DRG neurons and in spinal cord injury H₂O₂ levels were increased, which was abolished in p47^{phox} mutants (Hervera et al., 2018). When DRG neurons from *Nox2* mutants were co-cultured with bone marrow derived macrophages, the outgrowth response was preserved after the nerve injury, and inhibiting endocytosis abolished this response. Hence, the NOX2 complex originated from the macrophages surrounding the injury site, was maintained in endosomes and retrogradely transported to the neuronal cell body, where NOX2-mediated H₂O₂ could oxidize target proteins. Indeed, PTEN was found to be differentially regulated and significantly oxidized in response to H₂O₂ treatment after sciatic injury. PTEN inhibition results in PI3K/Akt pathway activation, which in turn promotes neuronal outgrowth. Through different signaling cascades, local production of ROS modulates axonal regeneration by

modifying cytoskeletal regulatory proteins and/or signaling mediators to re-arrange the cytoskeleton for regeneration of axons in response to injury.

1.6 Cellular antioxidant systems

Cellular ROS levels are controlled by antioxidant defense systems including endogenous antioxidant molecules such as glutathione, bilirubin, coenzyme Q, ferritin, and enzymes including SOD, catalase and glutathione peroxidase (Marengo et al., 2016). Presence of antioxidant defense system ensures cell homeostasis and redox regulation state by counterbalancing the over-production of ROS (Birben et al., 2012). Considering the importance of ROS mediated signaling, antioxidant systems are also crucial to monitor and control the intracellular ROS concentrations during development. Antioxidant mechanisms can be both constitutive, with constant regulation to maintain physiological ROS, and inducible, in which toxic accumulation of ROS causes a specific antioxidant response (Hahn, Timme-Laragy, Karchner, & Stegeman, 2015).

An important antioxidant defense mechanism against oxidative stress is nuclear factor erythroid 2 (Nfe2)-related factor 2 (Nrf2) activation (Nguyen, Nioi, & Pickett, 2009). Under physiological conditions, Nrf2 is bound to Keap1 and targeted for degradation (Sant et al., 2017). During oxidative stress, Nrf2 is freed from Keap1 and binds to specific DNA sequences called antioxidant response elements (ARE), which exist in the genes responsible for counterbalancing excess ROS and eliminate oxidative stress (Sant et al., 2017). Thus, Nrf2 acts as a master regulator for intracellular antioxidant defense system. The function of Nrf2 seem to be developmentally regulated. For instance, neuronal *Nrf2* expression was found to be decreased when NPCs start differentiating into neurons and Nrf2 inhibited proper maturation of neurons (Bell et al., 2015). Furthermore, the expression of *nrf2* was found to be lower in developing zebrafish embryos and increase gradually after 2 dpf (Hahn et al., 2015). These observations suggested that the major antioxidant system is kept inactive by controlled gene expression, allowing proper development during the early phases embryogenesis. Thus, the inactivity of Nrf2 system might favor the increase in intracellular ROS levels during development, which in turn regulates stem cell maintenance and differentiation as discussed above.

There are several other antioxidant mechanisms that are developmentally regulated. For instance, glutathione levels change during different stages of zebrafish development. While oxidized glutathione levels were higher during differentiation phases, it shifts to more reduced

glutathione during proliferative phases (Hahn et al., 2015; Timme-Laragy et al., 2013). Zebrafish embryos were shown to acquire substantial H₂O₂ levels during the first three days of development, and this coincides with the lower levels of catalase activity (Gauron et al., 2016). These observations suggest that antioxidant systems are not limited to eliminate excessive ROS production that are toxic to cell physiology. In summary, redox potentials during development are regulated both by ROS production and antioxidant defense control, and precise control of these two mechanisms ensure proper developmental response.

1.7 Retinal development in zebrafish

The visual system consists of the eyes and their connections in the brain. The receptive region in the eye is the retina, which is responsible for converting visual information into nerve signals. The vertebrate retina is organized into three nuclear layers containing cell bodies of seven major cell types. The cellular composition of the zebrafish retina is very similar to that of human retina. The three nuclear layers are: Ganglion cell layer (GCL) harboring cell bodies of retinal ganglion cells (RGCs), inner nuclear layer (INL) harboring cell bodies of horizontal, amacrine and bipolar cells, and outer nuclear layer (ONL) consisting of rod and cone photoreceptors. Finally, Müller glial cells (MG) have cell bodies residing in the INL, and they span the retinal layers to provide a structural support. The nuclear layers are separated by two synaptic layers: inner plexiform layer (IPL) and outer plexiform layer (OPL). The organization of the retinal layers and major cell types are shown in Figure 3. The major cell types are further divided into morphological and functional sub-types that underlie the complex circuitry in the vertebrate retina. The retina has a well-characterized laminar organization and within each layer neurons are not randomly positioned, but rather arranged in a mosaic organization. The ONL is well-known for its mosaic organization. For instance, ultraviolet (UV) -sensitive cones are arranged in rows with green cones, and green cones are flanked by red cones, and this characteristic arrangement is always specific to a cone subtype (Fadool & Dowling, 2008). This precise arrangement of neurons is required for proper visual information processing.

The visual signal is captured by photoreceptors residing in ONL. The information is then relayed from photoreceptors to interneurons in INL (amacrine, bipolar, horizontal cells), which in turn transmit information to RGCs in the GCL. RGCs are the neuronal output of the retina, sending

axons from the eye in a single bundle called optic nerve. Optic nerves from both eyes meet at the midline where they cross to the opposite side (optic chiasm) to grow dorsally into their final synaptic targets, the optic tectum in the midbrain, the main visual center in the zebrafish (Bilotta & Saszik, 2001). Each tectum receives input from contralateral RGC axons, which creates a topographic map of the visual field.

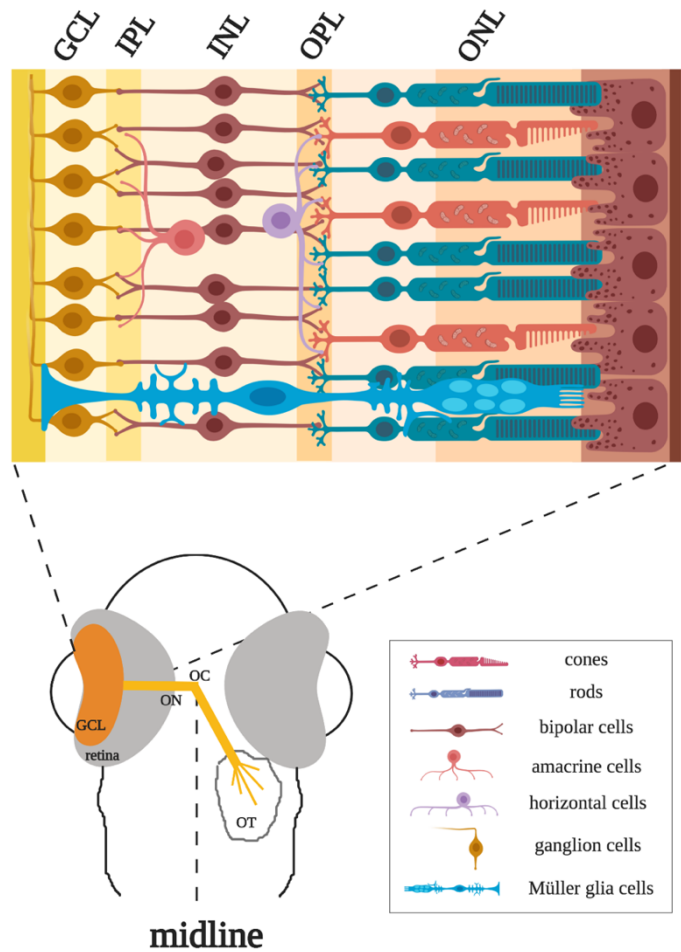


Figure 3: Structure of the zebrafish visual system.

The retina of zebrafish contains three major nuclear layers encompassing seven major types of retinal cells. Retinal ganglion cells (RGCs) reside at the innermost layer of the retina, the ganglion cell layer (GCL) and synapse with cells of the inner nuclear layer (INL). GCL and INL are separated by a synaptic inner plexiform layer (IPL). INL cells relay signals from photoreceptors that are found in the outer nuclear layer (ONL). INL and ONL are separated by a synaptic outer plexiform layer (OPL). Müller glial cells provide support to retinal cells. The RGC axons merge into a single bundle optic nerve (ON) which exit the retina and form the optic chiasm (OC) at the midline. From OC, axons grow dorsally to innervate optic tectum (OT) in the midbrain for processing visual information.

1.7.1 RGC neurogenesis

The neurogenesis in retina occurs in a wave-like manner. The first cells to exit cell cycle in the proliferative neuroepithelium are destined to become RGCs (Hu & Easter, 1999). This initial wave of differentiation is followed by differentiation of INL cells and finally photoreceptor cells in the ONL. RGC differentiation occurs between 28 and 36 hpf, and differentiation undergoes a spatiotemporal pattern during which neurons of each retinal cell population start differentiating sequentially (Burrill & Easter, 1994; Hu & Easter, 1999; Stenkamp, 2015). After RGC differentiation, INL cells become post-mitotic between 36 and 48 hpf, that is followed by specification of photoreceptors between 48 and 60 hpf (Stenkamp, 2015). Müller glia are the last cell type to become post-mitotic, around 72-96 hpf (Fadool & Dowling, 2008). Neurogenesis starts next to the optic stalk, progressing nasally, then dorsally and finally temporally – a trend that is similar to opening a fan (Stenkamp, 2015). The differentiation of each cell type is regulated by both intrinsic (transcription factors) and extrinsic factors (morphogens, cell-cell signaling). As RGCs are main focus of this study, RGC differentiation will be described here.

RGC specification requires basic helix-loop-helix (bHLH) transcription factor *atonal7* (also known as *atonal5* or *ath5*). *ath5* expression precedes RGC differentiation and its expression pattern is reminiscent of RGC neurogenesis wave in a spatiotemporal gradient (Masai, Stemple, Okamoto, & Wilson, 2000). Zebrafish *ath5* mutants are devoid of RGCs, and the progenitor cells remain in the cell cycle to differentiate into INL cells (amacrine and bipolar) and Müller glial cells instead (Kay, Finger-Baier, Roeser, Staub, & Baier, 2001). *ath5* also regulates RGC-specific genes later in RGC development, such as LIM-homeodomain transcription factor *islet-1* and POU-domain transcription factor *brn3b*, which has a role in development of RGC subtypes (Erskine & Herrera, 2014). Thus, *ath5* is required for RGC determination both during the initial neurogenesis wave and in later stages. Fgf signaling is also important in triggering RGC differentiation during the first neurogenic wave. Pharmacological and genetic inhibition of Fgf in zebrafish were shown prevent *ath5* expression and RGC production (Martinez-Morales et al., 2005; Picker & Brand, 2005). Interestingly, one study found that neither retinal environment nor the signals from retinal cells affected the *ath5* wave, however, midline-derived Shh acting before neurogenesis to regulate the timing of *ath5* expression and RGC differentiation (Kay, Link, & Baier, 2005). *shh* is also expressed by RGCs and required for driving neurogenic wave across the retina (Neumann & Nusslein-Volhard, 2000). This finding was controversial to other species and studies, as defects

in SHH signaling result in overproduction of RGCs in chick and mouse retina (Wang, Dakubo, Thurig, Mazerolle, & Wallace, 2005; Zhang & Yang, 2001). Extraretinal expression of SHH seems to be important to initiate intrinsic cell signaling mechanisms in RGC neurogenesis. Overall, RGC differentiation is mainly driven by transcription factor *ath5*, and requires additional intrinsic and extrinsic factors to take in place.

1.7.2 RGC axonal guidance

RGCs are the retinal neurons that send their axons to the brain to establish functional connections between the retina and the brain. Axonal pathfinding of RGCs is well-characterized in vertebrates, including in zebrafish (Erskine & Herrera, 2007, 2014; Kita, Scott, & Goodhill, 2015). Following their differentiation, RGCs start extending axons towards the exit point of the eye by 34-36 hpf (Stenkamp, 2015). These axons merge into a single bundle called the optic nerve (ON). Then, axons extend towards the ventral midline of the diencephalon where each optic nerve meets at a major brain commissure, the optic chiasm (OC). In zebrafish, all RGC axons project contralaterally to reach the optic tectum (OT) in the opposite side of the midbrain. By 46-48 hpf, first RGCs arrive to the OT and start innervating the tectal neuropil, forming a retinotopic map (Stuermer, 1988). Furthermore, within the OT, RGCs innervate different tectal layers in order to create topographic connections, depending on the RGC subtype (Robles, Filosa, & Baier, 2013). Hence, from exiting the eye to reach the final synaptic targets, RGC axons have multiple decision points in order to direct their correct targets. Steering the neuron towards the target requires the function of the growth cones located at the tip of RGC axons. RGC growth cones sense the environment and adopt changes in the cytoskeleton to direct the axon along the correct retinotectal pathway.

First, RGCs send axons medially towards the optic disc to aid exiting the eye. Several attractive and repulsive cues contribute to guidance within the retina. To ensure that RGC axons are within a single layer and extend toward the optic disc, inhibitory signals such as Slits are expressed, preventing RGC growth in the periphery. For instance, the neuroepithelium in front of the differentiated RGCs and lens secrete repulsive Slits to inhibit RGC growth in these areas (Halfter, 1996; Thompson, Camand, Barker, & Erskine, 2006). Netrin-1 is an essential cue for directing RGCs out of retina. Netrin-1 is secreted by the surrounding neuroepithelial cells and

attracts retinal axons that express the Netrin-1 receptor DCC (deleted in colorectal carcinoma) towards the disc (De La Torre et al., 1997; Deiner et al., 1997).

After exiting the eye, RGC growth is constrained to the optic nerve by inhibitory Sema5A signaling (Oster, Bodeker, He, & Sretavan, 2003; Oster, Deiner, Birgbauer, & Sretavan, 2004). In zebrafish, Sema3D is secreted at optic chiasm to guide RGC axons to the midline and grow towards the contralateral optic tract (Sakai & Halloran, 2006). After midline crossing, RGC axons grow dorsally into the optic tract. Slit family proteins and their receptors Robo are important to form an inhibitory barrier to prevent axons straying from the tightly fasciculated optic nerve (Plachez et al., 2008; Thompson, Barker, Camand, & Erskine, 2006). Zebrafish RGCs express only Robo2, which serves as a receptor to both slit1 and slit2 (Lee, Ray, & Chien, 2001). A subset of RGCs from zebrafish *astray (robo2)* mutants do not cross the midline properly and project into adjacent areas of OT (Fricke, Lee, Geiger-Rudolph, Bonhoeffer, & Chien, 2001; Hutson & Chien, 2002).

Once RGCs reach the optic tectum, they innervate the tectal neuropil. As the axons reach into the tectum, different guidance cues help navigating the growth cones to a particular location. RGC axons first project to four major retinorecipient areas at the surface of the tectum: the stratum opticum (SO), the stratum fibrosum griseum et superficiale (SFGS), the stratum griseum centrale (SGC) and the boundary zone between stratum album centrale and stratum periventriculare (SAC/SPV) (Xiao, Roeser, Staub, & Baier, 2005). Each RGC innervate only one sublamina in the neuropil, depending on the RGC subtype (Huberman et al., 2009; Xiao et al., 2005). RGC axons undergo extensive branching to form a terminal arbor at the target lamina (Xiao & Baier, 2007). Several guidance cues modulate the RGC guidance in the tectum. Slit1a-Robo2 interaction was shown to be a negative regulator of axon arbor formation and synaptogenesis in the zebrafish tectum and Slit/Robo signaling is also crucial for lamina-specific targeting of retinotectal connections (Campbell et al., 2007; Xiao et al., 2011). Furthermore, zebrafish *astray* mutants exhibit laminar targeting errors in addition to midline crossing that was described above (Xiao et al., 2011). Ephrin ligands and their receptors are crucial for mapping retinal axons in the tectum. Different Ephrin gradients were detected along rostro-caudal axis, contributing a precise mapping of RGCs into the tectal locations to provide a detailed topographic map organization (Kita et al., 2015). Overall, RGC axons face an extensive decision-making process from their birth in the GCL until they reach their synaptic targets in OT. A multitude of extrinsic and intrinsic factors work in cohort to guide RGC axons in their pathfinding.

1.8 Introduction to the project

The work described here is the examination of the role of Nox2-mediated H₂O₂ in axon guidance of zebrafish RGCs. There are several pieces of evidence outlined in the previous sections that support the cell-autonomous role of NOX in neuronal growth cones. Furthermore, NOX-mediated H₂O₂ is important in intracellular signaling that results in the post-translational modification of several redox-target proteins, many of which are important in regulating actin-based cytoskeleton machinery in the growth cones. NOX enzymes are multi-subunits enzymes that activation usually requires activation of several cytosolic subunits to assemble. Full assembly and activation of NOXes therefore require upstream signaling such as activation of protein kinases. Axonal guidance molecules modulate intracellular signaling upon interaction of cue-receptors, suggesting that the initiated signaling mechanism could act on several pathways in the cytosol. Hence, we sought to determine whether cell-autonomous Nox signaling could act downstream of a specific guidance cue-receptor interaction. The formation of zebrafish retinotectal connections is a well-established axonal guidance system in which retinal ganglion cell axons face several decisions. Therefore, we utilized the advantages of zebrafish as an animal model and this established guidance pathway to study whether Nox could act downstream of guidance of retinal ganglion cells. We used a *nox2* ^{-/-} mutant zebrafish line that was previously established in our group using CRISPR/Cas9 technology. Using these mutants as well as by inhibiting Nox pharmacologically, we analyzed nervous system development in general as well as specifically the retinotectal pathway.

CHAPTER 2. METHODS

2.1 General Methods

2.1.1 Zebrafish housing and breeding

All animal work and experimental protocols were approved by the Purdue Animal Care and Use Committee. Zebrafish (*Danio rerio*) of the AB, *Tg(ath5:GFP)*, *Tg(isl2b:Gal4;myl7:TagRFP)*, *nox2^{pu22}*, *astray^{ti272z}* lines were maintained according to standard procedures (M Westerfield, 2000). *nox2^{pu22}* mutant lines were generated in our lab previously (Weaver et al., 2018). *Tg(ath5:GFP)*, *Tg(isl2b:Gal4;myl7:TagRFP)* and *astray^{ti272z}* lines were obtained from Dr. Brian Link (Medical College of Wisconsin), Dr. Josh Bonkowsky (University of Utah), and Dr. Michael Granato (University of Pennsylvania), respectively. For zebrafish breeding, adult parents were placed into breeding tanks and separated by a clear divider overnight. The following morning, adults were moved to a new breeding tank with fresh water, the divider was removed to allow breeding. Embryos were collected at 15-minute intervals to obtain cohorts of the same stage. Embryos were maintained in E3 medium at 28°C and staged as described prior to harvest (Kimmel, Ballard, Kimmel, Ullmann, & Schilling, 1995). Medium was changed twice a day and dead embryos were removed to prevent bacterial and fungal infections. Embryos used for live-imaging were treated with 0.003% N-Phenylthiourea (PTU) (Sigma, St. Louis, MO) from 23 hours post fertilization (hpf) in E3 medium to inhibit melanization (Z. Li et al., 2012).

2.1.2 Genotyping

Genomic DNA was isolated from 24-96 hpf or adult tail biopsies (Wilkinson, Elworthy, Ingham, & van Eeden, 2013; Xing, Quist, Stevenson, Dahlem, & Bonkowsky, 2014). Samples were dissolved in 50 mM NaOH by incubating for 10 minutes at 95°C for DNA extraction. DNA samples are neutralized with 1 M Tris HCl pH 8.0 and the samples were stored at -20°C until further processing. *nox2* ^{-/-} mutants were genotyped routinely with DNA polyacrylamide gel (PAGE) method that was described previously (Zhu et al., 2014). Following PCR amplification with GoTaq Flexi (Promega, Madison, WI), samples were heated to 95°C and allowed to cool for 10 minutes at RT. Samples were then loaded onto a 15% acrylamide gel without SDS and run for 2.5 hours at 150 V. Gels were stained with GelRed Nucleic Acid stain (Biotium, Fremont, CA) for

10 minutes to visualize DNA bands. Heteroduplexes indicative of heterozygous mutants exhibited lower electrophoretic mobility, and homoduplexes were indicative of wild-type or homozygotes as described previously (Zhu et al., 2014). For genotyping validation, T7 Endonuclease Assay was performed as described previously (Jao, Wentz, & Chen, 2013). PCR products were combined with reaction buffer (New England Biolabs, Ipswich, MA) and heated to 95 °C for 5 min. Samples were slowly cooled down by removing from heat block to bench top. Once temperature fell below 30 °C, T7 endonuclease was added and reaction was incubated at 37 °C for 35 min. Finally, 0.5 M EDTA and DNA dye were added to stop the reaction. Samples were run on agarose gel for visualizing heteroduplexes. For sequencing, PCR products were purified with the Wizard SV Gel and PCR Clean-Up System (Promega) and then cloned into the pGEM-T Easy vector (Promega). *astray*^{+/-} and *astray*^{-/-} mutants were genotyped using site-specific primers to differentiate wild-type and mutant alleles. After PCR amplification, samples were loaded onto 2% agarose gel. Presence of amplification from both wild-type and mutant primers indicated heterozygosity. Genotyping primers are listed in Table 3.

Table 3: Genotyping Primers for PCR.

	Forward	Reverse
Nox2 (T7EI Assay)	GGGTGCAGTAAATACTACGAATAGA	AACAACAGAAGGAGAAGTGAGAG
Nox2 (DNA PAGE)	CCCGATAGCTTACGATAACAAA	CTCTCGATCTCATCTCCTGAT
Nox2 gRNA1 off-target	AATCCTCACAACCAGCTACTATG	TGTAACCGTCCCAGAACATAAC
Astray (wild-type)	GAATGACTCCTCGTCGCTCT	CAGCTCCTTTTGACATGTTT
Astray (mutant)	GAATGACTCCTCGTCGCTCT	CAGCTCCTTTTGACATGTTA

2.1.3 Microinjection

Microinjection plates were prepared by casting injection mold (Adaptive Science Tools) on 1.2% agarose in E3 media. Borosilicate glass microinjection needles (Sutter Instrument) were pulled with vertical pipette puller (David Kopf Instruments, Model 700C). Tips of the needles were cut off with forceps to give tip a sharp angle easier penetration, with an internal diameter of 10 µm. The amount of injecting volume was determined via mineral oil (Sigma-Aldrich). 1 nanoliter (nl) of the volume of the solution was measured by the stage that was calibrated with stage micrometer. One-cell stage embryos were aligned on a microinjection plate and each embryo was

injected with a 1-nl solution through their yolk with a microinjector (World Precision Instruments, Pneumatic PicoPump PV820). After injection, embryos were placed at 28°C incubator until further processing.

2.1.4 Statistical analysis

All data sets were analyzed using GraphPad Prism software version 6.0 or 8.4.2 (GraphPad Software, Inc, La Jolla, CA). All raw data was assessed for normality using the D'Agostino-Pearson omnibus test included in GraphPad, where applicable ($n \geq 8$). For $n < 8$, Shapiro-Wilk test was used to assess normality. Outliers were automatically identified and removed using the ROUT algorithm with a Q-value of 1%. For data sets containing 2 groups, Student's t-test (two-tailed) or Mann-Whitney U test were used to identify differences among means, depending on the sample distribution. Data sets containing three or more groups, one-way ANOVA or Kruskal-Wallis test were used to identify differences among means, depending on the sample distribution. If a significant difference was detected with the ANOVA, the Tukey HSD method was used for multiple comparisons among groups. If a significant difference was detected in Kruskal-Wallis test, Dunn's multiple comparisons test was used. Two-way ANOVA was used to detect differences when two independent factors are involved. p-values less than 0.05 were considered significant. All graphs show mean \pm standard error of the mean for each group. All data were averaged from at least two independent experiments.

2.2 Methods for Chapter 3

2.2.1 Whole-mount immunohistochemistry

At 23 hpf, 0.003% PTU (Sigma- Aldrich) in E3 medium was applied to embryos used for immunolabeling to inhibit melanization. At 48 hpf, samples were anesthetized in 0.016% tricaine methanesulfonate (Sigma-Aldrich) and fixed overnight in 4% paraformaldehyde (PFA)/1x PBS at 4°C in microcentrifuge tubes. 10-15 embryos were used in each staining. Embryos were then washed with PBT (1x PBS, 0.5% Triton X-100) at room temperature (RT). Next, samples were incubated in pre-chilled acetone for 30 min, at -20°C. They were then washed extensively in PBT at RT. To permit antibody penetrance, samples were incubated with 10 μ g/ml proteinase K at RT (Sigma-Aldrich) for 10 min. Embryos were then post-fixed in 4% PFA/1x PBS for 30 min and

washed extensively in PBT. Next, samples were incubated with blocking solution (10% goat serum in PBT; Sigma-Aldrich) for 2 hr at RT. To label all axons, a mouse anti-acetylated α -tubulin antibody (Sigma-Aldrich; RRID: AB_477585) was used. Primary antibody was diluted 1:500 in blocking solution. Samples were incubated in primary antibody solution overnight at 4°C and washed extensively in PBT the following day. Then, the secondary antibody, goat anti- mouse IgG Alexa Fluor 488 (Thermo Fisher), was diluted 1:250 in blocking solution. Samples were incubated overnight in secondary antibody solution at 4°C. The following day, the nuclear counterstain diamidino-2-phenylindole (DAPI; Thermo Fisher) was added to the secondary antibody solution at a 1:1000 dilution for 2 hours at RT. Finally, samples were washed extensively with PBT for 4 hr at RT and stored at 4°C in the dark.

For imaging, immunolabeled samples were positioned on glass-bottom dishes in 1% low-melting-point agarose dissolved in 1x PBS. The dishes were then filled with 1x PBS. Z-stacks were collected from dorsal perspective at 1- μ m intervals using a Zeiss LSM 710 inverted scanning confocal microscope equipped with a 40x LD C-Apochromat 1.1 numerical aperture (NA) W Corr M27 objective (Zeiss). Images were analyzed with ImageJ software. Maximum intensity projections were created for tubulin staining to reveal axonal phenotypes in zebrafish CNS, single DAPI sections were used to show nuclear staining.

2.2.2 Whole mount *in situ* hybridization

The *in situ* hybridization probes *fgf8*, *otx2*, *pax6a*, and *nestin* were characterized previously (Bishop et al., 2015; Mahler & Driever, 2007). Probe-containing vectors were linearized and riboprobes were synthesized using the DIG RNA labeling kit (Roche Diagnostics) and purified with 4 M LiCl (Sigma-Aldrich). Whole embryos were anesthetized in 0.016% tricaine methanesulfonate (Sigma-Aldrich) at 36 hpf before fixation in 4% PFA in PBS. The samples were dehydrated stepwise in methanol (30%, 50%, 70%, and 100%), digested with 10 μ g/ml proteinase K (Thermo Fisher) for 12 min, post-fixed in 4% PFA for additional 30 min, washed in 1x PBST (1x PBS, 0.1% Tween 20) 5 times, and prehybridized in hybridization buffer (50% formamide, 5x saline sodium citrate [SSC], 0.1% Tween 20, 5 mg/ml torula yeast RNA, 50 μ g/ml heparin) for 5 h at 65°C. Embryos were then incubated in 100 ng of riboprobe in hybridization buffer overnight at 65°C. Excess probes were washed with 50% formamide/2x SCCT (SSC, 0.1% Tween 20) twice, 2x SCCT once, and 0.2x SSC twice. Embryos were washed 3 times in 1x PBST and incubated

in blocking solution (2 mg/ml bovine serum albumin, 2% normal sheep serum, 1x PBST) for 4 h at room temperature. Embryos were then incubated with an alkaline phosphatase-labeled sheep anti-digoxigenin antibody (Roche Diagnostics; RRID: AB_514497) diluted 1:3000 in blocking solution overnight at 4°C on a shaker. Excess antibody was removed by washing in PBST three times. Samples were then incubated in staining solution (100 mM Tris, pH 9.5, 50 mM MgCl₂, 100 mM NaCl, 0.1% Tween 20, 1 mM levamisol). For color detection, the samples were incubated in 0.3 mg/ml nitroblue tetrazolium and 0.15 mg/ml 5-bromo-4-chloro-3-indolyl-phosphate (Sigma-Aldrich) diluted in 100 mM Tris, pH 9.5, at room temperature on a shaker. Upon reaching the desired color intensity, the reaction was stopped by fixing samples in 4% PFA overnight at 4°C. The next day, samples were washed 5 times in 1x PBST and then dehydrated stepwise in 30%, 50%, 70%, and 100% methanol and incubated in benzyl alcohol/ benzyl benzoate solution (2:1) for 2 min to wash out nonspecific signals. De-stained embryos were then rehydrated stepwise in 100%, 70%, 50%, and 30% methanol and washed in 1x PBST 3 times. Labeled embryos were kept in 4% PFA at 4°C. Whole-mount images of embryos were taken by mounting embryos in 3% methylcellulose using the Olympus SZX16 stereomicroscope with an SDF PLAPO 1x PF objective. Images were captured by using the RT3 2.0Mp Slider CCD camera (SPOT Imaging Solutions). At the minimum, five individual samples were processed for each gene in each of the three experimental replicates.

2.2.3 H₂O₂ imaging *in vivo*

The roGFP2-orp1 construct was received from Dr. Tobias Dick (DKFZ, Germany) and subcloned into pCS2+ vector by the lab of Dr. Qing Deng (Purdue University). roGFP2-orp1 mRNA was transcribed from pCS2+ vector using mMessage mMachine SP6 kit (Thermo Fisher). One nanoliter of 100 ng/ µl mRNA was injected into one-cell-stage embryos. Injected embryos were incubated at 28°C until they reached desired stage. At 2 and 5 dpf, embryos were anesthetized in 0.016% tricaine and mounted in 1% low-melting-point agarose on 35 mm glass bottom dishes and dishes were filled with fish water containing tricaine. Images were acquired from anterior perspective on a Zeiss LSM 710 laser scanning confocal microscope using 20X Plan-Apochromat 0.8 NA M2 objective. roGFP2-orp1 was excited with 405 and 488 nm excitation and corresponding emission was acquired with a 500–520 nm band-pass filter. For biosensor validation, time-lapse images were acquired over 20 min on a single optical section. H₂O₂ (20

mM) was added after taking the first image and 2.5 mM dithiothreitol (DTT) was added after 10 min of imaging. To measure basal levels of H₂O₂ in wild-type and mutant embryos, z-stacks were acquired with 5 µm section thickness. z-stacks were analyzed by ImageJ and the middle plane of each fish was selected to measure H₂O₂ levels as ratio of 405/480 images. To follow up same embryos, 2-dpf embryos were removed from agarose with forceps and placed in 24-well plates with PTU containing fish water without methylene blue individually until the next imaging session at 5 dpf.

To create ratiometric images of fish embryos, both 405 and 480 nm excitation images were opened in ImageJ. An average background value was subtracted from each channel and the intensity values of the 480 nm channel were added by “1” to eliminate pixel values of zero. Then, the 405 nm image was divided by the 480 nm image pixel by pixel using image calculator/divide function and the image was converted to 32-bit. Single optical sections in the middle of the eye were used to calculate average 405/480 ratio values in the retina. The region of interest (ROI) was defined by free-hand tool. Data were normalized to ratios before applying any oxidizing/reducing agents or control. For comparing basal levels in wild-type and *nox2* mutant fish embryos, ratio values were normalized to wild-type fish. To display ratio images, a binarized mask was created first in ImageJ, in which ROI pixels (embryo) received a value of 1, whereas background pixels were set to 0. The binarized mask was then multiplied with the ratio image and a factor of 2. The resulting ratiometric image was converted to 8-bit and pseudocolored by applying lookup table “Fire.” For following 2 and 5 dpf old animals in their ROS levels, slightly different protocol was applied for creating ratio images. Data were not normalized for reporting the 405/480 values. For image display, binarized mask multiplied with ratio image and a factor of 5 and 15, for 2 and 5 dpf old animals, respectively.

2.2.4 Optokinetic response (OKR) assay

We used a custom-built apparatus to assess optokinetic response in 5-dpf larvae (Ganzen, Venkatraman, Pang, Leung, & Zhang, 2017). The apparatus consists of a plastic drum with a lined paper made up of alternating black and white stripes, a stereoscope with a light source, and a variable speed motor and attached belt used to rotate the drum. Briefly, ~5 larvae were embedded ventrally in a 3% methyl-cellulose solution in a 35 mm plastic dish. The dish was placed in the

middle of the rotating drum. Each larva was screened for 1 min with a series of rotations lasting 15 s and alternating between clockwise and counterclockwise direction turning of the drum at 10 rpm. Each larvae was observed individually to assess the response to the rotating drum. The larvae that followed the rotating stripes and adapts changes in the direction of the turning drum were classified as OKR responsive, whereas the larvae that did not follow the stripes and exhibited no response at all to the rotating drum were classified as OKR nonresponsive. The test was repeated four-times independently and at least 10 fish were observed from each genotype per session.

2.2.5 Quantitative PCR

Total RNA was isolated by TRIzol reagent (Thermo Fisher Scientific, Waltham, MA) from age-specific embryos as previously described (Peterson & Freeman, 2009). 15 embryos were pooled from each genotype in a 1.5 ml microcentrifuge tube. 250 μ l of TRIzol reagent was added to embryos in microcentrifuge tube. The embryos were then lysed and homogenized with a pellet pestle (VWR, Radnor, PA) until tissue is disrupted. After homogenization, 250 μ l TRIzol was added and samples were incubated at RT for 5 mins to allow complete dissociation. 0.1 ml chloroform was then added and tubes for rocked for 15 sec to mix thoroughly. Next, samples were incubated at RT for 2 mins and centrifuged at 12,000 x g for 15 mins at 4°C. The top aqueous phase containing the RNA was transferred to a new RNase-free tube and 250 μ l of isopropanol was added to precipitate RNA. After 10 mins of incubation at RT, samples were centrifuged at 12,000 x g for 10 mins at 4°C. Supernatant was removed and the RNA pellet was washed with 0.5 ml of 75% ethanol by gentle inversion, followed by centrifuge at 7,500 x g for 5 mins. Ethanol was then removed, and samples were allowed to air dry to remove remaining ethanol for 10 mins. RNA pellet was resuspended in 50 μ L RNase-free water and incubated at 55°C for 10 mins rehydrate RNA. RNA isolation was followed by RNA clean up with Monarch RNA Cleanup Kit (New England Biolabs, Ipswich, MA). 100 ng of isolated and purified RNA was directly used in Luna Universal One-Step RT-qPCR Kit (New England Biolabs, Ipswich, MA) in a LightCycler 96 Real-Time PCR System (Roche). The expression fold-changes of mRNA were calculated with the $2^{-\Delta\Delta C_t}$ method (Rao, Huang, Zhou, & Lin, 2013), using *rp13a* as a housekeeping gene. The specificity of the primers was verified as a single peak in the melt-curves. No template-control (NTC) and no reverse transcriptase-control were used to check non-specific amplifications and DNA contamination in the samples, respectively. There was no amplification was detected in both

controls, validating the primers and pure RNA templates. Following primers were used for qPCR are listed in Table 4.

Table 4: qPCR primers.

	Forward Primer	Reverse Primer
<i>rp13a</i>	TCCTCCGCAAGAGAATGAAC	TGTGTGGAAGCATACCTCTTAC
<i>nox1</i>	GCTCCAAGACTCCAGTGAATTA	GACCCGCAATACTGGTGAATA
<i>noxo1</i>	CGAGACCAAAGACACCAAGAA	TCTACAAGCCACCAACCTTTC
<i>noxal</i>	GAGGCCGTAAAGGCAATAGA	GGACGCAACCACAAACATAG
<i>nef1</i>	TGGTCAGGAAAGGCGAGGAA	TGCTCTTCTGACCACGTCCC
<i>nef2</i>	GCAAAGGTTGTGGCTCTTTAC	AGCCACTCGTCATTGACTTT
<i>nox5</i>	TCATGTGCCGCTATCGTATG	CCACCTTCCTCAGCTTCATT
<i>duox</i>	CCTGGGAGGACTTTCACCTTC	CTTGTGCTGTCTGCCTAGTT

2.3 Methods for Chapter 4

2.3.1 Dissociated RGC neuronal culture

Protocol was modified from Chen et al. (Chen et al., 2013). At 33–34 hpf embryos were sterilized with 70% ethanol and then transferred to a new dish containing E2 medium (15 mM NaCl, 0.5 mM KCl, 1 mM MgSO₄, 0.15 mM KH₂PO₄, 0.05 mM Na₂HPO₄, 1.0 mM CaCl₂, 0.7 mM NaHCO₃). Chorions were removed with sharp forceps, and embryos were sacrificed by decapitation. Whole eyes were extracted, triturated 45 times using a P20 pipette in L15 medium (Invitrogen, Carlsbad, CA) supplemented with 2% FBS (Thermo Scientific, Waltham, MA), 0.4% pen/strep, and 12.5% saline solution (10 mM D-glucose, 5 mM Na-pyruvate, 1.26 mM CaCl₂, and 32 mM HEPES). Individual cells were then plated on coverslips pre-coated with 0.5 mg/ml poly-D-lysine (70–150 kD) (Sigma, St. Louis, MO) for 20 min, washed with PBS and then coated with 20 µg/ml laminin (Invitrogen, Carlsbad, CA) for 6 h. Cells were maintained in supplemented L15 medium in 35 mm petri dishes overnight at RT.

2.3.2 Growth cone collapse quantification

Percent growth cone collapse was determined by counting the number of growth cones that are collapsed in response to slit2 treatment per experiment. DIC images of before (time 0) and after (time 30) images were opened in ImageJ Software. If growth cones were healthy at time 0 and collapsed at time 30, they were counted as collapsed. Bullet shaped neurite tips, occasionally with a single filopodium and/or lacking lamellipodia were considered as collapsed growth cones. Growth cones harboring a flattened filopodia and/or with ≥ 2 filopodia were considered as healthy or not-collapsed growth cones.

2.3.3 H₂O₂ imaging *in vitro*

For analysis of H₂O₂ levels in RGC growth cones, roGFP2-orp1-expressing zebrafish embryos were selected for fluorescence at stage ~28 hpf and then killed via decapitation at 34 hpf. Retinas were dissected out and cells were plated as described above. For live-cell imaging, coverslips containing overnight retinal cultures were transferred from culture dishes to a custom-made open imaging chamber described previously (Suter, 2011). Prior to imaging, medium was replaced with serum-free L15 medium without phenol red. Imaging was performed with a Nikon TE2000 Eclipse microscope (Nikon, Melville, NY), a 60x 1.4 NA oil differential interference contrast (DIC) objective with additional 1.5x magnification (90x total), a OG590 long-pass red filter (Chroma Technology Corp., Bellows Falls, VT) and an iXon Ultra 888 EM CCD camera (Andor, Oxford Instruments). Using MetaMorph 7.8 software (Molecular Devices, Sunnyvale, CA), neurite lengths were measured from the base of the cell body to the tip of the growth cone lamellipodia on neurons and only neurons with processes $\geq 15 \mu\text{m}$ were imaged. Initial DIC images of isolated neurons were acquired at time = 0 min. Then, roGFP2-orp1 was excited with 405/20 and 480/30 nm excitation filters and corresponding emission was acquired at 535/30 nm using the dichroic mirror 505DCXR (R400/15 and 480/30, T510 –700 nm; Chroma). After time = 0 images were acquired, medium was replaced with L15 containing PBS (vehicle control) or slit2 (10 $\mu\text{g}/\text{ml}$; R&D Systems, Inc., Minneapolis, MN), and second set of images was taken after 30 min of incubation. Images were analyzed with ImageJ software. After average background subtraction in fluorescent images, 405/20 image was divided pixel-by-pixel by 480/30 image by image

calculator/divide function in order to get 405/480 ratio image that is representation of H₂O₂ levels. Measurements were done at the growth cone that is outlined in DIC image by free-hand tool.

To create ratiometric images of RGC neurons, both 405 and 480 nm excitation images were opened in ImageJ. An average background value was subtracted from each channel and the intensity values of the 480 nm channel were added by “100” to eliminate pixel values of zero. Then, the 405 nm image was divided by the 480 nm image pixel by pixel using image calculator/divide function and the image was converted to 32-bit. The growth cone was defined as the ROI by free-hand tool. For ratio image display, a binarized mask was created first in ImageJ, in which ROI pixels (growth cone) received a value of 1, whereas background pixels were set to 0. The binarized mask was then multiplied with the ratio image and a factor of 5. The resulting ratiometric image was pseudocolored by applying lookup table “Fire.” Data were normalized to before treatment (t = 0) values for each condition. Data were shown as mean ± SEM.

2.3.4 Whole-mount immunohistochemistry

Whole mount immunohistochemistry was performed as described in Chapter 2.2.1. 3-dpf embryos and 5-dpf larvae were used for staining. The incubation times were adjusted accordingly: Samples were incubated in pre-chilled acetone for 45 and 75 min; samples were digested with ProteinaseK for 15 and 35 min; for 3 and 5 dpf old animals, respectively. To label RGCs, the monoclonal zn-8 antibody raised against alcama (zn-8; Zebrafish International Resource Center; RRID: AB_10013774) was used as primary antibody. For imaging, immunolabeled samples were positioned on glass-bottom dishes in 1% low-melting-point agarose dissolved in 1x PBS. Samples were mounted on ventral and dorsal perspectives for OC and OT imaging, respectively. The dishes were then filled with 1x PBS. Z-stacks were collected at 2 µm intervals using a Zeiss LSM 710 inverted scanning confocal microscope equipped with a 40X LD C-Apochromat 1.1 numerical aperture (NA) W Corr M27 objective (Zeiss). Images were analyzed with ImageJ software. Maximum intensity projections were created for zn-8 staining to reveal RGC phenotypes in zebrafish OC and OT, single DAPI sections were used to show nuclear staining in OT.

For image analysis, ON thickness was measured for each embryo from single optic nerve at the chiasm using ImageJ software. For OT area, the tectal neuropil with RGC innervation and tectal neurons synapsing with RGCs were outlined for area measurements. All image analysis was

done on raw images with maximum intensity projections. Brightness/contrast were adjusted in ImageJ for better visualization of the phenotypes.

2.3.5 Imaging sparsely labeled RGCs

For sparse labeling of RGCs, transgenic bgug line *Tg(brn3c:GAL4, UAS: gap43-GFP)s318t* was obtained from Dr. Estuardo Robles, Purdue University (Robles, Laurell, & Baier, 2014). This line allows subset of RGCs to be labeled with GFP. We generated *nox2* heterozygous line in the bgug background. Embryos from bgug/*nox2*^{+/-} line were treated with PTU from 23 hpf to prevent pigment formation. At 2 dpf, embryos were pre-selected from GFP positive hair cells in zebrafish ear. From 3 to 5 dpf, live confocal imaging was conducted on a Nikon C2 confocal microscope equipped with solid-state laser for excitation of EGFP (488 nm). Embryos were anesthetized in 0.016% tricaine and embedded in 1.5 % low-melting-point agarose dorsally. Individual RGC growth cones in optic tectum were imaged using a Nikon 60x 1.0 NA water immersion objective. Optical sections were acquired using 0.6–2 μ m z-steps. For image analysis, Simple Neurite Tracer plugin was used in FIJI. This plugin allows tracing neurons over collected z-stacks.

2.4 Methods for Chapter 5

2.4.1 Cloning full length Zebrafish *nox2* gene

Total RNA was isolated from 2 dpf old embryos with TRIzol reagent as described in Chapter 2.2.5. Zebrafish *nox2* coding sequence (NM_200414) was amplified with reverse-transcriptase PCR (RT-PCR) by SuperScript IV One-Step RT-PCR (Invitrogen, Carlsbad, CA). Resulting cDNA was validated on agarose gel and a single 1.7 kilobase (kb) was observed corresponding to the size of full-length *nox2* sequence. In order to insert *nox2* coding sequence in zebrafish expression vector pCS2+, *nox2* cDNA was amplified by HiFi PCR Premix to add overhangs at 5' and 3' for pCS2+ insertion (Takara Bio, Mountain View, CA). pCS2-Hyper plasmid was linearized with BamHI and PstI to remove existing gene coding region. Later, *nox2* gene with pCS2+ overhangs that are complimentary to linearized pCS2+ vector was fused into linear pCS2+ by In Fusion Cloning Technology (Takara Bio, Mountain View, CA). Successful cloning of full length *nox2* coding sequence in pCS2+ vector was validated with restriction enzyme digestion, partial and whole plasmid sequencing. Later, with a similar approach, *nox2* coding

sequence was cloned into Gateway middle entry vector (pME). Overhangs that are complimentary to pME were added to 5' and 3' of the *nox2* gene by HiFi PCR premix. pME backbone was amplified from pME-Gal4-VP16 plasmid. Then, *nox2* coding sequence with overhangs was fused into linear pME by In Fusion technology. Successful insertions were confirmed with restriction enzyme digestions, partial and whole plasmid sequencing. Primers for *nox2* constructs are listed in Table 5.

2.4.2 Cloning roGFP2-orp1 in Gateway middle entry vector

Using pCS2+ vector containing roGFP2-orp1 sequence as a template, the roGFP2-orp1 was amplified by adding overhangs for Gateway pME vector using HiFi PCR Premix. For obtaining pME backbone, the existing pME-Gal4-VP16 plasmid was used. The backbone was first linearized, and then amplified to remove existing gene (Gal4-VP16). pME backbone and roGFP2-orp1 with pME homology regions were fused with In Fusion technology. Successful insertion of roGFP2-orp1 to pME vector was validated by whole plasmid sequencing. Later, roGFP2-orp1 was cloned into a middle entry vector containing Cas9 endonuclease. Existing pME-Cas9-2A-mCherry plasmid was used as a template to amplify pME-Cas9-2A region. roGFP2-orp1, from pCS2+ vector containing the sequence, was amplified with primers to add overhangs for inserting pME-Cas9-2A backbone. Successful insertions were confirmed by whole plasmid sequencing. Primers used for roGFP2-orp1 constructs are listed in Table 5.

Table 5: Primers for Gateway entry vector cloning.

	Forward	Reverse
<i>nox2</i> cDNA amplification	ATGGGAAACTTTGCTGCAAATG	TCCTTGAAAATAAACTC
<i>nox2</i> pCS2+ overhangs	AAAGCAGGCTGGACCATGGGAA ACTTTGCTGCAAATG	CAAGAAAGCTGGGTGTTAGA AGTTTTCTTGTTGAAAATAAAC
<i>nox2</i> pME overhangs	AAAGCAGGCTGGACCATGGGAA ACTTTGCTGCAAATG	CAAGAAAGCTGGGTGTTAGAAGTT TTCCTTGTTGAAAATAAAC
pME backbone for <i>nox2</i> insertion	CACCCAGCTTTCTTGACAAAG	GGTCCAGCCTGCTTTTTTGTAC
roGFP2-orp1 pME overhangs	AAAGCAGGCTGGACCA TGGTGAGCAAGGGCGAG	CAAGAAAGCTGGGTGCTATTC CACCTCTTCAAAGTTCT
pME backbone for roGFP2-orp1 insertion	CACCCAGCTTTCTTGACAAAG	GGTCCAGCCTGCTTTTTTGTAC
roGFP2-orp1 pME-Cas9-2A overhangs	GAAAACCCCGGTCTATGGTG AGCAAGGGCGAG	AGAACTAG GGATCCCTATTC CACCTCTTCAAAG
pME-Cas9-2A backbone for roGFP2-orp1 insertion	GGATCCACTAGTTCTAGAGCG	AGGACCGGGGTTTCTCCAC

2.4.3 Generating constructs for tissue-specific knockout

To generate RGC specific *nox2* mutants, I created constructs for tissue-specific Cas9 endonuclease expression along with ubiquitous guide RNA expression by Gateway cloning. Tissue specific knock-out approach was described previously (Ablain, Durand, Yang, Zhou, & Zon, 2015; Zhou et al., 2018) and the outline of the approach is shown in Figure 4. The final *Tol2:ath5:Cas9-2A-mCherry;U6a:nox2gRNA1-U6c:nox2gRNA2;cmcl2:GFP* construct was generated from individual Gateway entry vectors, which were validated by sequencing before cloning. 5' entry vector (p5E) contains RGC-specific promoter *atonal 5 (ath5)*. p5E-ath5 vector was obtained from Dr. Kristen Kwan (University of Utah). Middle entry vector (pME) contains the gene to be encoded in a tissue specific manner. pME-Cas9-2A-mCherry was obtained from Dr. Qing Deng (Purdue University). The 3' entry vector (p3E) containing the 2 different guide RNAs for *nox2* targeting were cloned in our lab. p3E-control guide vector was obtained from Dr. Qing Deng. Two guide

RNAs were cloned into p3E as previously described (Zhou et al., 2018). First, p3E-U6a-U6c with control guide RNA was digested with Sall (New England Biolabs, Ipswich, MA). Resulting small fragment of 0.5 kb and large fragment 3.5 kb were PCR amplified to replace control guide RNA sequences with two different gRNA sequences targeting *nox2*. *nox2* guide RNAs were previously designed by Dr. Cory Weaver in our group and general zebrafish mutants were already established with these guide RNAs. Primers were designed to add guide RNA sequences flanking the 0.5kb and 3.5 kb pieces of p3E, and the homology at the ends were used to paste two ends together (Table 6, p3E backbone sequences are underlined). Then, with In Fusion technology, the fragments were fused together and resulted in a plasmid containing gRNA1 and gRNA2 sequences under *U6a* and *U6c* promoters, respectively. Finally, destination vector containing a backbone with Tol2 sites and transgenesis marker *cmcl2*:GFP (pDEST-Tol2-CG2) was obtained from Dr. Qing Deng. To get final expression vector, all entry vectors with incubated together in the presence of LR Clonase II Plus (ThermoFisher Scientific, Waltham, MA) for 16 hr at 26 °C, following manufacturer's protocol. The successful cloning was identified with restriction enzyme digestions.

For an alternative approach, *Tol2:UAS:Cas9-2A-roGFP2-orp1;U6a:nox2gRNA1-U6c:nox2gRNA2; cmcl2: GFP* construct was generated. p5E-UAS was obtained from Dr. Qing Deng. pME-Cas9-2A-roGFP2-orp1 was generated in our lab as described in Chapter 2.4.2. p3E with guide RNAs was generated as described above. Resulting cloning product was confirmed with restriction enzyme digestions.

Table 6: PCR primers for cloning two guide RNAs in p3E vector.

	Forward	Reverse
p3E PCR with small fragment	GAAACTTTGCTGCAAATGAGTTT <u>AAGAGCTATGCTGGAAACAGCATAGC</u>	ATTCCATGAAGCACCAATCCGAAC <u>TAGGAGCCTGAGAACTGC</u>
p3E PCR with large fragment	GGTGCTTCATGGAATGTTTAAGAG <u>CTATGCTGGAAACAGCATAGC</u>	TTGCAGCAAAGTTTCCGAACC <u>AAGAGCTGGAGGGAGA</u>

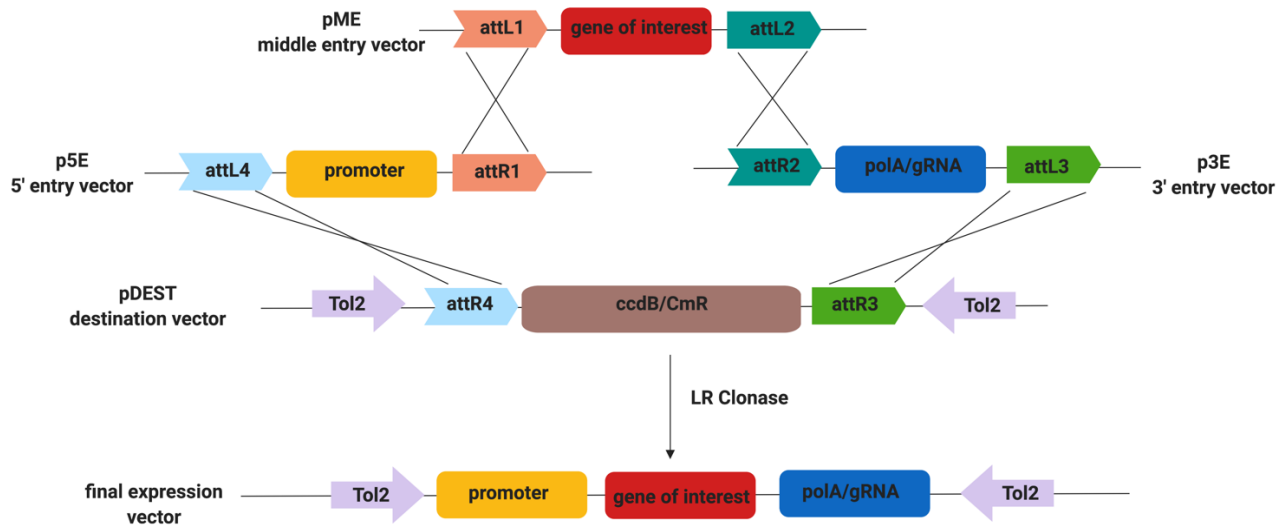


Figure 4: Gateway Cloning Principle.

Recombination-based cloning strategy for allowing directional cloning. The system consists of three entry vectors (p5E, pME and p3E) and one destination vector (pDEST). Each region of interest in vectors flanked by recombination sites (attL and attR). In the presence of clonase enzyme, L and R sites recombine to allow directional cloning. The end product allows expression of gene of interest under tissue-specific promoter in a vector backbone with transgenesis marker.

2.4.4 Zebrafish blastula stage cell transplantations

Blastula stage cell transplantation protocol was described in previously (Carmany-Rampey & Moens, 2006; Kemp, Carmany-Rampey, & Moens, 2009; Li, White, & Zon, 2011). We adopted the protocol with the help of Dr. Brian Perkins (Cleveland Clinic, Cole Eye Institute). Autoclaved fish water and sterilized materials were used throughout the protocol. Transplantation plates for holding embryos in individual wells were casted in a transplantation mold (Adaptive Science Tools) in 2% agarose in fish water. Transplantation needles were pulled with flaming-brown micropipette puller (Sutter Instruments, Model P-97) and the tip was cut with forceps to give 50-60 μm opening. On the day of experiment, donor embryos were microinjected with TexasRed-Dextran (ThermoFisher Scientific, Waltham, MA) to label donor cells for tracing, as described in Chapter 2.1.3. Then, both donor and host embryos were dechorionated with forceps on agarose-coated petri dishes. Embryos were then incubated at 28°C. Once they embryos reach blastula stage around 3 hpf (~1000 cells), they were aligned in the transplantation mold by using glass transfer pipettes. Donor and host embryos were aligned in adjacent columns to make easier transplantation. A transplantation rig with a micro-drive connected to oil syringe was used (Sutter Instruments,

Figure 5). Transplantation micropipette was placed on the pipette holder that was connected to syringe filled with mineral oil. The transplantation micropipette was filled with mineral oil until the point where needle becomes narrower. Micropipette was then filled with fish water from the transplantation plate, while leaving an air gap between the mineral oil. With the help of needle, donor embryos were oriented in a way that the mass of cells facing toward the micropipette as shown in Figure 6. Once positioned, very little suction was applied with the micro-drive to take out ~60-120 cells. For transferring cells to the host embryos; host embryo was aligned with the help of the micropipette to position embryo in a way that the mass of cells facing towards the pipette. While holding the embryo in position, a little pressure was applied to transport cells to the tip of the micropipette. Once cells were close to the tip, the micropipette was positioned to the center of top of the animal pole for proper fate determination (the region that will develop into forebrain/eye), and cells were ejected. For one host, ~60 cells could be transferred, and two hosts can receive cells from one donor. Once cells were transplanted, embryos were incubated in transplantation plate at 28°C overnight.

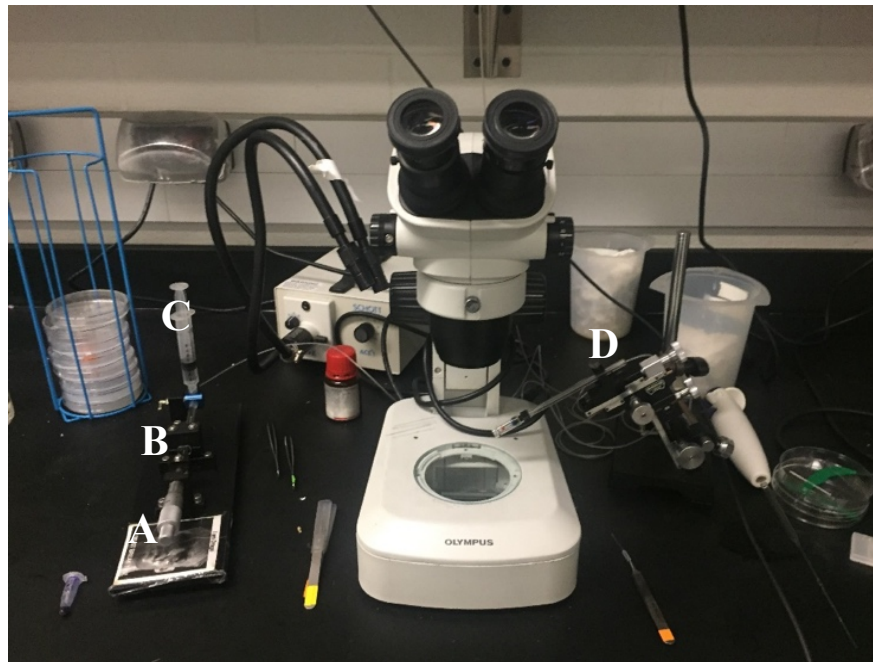


Figure 5: The setup of the transplantation rig.

A micro-drive (A) connected to a 25 μ L Hamilton-syringe filled with mineral oil (B) is connected to a syringe filled with mineral oil (C). The bigger syringe is connected to pipette holder that holds the transplantation needle (D). Micro-drive controls the suction and ejection pressures during cell transplantation.

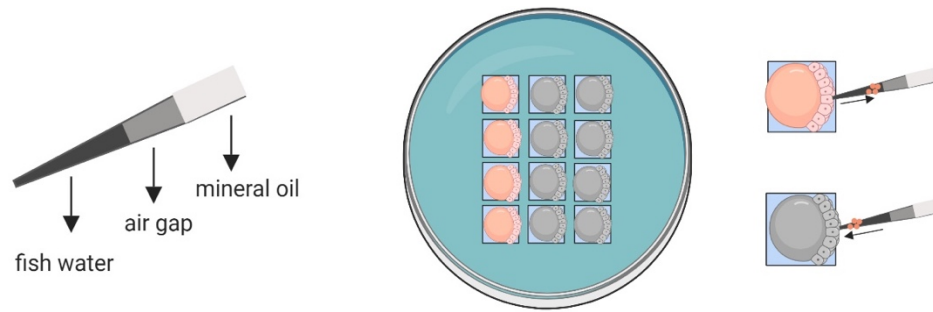


Figure 6: Schematic of transplantation micropipette and plate setup.

(Right) A transplantation needle will be filled with mineral oil and fish water that are connected via an air gap. (Left) The transplantation plate has individual wells for donors (red/labeled) and hosts (grey/unlabeled). Embryos are positioned to face toward the transplantation needle and suction applied to remove donor cells to eject into the animal pole of the host embryo.

2.4.5 Zebrafish embryo dissociation

Tg(ath5:GFP) embryos were used to isolate RGCs from zebrafish embryos for proceeding with fluorescence activated cell sorting (FACS). The protocol was adopted from (Covassin et al., 2006). 150 age-matched embryos were dechorionated with forceps and sorted in the 35 mm tissue culture dishes. Embryos were rinsed three times with calcium-free cold PBS (Fisher Scientific) on ice. To remove the yolk, embryos were passed through 200 μ l pipette tip and rinsed three times on ice with cold PBS. While on ice, 2 ml of warm PBS with 1x Trypsin (Fisher Scientific) and 1 mM EDTA were added to start digesting tissues. Next, dishes were incubated at 28.5 $^{\circ}$ C for 1 h. To aid dissociation of cells, embryos in solution were pipetted vigorously in every 10 mins during incubation. Digestion was stopped by adding 1 mM CaCl_2 and 10% fetal bovine serum (FBS). Then cells were passed through 40- μ m cell strainer (Fisher Scientific) to remove undigested clumps, and collected cells were centrifuged for 3 min at 3000 rpm at 4 $^{\circ}$ C. After removing supernatant, cells were resuspended in 500 μ l of 0.9x PBS/10%FBS. Cells were then kept on ice for further processing to FACS or NADPH oxidase assay.

2.4.6 NADPH Oxidase assay

To measure NADPH Oxidase activity in zebrafish embryos, we adopted NADP/NADPH Glo Assay (Promega, Madison, WI) that enables detection of total NADP⁺ and NADPH in cells. This assay is based on conversion of NADP⁺ to NADPH by the NADP cycling enzyme (G6P-DH). In the presence of NADPH, the reductase enzyme reduces pro-luciferin to luciferin that is quantified by the Ultra-Glo recombinant luciferase and the detected signal is proportional to the amount of NADP⁺ and NADPH in the sample. To validate that this assay is suitable for using in zebrafish cells, standard protocol was followed. Briefly, zebrafish cells from AB were dissociated as described in Chapter 2.4.5. Cell number were determined by counting with hemocytometer. Equal number of cells were added to white-walled 96-well plates in triplicates. Then, NADP/NADPH-Glo Detection reagent was added on the cells in a 1:1 ratio. Detection reagent is composed of luciferin detection reagent, reductase, reductase substrate (pro-luciferin), NADP cycling enzyme (G6P-DH) and NADP cycling substrate (G6P). After briefly shaking plate to mixing, luminescence was recorded in every 10 min for total of 90 minutes in Synergy 2 Microplate Reader (BioTek, Winooski, VT) with Gen5 Software. To measure NADP⁺ and NADPH levels individually, collected cells were lysed with 1% DTAB solution in base solution (100 mM sodium carbonate, 20 mM sodium bicarbonate, 10 mM nicotinamide, 0.05% Triton X-100). Then cells were divided into two pools. For NADP⁺ detection, cells were treated with 0.4 N HCl, heated at 60 °C for 15 minutes and incubated at RT for 10 mins, followed by addition of 0.5 M Trizma-Base. For NADPH detection: Cells were heated to 60 °C for 15 min and incubated at RT for 10 min. HCl/Trizma base solution was added. Finally, detection reagent was added on top of cells and luminescence was recorded with the microplate reader. The bioluminescence reading was proportional to the amount of NADP⁺ or NADPH individually. The protocol is summarized in Figure 7.

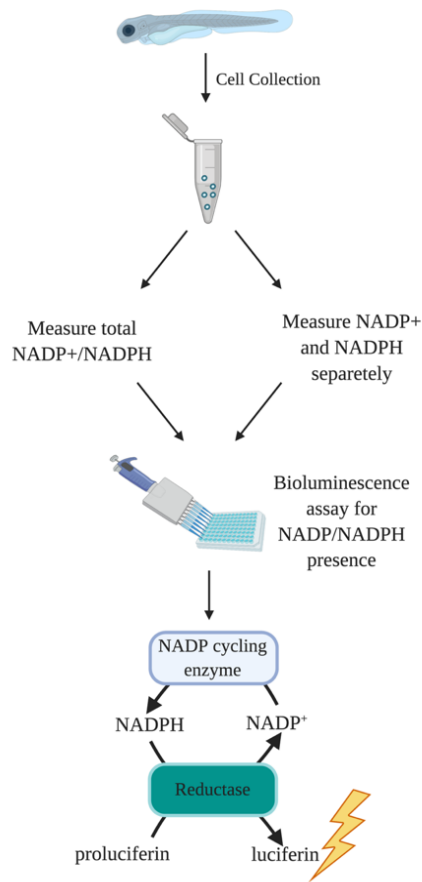


Figure 7: The principle of NADP/NADPH Glo Assay.

NADP/NADPH Glo Assay from Promega allows detection of total or individual NADP⁺ and NADPH content in cells. After cell dissociation from whole zebrafish embryos, cells were treated differently to measure NADP⁺ and NADPH individually. After specific treatments, the bioluminescence assay was conducted by adding a mixture of reductase enzyme that converts pro-luciferin into luciferin and NADP cycling enzyme that converts existing NADP⁺ to NADPH. The luminescence readout was collected to assess levels of NADP⁺ and NADPH.

CHAPTER 3. CHARACTERIZATION OF NOX2 ^{-/-} MUTANT ZEBRAFISH DURING DEVELOPMENT

Part of the work described in this chapter was previously published. The text presented here is adapted, with permission, from the original publication to highlight my individual contributions (Weaver et al., 2018).

3.1 Introduction

To investigate the role of Nox-mediated ROS in axon growth and guidance *in vivo*, our lab previously established *nox2* ^{-/-} mutants by CRISPR/Cas9 genome editing (Weaver et al., 2018). Two separate *nox2* ^{-/-} lines were generated from two different guide RNAs targeting the N-terminus of the *nox2* gene. The mutant line generated from gRNA I had a 5 bp deletion, whereas the line from gRNA II carried a 23 bp deletion (Figure 8A). Each mutation causes a premature stop codon early in the coding sequence for Nox2, which results in a significant truncation of the Nox2 protein. While wild-type Nox2 protein consists of 565 amino acids (aa), gRNA I and II-mediated mutations result in 33 and 221 aa long Nox2 proteins (Figure 8B). Both Nox2 mutant enzyme types have lost the substrate binding domain and at least one of the critical histidine residues which are essential for electron transport to oxygen. Without these critical functional domains, the mutant Nox2 enzymes are expected to be non-functional.

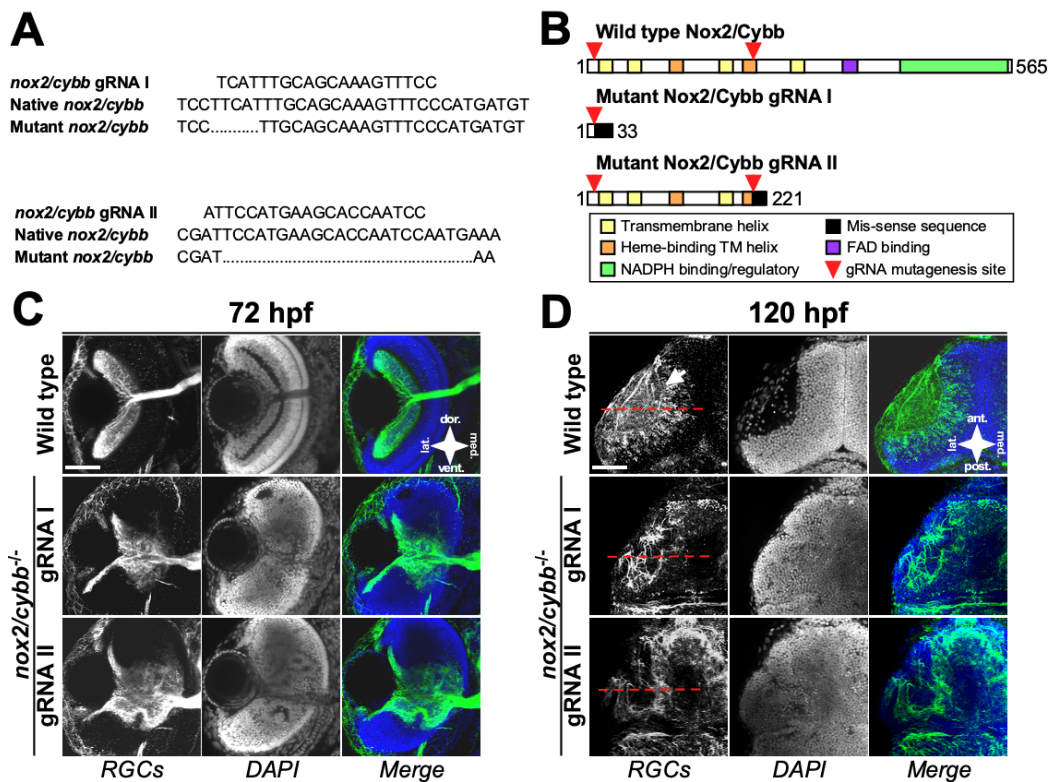


Figure 8: Characterization of zebrafish *nox2* mutant lines that were generated by CRISPR/Cas9 genome editing.

(A) Genomic sequences of gRNA target sites along with *nox2* mutants showing the 5 and 23 base pair deletions generated from gRNA I and II, respectively. (B) Schematic of the mutant Nox2 proteins based on translated mRNA sequences and alignment to the human protein sequence. (C) *nox2*^{-/-} eyes at 72 hpf labeled with zn-8 and DAPI showing that mutants with defects in RGC outgrowth and retinal lamination. (D) Micrographs of 120 hpf wild type and *nox2*^{-/-} midbrains labeled with zn-8 and DAPI. Mutants show defects in tectal innervation and formation. The figure is adopted from *Weaver et al., 2018*. Scale bars = 100 μ m.

Both type of mutants exhibited defects in retinal development and axon guidance. First, the GCL was expanded in both mutants, suggesting that Nox2 is required for proper lamination in zebrafish retina (Figure 8C). Second, the RGC axons were mis-targeted outside of the OT and in the adjacent midbrain area (Figure 8D). Normally, RGC axons are found in the tectal neuropil, where they make synapses with the tectal neurons. However, RGCs from *nox2*^{-/-} larvae were not confined to such area and the axons were found throughout the midbrain. Finally, the neuropil area, which is normally devoid of cell bodies and mainly consists of axons, exhibited nuclear staining in both *nox2*^{-/-} mutants (Figure 8D). This observation suggested that proper formation of OT is also disrupted in *nox2*^{-/-} mutants.

Although these mutants exhibited clear effects in RGC development and guidance, a more detailed characterization was needed to elucidate other potential effects during development. In this chapter, I will present the characterization of a broader CNS development and overall phenotypes of the *nox2* *-/-* mutants.

3.2 Results

3.2.1 Nox2 mutant zebrafish exhibit aberrant axon projections along CNS

To determine whether axonal mis-targeting in *nox2* *-/-* mutants is specific to the retinotectal pathway, we investigated other areas of the CNS. We only used *nox2* *-/-* mutants that were generated from gRNA I (*nox2^{pu22}*), since the premature stop codon results in a shorter transcript than the *nox2* *-/-* mutant generated by gRNA II. Unless otherwise stated, the experiments were performed with the *nox2^{pu22}*, and will be referred to *nox2* *-/-* hereafter. In order to analyze axonal phenotypes throughout the CNS, we immunolabeled wild-type and *nox2* *-/-* homozygous mutants with anti-acetylated tubulin antibody at 48 hpf. Acetylated tubulin staining of axons in the forebrain showed aberrant axonal projections in *nox2* *-/-* mutant zebrafish embryos (Figure 8). In wild-type embryos, the anterior-forebrain commissure (AC) in the telencephalon consists of fasciculated axons (Figure 9A-A’'). However, in *nox2* *-/-* homozygous mutants, the axons in the AC are not held together and the projections exhibit an irregular pattern (Figure 9B-B’'). The diminished fasciculation of axons in the AC can also be seen in the dorsal views (Figure 9C, D). Lastly, abnormal axonal projections were detected in the dorsal longitudinal fascicle of the spinal cord in 48 hpf *nox2* *-/-* mutants (Figure 9E-F).

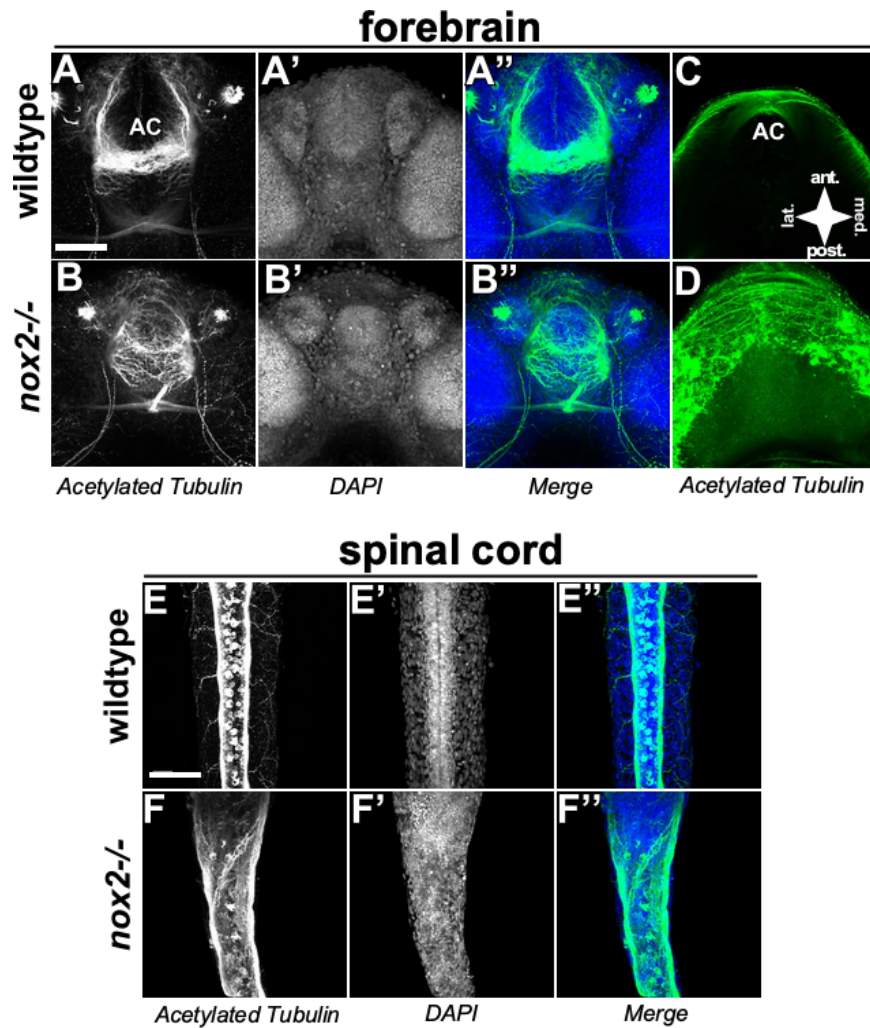


Figure 9: Axons are mistargeted in the CNS of homozygous *nox2* mutants.

Micrographs of 48 hpf wild-type (A, C) and *nox2* $-/-$ (B, D) forebrains labeled with anti-acetylated α -tubulin antibody and DAPI. *nox2* $-/-$ embryos exhibit aberrant axonal projections at the forebrain AC. Ventral views are shown in A and B; dorsal views in C and D. Micrographs of 48 hpf wild-type (E-E'') and *nox2* $-/-$ (F-F'') spinal cord labeled with anti-acetylated α -tubulin antibody and DAPI. The spinal cord is wider and shows aberrant projections of the dorsal longitudinal fascicle in *nox2* $-/-$ embryos (F-F'') compared with wild-type embryos (E-E''). Scale bars = 100 μ m.

3.2.2 *nox2* mutant zebrafish exhibit normal brain development

Because axonal tracts in different parts of the CNS are affected in *nox2* *-/-* mutants, we investigated whether the early development of the nervous system such as patterning is altered in these mutants to distinguish early developmental versus axonal guidance deficits. Therefore, we performed *in situ* hybridization experiments with known CNS gene markers for forebrain (*pax6a*), midbrain (*otx2*), and midbrain–hindbrain boundary (*fgf8*) on 36 hpf wild-type and *nox2* *-/-* mutant embryos (Figure 10A-C). We did not find any obvious difference in the expression pattern of these marker genes between wild-type and *nox2* *-/-* mutant embryos. *pax6a* expression was found in the lens, retina, telencephalon, and hindbrain (Figure 10A-A’). *otx2* expression was detected in the midbrain (Figure 10B-B’) and *fgf8* expression at the midbrain–hindbrain boundary (Figure 10C-C’). A recent study showed that both the number of neural progenitor cells and the level of *nestin* expression, a marker for neural progenitor cells, are decreased in *nox2*-deficient adult mice (Nayernia et al., 2017). We did not find any difference in *nestin* expression pattern between wild-type and mutant embryos at 36 hpf (Figure 10D-D’). In summary, these data suggest that the major brain regions are intact and that the early development of CNS is not significantly altered in *nox2* *-/-* mutants. Overall, the results suggest that the axonal deficits in *nox2* *-/-* mutants are not due to general developmental problems and that Nox2 plays a role in axonal pathfinding and targeting.

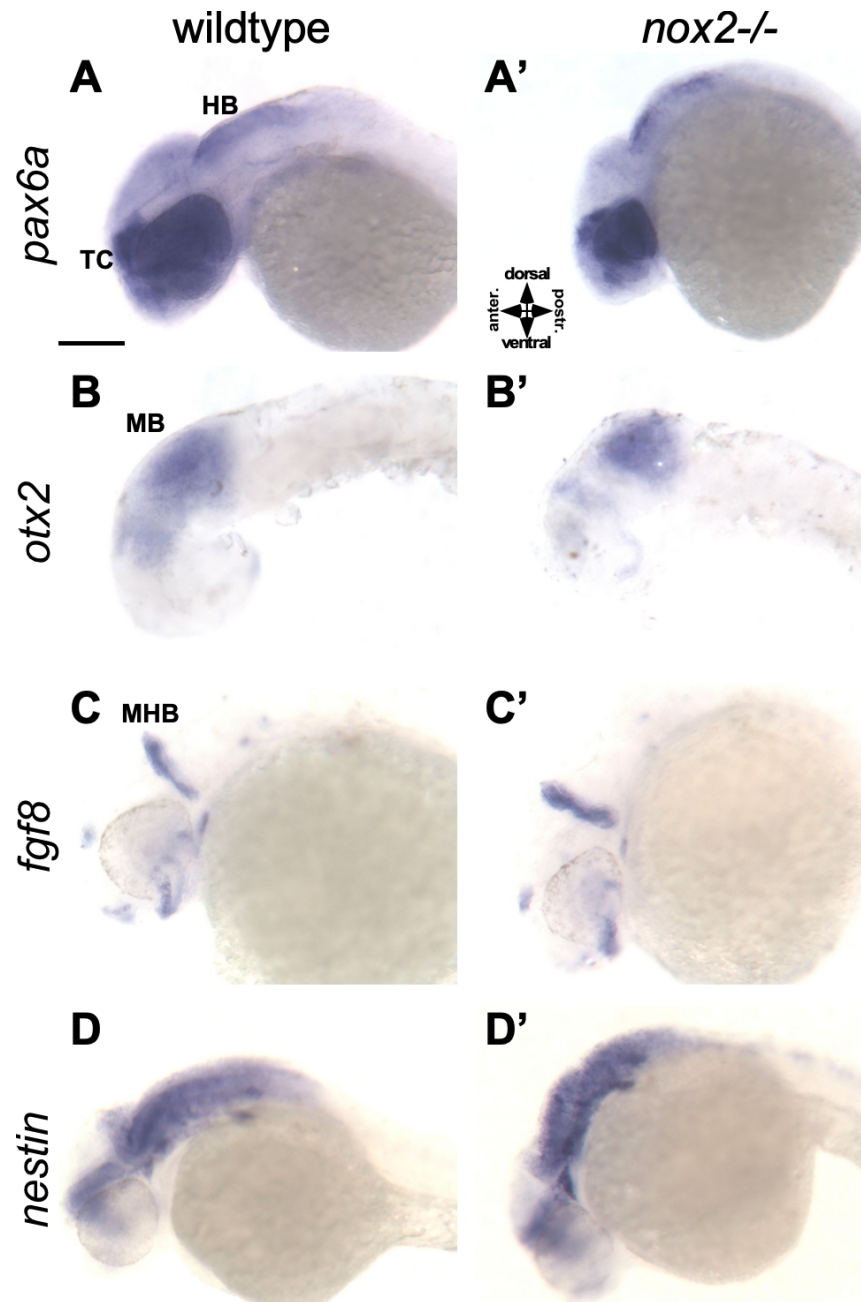


Figure 10: Early development of CNS is normal in homozygous *nox2* mutants.

In situ hybridization with probes for marker genes of CNS patterning in 36 hpf wild-type and *nox2*^{-/-} mutant embryos. (A–A') *pax6a* expression was found in the telencephalon (TC), lens, retina, and hindbrain (HB) in both wild-type and *nox2*^{-/-} embryos. *otx2* expression was detected in midbrain (MB; B–B') and *fgf8* expression at the midbrain-hindbrain boundary (C–C') in both wild-type and mutant embryos. Eyes and yolk were removed for better visualization of *otx2* expression in B–B'. The development of major brain regions was not affected in *nox2*^{-/-} embryos. D–D', Expression pattern of *nestin*, a marker for neural progenitor cells, was similar in wild-type and mutant embryos and *nestin* expression was found in all major brain regions. Scale bar = 200 μ m.

3.2.3 *nox2* ^{-/-} mutants have impaired vision

nox2 ^{-/-} zebrafish larvae have smaller eyes compared to wild-types and RGCs in *nox2* ^{-/-} mutants fail to innervate OT properly. As this innervation is crucial for the relay of visual information to the brain for processing and initiating a behavioral response, we sought to determine the visual activity in *nox2* ^{-/-} mutants. To measure visual activity, we examined larval eye movements in response to a visual cue (i.e, rotating stripes) as described in Chapter 2.2.4. This behavior is named as optokinetic response (OKR) and widely used to assess zebrafish visual function (Ganzen et al., 2017). The OKR behavior appears as early as 3 dpf, the time when most of the retinal neurons are identifiable and startle responses can be evoked (Fadool & Dowling, 2008). Here, we tested at 5 dpf, as >95% of zebrafish response to visual stimuli and widely used to assess OKR (Fadool & Dowling, 2008). At 5 dpf, wild-type larvae respond to visual cue by following the direction of the movement of rotating stripes. However, none of the *nox2* ^{-/-} mutants displayed an OKR. We tested at least 10 fish in each session over four-independent sessions. As the mutants failed to respond to the visual cue, they are considered to have impaired vision and unable to detect the motion.

3.2.4 H₂O₂ levels in homozygous *nox2* ^{-/-} mutants

We reported that reducing Nox activity in general (through pharmacological Nox inhibition) or reducing Nox2 activity in particular (in *nox2* ^{-/-} mutants) affects GCL formation and tectal innervation (Weaver et al., 2018). To determine whether ROS levels are altered in *nox2* ^{-/-} mutants, we transiently expressed a genetically encoded H₂O₂-biosensor, roGFP2-orp1, in developing zebrafish embryos (Gutscher et al., 2009). Although superoxide is the primary ROS produced by Nox, superoxide can quickly react into H₂O₂, which has a longer half-life and therefore likely acts as the main ROS signaling molecule. First, we validated this H₂O₂ biosensor by treating 48 hpf zebrafish embryos with 20 mM H₂O₂ for 10 min, followed by 2.5 mM DTT for another 10 min while collecting ratiometric fluorescent images of the head region (Figure 11A). We observed that H₂O₂ levels in the retina increased threefold with H₂O₂ treatment (p < 0.0001; paired t-test), which was then reduced to 146% of the baseline level after the DTT treatment (Figure 11B). As the biosensor specifically detected H₂O₂ levels and responded real-time changes, we next compared the basal H₂O₂ levels in wild-type and *nox2* ^{-/-} embryos at 48 hpf. Although we

observed a slightly increased level of H_2O_2 in the mutant embryos, the trend was not significant ($p = 0.2675$; Figure 11C). The fact that the H_2O_2 levels were not significantly different between wild-type and mutant embryos could be explained by compensatory mechanisms and does not eliminate the possibility that the *nox2* $-/-$ mutants exhibit different levels in earlier stages of development.

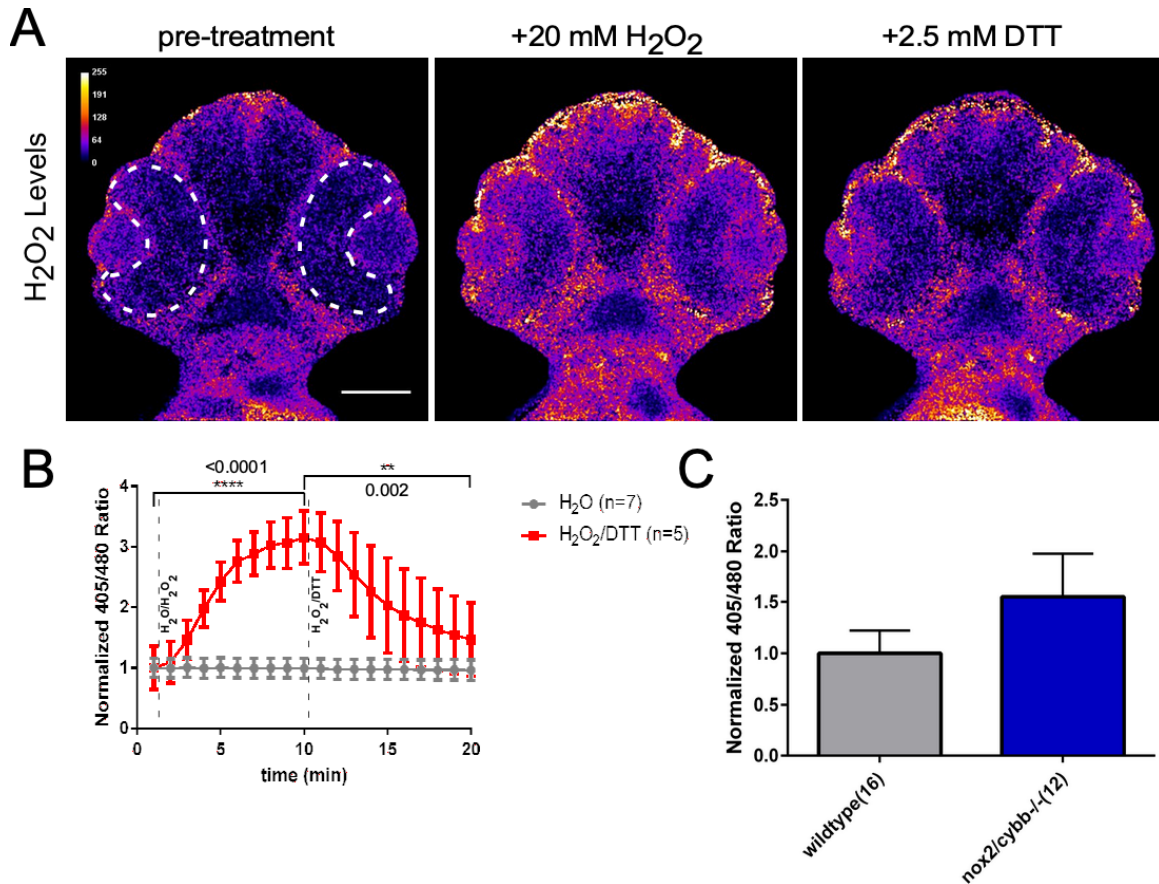


Figure 11: H_2O_2 levels in retinas of homozygous *nox2* $-/-$ mutants.

(A) Ratiometric images depicting H_2O_2 levels in the head of a 48 hpf wild-type zebrafish embryo expressing roGFP2-orp1, before (left), 10 min after 20 mM H_2O_2 (middle), and 10 min after 2.5 mM DTT (right) addition. Dashed white line demarks retina, in which H_2O_2 levels were quantified in B and C. Scale bar = 100 μm . (B) Graph showing the normalized 405/480 ratios of wild-type embryos at 1 min intervals in response to either H_2O_2/DTT (red line; $n = 5$ embryos) or H_2O (gray line; $n = 7$ embryos) addition. Data are presented as mean \pm SEM. p -values are indicated for paired t tests between H_2O and H_2O_2 ($p = 0.0001$) and H_2O_2 and DTT ($p = 0.002$). (C) Bar graph showing the basal H_2O_2 levels in retinas of wild-type ($n = 16$) and *nox2* $-/-$ mutant ($n = 12$) embryos. *nox2* $-/-$ mutant embryos do not have significantly different H_2O_2 levels compared with wild-type embryos ($p = 0.2675$, unpaired t test with Welch's correction).

3.2.5 The *nox2* mutation exhibits incomplete penetrance

Once the homozygous line was generated from *nox2* $-/-$ mutants, we have seen an unexpected pattern. Initial experiments were conducted with homozygous embryos that were obtained from breeding of heterozygous parents. A portion of the homozygous embryos grew into adulthood and bred normally. However, the progeny derived from homozygous parent breeding resulted in two phenotypes: $\sim 75\%$ of the embryos developed normally, and they were comparable with the wild-types throughout their development. On the other hand, $\sim 25\%$ of the embryos initially looked underdeveloped, and they accumulated defects in their overall body shape, eyes and heart. These embryos died at 6-9 dpf and did not grow into the adulthood. To better understand how the two different *nox2* $-/-$ population diverge from each other, we monitored wild-type and *nox2* $-/-$ embryos from 1 to 4 dpf (Figure 12). While wild-type and some of the *nox2* $-/-$ embryos showed similar development pattern, some of *nox2* $-/-$ embryos looked underdeveloped at 1 dpf (Figure 12A-C). By 2 dpf, mutants had obvious morphological defects: curved bodies, tilted tails and had smaller eyes (Figure 12A'-C'). By 3 dpf, the phenotypic difference becomes more obvious. *nox2* $-/-$ mutants with the mutant phenotype now exhibit clear differences in their eyes and also have pericardial edema (Figure 12A''-C''). At 4 dpf, the differences in the phenotypes were even more pronounced (Figure 12A'''-C'''), and this continued until the larvae died (not shown). Interestingly, the percentage of *nox2* $-/-$ embryos with and without the mutant phenotype were consistent through different breeding times and generations (Figure 12D). Throughout two generations, the *nox2* $-/-$ progeny exhibited similar trend: $\sim 25\%$ of *nox2* $-/-$ embryos exhibited mutant phenotype, while $\sim 75\%$ of the *nox2* $-/-$ embryos did not exhibit mutant phenotype .

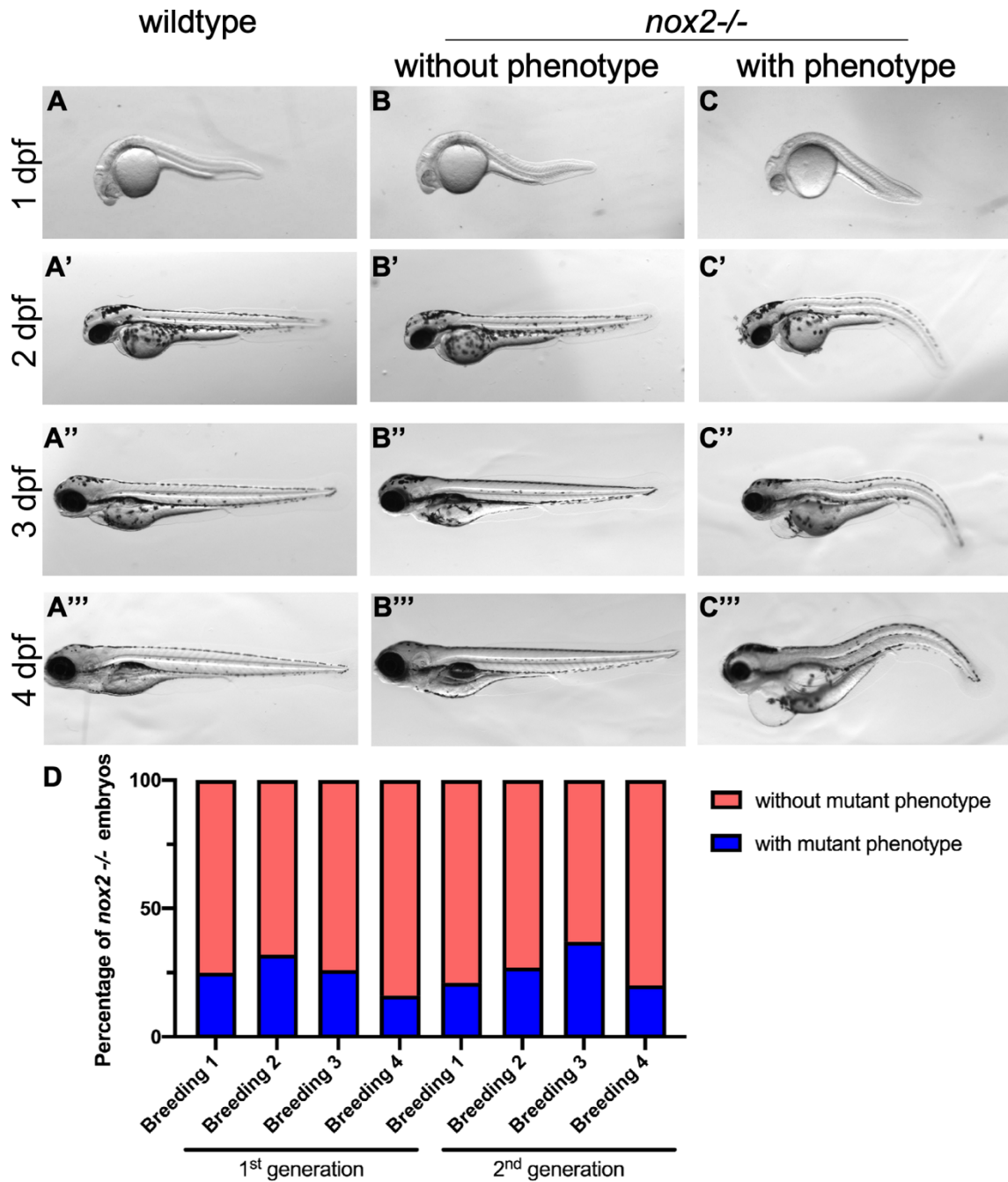


Figure 12: The phenotypic characterization of *nox2*^{-/-} mutants.

Wild-type (A), *nox2*^{-/-} without a mutant phenotype (B) and *nox2*^{-/-} with a mutant phenotype (C) embryos were monitored from 1-4 dpf. Wild-type and *nox2*^{-/-} without a mutant phenotype exhibited similar pattern of development (A-A''', B-B'''), while *nox2*^{-/-} with mutant phenotype embryos exhibit smaller eyes, curved body, and pericardial edema (C-C'''). Quantification of the percentage of *nox2*^{-/-} embryos with and without mutant phenotype, showing four-independent breeding in each generation. There was a consistent pattern in each generation that on average 25% of *nox2*^{-/-} embryos exhibited the mutant phenotype and 75% of the *nox2*^{-/-} embryos did not exhibit the mutant phenotype (Chi-square test, **p* = 0.0192).

To see if these phenotypes matched with the RGC phenotypes, we stained these embryos with anti-acetylated tubulin antibody at 4 dpf and examined the retina (Figure 13). Wild-type (Figure 13A-A') and normal-looking *nox2* *-/-* embryos (Figure 13B-B') were indistinguishable, however, the *nox2* *-/-* embryos with the mutant phenotype, also exhibited enlarged GCL (Figure 13C-C'). These results suggested that the *nox2* *-/-* mutants, that do not show an overall phenotype, also lacks the RGC-specific phenotypes that we initially observed. On the other hand, a quarter of *nox2* *-/-* mutants exhibit both overall mutant phenotype in their bodies, as well as RGC-specific phenotypes such as increased GCL in the retina.

Later, we looked at the second type of *nox2* *-/-* mutants that were mentioned above, to ensure the specificity of the mutagenesis. We generated *nox2* *-/-* (*II*) mutants in the transgenic background, *Tg(ath5:GFP)*, which expresses GFP in their RGCs that is driven by *ath5* promoter. At 3 dpf, wild-type embryos exhibited proper GCL formation, however, the *nox2* *-/-*(*II*) mutants had increased GCL layer (Figure 14A-B). Furthermore, we have seen that embryos derived from homozygous *nox2* *-/-* (*II*) mutants are also different in their phenotypes (Figure 14C-C'). 22% of the progeny exhibited phenotype, similar to *nox2* *-/-* (*I*) mutants. Furthermore, we looked at the embryos that have the both *nox2* mutations (Figure 8A) in order to test whether the same penetrance pattern will be seen. When the adults from *nox2* *-/-* (*I*) and *nox2* *-/-* (*II*) crossed, 26% of the progeny exhibited a mutant phenotype. These results supported the specificity of the mutation in *nox2* gene and validated loss of Nox2 as the source for differences in the phenotypes. Thus, two different mutations resulting in different truncated proteins, resulted in similar RGC phenotypes and penetrance.

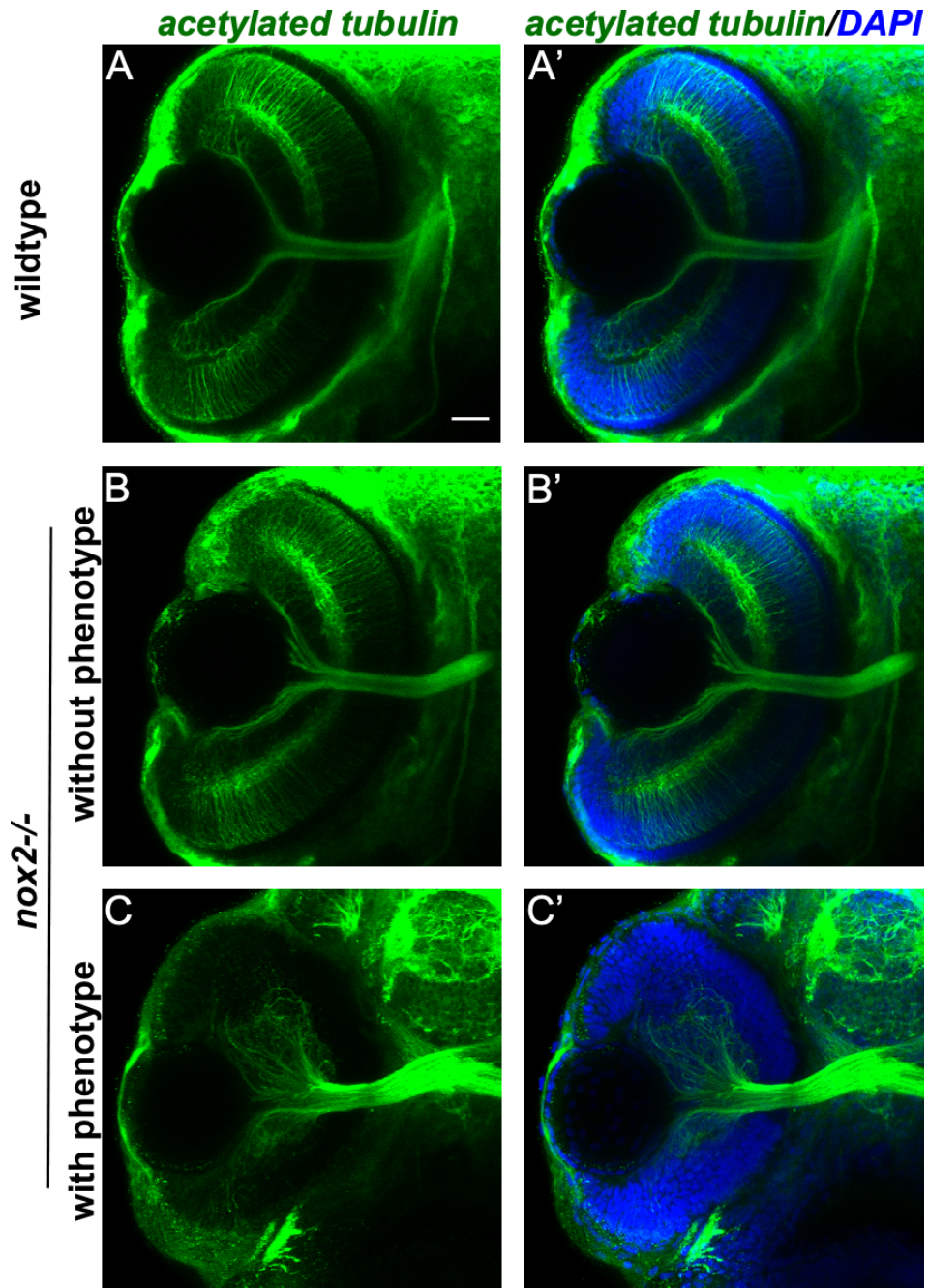


Figure 13: The overall phenotypic difference coincides with the RGC phenotypes in *nox2*^{-/-} mutants.

Micrographs of 4 dpf old wild-type (A, A') and *nox2*^{-/-} without mutant phenotype (B, B') and *nox2*^{-/-} with mutant phenotype (C, C') retinas labeled with anti-acetylated α -tubulin antibody and DAPI. *nox2*^{-/-} embryos with mutant phenotype exhibited enlarged GCL formation, thickened ON and smaller retina. Scale bar = 25 μ m.

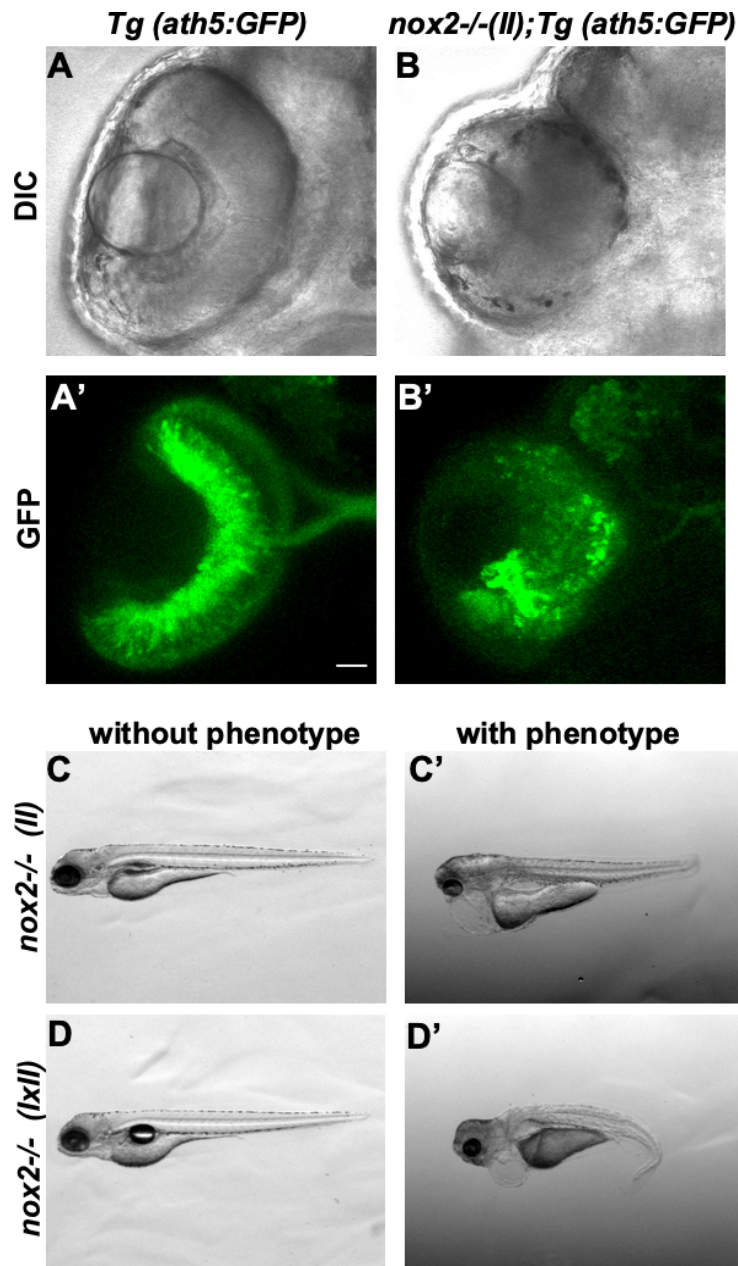


Figure 14: Phenotypes in *nox2* $-/-$ (II) mutants are comparable to *nox2* $-/-$ (I) mutants.

(A-B) DIC and fluorescent images of transgenic lines with RGC-specific GFP expression at 3 dpf. (A-A') Wild-type embryos exhibit normal retina and GCL formation. (B-B') *nox2* Type II homozygous mutants exhibit smaller retina and disrupted GCL formation, similar to that of *nox2* Type I homozygous mutants. (C-D) Overall phenotypes of Type II mutants exhibited same trend of population. (C-C') While 22% of the embryos from *nox2* Type II homozygous crossing exhibited mutant phenotype with smaller eyes, pericardial edema and smaller body shape (C'), remaining embryos looked normal (C). (D-D') *nox2* $-/-$ (I) and *nox2* $-/-$ (II) parents were bred to obtain embryos carrying two different loss-of-function *nox2* mutations. These embryos same similar trend with individual *nox2* mutant embryos. Scale bar = 25 μ m.

To further confirm that the *nox2* homozygous mutants and whether our genotyping strategy is reliable, we genotyped and sequenced the adult fish that were used in the experiments. We use DNA PAGE approach to genotype *nox2* *-/-* mutants on a regular basis. Wild-type and homozygous *nox2* *-/-* mutants exhibited single band corresponding homoduplexes and can be differentiated by their size since *nox2* *-/-* mutants have a 5 bp deletion (Figure 15A). Mixing of wild-type and *nox2* *-/-* PCR samples would mimic heterozygous mutants and exhibited heteroduplexes as their electromobility is different from homoduplexes (Figure 15A, red bracket). Next, we used T7 endonuclease assay to validate our genotyping strategy. We used same samples in T7 endonuclease assay, which can detect heteroduplexes (Figure 15B). While homozygous mutants and wild-types were detected as single band, heteroduplexes were recognized and cut by the T7 endonuclease and result in additional bands (Figure 15B, red arrows). The genotypes were also validated with high-resolution melt analysis, further validating the accuracy of our genotyping approach (data not shown). Finally, we sequenced the adult wild-type and *nox2* *-/-* mutants. The 5 bp deletion near *nox2* gRNA I target site was detected in all *nox2* *-/-* mutants (Figure 15C). Furthermore, the predicted off-target of *nox2* gRNA I sequence was found to be unaltered in all tested animals (Figure 15C, lower panel). Overall, we gathered evidence that the phenotypes that are seen in the 25% of the *nox2* *-/-* homozygous mutants were specific to loss of functional Nox2.

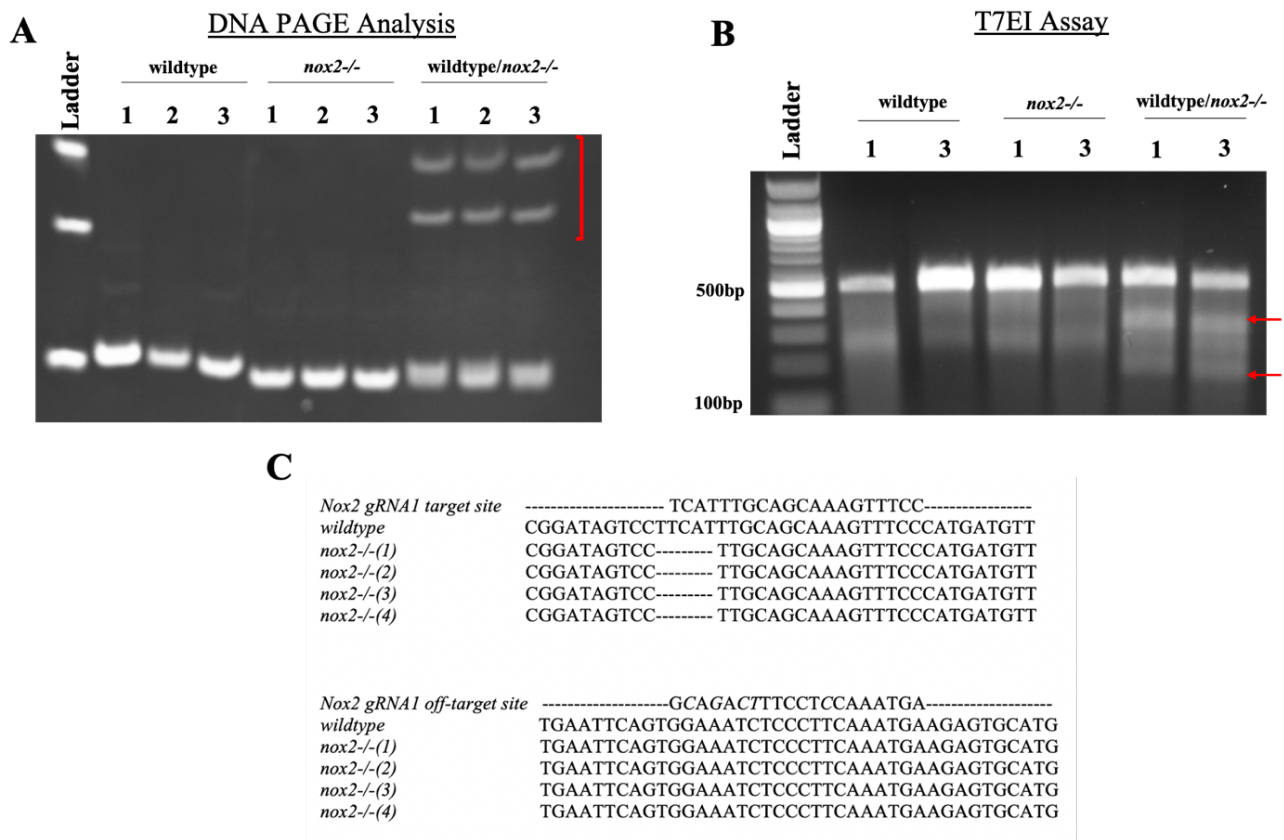


Figure 15: The validation of the genotypes of *nox2*^{-/-} fish.

Wild-type and *nox2*^{-/-} mutant adult fish were genotyped from their tail biopsies by DNA PAGE analysis (A) and T7 endonuclease assay (B). Wild-type and *nox2*^{-/-} homozygous mutants produce homoduplexes while combination of both forms heteroduplexes (red bracket) in DNA PAGE analysis (A). T7 endonuclease recognizes and digests at mis-matched base pairs that were found in heterozygous mutants. Additional bands were detected in the wild-type and *nox2*^{-/-} sample mixing (red arrows, 350 and 180 bp) (B). Sanger sequencing results for wild-type and *nox2*^{-/-} adult fish. *Nox2* gRNA I target site is shown on top row; 5 bp deletion in *nox2*^{-/-} fish validated the genotype of the mutants (top). *Nox2* gRNA I off-target site is shown on top row, mismatched residues are shown in italic. The off-target site was not affected in *nox2*^{-/-} mutant fish (bottom).

3.2.6 Loss of functional Nox2 is compensated by other Nox isoforms

We wanted to identify the underlying reason for the two mutant phenotypes, which is critical for understanding the mechanistic differences in these phenotypes. To elucidate the potential cause for these different phenotypes, we first assessed the *in vivo* H₂O₂ levels at 2 dpf and 5 dpf using roGFP2-orp1 biosensor. In 2 dpf embryos, we did not find any difference in H₂O₂ levels when comparing retinas of wild-type, *nox2* *-/-* without the mutant phenotype, and *nox2* *-/-* with the mutant phenotype (Figure 16A, A'). On the other hand, 5 dpf old larvae exhibited higher H₂O₂ levels in the retina when compared to 2 dpf embryos for all experimental groups (Figure 16B, B'). At 5 dpf, the *nox2* *-/-* larvae with the mutant phenotype had significantly higher H₂O₂ levels (3.8 ± 0.4) compared to wild-type (2.5 ± 0.2 ; **p* = 0.0471) and *nox2* *-/-* without the mutant phenotype (2.1 ± 0.1 ; ***p* = 0.0042; Figure 16B, B'), while the levels in *nox2* *-/-* larvae without the phenotype were similar to wild-type.

This observation led us to investigate the potential source of the increased H₂O₂. One possibility could be compensation by other Nox isoforms in *nox2* *-/-* mutants. Previously, it was shown that Nox1 can partially compensate Nox2, and Nox2 cytosolic subunits could activate Nox1 (Bánfi et al., 2003; Miklós Geiszt et al., 2003). To test whether other Nox isoforms are upregulated in the *nox2* *-/-* mutants, we isolated total RNA from 2 and 5 dpf larvae and performed RT-qPCR analysis to determine expression levels of different Nox isoforms and subunits. We determined mRNA levels of *nox1* and its cytosolic subunits *noxo1* and *noxal*, Nox2 subunits *ncf1* (p47^{phox}) and *ncf2* (p67^{phox}), *nox5* and *duox*. At 2 dpf, both types of *nox2* *-/-* mutants (with and without mutant phenotype) showed elevated *nox1* expression compared to wild-type larvae (*****p* < 0.0001; Figure 16C). However, at 5 dpf, *nox2* *-/-* larvae with the phenotype exhibited significantly higher *noxo1* expression compared to both wild-type and *nox2* *-/-* without the mutant phenotype (*****p* < 0.0001; Figure 16D). Furthermore, *nox5* gene expression was elevated in *nox2* *-/-* larvae with mutant phenotype when compared to wild-type (**p* = 0.0137) and *nox2* *-/-* larvae without the mutant phenotype (***p* = 0.0096; Figure 16D). These results suggest that at 2 dpf, loss of Nox2 can be compensated by Nox1 activation in both mutants, resulting in comparable H₂O₂ levels compared to wild-type. Hence, at 5 dpf, the higher H₂O₂ levels in *nox2* *-/-* showing the mutant phenotype could be attributed to overexpression of Nox1 and Nox5, which we did not observe in the mutants lacking the mutant phenotype. However, how these increased H₂O₂ levels relate to the different phenotypes in *nox2* *-/-* is unclear and requires further investigation.

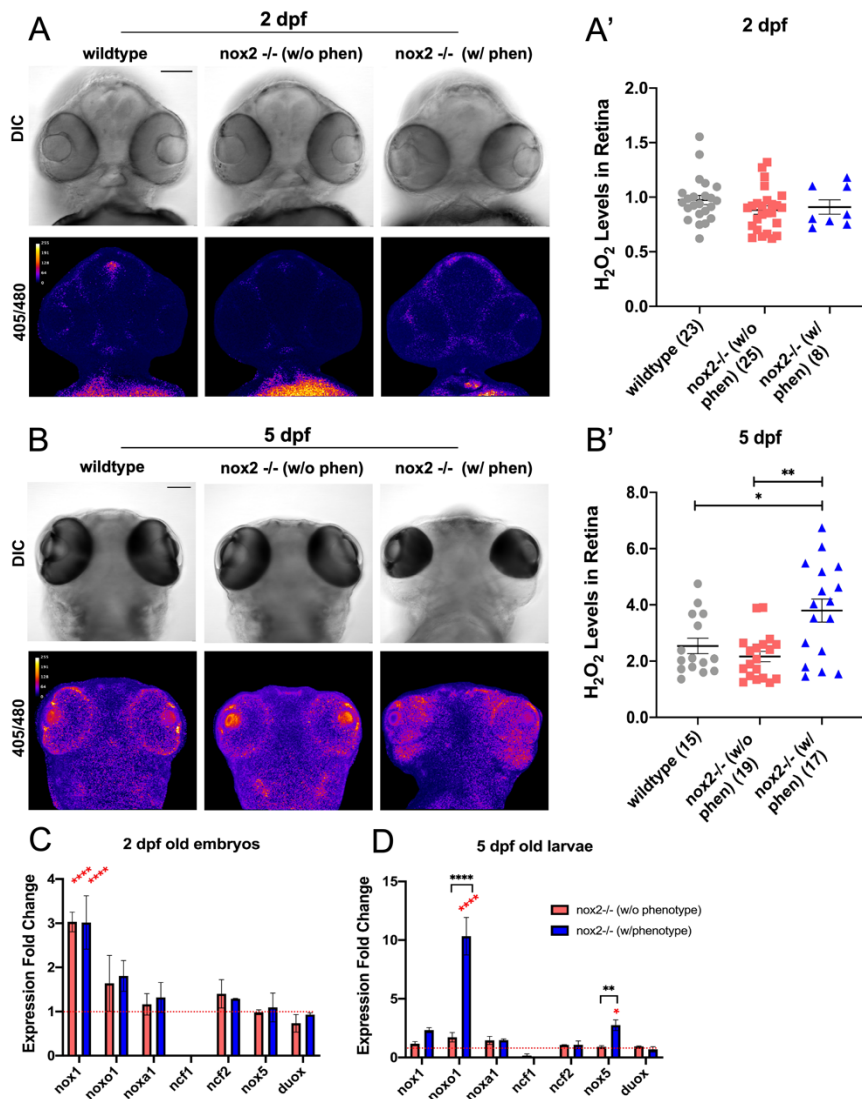


Figure 16: Loss of Nox2 is compensated by other Nox isoforms.

(A) Micrographs of DIC and 405/480 ratio images of 2 dpf wild-type, *nox2* ^{-/-} without the mutant phenotype (w/o phen) and *nox2* ^{-/-} with the mutant phenotype (w/ phen) embryos. (B) DIC and 405/480 ratio images of 5 dpf wild-type, *nox2* ^{-/-} without the mutant phenotype (w/o phen) and *nox2* ^{-/-} with the mutant phenotype (w/ phen) larvae. (C, D) Quantification of H₂O₂ levels in the retinas of 2 dpf embryos (C) and 5 dpf larvae (D). Average ratio values from retinas were calculated from each fish. (E, F) Expression fold-change analysis calculated by 2^{-ΔΔCt} method for 2 dpf (E) and 5 dpf (F) old animals. Ribosomal *rp13a* was used as a housekeeping gene. Expression fold-changes were shown in respect to wild-type expression (red dashed line). Statistical difference between mutant with wild-type shown as red asterisks while difference between two mutant types shown in black. Scale bars = 50 μm. Data are shown as mean ± SEM; n-value in parenthesis indicates the number of embryos. Kruskal-Wallis/ Dunn's multiple comparisons test (C); Brown-Forsythe ANOVA/ Dunnett's T3 multiple comparisons test (D); two-way ANOVA (E, F); *p < 0.05; **p < 0.01, ***p < 0.001, ****p < 0.0001.

3.3 Discussion

3.3.1 The role of Nox2 in zebrafish CNS development

The aim of this chapter was to present a detailed characterization of the *nox2* homozygous mutants that were established in our group by the work of former graduate student Cory Weaver. First, we performed immunohistochemistry with anti-acetylated tubulin antibody in order to visualize all axons throughout the CNS. We have already known that axon guidance defects existed in the midbrains of *nox2* mutants since RGCs failed to properly innervate OT (Figure 8). First, we found that axons in the forebrain also projected abnormally (Figure 9). The anterior commissure in the forebrain exhibited clear guidance defects as the axons were not confined in a tight bundle, instead they projected aberrantly in the forebrain. Next, we have shown that dorsal longitudinal fascicle of the spinal cord failed to make proper projections. Although we did not investigate in great detail, the axons in the hindbrain also exhibited aberrant projections especially close to midbrain-hindbrain boundary (Figure 17). Taken together, *nox2* $-/-$ zebrafish have axon guidance defects throughout the CNS, including telencephalon in the forebrain, OT in the midbrain, hindbrain, and spinal cord (Figure 18). These results suggest that Nox2 plays a role in axon guidance signaling common these specific axon projections.

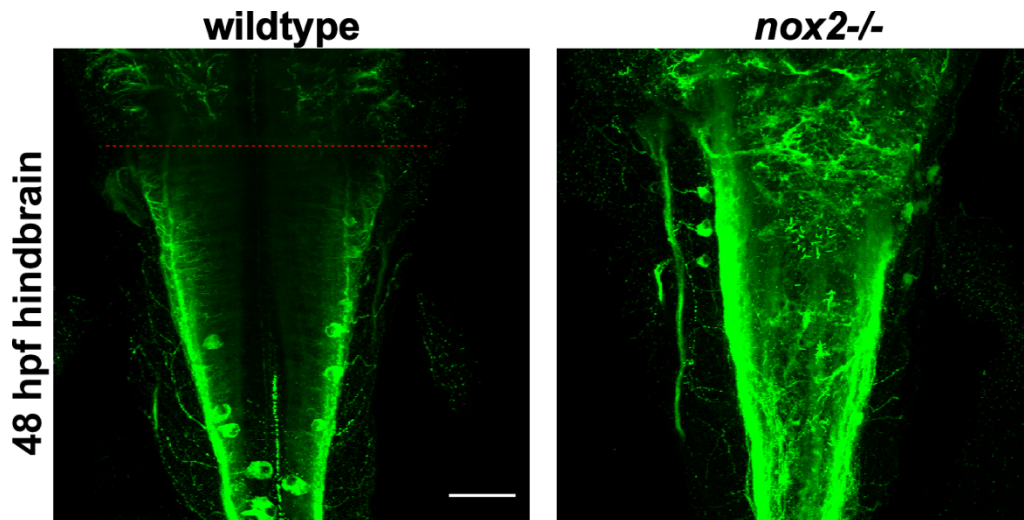


Figure 17: Aberrant axon projections in *nox2* $-/-$ hindbrain area.

Anti-acetylated tubulin staining of hindbrains from 48 hpf wild-type and *nox2* $-/-$ zebrafish embryos. Mutant embryos exhibit excessive axon projections around midbrain-hindbrain boundary (red line). Scale bar = 50 μ m.

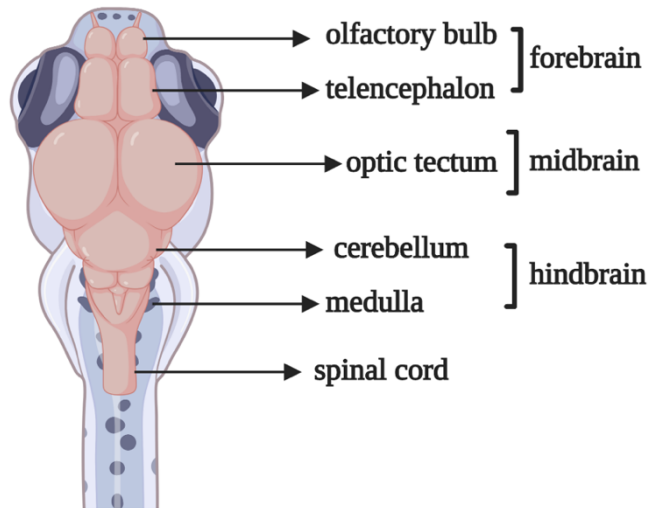


Figure 18: Schematic representation of zebrafish neuroanatomy.

Next, we wanted to check whether Nox2 deficiency had general morphological defects early in brain development or directly affected axon projections. To test this, we performed *in situ* hybridization experiments with major brain markers for forebrain (*pax6a*), midbrain (*otx2*) and midbrain-hindbrain (*fgf8*) at 36 hpf, the earliest time point that we could detect phenotypic differences in *nox2* *-/-* mutants confidently. We did not observe any differences in the expression pattern of the forebrain, midbrain and midbrain-hindbrain boundary markers, where we detected axonal projection errors (Figure 10). Thus, the early brain development was normal in *nox2* *-/-* mutants, suggesting that loss of functional Nox2 affects later nervous system development including axon guidance. In support of our findings, *Nox2* and *p47^{phox}* knockout mice had normal brains, cortex and hippocampus (Kishida et al., 2006).

3.3.2 The role of Nox2 in neurogenesis

Nox2-mediated ROS signaling is an important regulator of neural stem cell proliferation and differentiation as described in Chapter 1. The dentate gyrus and subventricular zone showed decreased *nestin* expression along with decreased neural progenitor cells (NPC) in *Nox2* deficient mice (Nayernia et al., 2017). Nestin, neuroepithelial stem cell protein, is an intermediate filament and a major cytoskeletal component that is also important in zebrafish retina and brain development (Chen, Yuh, & Wu, 2010). *nestin* expression was found throughout the developing

CNS at 24 hpf and later, the expression pattern was restricted to neurogenic zones. The progenitor pools were found in telencephalon, diencephalon, midbrain-hindbrain boundary and ciliary marginal zone in the retina (Mahler & Driever, 2007). In contrast to *Nox2*^{-/-} mice, we did not see a difference in pattern of *nestin* expression in CNS of *nox2*^{-/-} zebrafish embryos at 36 hpf (Figure 9 D-D'). Hence, in earlier neurogenesis *nox2* deficiency does not seem to have an effect on NPC pool. However, further quantitative analysis at later time points using qPCR to detect *nestin* expression in *nox2* mutants are needed to better understand the role of Nox2 in zebrafish CNS neurogenesis. To determine to number of proliferating cells in retina, BrdU staining can also be performed. BrdU is a synthetic analog of thymidine and is commonly used to detect proliferating cells. We have stained whole-mount embryos with anti-BrdU antibody; however, whole-mount has limitations for reliable quantification of individual cells (data not shown). Therefore, antibody staining should be performed on sections instead of whole embryos. Ideal BrdU incubation time is from 36 to 48 hpf, since RGCs exit cell cycle around 36 hpf and retinal progenitors start taking fate to become INL cells from 36-48 hpf. At this time frame, the GCL should be devoid of proliferating cells. If Nox2 is involved in RGC differentiation, a higher number of proliferating cells is expected to be seen in *nox2*^{-/-} GCL after 36 hpf. Furthermore, this analysis can be extended to analyze differentiation pattern of other retinal cells.

To test whether RGC specification was affected in *nox2* mutants, we also performed *in situ* hybridization with *ath5* antisense RNA. *ath5* is a transcription factor that is expressed in differentiating cells that are destined to become RGCs and a key regulator of vertebrate retina (Del Bene et al., 2007; Kay et al., 2001; Souren, Martinez-Morales, Makri, Wittbrodt, & Wittbrodt, 2009). *In situ* hybridization was performed on 36 hpf embryos, when the first wave of RGC differentiation is expected to be finalized, to see if there is a delay in differentiation of RGCs. There were two populations of embryos in both wild-type and *nox2*^{-/-} mutants, showing intense staining (Figure 18 A-A', C-C') and less staining with more restricted pattern (Figure 18 B-B', D-D'). This might be because the developmental stage of individual fish was different from each other, and not all embryos were stage-matched during staining. Therefore, more experiments with a better control of timing are required to make reliable conclusions. However, the overall pattern is similar with both wild-type and *nox2*^{-/-}, which could be attributed to normal RGC specification. Future experiments investigating the other retinal cells are also important to better understand the role of Nox2 in retinal neurogenesis.

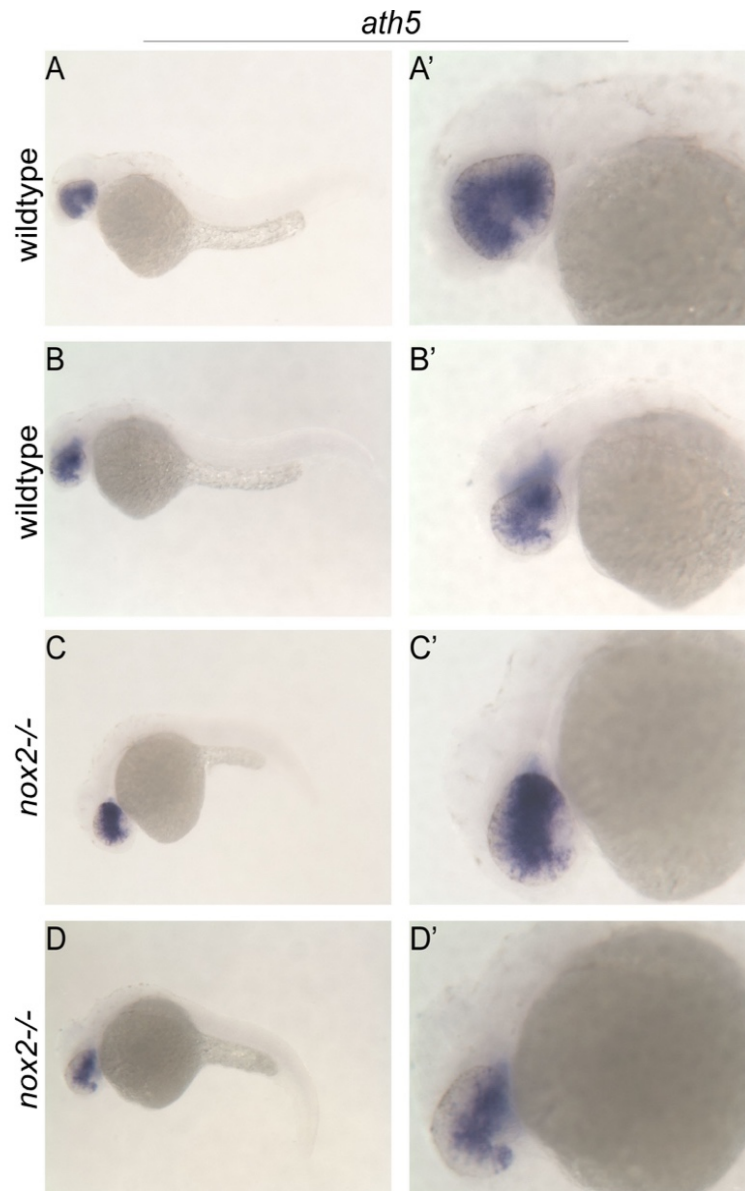


Figure 19. RGC specification seems unaffected in *nox2*^{-/-} mutants.

In situ hybridization with probes for *ath5* in 36 hpf wild-type and *nox2*^{-/-} mutant embryos. (A–B) Two distinct staining pattern was observed in wild-type embryos. (A'–B') enlarged views of the retina. (C–D) Same pattern existed in *nox2*^{-/-} embryos.

3.3.3 Analysis of incomplete penetrance in *nox2* mutants

Interestingly, we observed that both type of *nox2* mutants exhibit incomplete penetrance, a phenomenon in which a deleterious mutation produces a phenotype only in a subset of mutant individuals. 25% of the embryos from both mutant parents exhibited a mutant phenotype consistently through generations. We performed additional genotyping and sequencing experiments to exclude any genotyping errors and off-target modifications by CRISPR/Cas9. Although our findings suggest that the genotypes correspond to mutant sequence and off-target was not affected, whole-genome sequencing in these mutants should be established for further validation that no other parts of the genome are affected.

The proposed mechanisms that explain how zebrafish mutants overcome deleterious mutants include alternative mRNA splicing and genetic compensation (Anderson et al., 2017; Rossi et al., 2015). Functional splice variants of *Nox1* and *Nox4* have been established in mice knockout models, however, there is only one splice variant found for *Nox2*, which regulates NOX2 activity in mice and human macrophages (Altenhöfer et al., 2012; Harrison et al., 2012). There is also *Nox2S* variant that was described before, however whether *Nox2S* translates into a protein is still unknown (Heidari, Shah, & Gove, 2004). Thus, there is currently no evidence that supports the presence of an alternative splice variant of *Nox2* that could function in the nervous system. Possible splice variants should also be tested in the current zebrafish *nox2* *-/-* mutants to safely exclude this mechanism behind incomplete penetrance.

Genetic compensation, on the other hand, can work at two different pathways: (1) Tuning genetic circuitry complements by activating another player in the pathway in which the deleterious mutation occurred, or (2) transcriptional adaptations of compensatory genes. Sucharov et al. showed that in zebrafish *mef2ca* (myocyte enhancer factor 2ca) mutants, Notch signaling differs with phenotypic variability, suggesting that gene circuitry adaptations determine the susceptibility or resilience in genetic mutations (Sucharov, Ray, Brooks, & Nichols, 2019). On the other hand, we found that zebrafish *nox2* *-/-* mutants exhibit incomplete penetrance by altering transcription of compensatory genes. Both type of mutants (with and without mutant phenotypes) exhibit increased *nox1* expression at earlier stages of development, suggesting that they respond similarly to the *nox2* mutation, however, towards later stages of development, gene expression differs between two types of mutants.

At 2 dpf, in both types of *nox2* *-/-* mutants (with and without phenotype), expression of *nox1* gene was elevated compared to wild-type embryos, suggesting that mutant fish might compensate loss of functional Nox2 by upregulation of Nox1. Furthermore, the H₂O₂ levels in the retinas of 2 dpf old mutant embryos (with and without mutant phenotype) were not different from wild-type, suggesting a functional compensation. Later at 5 dpf, about 25% of *nox2* *-/-* mutants exhibit a mutant phenotype, while the remaining *nox2* *-/-* larvae look normal. We found that mutants with a mutant phenotype have higher H₂O₂ levels in their retina, while mutants without the mutant phenotype had H₂O₂ levels comparable to wild-type (Figure 15). At this stage, *nox2* *-/-* mutants with the phenotype have significantly higher *nox1* and *nox5* expression compared to *nox2* *-/-* mutants without the mutant phenotype and wild-types. These results suggest that the strong phenotype in 25% of *nox2* *-/-* mutants correlates with an accumulation of H₂O₂ and is possibly caused by the increase in H₂O₂. Thus, the difference of the phenotypes in *nox2* *-/-* mutants possibly originates from the level of overexpression of other Nox isoforms. While some of the mutants can keep the H₂O₂ levels similar to wild-type and fully rescue the loss of Nox2, 25% of the *nox2* *-/-* mutants cannot control the over-activation of Noxes and continue to accumulate H₂O₂.

It was a surprise to us that the incomplete penetrance was an inherited trait. We kept seeing same percentage of embryos manifesting phenotype after second generation (data not shown). This observation could be explained with genetic liability-threshold model. This model is associated with multifactorial disorders in genetics. In this model, liability is described as a single entity encompassing all contributors to the development of a certain phenotype and liability is under control of multiple genes (Dahlqwist, Magnusson, Pawitan, & Sjölander, 2019). When individuals accumulate certain level of liability, they reach a threshold level at which individuals exhibit the associated trait. Furthermore, Sucharov et al. were able to fit their penetrance inheritance pedigree in zebrafish to this model (Sucharov et al., 2019). Hence, in our system, liability can be described as Nox expression pattern from different isoforms. Once individual embryos pass the threshold and accumulate higher Nox expression, they exhibit associated traits in their overall development and axon projection errors. Further experiments on detailed analysis of number of individuals with phenotype and genetic screening to generate a standard distribution of liability within a population needs to be performed to test this possibility.

Furthermore, we found that *nox2* gene expression was similar in *nox2* *-/-* mutants with and without the mutant phenotypes and that was comparable to wild-type expression at 2 dpf (Figure 20). However, it will be interesting to see if the mRNA levels change at 5 dpf, when there are over-compensatory mechanisms take over in some of the *nox2* *-/-* mutants. On the other hand, Nox2 subunit *p47phox* exhibited total loss of mRNA expression in *nox2* *-/-* mutants, while *p67phox* expression did not change compared to wild-type littermates (Figure 16C-D). In support of this, p47phox protein levels were found to be decreased while p67phox was unchanged in neutrophils from patients with cirrhosis in which NOX2 was depleted (Rolas et al., 2018). This suggests that *p47phox* expression might depend on functional Nox2 presence.

3.3.4 The function of H₂O₂ in *nox2* mutants

nox2 *-/-* zebrafish exhibiting overall and RGC phenotypes accumulate higher levels of H₂O₂ in their retina. We cannot be sure how this high level of H₂O₂ affects individual cell physiology. Previously, we have shown that embryos treated with CST exhibited defects in RGC innervation in the OT similar to that of *nox2* *-/-* mutants, and some of these effects were rescued by exogenous H₂O₂ treatment (Weaver et al., 2018), suggesting that the RGC pathfinding errors are due to insufficient H₂O₂ production. In support of our findings, Nox-inhibition caused decreased tectal innervation, but this effect was rescued by H₂O₂ treatment (Gauron et al., 2016). One caveat here is the lack of precise measurements of H₂O₂ concentrations that are required for carrying out normal physiology. Nox2 is lost in the whole organism in these *nox2* *-/-* mutants, possibly triggering events at an organism level as seen with expression changes that may overshadow Nox2 reduction effects at the single cell level. Therefore, tissue-specific *nox2* mutants could reveal the importance in cell-autonomous activities of RGCs. The different approaches for studying RGC-specific *nox2* mutants will be described in Chapter 5.1. Overall, our *in vivo* data indicates that RGC guidance along optic tract requires functional Nox2. Thus, proper H₂O₂ production by Nox2 is required for the development of zebrafish visual system, although the details of how up- and down

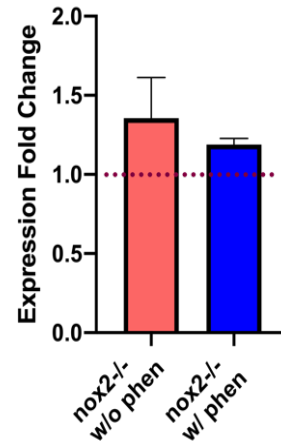


Figure 20: *nox2* mRNA expression fold-changes in 2 dpf old embryos.

Expression fold-change analysis calculated by 2- $\Delta\Delta$ Ct method for 2 dpf *nox2* *-/-* embryos. Ribosomal *rp13a* was used as a housekeeping change. Expression fold-changes were shown in respect to wild-type expression (red dashed line).

regulation of H₂O₂ regulates growth cone behavior at the single cell level are unclear at this point. These studies will require RGC-specific *nox2* mutants and imaging of ROS levels and axonal phenotype at the single cell level.

CHAPTER 4. NOX2 AND SLIT2/ROBO2 SIGNALING DURING RGC GUIDANCE

4.1 Introduction

Growth cones make directional decisions by sensing different environmental cues via receptors on the surface to navigate throughout the nervous system. There is a highly coordinated spatiotemporal expression of attractive and repellent guidance cues, which enables growth cones to make directional movements in response to presented cues. This dynamic response to changing environment is established by the modulation of the actin cytoskeleton at the growth cones (Dent et al., 2011). Growth cones connect the extracellular signals to intracellular signaling and modulated actin-based machinery for directional movement. Briefly, a specific guidance cue binds to its receptor on the growth cone surface, initiating an intracellular signaling cascade that alters the cytoskeletal dynamics (Bashaw & Klein, 2010; Lowery & Vactor, 2009; Omotade et al., 2017).

Our lab previously showed that NOX2 and its cytosolic subunit p40^{phox} localized at the growth cone periphery of *Aplysia* bag cell neurons (Munnamalai et al., 2014). Furthermore, pharmacological NOX inhibition altered the F-actin dynamics, reduced retrograde F-actin flow and decreased neurite outgrowth in these neurons (Munnamalai & Suter, 2009; Munnamalai et al., 2014). NOX2 and its subunits were also detected in the axons and axon tip of the cultured hippocampal neurons (Wilson et al., 2015). Moreover, NOX inhibition caused decrease in lamellar area as well as the number, length and the lifetime of filopodia in cultured hippocampal neurons (Wilson et al., 2015). Overall, these observations suggested that sufficient ROS production is required to maintain proper actin dynamics at the growth cones.

Finally, recent evidences indicate a role for Nox-derived ROS in the development of retinotectal connections in zebrafish. Pharmacological and genetic inhibition of Nox2 attenuated proper OT innervation in developing zebrafish embryos (Gauron et al., 2016; Weaver et al., 2018). Pharmacological Nox inhibition resulted in attenuation of the length, branching and tectal projection of RGCs, a phenotype that could be rescued by H₂O₂ application (Gauron et al., 2016). Previous work from our group also showed that Nox inhibition alters the behavior zebrafish RGCs in response to netrin-1, slit2 and BDNF *in vitro* (Haley Roeder, unpublished data); suggesting that these cues could act through Nox signaling in order to modulate RGC growth cone guidance. In

this chapter, I will present both *in vitro* and *in vivo* studies where we further investigated the link between Slit2/Robo2 and Nox2 pathways in zebrafish RGC guidance.

4.2 Results

4.2.1 Nox inhibition abolishes slit2-mediated growth cone collapse *in vitro*

To determine whether Nox could act downstream of slit2/Robo2 signaling, we cultured RGCs from zebrafish embryos as described in Chapter 2.3.1. To assess the effects of slit2 on cultured RGCs, I used data that was previously collected by Haley Roeder in our research group and combined with additional data that I collected to measure percentage of RGC growth cone collapse in response to slit2. In the first set of experiments, RGCs were cultured from wild-type embryos, and treated with control (0.1% DMSO), pan-Nox inhibitor CST (0.05 μ M), slit2 (10 μ g/mL), or slit2 with CST for 30 min. We quantified the percentage of growth cone collapse in at least three independent experiments (Figure 21C). While slit2 caused growth cone collapse in wild-type RGCs (41.1% \pm 4.7) compared to vehicle treatment (18.7% \pm 3.7, * p = 0.0126), this effect was abolished when Nox enzymes were inhibited with CST treatment, reducing percent growth cone collapse to the control levels (19.3% \pm 3.1, * p = 0.0269). Later, we looked at whether this response could be recapitulated with RGCs from *nox2* $-/-$ embryos. Similar to inhibitor treatment, slit2 mediated growth cone collapse (41.4% \pm 6.8) was lost in *nox2*-deficient RGCs (17.6% \pm 4.3, * p = 0.0147; Figure 21A-B, D). These results supported the previous observations (Haley Roeder, unpublished data) that slit2-mediated growth rate and guidance responses are Nox2-dependent.

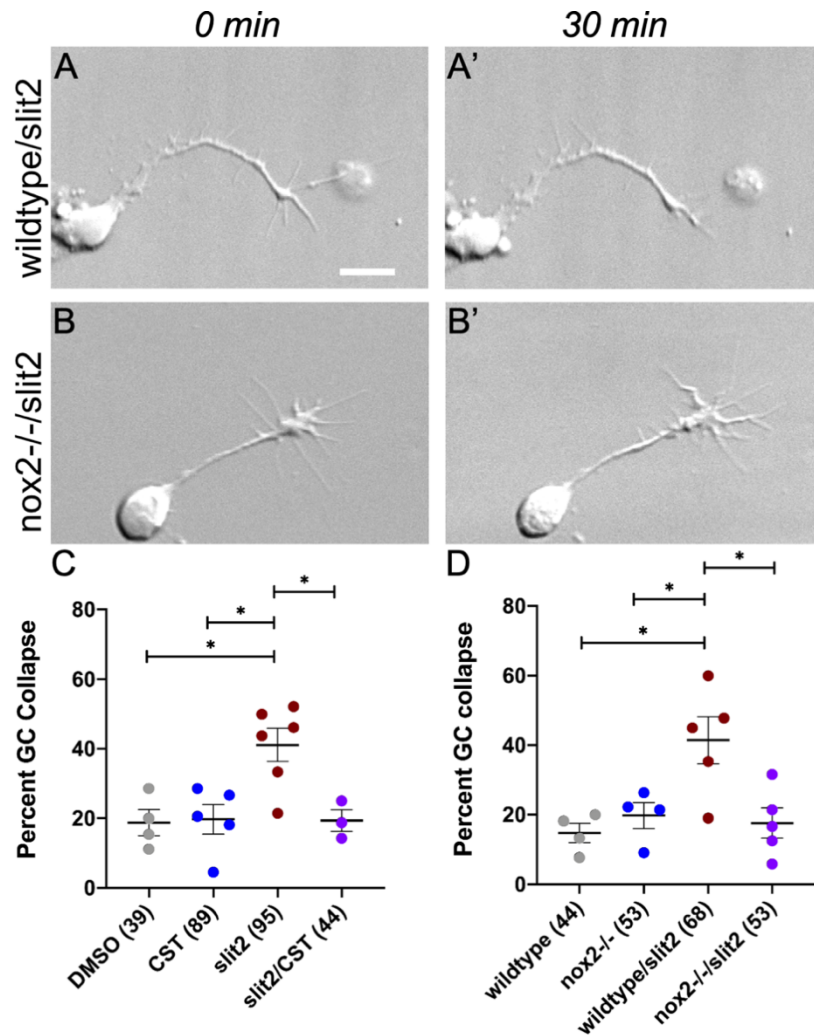


Figure 21: Nox inhibition abolishes slit2 mediated growth cone collapse.

(A-B) Representative DIC images of cultured zebrafish RGCs before (0 min) and after (30 min) slit2 treatment. (A-A') Wild-type RGC growth cones collapse with slit2 treatment. Collapsed growth cones exhibit loss of filopodia and a bullet shaped tip. (B-B') *nox2* ^{-/-} RGC growth cones do not collapse upon slit2 treatment. (C-D) Percent growth cone collapse quantification. (C) Average percentage of growth cones collapsed in response to pharmacological Nox inhibition. Slit2 treated wild-type growth cones exhibited significantly higher growth cone collapse compared to control (DMSO) and Nox inhibitor (CST) treated growth cones, while slit2 mediated growth cone collapse was lost when Nox enzymes were inhibited with CST. (D) Average percentage of growth cones collapsed in response to genetic loss of Nox2. While wild-type RGCs treated with slit2 exhibited higher growth cone collapse compared to wild-type and *nox2* ^{-/-} RGCs alone; *nox2* ^{-/-} RGCs did not collapse upon slit2 treatment. Total number of cells tested in each condition are shown in parentheses. Individual data points represent number of experiments in which percent growth cone collapse was calculated.

4.2.2 Nox2 is required for slit-2 mediated H₂O₂ production

We showed that Nox2 is required for slit2-mediated growth cone collapse. To be able to functionally link the Nox2 and slit2-Robo2 interactions, we measured the enzymatic product of Nox2, H₂O₂. We transiently expressed H₂O₂ specific biosensor roGFP2-orp1 in zebrafish embryos by injecting mRNA at one-cell stage. roGFP2-orp1 expressing zebrafish embryos were pre-selected and used for dissociated RGC neuronal cultures. We first treated wild-type RGCs with control (PBS) or 10 μg/mL slit2 for 30 minutes and measured the H₂O₂ levels in the growth cones before (time = 0) and after (time = 30) treatment. When wild-type RGCs were incubated with slit2, significantly higher levels of H₂O₂ at the growth cones were detected (1.3 ± 0.06 ; *p = 0.0195) compared to wild-type RGCs treated with PBS only (1.05 ± 0.07 ; Figure 22A). However, the H₂O₂ levels in *nox2*^{-/-} RGCs treated with slit2 were comparable to that of PBS-treated RGCs, suggesting the slit2 mediated H₂O₂ production at the growth cone requires functional Nox2 (Figure 22B). Furthermore, we tested zebrafish *astray*^{-/-} mutants that are defective in the *robo2* gene, which is the receptor for slit2. Similar to *nox2*^{-/-}, *astray*^{-/-} RGCs also did not exhibit slit2-mediated H₂O₂ production (Figure 22C). Overall, these data showed that zebrafish RGCs respond to slit2 by increasing intracellular H₂O₂ through Nox2 activity *in vitro*.

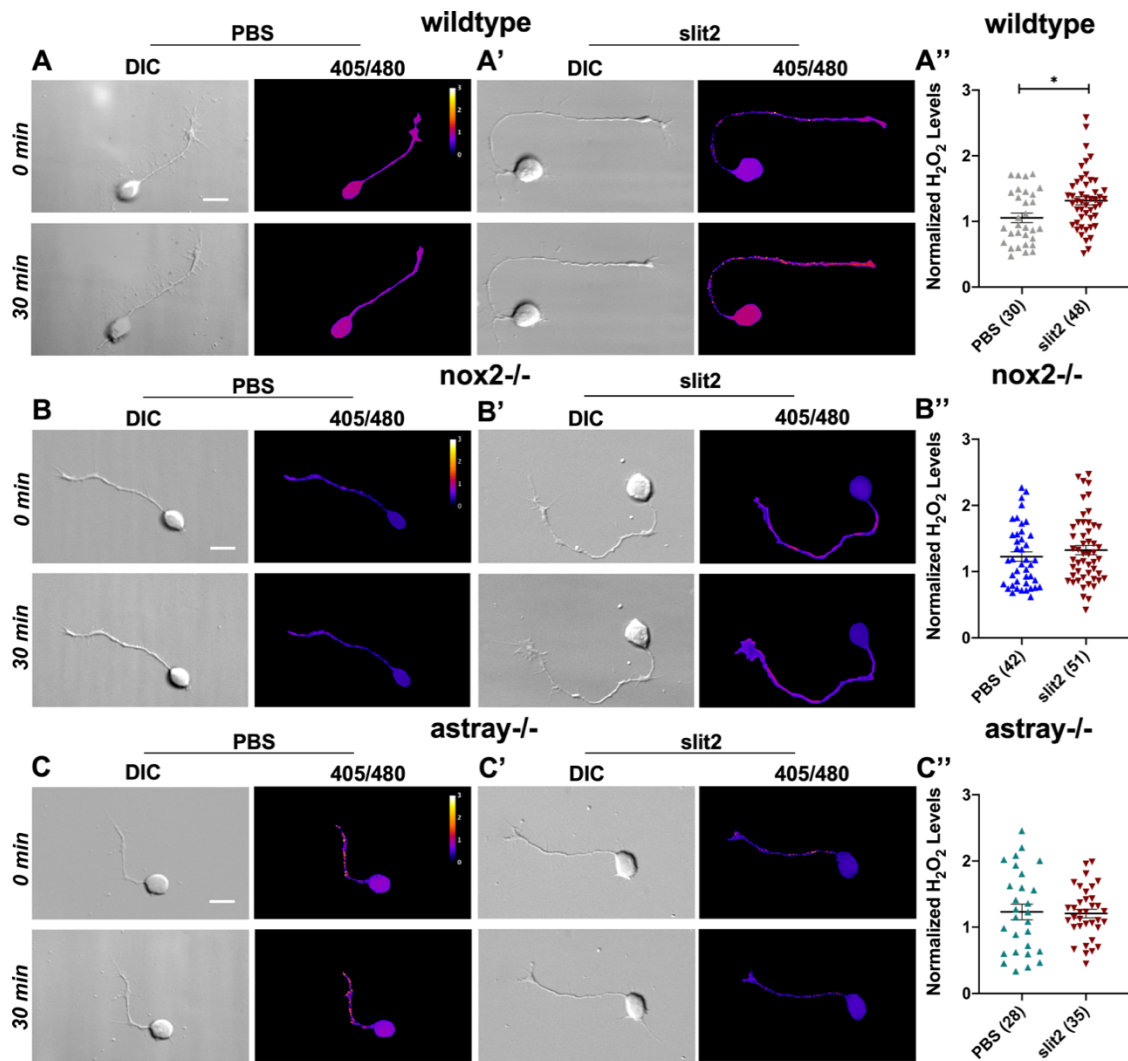


Figure 22: Slit2 causes an increase in intracellular H_2O_2 levels in wild-type RGCs, but not in *nox2*^{-/-} or *astray*^{-/-} RGCs.

(A) DIC and 405/480 ratio image of wild-type RGCs before (upper panel) and after 30 min (lower panel) of control (PBS) treatment. (A') DIC and 405/480 ratio image of wild-type RGCs before (upper panel) and after 30 min (lower panel) of slit2 treatment. (B-B') DIC and 405/480 ratio image of *nox2*^{-/-} RGCs before (upper panel) and after 30 min (lower panel) of control (PBS) (B) and slit2 (B') treatment. (C-C') DIC and 405/480 ratio image of *astray*^{-/-} RGCs before (upper panel) and after 30 min (lower panel) of control (PBS) (C) and slit2 (C') treatment. (A''-C'') Quantification of intracellular H_2O_2 levels at the growth cones measured as the average intensity in the 405/480 ratio images in RGC growth cones. 405/480 ratios were normalized to corresponding before treatment (0 min) ratio values for each condition. Data are shown as mean \pm SEM; n-value in parenthesis indicates the number of cells analyzed. Scale bars, 10 μ m. Mann-Whitney U test (A'', B''), Two-tailed Student's t-test (C''); * $p < 0.05$.

4.2.3 Partial loss of Nox2 and Robo2 combined does not affect formation of optic chiasm

Next, we investigated the relationship between slit2/Robo2 and Nox2 pathways *in vivo*. *astray* (*Robo2*) mutants have RGC axon pathfinding defects including midline crossing and projection in the optic tectum (Fricke et al., 2001; Hutson & Chien, 2002; Karlstrom et al., 1996). Similarly, *nox2* *-/-* mutants have defects in optic tectum innervation (Figure 8D; Weaver et al., 2018). To address whether Nox2 and slit2/Robo2 are in the same signaling pathway controlling RGC pathfinding, we performed genetic interaction experiments *in vivo*. Genes that are in the same signaling pathway are typically not expected to show an enhanced phenotype in double homozygous knockouts or mutants when compared to individual gene knockouts/mutants. On the other hand, weak phenotypes produced by heterozygotes or weaker alleles of different genes in the same pathway can be enhanced when combined. Since we were unable to generate double homozygous mutants for Nox2 and Robo2 thus far, we tested our hypothesis that Nox2 and Robo2 are in the same pathway with *astray/nox2* double heterozygous mutants along with individual heterozygous and homozygous mutants (Figure 22). The larvae were immunolabeled with RGC antibody zn-8 at 3 and 5 dpf to investigate the formation of the OC and innervation of the OT by RGC axons, respectively (Figure 23A). At 3 dpf, RGC axons from *nox2* *-/-* embryos were not as confined to the optic nerve as in wild-type embryos resulting in a wider ON, especially at the OC (Figure 23B). Similarly, *astray* *-/-* embryos also exhibited wider optic nerves along with pathfinding errors after crossing the OC, which is in agreement with previous reports (Fricke et al., 2001; Hutson & Chien, 2002; Xiao et al., 2011) (Figure 23B). We measured the thickness of ON originating from one eye at the chiasm (shown as red line in Figure 23B). ON thickness from individual homozygous mutants were significantly different from wild-type, *nox2* *+/-*, *astray* *+/-*, and *astray/nox2* *+/-* (Figure 23D). In all *nox2* *+/-*, *astray* *+/-* and *astray/nox2* *+/-* embryos, we did not observe mis-targeted RGC axons either before or after midline crossing, and the optic nerve thickness was not different in *astray/nox2* *+/-* when compared to individual heterozygous mutants (Figure 23B, D).

4.2.4 Partial loss of Nox2 and Robo2 combined alters tectal innervation *in vivo*

Then, we investigated at the final synaptic target of RGCs, the OT in midbrain. RGC axons project into the tectal neuropil, where they synapse with the tectal neurons to relay information from retina to brain. We have previously reported that *nox2* *-/-* mutants exhibit a diffuse innervation of the OT; however, we did not carry out a detailed quantification (Weaver et al., 2018). Here, we measured the OT area as outlined in Figure 23C. Since *nox2* *-/-* mutants have drastic RGC axon innervation defects and do not exhibit a clearly defined OT neuropil area that is quantifiable, we excluded this genotype from our quantitative analysis. *astray* *+/-* ($11839 \pm 403 \mu\text{m}^2$) and *nox2* *+/-* ($10471 \pm 385 \mu\text{m}^2$) individual heterozygous mutants did not show a difference in OT area compared to wild-type larvae ($11419 \pm 360 \mu\text{m}^2$; Figure 23E). However, *astray/nox2* *+/-* double heterozygous mutants had significantly decreased OT innervation area compared to wild-type ($8631 \pm 389 \mu\text{m}^2$; **** $p < 0.0001$), *nox2* *+/-* (* $p = 0.0159$), *astray* *+/-* (**** $p < 0.0001$), and *astray* *-/-* ($11001 \pm 454 \mu\text{m}^2$; *** $p = 0.0006$). *astray* *-/-* larvae did not show difference in overall OT area; however, mistargeted RGC axons were evident outside the tectal area in both *astray* *-/-* and *astray/nox2* *+/-* larvae (Figure 23C, red arrows). Taken together, partial loss of Nox2 and Robo2 individually did not affect RGC innervation of the OT; however, when combined partial loss of both genes affected retinotectal innervation *in vivo*.

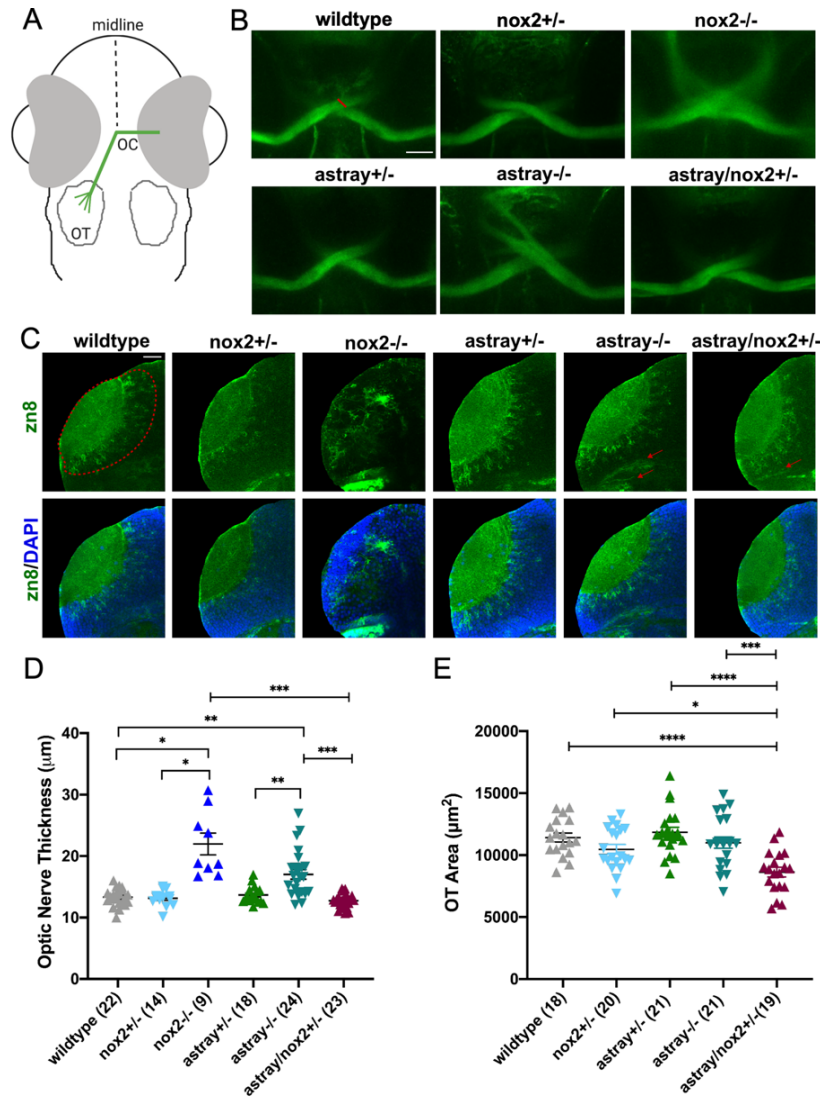


Figure 23: Partial loss of Nox2 and Robo2 together alters RGC pathfinding *in vivo*.

(A) Schematic presentation of zebrafish retinotectal pathway. RGCs (green) exit the eye as a single bundle optic nerve, cross the midline forming OC and grow dorsally to the contralateral OT in the midbrain, where they make synaptic connections. (B) Ventral views of zn8 staining from 3 dpf old embryos showing the OC. Measurements of optic nerve thickness were done from single optic nerves crossing the chiasm (red line). Optic nerve thickness from individual homozygotes (*nox2*^{-/-}, 21.9 ± 1.7 μm; *astray*^{-/-}, 17 ± 0.7 μm) were significantly different from wild-type (13.3 ± 0.3 μm; vs. *nox2*^{-/-} *p = 0.0154; vs. *astray*^{-/-} **p = 0.0016), *nox2*^{+/-} (13.1 ± 0.3 μm; vs. *nox2*^{-/-} *p = 0.0106; vs. *astray*^{-/-} **p = 0.0011), *astray*^{+/-} (13.6 ± 0.3 μm; vs. *nox2*^{-/-} *p = 0.0153; vs. *astray*^{-/-} **p = 0.0055) and *astray/nox2*^{+/-} (vs. *nox2*^{-/-} **p = 0.01; vs. *astray*^{-/-} ***p = 0.0002). (C) Dorsal views of zn8 staining from 5 dpf old larvae showing the optic tectum. Measurements of OT area were done by the outlined area in wild-type micrograph (dashed red line). Mis-guided RGC axons were evident in *astray*^{-/-} and *astray/nox2*^{+/-} larvae outside the OT (red arrows). (D) Quantification of optic nerve thickness. (E) Quantification of OT area. Data are shown as mean ± SEM; n-value in parenthesis indicates the number of embryos. Scale bar = 25 μm. Brown-Forsythe ANOVA, Dunnet's T3 multiple comparisons test (D); One-Way ANOVA/post-hoc Tukey test (E); *p < 0.05; **p < 0.01 ***, p < 0.001, ****p < 0.0001.

4.3 Discussion

4.3.1 Nox2-slit2/Robo2 interaction *in vitro*

In this chapter, we aimed to find a relationship between Nox2 and Slit/Robo guidance signaling. Slit1/2-Robo signaling plays a crucial role in preventing pathfinding errors in the optic nerve, in facilitating ventral midline crossing at the OC, and in formation of the optic tract (Fricke et al., 2001; Hutson & Chien, 2002; Plachez et al., 2008; Plump et al., 2002; Thompson, Barker, et al., 2006). We showed that Nox2 is required for slit2-mediated growth cone collapse *in vitro* (Figure 21). Pharmacological and genetic inhibition of Nox2 abolished the response of RGC growth cones to slit2. Hence, we speculate that slit2 might activate Nox2 to promote growth cone collapse. It was previously shown that phorbol ester induces growth cone collapse and causes actin bundle loss; since phorbol esters act as PKC activators, one possible scenario is that Nox2 activation via PKC could promote growth cone collapse (Zhou & Cohan, 2001). Furthermore, we found that slit2 increased intracellular H₂O₂ levels in the RGC growth cones, and we showed that this slit2-mediated H₂O₂ production requires functional Nox2 and Robo2 (Figure 22). These results suggested that slit2-mediated RGC growth cone collapse requires Nox2 *in vitro*. Further *in vitro* experiments can be performed on RGCs, such as growth cone turning assay. This assay allows measuring the response of a growth cone of cultured RGCs in response to a cue that is presented from an angle. It will be very interesting to perform this assay in roGFP2-orp1 expressing wild-type and *nox2* *-/-* RGCs. This will allow measuring both the response of the RGC and the H₂O₂ levels, hence, functionally linking the growth cone guidance to Nox2-mediated H₂O₂ production.

4.3.2 Nox2-Slit2/Robo2 interaction *in vivo*

Astray mutants, which are deficient in Robo2, have major pathfinding defects including axons diverging from optic nerve and RGCs projecting outside the tectal area (Fricke et al., 2001; Hutson & Chien, 2002). We used *astray*^{ti272z} allele, which is the functional null mutation for Robo2, to investigate the relationship between Nox2 and slit2/Robo2 *in vivo* (Figure 23). Since we did not have double homozygous *astray/nox2* *-/-* available for analysis, we investigated RGC guidance in double heterozygous mutants that have partial loss of functional Nox2 and Robo2 in addition to individual heterozygous and homozygous mutants. We theorized that if the Nox2 and Robo2 are in the same pathway, partial loss of functions could exhibit additive effects on RGC

guidance. A subset of RGCs from *astray* *-/-* embryos failed to cross midline properly and ended up projecting outside of OT, as reported previously (Fricke et al., 2001; Xiao et al., 2011). *nox2* *-/-* RGCs also exhibited pathfinding errors at optic chiasm, as the ON thickened and did not stay as a tight bundle. On the other hand, neither *astray* *+/-* and *nox2* *+/-*, or *astray/nox2* *+/-* showed any such clear pathfinding errors near the OC. One possible explanation for this result could be that if only a few axons have pathfinding errors in double heterozygous mutants, the immunolabeling of all RGCs might hinder visualizing those mistargeted axons, since the staining is too dense around OC. Hence, additional experiments are required to investigate detailed pathfinding phenotypes in double heterozygotes. For instance, sparse labeling of RGCs in double heterozygotes could reveal how individual RGC axons behave during midline crossing.

After midline crossing, RGC axons must project to their final synaptic targets in the OT. RGCs mainly project to the neuropil, where they synapse with tectal neurons to create a topographic map of the visual field. Slit family proteins are expressed in OT, and Robo2 has been shown to negatively regulate axon arbor formation (Campbell et al., 2007). Slit1a, but not Slit2, was found to be required for proper laminar pathfinding of RGCs through Robo2 signaling in OT (Xiao et al., 2011). In the work presented here, we found that the total OT area was decreased in double heterozygous *astray/nox2* *+/-* larvae, when compared to wild-type or single *astray* *+/-* and *nox2* *+/-* heterozygous mutant larvae (Figure 23). *nox2* *-/-* larvae had a strongly reduced OT innervation to a level where the OT was not clearly defined and prevented us from quantification (Figure 23C). *astray* *-/-* larvae showed RGC pathfinding errors at the OC and outside the OT, but the OT area itself was not significantly reduced (Figure 23C and E). Similar to *astray* *-/-* larvae, we also found RGCs projecting outside the OT in *astray/nox2* *+/-* larvae. Two conclusions can be drawn from these observations: (1) Slit2/Robo2/Nox2 signaling directs RGC guidance at the OC resulting in pathfinding errors in mutants thereafter. (2) Slit1-2/Robo2/Nox2 signaling could guide RGC axons in OT to the correct sublamina. However, in our study we did not investigate the pathfinding of individual RGC axons, which could reveal more details about the mutant phenotypes. Sparse labeling in *astray/nox2* *+/-* larvae could possibly provide further information. Taken together, we propose that targeting RGC axons in the OT is Nox-dependent, possibly through mechanisms involving Slit1-2/Robo2/Nox2 signaling.

Our results with cultured RGC neurons strongly suggest that Nox2 acts cell-autonomously with respect to cue-mediated growth and guidance. Our *in vivo* data on the other hand do not

provide direct proof that Nox2 acts cell-autonomously in RGC pathfinding because experiments were performed with larvae that are Nox2-deficient in all cells. There is the possibility that part of the severe OT innervation defects of *nox2*^{-/-} larvae is due to RGC-independent effects. *nox2*^{-/-} mutant larvae with a phenotype exhibit neuronal cell bodies in neuropil, which is normally devoid of cell bodies (Figure 23C). Hence, the altered RGC innervation of the OT in *nox2*^{-/-} larvae could be caused not only by an axonal pathfinding defect of RGC neurons lacking Nox2, but also by an improper formation of the OT due to the lack of Nox2 (and possibly Nox1 activation) in tectal cells. Thus, additional experiments will be required to test whether Nox2 has a cell-autonomous role in RGC pathfinding *in vivo*. The RGC-specific Nox2 knockout approach is very important to dissect the role of Nox2 solely in RGC guidance.

4.3.3 Analysis of individual RGC growth cone guidance

We conducted experiments on an established *bbug* zebrafish line *Tg(brn3c:GAL4, UAS:gap43-GFP)*, that express GFP in subset of RGCs, as well as other neurons such as hair cells (Robles et al., 2014). First, we generated *nox2* heterozygous line with the *bbug* background. This allowed us to generate *nox2* homozygous embryos and analyze the individual RGCs. Zaiyang Zang and Garima Baral, two rotation students, have worked on this project to analyze OT innervation by single RGCs. We looked from 3 dpf to 5 dpf zebrafish larvae and captured snapshots in time to compare the filopodial length, branching, and overall tectal projection of RGCs in wild-type and *nox2* mutant embryos. Examination of the overall phenotype of the RGC axons in wild-type and *nox2* mutant embryos showed that there is no difference in following criteria between wild-type and *nox2* mutant RGCs *in vivo*: total filopodial length, thickness of the innervated layer, number of branch points, and filopodia density (Figure 24).

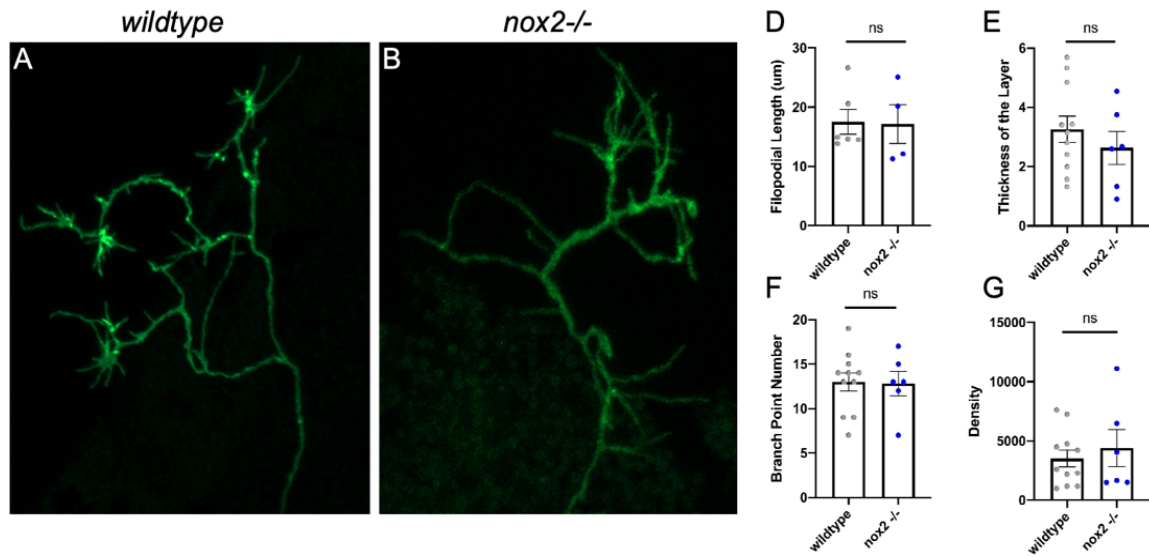


Figure 24: Imaging of individual RGCs in wild-type and *nox2*^{-/-} larvae.

The maximum intensity projections of RGCs from 3 dpf wild-type (A) and *nox2*^{-/-} (B) embryos were imaged in optic tectum. Total filopodial length (D), thickness of the tectal layer that each RGC innervated (E), number of branches (F) and the density of filopodial area (G) were measured. There was no difference found between wild type and mutants RGCs in all tested parameters (Mann Whitney Test for filopodial length, Student's t-test for others). Data are shown as mean ± SEM.

There are several possible reasons for not seeing difference between wild-type and mutant RGCs:

(1) The labeling of RGCs is random in each fish, and there are several types of RGCs that originate in retina and innervate different layers of OT. Currently, we do not have a way to differentiate between what type of RGC we are imaging and which layer it is innervating. However, a previous study showed that some of the RGC phenotypes change with pharmacological inhibition of Nox in sparsely labeled transgenic fish (Gauron et al., 2016).

(2) We reported that in general *nox2* mutant fish, only the 25% of the embryos from homozygous parents exhibit the mutant phenotype and the mechanism behind it was discussed in Chapter 3. Considering that, there is a very low chance to see a *nox2*^{-/-} with mutant phenotype, as not all of *bbug* crossing exhibit individual RGC labeling. Furthermore, the sparse labeling is not seen in every embryo, some do not show labeling at all. Altogether, this limits our ability to look at mutants that are exhibiting loss-of-Nox2 effects.

(3) Finally, we have tried treating embryos with Nox inhibitor Celastrol, to repeat previous findings by Gauron et al. and also prevent possible compensation mechanisms (Gauron et al., 2016). However, we showed that compensation could cause a phenotype only in a subset of *nox2*

-/- embryos (Chapter 3) and we did not see an effect of Celestrol (data not shown). As discussed above, we have limitations to study *nox2* -/- with the mutant phenotype with the current approach. Furthermore, the regime for Celestrol treatment still needs to be adjusted. Future experiments with dose-response analysis and different incubation times might enlighten some of the discrepancies we observed with Nox inhibition.

4.3.4 The role of Slit/Robo during midline crossing

Slit/Robo pathway is not only essential for RGC axon guidance but also for commissural axon guidance at the midline crossing. Accordingly, in addition to optic tract in general *nox2* -/- mutants, we observed defects in axon projections at anterior commissure and spinal cord, all of which require guidance of commissural axons (Chapter 3.2.1). Hence, the proposed interaction between Slit/Robo and Nox signaling could be broader, affecting axon guidance throughout the CNS. Here, I will discuss a more general role of Slit/Robo signaling and its interaction with Nox.

Zebrafish CNS has a bilateral symmetry along the midline like other organisms and axon tracts interconnects the left side of the organism to their right side. These connections are named commissures, and by 28 hpf zebrafish develops major axon tracts along commissures throughout the CNS (Chitnis & Kuwada, 1990). During development, commissural axons cross the midline with the help of guidance cues that are secreted by cells at the midline (Neuhaus-Follini & Bashaw, 2015). First, attractive cues draw the commissural axons to the midline. Then, axons become gain sensitivity to repulsive cues to exit the midline and these repulsive cues also prevent re-crossing after reaching the midline.

While netrin-1 and SHH attracts the commissural axons to midline, slits act as midline repellents (Long et al., 2004; Tessier-lavigne & Goodman, 1996). *Slit* mutants exhibit aberrant projection of commissural axons or stalled axons around the midline (Long et al., 2004). Furthermore, commissural axons from *Robo* mutants exhibit several axon pathfinding defects at the midline, including re-crossing the midline (Kidd et al., 1998; Seeger, Tear, Ferres-Marco, & Goodman, 1993). Slits and netrin-1 are both expressed at the midline; however, the response of axons are different before and after the midline. The netrin-1 attraction brings commissural axons to the midline and after crossing, slits repel the commissural axons to keep them in tract. But how do axons respond to slits but not netrin-1 after midline crossing, considering that netrin-1 still exist at the midline? Netrin-1-DCC pathway could actually interact with slit-Robo2 signaling to

modulate axonal guidance: Robo activation ceases the attractiveness to netrin-1 by binding to DCC after midline crossing in mammalian commissural axons (Stein & Tessier-Lavigne, 2001). Moreover, slit-Robo2 signaling suppresses attractive netrin-1 signal for proper anterior commissure and supraoptic tract formation during zebrafish anterior telencephalic neuron development (Zhang, Gao, Zhang, Sun, & Peng, 2012). Hence, slits can work together with other guidance cues, such as netrin-1 by interfering with growth cone responsiveness. In support of this, we also showed that cultured RGC growth cone response to netrin-1 cue depends on Nox activity (Haley Roeder, unpublished data). Considering both cues regulate axon guidance in optic tract and midline crossing, and *nox2* *-/-* mutants exhibit axon projection errors in both places, it is highly likely that Nox2 involvement in guidance regulation is a more general mechanism. Therefore, it will be interesting to investigate whether such interaction between netrin-1 and slit2/Robo2 signaling occurs during different stages of RGC guidance, and whether this interaction involves Nox activity.

CHAPTER 5. TOOLS TO INVESTIGATE NOX2 IN RGC DEVELOPMENT

5.1 Studying cell-autonomous effects of Nox2 in RGC guidance

5.1.1 Introduction

Current general *nox2* $-/-$ mutants revealed the Nox2-specific roles in overall development of zebrafish; however, because *nox2* $-/-$ mutant larvae with mutant phenotype have additional defects inside and outside the nervous system, RGC-specific role of Nox2 *in vivo* remains to be determined. *nox2* $-/-$ mutants recapitulated the RGC phenotypes that were observed by transient pharmacological Nox inhibition, suggesting that the effects on RGC phenotypes were specific to loss of functional Nox2. However, both incomplete penetrance of the mutation (Chapter 3.2.5) and defects other than RGC guidance (Chapter 3.2.1) suggest that RGC-specific roles of Nox2 need further investigation. Our *in vitro* studies with *nox2* mutant RGCs support the cell-autonomous effects of Nox2 on RGC guidance. Here, I describe additional tools that I have developed to investigate the role of Nox2 in RGC-specific manner, as well as general tools that can be used to further investigate Nox2 function in zebrafish system.

5.1.2 Generating RGC-specific *nox2* mutant zebrafish

Tissue-specific mutation approaches for zebrafish have been recently published (Ablain et al., 2015; Zhou et al., 2018). The approach utilizes the Tol2 system for inducing germline transgenesis (Kwan et al., 2007). Tol2 is an autonomously active transposon and can create insertions in zebrafish genome very efficiently (Kawakami et al., 2004). The cloning principle is recombination based to achieve site specific cloning. 5' entry vectors (p5E) harbor the promoter of interest, middle entry vectors (pME) have the gene-of-interest, and 3' entry vectors (p3E) have the 3' regulatory regions. Each sequence of interest flanked by recombination sites. Finally, there is a destination vector in which all entry vectors are cloned into and carries a transgenesis marker for positive selection. In the presence of recombinase enzyme, these recombination sites allow gene expression under the control of a specific promoter as described in Figure 4.

In order to study RGC-specific effects of Nox2, we adopted the Tol2 transgenesis approach. We used *ath5* promoter to drive expression of Cas9-2A-mCherry, and ubiquitous expression of

two guide RNAs targeting zebrafish *nox2* gene in a Tol2 construct that has GFP expression under heart promoter *cmcl2* (Figure 25A). The construction of the plasmid was described in Chapter 2.4.3. Once integrated into the genome, this plasmid allows expressing Cas9 endonuclease and mCherry specifically in RGCs, when *ath5* promoter is turned on with RGC differentiation onset. Alternatively, we generated a construct for sparse-labeling RGCs with H₂O₂ biosensor roGFP2-orp1 (Figure 25B). For this approach, we received an established transgenic zebrafish line *Tg(isl2b:Gal4;myl7:TagRFP)* and generated a Tol2 construct for injecting into embryos of this transgenic line. The construct expresses Cas9 and roGFP2-orp1 under UAS promoter and two guide RNAs targeting *nox2* ubiquitously. This system relies on the transcription activation by Gal4-UAS system, which enables expression of desired gene in tissue-of-interest (Kawakami et al., 2016). In our construct, UAS-driven *cas9* and roGFP2-orp1 expression will only be initiated in the presence of Gal4, and Gal4 expression is driven by another RGC-specific promoter *isl2b*. *isl2b* promoter turns on by 30 hpf in ventro-anterior retina, and labels vast majority of RGCs (Pittman, Law, & Chien, 2008). Sparse labeling will be achieved through injection and will allow us to visualize individual RGC growth cone dynamics, while enabling measurement of intracellular H₂O₂ levels. Although this construct was validated by sequencing, signal was not detected upon injecting the construct into the Gal4 line. Hence, additional verifications are needed to be performed.

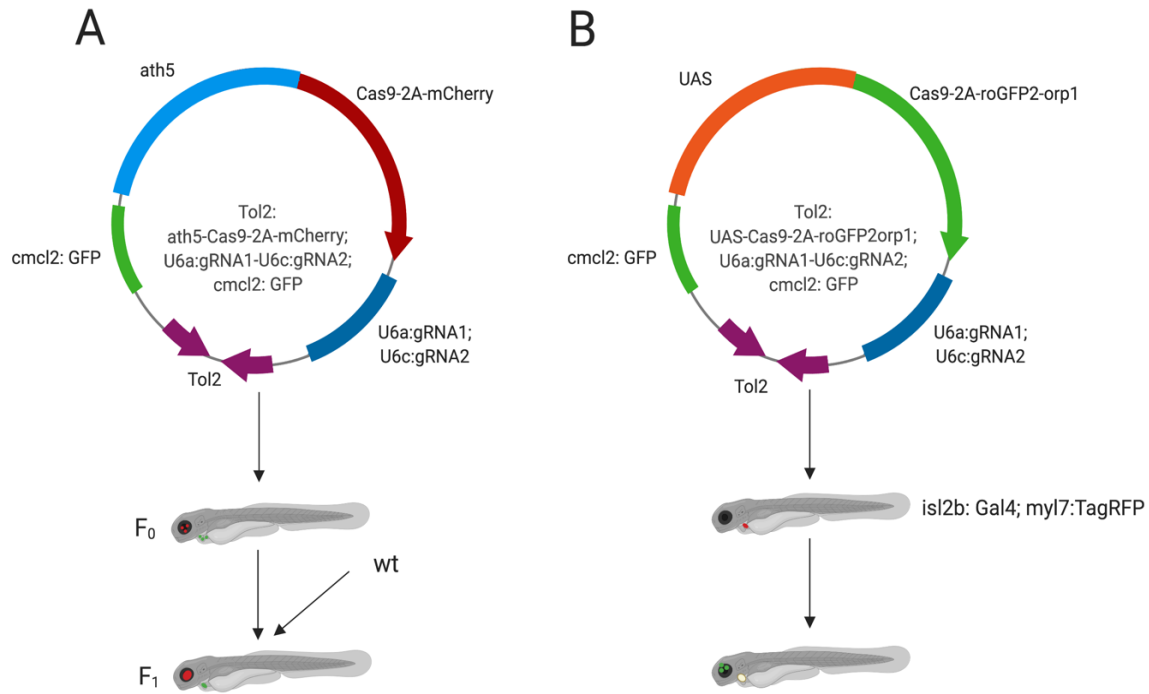


Figure 25: Construct design for tissue-specific knock-out approach.

(A) RGC-specific *nox2* knockout approach. *Tol2:ath5-Cas9-2A-mCherry;U6a:nox2gRNA1-U6c:nox2gRNA2; cmcl2:GFP* construct was generated by Gateway cloning. The injection of this construct will create chimeric embryos with an insertion of the construct through Tol2 sites. Upon breeding the initial injectants with wild-type (wt) fish, stable lines will be created in the F1 generation. (B) Sparsely labeled RGC-specific *nox2* knockout approach. *Tol2:UAS-Cas9-2A-roGFP2orp1; U6a:nox2gRNA1-U6c:nox2gRNA2; cmcl2:GFP* construct was generated by Gateway cloning. Transgenic fish line *Tg(isl2b:Gal4;myl7:TagRFP)* was obtained from Bonkowsky lab. The injection of Tol2 construct into the line allows expression of Cas9 and roGFP2-orp1 in subset of RGGs.

Initial injections of the tissue-specific knockout plasmids (Figure 25) exhibited transgenesis marker, however, the RGCs labeling was not clear. Recently, Dr. Deng's research group (Yueyang Wang) established an alternative approach because mCherry expression was found to be dim when expressed along with Cas9. Hence, the Cas9 and tissue labeling needs to be separate for a higher imaging resolution. In this approach, two separate Tol2 constructs needs to be generated in order to achieve better labeling of the tissue of interest: (1) Cas9 expression under tissue specific promoter (*Tol2:ath5-Cas9; cmcl2:GFP*), (2) Fluorescent marker expression under tissue specific promoter and guide RNAs targeting gene of interest (*Tol2:ath5-GFP-U6a:nox2 gRNA1-U6c:nox2 gRNA2*) (Figure 26). Alternatively, roGFP2-orp1 can be used as RGC marker instead of GFP to

record the H₂O₂ levels. After establishing stable lines for both, resulting adults can be crossed to bring two components together.

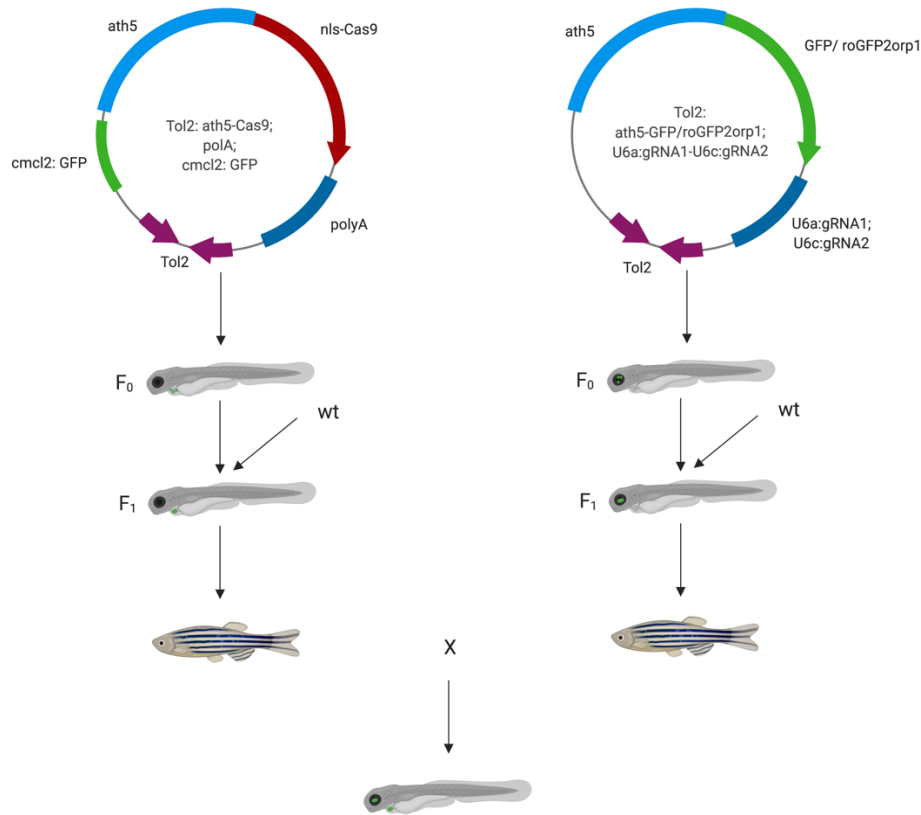


Figure 26: Alternative approach for tissue-specific knockout construct design.

Two different Tol2 constructs are needed for driving expression under RGC-specific promoter *ath5*. *Tol2:ath5-Cas9; cmcl2:GFP* construct allows Cas9 expression in RGCs, while *Tol2:ath5-GFP-U6a:nox2 gRNA1-U6c:nox2 gRNA2* construct allows GFP expression in RGCs and ubiquitous expression of *nox2* targeting gRNAs. Alternatively, roGFP2-orp1 can be used instead of GFP to measure H₂O₂ levels simultaneously.

5.1.3 Cell Transplantation

Cell-autonomous effects of Nox2 in RGC growth and guidance can also be analyzed with the current general *nox2* mutants. Cell transplantation between wild-type and mutant embryos enables investigation of cell-autonomous effects by transferring wild-type cell-of-interest in mutant background, or mutant cell-of-interest in wild-type background (Carmany-Rampey & Moens, 2006; Kemp et al., 2009). In order to investigate the cell-specific role of Nox2 in RGC guidance, the wild-type and *nox2* ^{-/-} mutant cells can be transplanted to the global *nox2* ^{-/-} mutant and wild-type embryos, respectively. If the effects of Nox2 is cell-autonomous, then regardless of

the genotype of surrounding cells, the RGCs will exhibit mutant phenotype. However, if Nox2 acts non cell-autonomously, then the behavior of RGCs will depend on the environment that they are transplanted into: *nox2* ^{-/-} cells in wild-type embryos will behave normally, while wild-type cells in mutant embryos will have mutant phenotype. The approach for cell transplantation in zebrafish embryos has previously been published (Kemp, Carmany-Rampey, & Moens, 2009; Li, White, & Zon, 2011) and outlined in Chapter 2.4.4. The optimal time window for cell transplantation is between 1000-cell stage and dome stage. Although cells are not committed to a fate at this stage, blastula-stage cell transplantations yield in higher number of embryos to work with. Cells located at the top of the animal pole are destined to become forebrain and eye, hence, transplanted cells should be transplanted into this region when studying RGCs.

So far, we have only been able to practice blastula-stage transplantations. The most important aspect has been the timing. Manual dechoriation is highly time-consuming process and interferes with the time window of cell transplantation scheme. Once cells are beyond 4 hpf, the individual cells cannot be taken via this method. We ideally want to be able to transplant ~50-100 embryos in each session to have enough samples to analyze per experiment. So far, it was hard to get ~10 embryos that remain alive throughout the process. Furthermore, the injected donor embryos are more prone to dying after dechorionated. Therefore, additional practice is highly recommended to get better in hand dechorionation of early stage embryos in a relatively short amount of time.

5.1.4 RGC-specific Nox2 rescue in general *nox2* $-/-$ mutants

Tissue-specific rescue of the phenotype is another approach to support cell-autonomous role for Nox2 in the current general *nox2* $-/-$ mutants. The goal here is to express wild-type Nox2 in RGCs in *nox2* $-/-$ background. I cloned the full-length zebrafish *nox2* gene first into zebrafish expression vector pCS2+, and into Gateway middle entry vector pME as described in Chapter 2.4.1. Using validated pME-*nox2* construct, the full-length *nox2* gene needs to be expressed under RGC-specific promoter *ath5* with Gateway cloning. Resulting Tol2 plasmid can be injected to *nox2* $-/-$ mutants in order to create a stable *nox2* $-/-$ line with wild-type *nox2* expression only in RGCs (Figure 27). To visualize RGC behavior, fluorescent protein can be expressed in RGCs or, RGCs can be immunolabeled with zn8 antibody, or through lipophilic dye injections directly into GCL, the projections can be detected throughout the retinotectal pathway (Monte Westerfield, Zon, & Detrich III, 2009).

5.1.5 Conclusion

The RGC-specific approaches described here provide essential information on the specific involvement of Nox2 in guidance and development of RGCs. Cell transplantation and RGC-specific *nox2* expression allow immediate analysis in existing general *nox2* $-/-$ mutants. However, I believe that the RGC-specific *nox2* mutant approach is more reliable and efficient than the other two approaches. For cell transplantation, although there is some targeting for tissue specificity, it

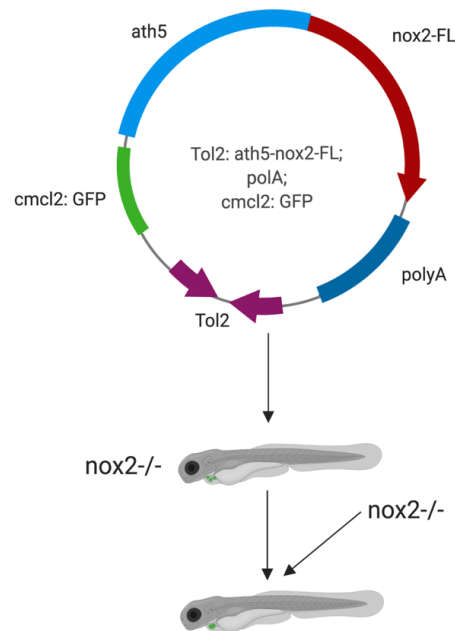


Figure 27: RGC-specific full length Nox2 expression.

Proposed construct design for *Tol2:ath5-nox2-FL; cmcl:GFP*. Individual entry and destination vectors are ready to use, and Gateway reaction is needed to complete the construct.

will be hard to keep it very consistent among different animals and experiments. Furthermore, there can always be other cell types transplanted and affected by the mutation, which will prevent a pure assessment of cell-autonomous activity of Nox2. RGC-specific Nox2 expression is a good approach to validate the current *nox2* mutants, that could show that RGC effects are specific. However, at this point starting over RGC-specific knockout approach and investigating loss of Nox2 directly in RGCs seem to be more efficient in terms of time and resources. This approach allows examination of RGCs directly by fluorescent labeling and is very accurate to induce mutations in tissue-specific manner (Ablain et al., 2015; Zhou et al., 2018). Therefore, in the near future this approach can be used to study cell autonomous effects of Nox2 during RGC guidance.

5.2 Alternative Ways for Measuring Nox activity in Zebrafish Cells

5.2.1 Introduction

An essential way to show that the mutation causes non-functional protein is to use antibodies targeting the specific portion of the protein that is not expected to be found in the mutant protein. However, we do not have any Nox2 antibody that specifically recognizes zebrafish Nox2 protein at the moment. In order to prove non-functionality of the Nox2 in our mutants, we used H₂O₂-biosensor imaging in zebrafish embryos. Although this is a powerful tool, it has some limitations. (1) Detection occurs at a whole tissue (i.e., retina or whole body) and lacks information on the levels in specific cell types, (2) H₂O₂ detection is not specific to Nox enzymes. To overcome these limitations, alternative ways for detection of H₂O₂ at the cellular level and measuring Nox enzymatic activity can be achieved. Here, I will describe two possible approaches that I initiated and can be extended further in the future.

5.2.2 RGC-specific expression of roGFP2-orp1 biosensor

Avoiding measurements of H₂O₂ production from surrounding tissue and assessing H₂O₂ levels specifically in RGCs will provide more insight on the relationship with guidance and Nox pathway. To achieve this, the H₂O₂-specific biosensor roGFP2-orp1 could be expressed in RGCs only. Tissue-specific gene expression strategy was described in Chapter 5.1.2. roGFP2-orp1 has already been cloned in pME vector, and it is ready to use (pME-roGFP2-orp1). roGFP2-orp1 can be cloned under *ath5* or *isl2b* promoter in order to drive expression in RGCs with Gateway cloning.

For instance p5E-ath5, pME-roGFP2orp1, p3E-polyA and pDEST-Tol2-CG2 vectors could be combined through Gateway cloning to generate *Tg(ath5:roGFP2-orp1; cmcl2:GFP)* (Figure 28A). Alternatively, RGCs can be sparsely labeled to study H₂O₂ levels in individual RGCs. To do so, Gal4-UAS approach can be taken. In this approach, transgenic fish *Tg(isl2b:Gal4; myl7:TagRFP)* can be injected with a UAS:roGFP2-orp1 construct (Figure 28B). For this approach, roGFP2-orp1 needs to be cloned under UAS promoter. Both approaches will allow measuring intracellular H₂O₂ levels either in all RGCs, or in individual RGCs. Sparse labeling approach is more advantageous, since it can allow detection of H₂O₂ levels in individual RGCs. Through time-lapse confocal imaging, how different dynamics and axon guidance relates to intracellular H₂O₂ levels can be investigated. For instance, tracing a single RGC along optic tract will allow correlating the intracellular H₂O₂ levels with the certain guidance cues.

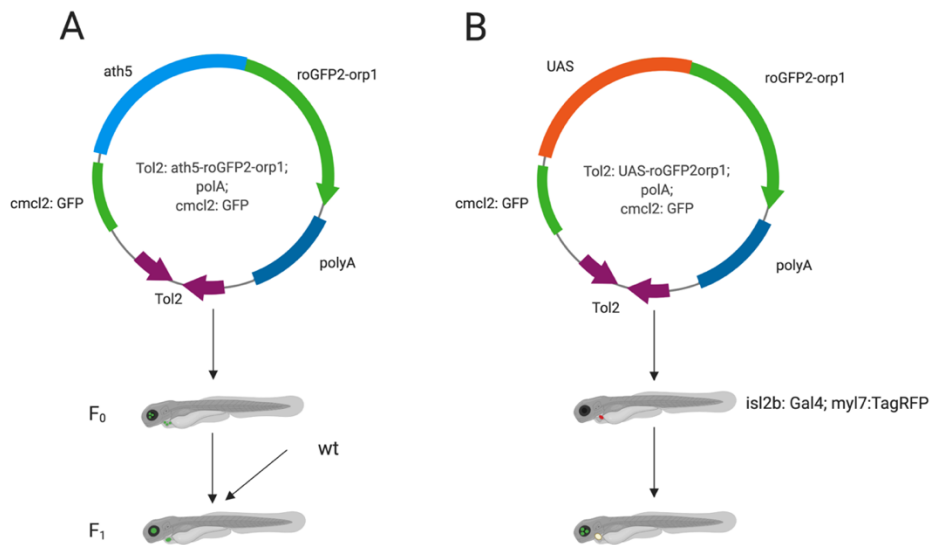


Figure 28: Construct design for RGC-specific roGFP2-orp1 expression.

(A) RGC-specific roGFP2-orp1 expression can be achieved with establishing transgenic line *Tg(ath5:roGFP2-orp1; cmcl2:GFP)*. (B) Alternatively, transgenic fish *Tg(isl2b:Gal4; myl7:TagRFP)* can be injected with *Tol2:UAS-roGFP2orp1* construct for sparse labeling of RGCs.

5.2.3 NADPH Oxidase Assay

An alternative approach to measuring Nox activity is detecting the NADPH/NADP⁺ ratio. As described in Chapter 1, Nox enzymes transfer an electron from NADPH to oxygen and generate

NADP⁺ and superoxide. Thus, bioluminescent cell-based NADP⁺/NADPH detection assays could be a powerful alternative to detect the activity of Nox enzymes. These assays have mainly been used in cell culture systems and were not previously adopted for detection in zebrafish cells. To test whether we can use this assay in our system, total zebrafish cells from 2 dpf embryos were dissociated as described in Chapter 2.4.5. Different number of cells were subjected to the assay for validation and PBS was used as a background luminescence control. We measured luminescence every 10 min to measure total NADP⁺ and NADPH levels and saw that the NADP⁺/NADPH ratio can be detected from zebrafish cells. The luminescence levels increased with increasing cell numbers, and plateau was reached with the highest number tested (Figure 29A). Although this system is good to detect total levels, this information does not provide any insight into Nox activity because it allows detection of both NADP⁺ and NADPH presence. In cells with active Nox, NADPH levels are expected to be less and NADP⁺ levels are expected to be higher, compared to cells with less active Nox. Hence, individual detection of NADP⁺ and NADPH was required to be able to correlate with Nox activity, and this assay allows such detection. By measuring NADP⁺ and NADPH separately, we were able to measure the ratio of the abundance of NADPH to NADP⁺ as a measure of Nox activity (Figure 29B-D). The ratio of the NADPH/NADP⁺ was consistent among different cell numbers, although there was a higher ratio in 25,000 cells, which seems to be an experimental artifact. This experiment also suggested that low-cell numbers, such as 10,000, might not be reliable since the luminescence reading was not very different from the background (PBS). Additional experiments are required to validate that Nox activity can be assessed through this assay. We performed the assay on embryos that were treated with either vehicle control (0.1% DMSO) or Nox-inhibitor Celastrol, however, results were not consistent (data not shown). Hence, further verifications are still required to detect Nox activity. Once it is validated, this assay can be used in mutant embryos as an assessment of Nox activity.

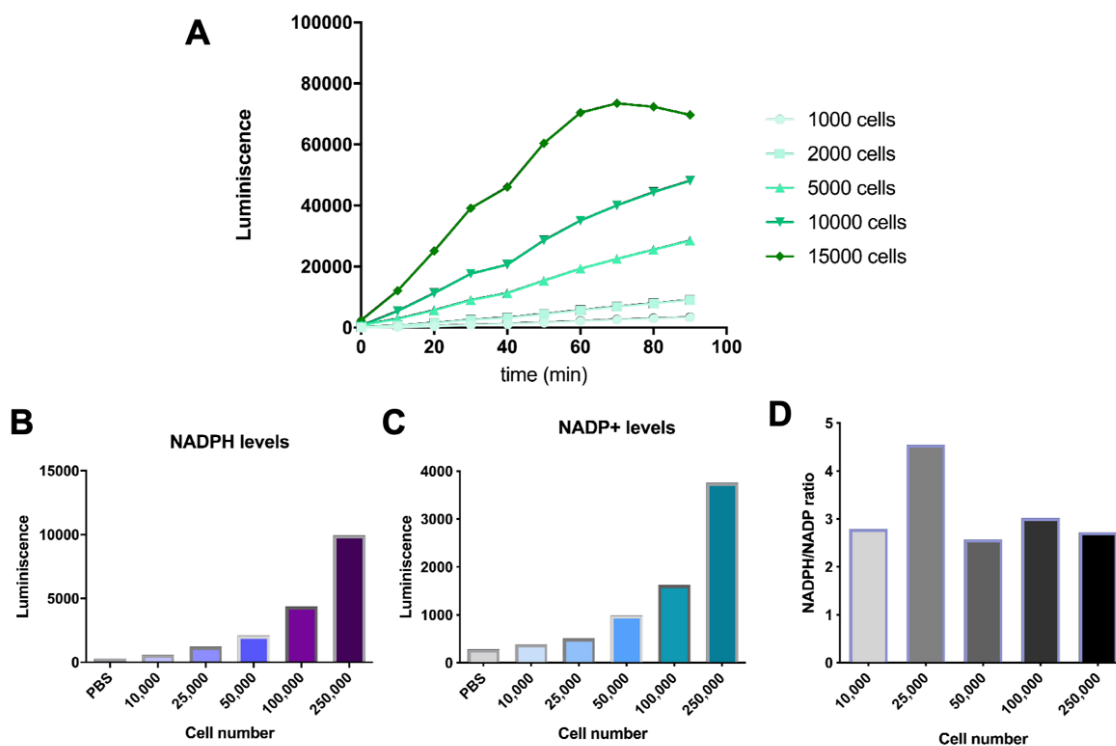


Figure 29: NADP/NADPH Glo assay validation in zebrafish cells.

Assay validation with increasing number of zebrafish cells demonstrated successful reading of bioluminescence from isolated zebrafish cells (A). The luminescence signal seemed to reach plateau for the 15000 cells after 90 min of incubation. Measurement of NADPH (B) and NADP+ (C) levels individually in different number of zebrafish cells. The ratio of NADPH/NADP+ (D) can be used to assess Nox activity.

CHAPTER 6. GENERAL DISCUSSION

The data presented in previous chapters suggest an interaction between Slit2/Robo2 and Nox2 signaling that eventually generates intracellular H_2O_2 to modulate growth cone guidance. Our proposed mechanism is shown in Figure 30. From the data presented so far, we propose that slit2-Robo2 interaction at the surface of RGC growth cones could initiate a signaling pathway that leads to activation of Nox2 via cytosolic subunits such as p47phox or Rac. Cytosolic subunits are translocated to the plasma membrane, where gp91^{phox}-p22^{phox} resides for a full activation of the enzyme complex. Once active, Nox2 transfers an electron from NADPH to molecular oxygen to produce superoxide, which is almost immediately converted to H_2O_2 either spontaneously or by extracellular dismutase enzyme (Sod3). H_2O_2 can either enter the cell through aquaporins to post-translationally modify redox-sensitive proteins such as actin or oxidize receptor proteins extracellularly. The exact target(s) of H_2O_2 in this signaling pathway is not known in RGCs; however, there are multiple candidate redox-sensitive proteins that are involved in growth and guidance regulation. Upon target oxidation, a change in cytoskeletal dynamics cause growth cone collapse and repel the growth cone from slit2.

The intracellular signaling initiated by Nox2-mediated H_2O_2 is not limited to actin and actin regulatory proteins that modulate growth cone dynamics. Although our focus is the redox targets that modulate actin machinery, there are several other mechanisms in which Nox2 could act downstream of slit2/Robo2 at the growth cones. For instance, Nox2 activation can be an intermediate mechanism that could alter gene expression for prolonged effects of guidance cues (Turpaev, 2002). Another possible mechanism is interfering with microRNA action to modulate actin-severing protein, which will be discussed in Chapter 6.1.3. In addition, ROS could potentially modify extracellular proteins to modulate long-range, extracellular signaling. One possible scenario is the redox regulation of extracellular matrix proteins, which in turn regulates the growth cone guidance (Eble & De Rezende, 2014).

This proposed mechanism is expected to be valid only if the ROS increase is very local and not spread over the whole growth cone. Considering the half-life of ROS molecules (10^{-9} to 10^{-5} sec), local ROS activity is favored (Giorgio et al., 2007). The longer ROS molecules stay in the environment, there is a higher probability that cellular antioxidant mechanisms act and eliminate their presence (Birben et al., 2012). Hence, it is highly likely that local ROS production

at the growth cones start autocrine signaling and do not affect neighboring growth cones. However, whether cue-mediated ROS initiate a paracrine signaling and help directing the adjacent growth cones should also be investigated.

In this chapter, I will discuss the signaling downstream of Slit2/Robo2 which could potentially result in Nox2 activation. Then, I will discuss the role of Nox-mediated H_2O_2 in intracellular signaling that could modulate the cytoskeletal dynamics for growth cone guidance.

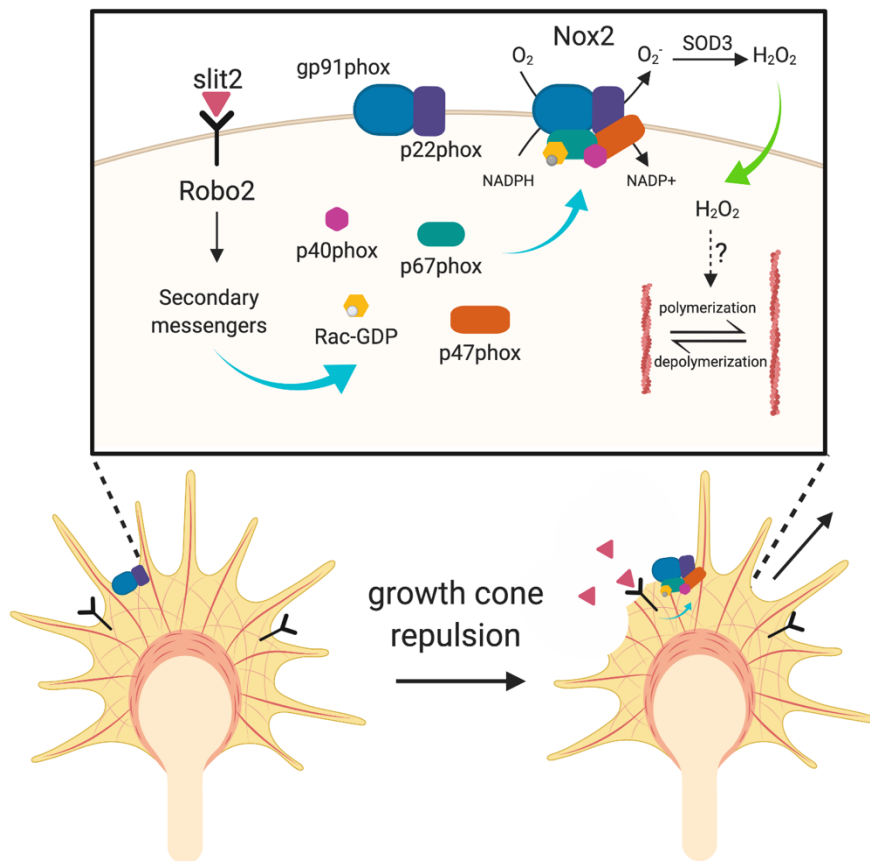


Figure 30: Proposed mechanism for Slit/Robo mediated Nox2 activation at growth cones.

Schematic representation of the signaling events leading to Nox2 activation at the growth cone plasma membrane in response to repulsive slit2 is shown. Slit2-Robo2 downstream secondary messengers such as srGAPs or microRNAs could initiate Nox2 activation through cytosolic subunits. Active Nox2 produces H_2O_2 which can alter actin machinery to modulate growth cone collapse.

6.1 The signaling downstream of Slit/Robo interaction

Slits are highly conserved chemorepellents and bind to Robo receptors, which are single pass transmembrane proteins without any enzymatic activity. Hence, downstream intracellular signaling events are required to propagate Slit-mediated growth cone guidance. Main targets downstream of Slit/Robo signaling involves cytoplasmic kinases, actin and microtubule cytoskeleton (Blockus & Chédotal, 2016). Upon slit binding to Robo on growth cone surface, key players in cytoskeletal arrangement are recruited to promote proper growth cone response. Here, I will describe some of the downstream targets of Slit/Robo signaling. Although their connection to Noxes are not established yet, I will discuss the possible mechanisms that potentially link Noxes to Slit-mediated signaling.

6.1.1 Slit-Robo GTPase activating proteins (srGAPs)

One important downstream effector of Slit/Robo signaling is Slit-Robo GTPase activating proteins (srGAPs). There are several srGAPs that have been identified in Slit-mediated signaling so far, and each selectively act on different Rho family GTPases, Rho, Rac and Cdc42, to modulate their actions. The current understanding of the function of srGAPs is that, upon Slit-Robo interaction at the growth cone, srGAPs are activated by binding to Robo and block Rho GTPases (Wong, Park, Wu, & Rao, 2002). Inactivation of Rho GTPases in turn inhibits actin polymerization and lead asymmetric rearrangement of cytoskeleton, depending on the localization of secreted slit. Thus, growth cones are repelled from Slit source (Lucas & Hardin, 2017).

The function of srGAPs could be a more complex mechanism than the direct inactivation of Rho GTPases and actin depolymerization. For instance, srGAP2 inhibits Rac1 activity, which in turn blocks formin-mediated actin severing during phagocytosis (Mason, Heimsath, Higgs, & Soderling, 2011). srGAP3 mediated Rac1 inactivation requires srGAP1 and srGAP2 binding to srGAP3, independent from their GTPase activities; suggesting srGAPs could have a wider function in regulating intracellular signaling (Ma et al., 2013). Furthermore, Rac inactivation could promote Cdc42 activity that stimulates F-actin bundling and filopodia formation, or RhoA activation which could promote formin-mediated actin nucleation (Narumiya, Tanji, & Ishizaki, 2009; Nimnual, Taylor, & Bar-Sagi, 2003; Raftopoulou & Hall, 2004). Thus, srGAP activity does not always

promote actin depolymerization and its action could participate in the dynamic nature of the cytoskeleton.

Although there has been no evidence for an interaction between srGAPs and ROS signaling so far, there are two important characteristics of srGAPs that could link them to Nox-mediated signaling. (1) srGAPs bind to membrane bound Robo intracellularly upon Slit-Robo interaction. Furthermore, srGAPs harbor an SH3-domain that could potentially bind and recruit cytosolic subunits of Nox2 to the membrane, in close proximity to Robo. Once Nox2 is activated locally, it can produce H₂O₂ to modulate intracellular signaling near Slit-Robo interaction, which could contribute to local alteration of cytoskeleton. (2) srGAPs could alter activity of Rac, which is a component of Nox2 cytosolic subunits. Either inactivation of Rac directly, or leading activation of Rac by modulating other Rho GTPases could alter the Nox2 activity. Future experiments investigating the binding of srGAPs to Nox2 and assessing their cellular localization will give more insights to these possibilities. Furthermore, srGAP knockdown studies can be conducted to see how Nox2 activity is modulated. A simple experiment would be measuring the H₂O₂ levels in srGAP mutant RGCs in response to slit2.

6.1.2 Cofilin

Cofilin is an actin binding protein that promotes disassembly of actin filaments. It is also an important candidate for supporting interaction between slit2/Robo2 and Nox2, as cofilin itself is a redox target. In non-neuronal cells, slit2 can activate cofilin to prevent epithelial cell migration (Huang et al., 2011). In neuronal cells, slit2 was shown to increase cofilin in growth cones of *Xenopus* RGCs through mechanisms involving protein translation (Piper et al., 2006). Until recently, the mechanism how slit2 increases cofilin translation was unknown. Bellon et al. showed that developing *Xenopus* RGC have a rich microRNA repertoire, and miR-182 is the most abundant microRNA (Bellon et al., 2017). miR-182 normally blocks translation of cofilin mRNA, and slit2/Robo interaction inhibits the miR-182 to release repression on cofilin mRNA. Cofilin seems to be an interesting target to investigate, as its action can be regulated by both slit2/Robo and Noxes. Redox regulation of cofilin will be further discussed in Chapter 6.2.2.

6.1.3 microRNAs

As discussed above, microRNAs can be a downstream target of slit/Robo signaling. On the other hand, slit/Robo signaling is also under control for microRNAs. Recently, miR-92 was shown to repress Robo1 translation to modulate sensitivity of commissural axons during midline crossing (Yang et al., 2018). Furthermore, miR-218 was found to be expressed from the intron of slit genes, that in turn negatively regulated slit/Robo signaling during vascular patterning (Small, Sutherland, Rajagopalan, Wang, & Olson, 2010). Considering the complex involvement of microRNAs in slit/Robo signaling, can there also be a mechanism by which ROS can mediate microRNA function at the growth cones? It is known that microRNAs can be regulated by oxidative stress in neurological disorders (Konovalova, Gerasymchuk, Parkkinen, Chmielarz, & Domanskyi, 2019). Furthermore, the interplay between microRNAs and ROS is studied in detail in cancer (Babu & Tay, 2019). While microRNA can modulate the activity of Noxes (Nox2 and Nox4), ROS can also regulate microRNA activity (Carbonell & Gomes, 2020; Konovalova et al., 2019). ROS-dependent microRNA regulation involves microRNA biogenesis machinery and microRNA expression (He & Jiang, 2016). Hence, it will be interesting to investigate whether ROS can interfere with microRNA function at the growth cones.

For example, the mechanism of how miR-182 inhibition occurs in response to Slit/Robo signaling is not known. We showed that Slit2 can induce H₂O₂ production in the RGC growth cones. One possible scenario is that Slit2/Robo2 signaling activates Nox2, and Nox2-derived H₂O₂ can inhibit miR-182 action to promote cofilin translation. Another possibility is that other microRNAs are expressed upon Nox2-mediated ROS production to alter actin machinery at the growth cones. To investigate the role of microRNAs in RGC growth cones, microRNA profiling can be conducted for zebrafish RGCs. The approach for microRNA profiling in zebrafish has been studied before in neutrophils (Hsu et al., 2017, 2019). For instance, GFP labeled RGCs from transgenic zebrafish embryos *Tg(ath5:GFP)* can be FACS-sorted to subject microRNA sequencing. Then, the role of individual microRNAs in RGC guidance can be examined by individually knocking down the candidate microRNAs specifically in RGCs. To test whether candidate microRNAs are involved downstream of slit2/Robo2, *in vitro* growth and guidance assays can be conducted on cultured RGC neurons. To test whether microRNAs are involved in Nox2 activity, H₂O₂-imaging can be performed. RGC phenotypes in microRNA knockdown and

Nox2 knockdown in RGCs can be compared and rescue experiments can be conducted to show involvement of microRNAs in RGC guidance.

6.2 The role of Nox2-derived H₂O₂ in cellular signaling during axonal guidance

How could Nox-derived ROS act as intracellular signaling molecule during axonal guidance? One possibility is by affecting Ca⁺² signaling. Ca⁺² is an important second messenger that regulates cell functions including gene expression, migration, cell survival and death (Görlach, Bertram, Hudcová, & Krizanová, 2015). Crosstalk between Ca⁺² and ROS modulates cellular signaling (Figure 31). As mentioned before, Ca⁺² itself can activate Nox enzymes with EF-hand motif to initiate ROS signaling (Rigutto et al., 2009). Consequently, other Nox isoforms can be activated via Ca⁺² signaling. Ryanodine receptors (RyR) on ER membrane release Ca⁺² ions and harbor a free cysteine residue that makes RyR itself susceptible to oxidative modifications (Yan, Wei, Zhang, Cheng, & Liu, 2006). In neurons, NOX-derived H₂O₂ enhance RyR-mediated Ca⁺² release to activate actin regulatory protein Rac1, which can further activate Nox enzymes (Wilson, Muñoz-Palma, et al., 2016; Zhang & Forscher, 2009). In future experiments, investigation of the cytoplasmic Ca⁺² levels in response to Nox2 activation can be conducted to examine its importance in Nox-mediated signaling at growth cones. For instance, *in vivo* Ca⁺² biosensor imaging in RGC growth cones during RGC development is a promising experiment.

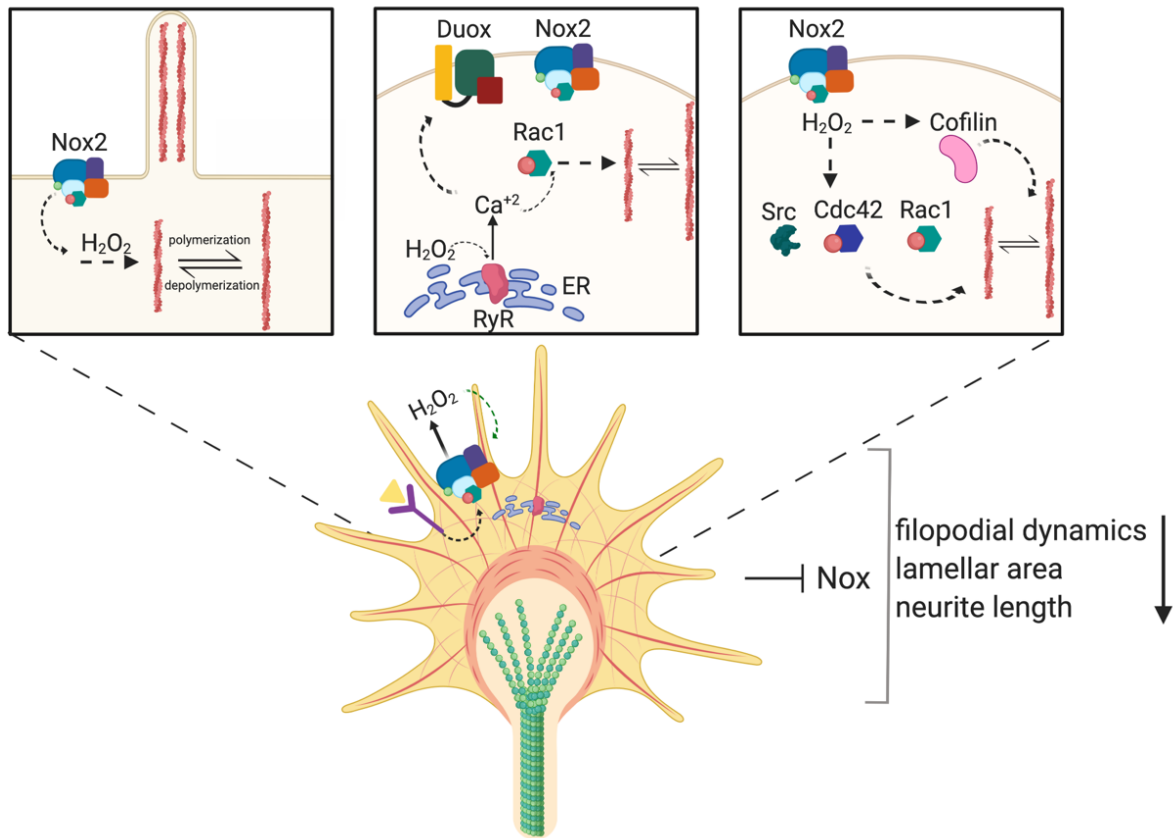


Figure 31: Nox-mediated ROS affects neuronal cytoskeleton during neurite growth.

The growth cone at the distal axon in developing neurites is heavily populated by F-actin, which forms filopodia and lamellipodia. Nox2 subunits are located at the growth cones, in close association with F-actin. Active Nox2 produces H₂O₂ that can oxidize actin to modify its polymerization state. Nox inhibition decreases neurite outgrowth, actin retrograde flow, filopodial actin dynamics and lamellar area, while H₂O₂ increases neurite growth. The ryanodine receptors (RyR) on endoplasmic reticulum (ER) can be oxidized by Nox-mediated H₂O₂ to release Ca²⁺ into cytoplasm, which can activate actin regulatory protein Rac1, possibly Duox enzymes as well. Actin binding proteins such as cofilin, and actin regulatory proteins such as Rho GTPases (Rac1, Cdc42) and Src kinase can be post-translationally modified by H₂O₂, which affects the association with the actin and ultimately the organization and dynamics of the actin cytoskeleton.

6.2.1 Redox regulation of actin cytoskeleton

Another mechanism through which ROS could exert their signaling effects is by redox modification of cytoskeletal target proteins (Figure 31). Actin itself is susceptible to oxidation of its cysteine and methionine residues; therefore, actin dynamics can be regulated by ROS via direct redox modifications of actin (Wilson & González-Billault, 2015; Wilson, Terman, González-Billault, & Ahmed, 2016). In oxidative stress conditions, actin undergoes reversible S-glutathionylation, and this modification on a specific cysteine residue alters its polymerization capacity (Dalle-Donne, Giustarini, Rossi, Colombo, & Milzani, 2003). Nox-derived H₂O₂ can modify actin polymerization via reversible glutathionylation in active neutrophils to regulate recruitment and phagocytic activity (Sakai et al., 2012). In plants, Nox-derived H₂O₂ modulates actin remodeling during innate immunity response (Li, Cao, & Staiger, 2017; Ryder et al., 2013). H₂O₂ can affect the lamellipodium and lamella through F-actin networks in migrating epithelial cells to regulate leading edge protrusion (Taufet, Delorme-Walker, & DerMardirossian, 2012). Moreover, oxidation of actin can alter the effects of actin regulatory proteins; for example, cofilin-dependent actin depolymerization was facilitated when actin was oxidized by MICALs (Grintsevich et al., 2017, 2016). Therefore, it will be important to assess the oxidation levels of actin at the growth cones during axon guidance.

6.2.2 Redox regulation of actin binding proteins

In addition to actin itself, proteins that regulate actin dynamics can also be redox target. In particular, actin-binding proteins myosin II and cofilin, as well as actin regulatory proteins Rac1, Cdc42, Src, and PKC can be modified through oxidation, eventually altering the interactions with actin and modulating actin dynamics (Hobbs, Zhou, Cox, & Campbell, 2014; Truong & Carroll, 2013; Xu, Huff, Fujii, & Griendling, 2017). For instance, cofilin oxidation interfered with the cofilin binding to actin molecules and prevented cofilin-mediated F-actin depolymerization (Cameron et al., 2015; Klamt et al., 2009). On the other hand, cofilin oxidation at different cysteine residues did not alter its capability to bind actin but prevented cofilin-mediated F-actin severing (Klemke et al., 2008). How does the same type of post-translational modification (i.e., oxidation) result in a different inhibitory effect on cofilin? When cofilin's ability to actin binding was inhibited through oxidation, cofilin translocated to mitochondria where it can release cytochrome

c to induce apoptosis (Klamt et al., 2009). Thus, oxidation site at cofilin could also determine the downstream signaling; by preventing actin binding, cofilin is available to modulate different cellular events. This suggests that the level of regulation through oxidation is highly multifaceted.

Furthermore, oxidation of cofilin regulatory phosphatase slingshot-1L indirectly activated cofilin and induced formation of cofilin-actin rods (Kim, Huang, & Bokoch, 2009). Hence, redox regulation of cofilin appears to be quite complex. Both Nox1 and Nox2 lead to dephosphorylation of cofilin to allow actin remodeling and membrane ruffle formation in macrophages during macropinocytosis, demonstrating the different levels of modifications that can alter actin regulators (Csányi et al., 2017; Ghoshal et al., 2017).

6.2.3 Redox regulation of actin regulatory proteins

Actin can be modulated by Rho GTPases. Rac1 modulates lamellipodia and membrane ruffle formation, while Cdc42 promotes filopodia formation at the growth cones. Hence, changes in their association with actin can change the structure of the growth cone as well as reorganizing the cytoskeleton (Figure 31). Rac-mediated lamellipodia formation required H₂O₂-induced Rho inactivation, and the source of H₂O₂ inactivating Rho is activated by Rac itself (Nimnual et al., 2003). Indeed, the positive feedback loop between Rac and H₂O₂ production was shown in a study where Rac1-mediated Nox2 activation stimulated further Rac1 activation during directional migration of neutrophils (Kuiper, Sun, Magalhães, & Glogauer, 2011) and axonal growth of hippocampal neurons (Wilson, Muñoz-Palma, et al., 2016). Inhibiting H₂O₂ attenuated N-formyl-L-methionyl-L-leucyl-L-phenylalanine (fMLP)-induced uncapping of F-actin in response to Rac1 activation, showing the functional coupling between ROS, Rac1 and actin cytoskeleton rearrangement during migration (Kuiper et al., 2011). Although Cdc42 has a redox-sensitive cysteine similar to Rac1, little is known about Nox-mediated redox regulation of Cdc42. Wilson et al. showed a small decrease in Cdc42 activity in axonal tips (Wilson et al., 2015); however, more research is required to determine whether Cdc42 is a true target of Nox-derived H₂O₂. Furthermore, the activity of Cdc42 activating protein Cdc42GAP was shown to be suppressed by Nox-mediated H₂O₂ production during smooth muscle contraction (Li & Tang, 2009). Thus, the modification of Rho GTPases are important not also in Nox activation, but also relaying the downstream signaling.

6.2.4 Redox regulation of signaling proteins

Src, a cytoplasmic protein tyrosine kinase, is an important signaling enzyme that regulates actin organization and dynamics during axonal growth and guidance. Our work has recently shown that Src phosphorylates the actin-regulatory protein cortactin at a specific tyrosine residue, which increases filopodia formation as well as F-actin density in lamellipodia of neuronal growth cones (He et al., 2015; Ren et al., 2019). Oxidation of Src increases its kinase activity (Giannoni, Buricchi, Raugei, Ramponi, & Chiarugi, 2005; Xu et al., 2017). Direct oxidation and activation of Src by DUOX1-mediated H₂O₂ was shown in lung epithelial cells (Sham, Wesley, Hristova, & van der Vliet, 2013). Src expression was increased following H₂O₂ treatment after the sciatic injury, during which the cellular cytoskeleton undergoes extensive modifications for axonal regeneration (Hervera et al., 2018). In summary, NOX-derived ROS can control the oxidation state of both actin and actin-modifying proteins thereby actin dynamics and related axonal growth and guidance.

6.3 Conclusion

Here, I described several downstream signals of Slit/Robo interaction that could result in Nox2 activation at the growth cones. Then, I listed important redox targets which can alter actin cytoskeleton to modulate directional movement of growth cones in response to Nox2 activation. I believe the investigation of the role of microRNAs in growth cone guidance will be an important area in the near future. As they emerged as mediators of variety of signaling events, it will be essential to discover the function of microRNAs in developing neurons. Furthermore, microRNAs will highly likely provide a bridge between cue-mediated signaling and Nox activation, considering their involvement in both parts of the pathway. Other important targets involve cofilin and Rac that could modulate actin machinery at the growth cones. Evidence suggest that there is a highly complicated maintenance of these proteins with post-translational modifications and other regulatory proteins such as srGAPs. Hence, cell-specific activity of cofilin and Rac should be investigated in detail to discover such a link between Nox signaling.

How do H₂O₂ levels control the growth cone guidance? We have evidence that adequate amount of H₂O₂ is required for proper formation of F-actin, either low levels or high levels of ROS leads loss of F-actin. I speculate that the exact amount of H₂O₂ is important in regulating cellular

signaling, while still in physiological range. H_2O_2 has a longer half-life compared to other ROS, however, its activity is still limited to the proximity of target proteins. Hence, I believe once H_2O_2 initiates a signaling cascade, the duration of that signaling response is determined by the sequential activation/inactivation of target proteins. For instance, small changes in H_2O_2 levels could alter a certain signaling pathway that the distance of action will be limited because of the lower levels of H_2O_2 presence. However, if there is more H_2O_2 produced, or consistently produced for a longer amount of time, then there will be more time for the target modifications. This will lead more signaling proteins to be affected and different signaling cascades to be initiated.

In support of this, we found that cultured RGC guidance responses to both attractive (netrin-1) and repulsive (slit2) affected by Nox inhibition (Haley Roeder, unpublished data). Although we propose a pathway between slit2/Robo2 and Nox2, it is highly likely that Nox signaling is also important in other growth cone responses. This suggests a broader regulatory mechanism involving Nox2 and guidance cues to steer the growth cone during directional decision making. Testing these hypotheses is not easy and is currently limited to detection of intracellular H_2O_2 levels *in vivo*. Therefore, future experiments are needed to focus studying growth and guidance at a single-cell level with a more sensitive H_2O_2 -detection limit *in vivo*.

REFERENCES

- Ablain, J., Durand, E. M., Yang, S., Zhou, Y., & Zon, L. I. (2015). A CRISPR/Cas9 vector system for tissue-specific gene disruption in zebrafish. *Developmental Cell*, *32*(6), 756–764. <https://doi.org/10.1016/j.devcel.2015.01.032>
- Abramov, A. Y., Jacobson, J., Wientjes, F., Hothersall, J., Canevari, L., & Duchen, M. R. (2005). Expression and modulation of an NADPH oxidase in mammalian astrocytes. *Journal of Neuroscience*, *25*(40), 9176–9184. <https://doi.org/10.1523/JNEUROSCI.1632-05.2005>
- Accetta, R., Damiano, S., Morano, A., Paolo, M., Paternò, R., Avvedimento, E. V., & Santillo, M. (2016). Reactive oxygen species derived from NOX3 and NOX5 drive differentiation of human oligodendrocytes. *Frontiers in Cellular Neuroscience*, *10*(146), 146. <https://doi.org/10.3389/fncel.2016.00146>
- Al Ghouleh, I., Khoo, N. K. H., Knaus, U. G., Griendling, K. K., Touyz, R. M., Thannickal, V. J., ... Pagano, P. J. (2011). Oxidases and peroxidases in cardiovascular and lung disease: new concepts in reactive oxygen species signaling. *Free Radical Biology and Medicine*, *51*(7), 1271–1288. <https://doi.org/10.1016/j.freeradbiomed.2011.06.011>
- Altenhöfer, S., Kleikers, P. W. M., Radermacher, K. A., Scheurer, P., Hermans, J. J. R., Schiffers, P., ... Schmidt, H. H. H. W. (2012). The NOX toolbox: Validating the role of NADPH oxidases in physiology and disease. *Cellular and Molecular Life Sciences*, *69*(14), 2327–2343. <https://doi.org/10.1007/s00018-012-1010-9>
- Ambasta, R. K., Kumar, P., Griendling, K. K., Schmidt, H. H. H. W., Busse, R., & Brandes, R. P. (2004). Direct interaction of the novel Nox proteins with p22phox is required for the formation of a functionally active NADPH oxidase. *Journal of Biological Chemistry*, *279*(44), 45935–45941. <https://doi.org/10.1074/jbc.M406486200>
- Anderson, J. L., Mulligan, T. S., Shen, M. C., Wang, H., Scahill, C. M., Tan, F. J., ... Farber, S. A. (2017). mRNA processing in mutant zebrafish lines generated by chemical and CRISPR-mediated mutagenesis produces unexpected transcripts that escape nonsense-mediated decay. *PLoS Genetics*, *13*(11), e1007105. <https://doi.org/10.1371/journal.pgen.1007105>
- Aviello, G., & Knaus, U. G. (2018). NADPH oxidases and ROS signaling in the gastrointestinal tract. *Mucosal Immunology*, *11*, 1011–1023. <https://doi.org/10.1038/s41385-018-0021-8>

- Babu, K. R., & Tay, Y. (2019). The Yin-Yang regulation of reactive oxygen species and microRNAs in cancer. *International Journal of Molecular Sciences*, *20*(21), 5335. <https://doi.org/10.3390/ijms20215335>
- Bánfi, B., Clark, R. A., Steger, K., & Krause, K. H. (2003). Two novel proteins activate superoxide generation by the NADPH oxidase NOX1. *Journal of Biological Chemistry*, *278*(6), 3510–3513. <https://doi.org/10.1074/jbc.C200613200>
- Bánfi, B., Malgrange, B., Knisz, J., Steger, K., Dubois-Dauphin, M., & Krause, K. H. (2004). NOX3, a superoxide-generating NADPH oxidase of the inner ear. *Journal of Biological Chemistry*, *279*(44), 46065–46072. <https://doi.org/10.1074/jbc.M403046200>
- Bánfi, B., Molnár, G., Maturana, A., Steger, K., Hegedûs, B., Demarex, N., & Krause, K. H. (2001). A Ca²⁺-activated NADPH oxidase in testis, spleen, and lymph nodes. *Journal of Biological Chemistry*, *276*(40), 37594–37601. <https://doi.org/10.1074/jbc.M103034200>
- Barth, B. M., Stewart-Smeets, S., & Kuhn, T. B. (2009). Proinflammatory cytokines provoke oxidative damage to actin in neuronal cells mediated by Rac1 and NADPH oxidase. *Molecular and Cellular Neuroscience*, *41*(2), 274–285. <https://doi.org/10.1016/j.mcn.2009.03.007>
- Bashaw, G. J., & Klein, R. (2010). Signaling from axon guidance receptors. *Cold Spring Harbor Perspectives in Biology*, *2*(5), a001941. <https://doi.org/10.1101/cshperspect.a001941>
- Bedard, K., Lardy, B., & Krause, K.-H. (2007). NOX family NADPH oxidases: Not just in mammals. *Biochimie*, *89*(9), 1107–1112. <https://doi.org/10.1016/j.biochi.2007.01.012>
- BelAiba, R. S., Djordjevic, T., Petry, A., Diemer, K., Bonello, S., Bánfi, B., ... Görlach, A. (2007). Nox5 variants are functionally active in endothelial cells. *Free Radical Biology and Medicine*, *42*(4), 446–459. <https://doi.org/10.1016/j.freeradbiomed.2006.10.054>
- Bell, K. F. S., Al-Mubarak, B., Martel, M. A., McKay, S., Wheelan, N., Hasel, P., ... Hardingham, G. E. (2015). Neuronal development is promoted by weakened intrinsic antioxidant defences due to epigenetic repression of Nrf2. *Nature Communications*, *6*, 7066. <https://doi.org/10.1038/ncomms8066>
- Bellon, A., Iyer, A., Bridi, S., Lee, F. C. Y., Ovando-Vázquez, C., Corradi, E., ... Baudet, M. L. (2017). miR-182 regulates slit2-mediated axon guidance by modulating the local translation of a specific mRNA. *Cell Reports*, *18*(5), 1171–1186. <https://doi.org/10.1016/j.celrep.2016.12.093>

- Benna, J. El, Dang, P. M., Andrieu, V., Vergnaud, S., Dewas, C., Cachia, O., ... Gougerot-Pocidalò, M.-A. (1999). p40phox associates with the neutrophil triton X-100-insoluble cytoskeletal fraction and PMA-activated membrane skeleton: a comparative study with p67phox and p47phox. *Journal of Leukocyte Biology*, 66(6), 1014–1020.
<https://doi.org/10.1002/jlb.66.6.1014>
- Bentley, D., & Toroian-Raymond, A. (1986). Disoriented pathfinding by pioneer neurone growth cones deprived of filopodia by cytochalasin treatment. *Nature*, 323(6090), 712–715.
<https://doi.org/10.1038/323712a0>
- Berman, S.A., Moss, D., Bursztajn, S. (1993). Axonal branching and growth cone structure depend on target cells. *Developmental Biology*, 159(1), 153–162.
<https://doi.org/10.1006/dbio.1993.1229>
- Bernard, K., Logsdon, N. J., Miguel, V., Benavides, G. A., Zhang, J., Carter, A. B., ... Thannickal, V. J. (2017). NADPH Oxidase 4 (Nox4) suppresses mitochondrial biogenesis and bioenergetics in lung fibroblasts via a nuclear factor erythroid-derived 2-like 2 (Nrf2)-dependent pathway. *Journal of Biological Chemistry*, 292(7), 3029–3038.
<https://doi.org/10.1074/jbc.M116.752261>
- Bienert, G. P., Møller, A. L. B., Kristiansen, K. A., Schulz, A., Møller, I. M., Schjoerring, J. K., & Jahn, T. P. (2007). Specific aquaporins facilitate the diffusion of hydrogen peroxide across membranes. *The Journal of Biological*, 282(2), 1183–1192.
<https://doi.org/10.1074/jbc.M603761200>
- Bienert, G. P., Schjoerring, J. K., & Jahn, T. P. (2006). Membrane transport of hydrogen peroxide. *Biochimica et Biophysica Acta*, 1758(8), 994–1003.
<https://doi.org/10.1016/j.bbamem.2006.02.015>
- Bilotta, J., & Saszik, S. (2001). The zebrafish as a model visual system. *International Journal of Developmental Neuroscience*, 19(7), 621–629. [https://doi.org/10.1016/S0736-5748\(01\)00050-8](https://doi.org/10.1016/S0736-5748(01)00050-8)
- Birben, E., Sahiner, U. M., Sackesen, C., Erzurum, S., & Kalayci, O. (2012). Oxidative stress and antioxidant defense. *World Allergy Organization Journal*, 5(1), 9–19.
<https://doi.org/10.1097/WOX.0b013e3182439613>

- Bishop, B., Ho, K. K., Tyler, K., Smith, A., Bonilla, S., Leung, Y. F., & Ogas, J. (2015). The chromatin remodeler chd5 is necessary for proper head development during embryogenesis of *Danio rerio*. *Biochimica et Biophysica Acta - Gene Regulatory Mechanisms*, *1849*(8), 1040–1050. <https://doi.org/10.1016/j.bbagrm.2015.06.006>
- Block, K., Gorin, Y., & Abboud, H. E. (2009). Subcellular localization of Nox4 and regulation in diabetes. *Proceedings of the National Academy of Sciences of the United States of America*, *106*(34), 14385–14390. <https://doi.org/10.1073/pnas.0906805106>
- Blockus, H., & Chédotal, A. (2016). Slit-robo signaling. *Development*, *143*(17), 3037–3044. <https://doi.org/10.1242/dev.132829>
- Bórquez, D. A., Urrutia, P. J., Wilson, C., Van Zundert, B., Núñez, M. T., & González-Billault, C. (2016). Dissecting the role of redox signaling in neuronal development. *Journal of Neurochemistry*, *137*(4), 506–517. <https://doi.org/10.1111/jnc.13581>
- Borregaard, N., Heiple, J. M., Simons, E. R., & Clark, R. A. (1983). Subcellular localization of the b-cytochrome component of the human neutrophil microbicidal oxidase: translocation during activation. *Journal of Cell Biology*, *97*(1), 52–61. <https://doi.org/10.1083/jcb.97.1.52>
- Brandes, R. P., Weissmann, N., & Schroder, K. (2014). Nox family NADPH oxidases: molecular mechanisms of activation. *Free Radical Biology and Medicine*, *76*, 208–226. <https://doi.org/10.1016/j.freeradbiomed.2014.07.046>
- Burrill, J. D., & Easter, S. S. (1994). Development of the retinofugal projections in the embryonic and larval zebrafish (*Brachydanio rerio*). *Journal of Comparative Neurology*, *346*(4), 583–600. <https://doi.org/10.1002/cne.903460410>
- Buvelot, H., Jaquet, V., & Krause, K. H. (2019). Mammalian NADPH oxidases. In *Methods in Molecular Biology* (pp. 17–36). https://doi.org/10.1007/978-1-4939-9424-3_2
- Caillou, B., Dupuy, C., Lacroix, L., Nocera, M., Talbot, M., Ohayon, R., ... Virion, A. (2001). Expression of reduced nicotinamide adenine dinucleotide phosphate oxidase (ThoX, LNOX, Duox) genes and proteins in human thyroid tissues. *The Journal of Clinical Endocrinology & Metabolism*, *86*(7), 3351–3358. <https://doi.org/10.1210/jcem.86.7.7646>
- Cameron, J. M., Gabrielsen, M., Chim, Y. H., Munro, J., McGhee, E. J., Sumpton, D., ... Olson, M. F. (2015). Polarized cell motility induces hydrogen peroxide to inhibit cofilin via cysteine oxidation. *Current Biology*, *25*(11), 1520–1525. <https://doi.org/10.1016/j.cub.2015.04.020>

- Campbell, D. S., Stringham, S. A., Timm, A., Xiao, T., Law, M. Y., Baier, H., ... Chien, C. Bin. (2007). Slit1a Inhibits retinal ganglion cell arborization and synaptogenesis via robo2-dependent and -independent pathways. *Neuron*, 55(2), 231–245.
<https://doi.org/10.1016/j.neuron.2007.06.034>
- Cao, X., Dai, X., Parker, L. M., & Kreulen, D. L. (2007). Differential regulation of NADPH oxidase in sympathetic and sensory ganglia in deoxycorticosterone acetate-salt hypertension. *Hypertension*, 50(4), 663–671.
<https://doi.org/10.1161/HYPERTENSIONAHA.107.089748>
- Cao, X., Demel, S. L., Quinn, M. T., Galligan, J. J., & Kreulen, D. (2009). Localization of NADPH oxidase in sympathetic and sensory ganglion neurons and perivascular nerve fibers. *Autonomic Neuroscience: Basic and Clinical*, 151(2), 90–97.
<https://doi.org/10.1016/j.autneu.2009.07.010>
- Carbonell, T., & Gomes, A. V. (2020). MicroRNAs in the regulation of cellular redox status and its implications in myocardial ischemia-reperfusion injury. *Redox Biology*, 36(June), 101607. <https://doi.org/10.1016/j.redox.2020.101607>
- Carmany-Rampey, A., & Moens, C. B. (2006). Modern mosaic analysis in the zebrafish. *Methods*, 39(3), 228–238. <https://doi.org/10.1016/j.ymeth.2006.02.002>
- Case, A. J., Li, S., Basu, U., Tian, J., & Zimmerman, M. C. (2013). Mitochondrial-localized NADPH oxidase 4 is a source of superoxide in angiotensin II-stimulated neurons. *AJP: Heart and Circulatory Physiology*, 305(1), H19–H28.
<https://doi.org/10.1152/ajpheart.00974.2012>
- Cavaliere, F, Urrea, O., Alberdi, E., & Matute, C. (2012). Oligodendrocyte differentiation from adult multipotent stem cells is modulated by glutamate. *Cell Death & Disease*, 3, e268.
<https://doi.org/10.1038/cddis.2011.144>
- Cavaliere, Fabio, Benito-Muñoz, M., Panicker, M., & Matute, C. (2013). NMDA modulates oligodendrocyte differentiation of subventricular zone cells through PKC activation. *Frontiers in Cellular Neuroscience*, 7(261), 261. <https://doi.org/10.3389/fncel.2013.00261>
- Challacombe, J. F., Snow, D. M., & Letourneau, P. C. (1997). Dynamic microtubule ends are required for growth cone turning to avoid an inhibitory guidance cue. *Journal of Neuroscience*, 17(9), 3085–3095. <https://doi.org/10.1523/JNEUROSCI.17-09-03085.1997>

- Chandran, R., Kim, T. H., Mehta, S. L., Udho, E., Chanana, V., Cengiz, P., ... Vemuganti, R. (2018). A combination antioxidant therapy to inhibit NOX2 and activate Nrf2 decreases secondary brain damage and improves functional recovery after traumatic brain injury. *Journal of Cerebral Blood Flow and Metabolism*, *38*(10), 1818–1827. <https://doi.org/10.1177/0271678X17738701>
- Chandrasekaran, V., Lea, C., Sosa, J. C., Higgins, D., & Lein, P. J. (2015). Reactive oxygen species are involved in BMP-induced dendritic growth in cultured rat sympathetic neurons. *Molecular and Cellular Neuroscience*, *67*, 116–125. <https://doi.org/10.1016/j.mcn.2015.06.007>
- Chao, J., Yang, L., Buch, S., & Gao, L. (2013). Angiotensin II increased neuronal stem cell proliferation: role of AT2R. *PLoS ONE*, *8*(5), e63488. <https://doi.org/10.1371/journal.pone.0063488>
- Chen, H., Yuh, C., & Wu, K. K. (2010). *Nestin Is Essential for Zebrafish Brain and Eye Development through Control of Progenitor Cell Apoptosis*. *5*(2). <https://doi.org/10.1371/journal.pone.0009318>
- Chen, J., He, R., Minshall, R. D., Dinauer, M. C., & Ye, R. D. (2007). Characterization of a mutation in the phox homology domain of the NADPH oxidase component p40phox identifies a mechanism for negative regulation of superoxide production. *Journal of Biological Chemistry*, *282*(41), 30273–30284. <https://doi.org/10.1074/jbc.M704416200>
- Chen, K., Kirber, M. T., Xiao, H., Yang, Y., & Keaney, J. F. (2008). Regulation of ROS signal transduction by NADPH oxidase 4 localization. *Journal of Cell Biology*, *181*(7), 1129–1139. <https://doi.org/10.1083/jcb.200709049>
- Chen, Z., Lee, H., Henle, S. J., Cheever, T. R., Ekker, S. C., & Henley, J. R. (2013). Primary Neuron Culture for Nerve Growth and Axon Guidance Studies in Zebrafish (*Danio rerio*). *PLoS ONE*, *8*(3). <https://doi.org/10.1371/journal.pone.0057539>
- Cheng, G., Cao, Z., Xu, X., van Meir, E. G., & Lambeth, J. D. (2001). Homologs of gp91phox: cloning and tissue expression of Nox3, Nox4, and Nox5. *Gene*, *269*(1–2), 131–140. [https://doi.org/10.1016/S0378-1119\(01\)00449-8](https://doi.org/10.1016/S0378-1119(01)00449-8)
- Cheng, G., Diebold, B. A., Hughes, Y., & Lambeth, J. D. (2006). Nox1-dependent reactive oxygen generation is regulated by Rac1. *Journal of Biological Chemistry*, *281*(26), 17718–17726. <https://doi.org/10.1074/jbc.M512751200>

- Cheng, G., Ritsick, D., & Lambeth, J. D. (2004). Nox3 regulation by NOXO1, p47phox, and p67phox. *Journal of Biological Chemistry*, 279(33), 34250–34255.
<https://doi.org/10.1074/jbc.M400660200>
- Cheng, L., Chen, L., Wei, X., Wang, Y., Ren, Z., Zeng, S., ... Liu, H. (2018). NOD2 promotes dopaminergic degeneration regulated by NADPH oxidase 2 in 6-hydroxydopamine model of Parkinson's disease. *Journal of Neuroinflammation*, 15(1), 243.
<https://doi.org/10.1186/s12974-018-1289-z>
- Chéret, C., Gervais, A., Lelli, A., Colin, C., Amar, L., Ravassard, P., ... Mallat, M. (2008). Neurotoxic activation of microglia is promoted by a Nox1-dependent NADPH oxidase. *Journal of Neuroscience*, 28(46), 12039–12051. <https://doi.org/10.1523/JNEUROSCI.3568-08.2008>
- Chessa, T. A. M., Anderson, K. E., Hu, Y., Xu, Q., Rausch, O., Stephens, L. R., & Hawkins, P. T. (2010). Phosphorylation of threonine 154 in p40phox is an important physiological signal for activation of the neutrophil NADPH oxidase. *Blood*, 116(26), 6027–6036.
<https://doi.org/10.1182/blood-2010-08-300889>
- Chitnis, A. B., & Kuwada, J. Y. (1990). Axonogenesis in the brain of zebrafish embryos. *Journal of Neuroscience*, 10(6), 1892–1905. <https://doi.org/10.1523/jneurosci.10-06-01892.1990>
- Choi, S.-A., Kim, Y., Park, Y.-H., Yang, H.-J., Jeong, P.-S., Cha, J.-J., ... Chang, K.-T. (2019). Novel crosstalk between Vps26a and Nox4 signaling during neurogenesis. *Cell Death & Differentiation*, 26, 1582–1599. <https://doi.org/10.1038/s41418-018-0226-0>
- Clark, R. A., Volpp, B. D., Leidal, K. G., & Nauseef, W. M. (1990). Two cytosolic components of the human neutrophil respiratory burst oxidase translocate to the plasma membrane during cell activation. *Journal of Clinical Investigation*, 85(3), 714–721.
<https://doi.org/10.1172/JCI114496>
- Coant, N., Mkaddem, S. Ben, Pedruzzi, E., Guichard, C., Tréton, X., Ducroc, R., ... Ogier-Denis, E. (2010). NADPH oxidase 1 modulates WNT and NOTCH1 signaling to control the fate of proliferative progenitor cells in the colon. *Molecular and Cellular Biology*, 30(11), 2636–2650. <https://doi.org/10.1128/MCB.01194-09>

- Coleman, C. G., Wang, G., Faraco, G., Lopes, J. M., Waters, E. M., Milner, T. A., ... Pickel, V. M. (2013). Membrane trafficking of NADPH oxidase p47phox in paraventricular hypothalamic neurons parallels local free radical production in angiotensin II slow-pressor hypertension. *Journal of Neuroscience*, *33*(10), 4308–4316.
<https://doi.org/10.1523/JNEUROSCI.3061-12.2013>
- Collins, S. J., Tumpach, C., Groveman, B. R., Drew, S. C., & Haigh, C. L. (2018). Prion protein cleavage fragments regulate adult neural stem cell quiescence through redox modulation of mitochondrial fission and SOD2 expression. *Cellular and Molecular Life Sciences*, *75*(17), 3231–3249. <https://doi.org/10.1007/s00018-018-2790-3>
- Cooney, S. J., Zhao, Y., & Byrnes, K. R. (2014). Characterization of the expression and inflammatory activity of NADPH oxidase after spinal cord injury. *Free Radical Research*, *48*(8), 929–939. <https://doi.org/10.3109/10715762.2014.927578>
- Cooney, Sean J., Bermudez-Sabogal, S. L., & Byrnes, K. R. (2013). Cellular and temporal expression of NADPH oxidase (NOX) isoforms after brain injury. *Journal of Neuroinflammation*, *10*(1), 155. <https://doi.org/10.1186/1742-2094-10-155>
- Corcoran, A., & Cotter, T. G. (2013). Redox regulation of protein kinases. *FEBS Journal*, *280*(9), 1944–1965. <https://doi.org/10.1111/febs.12224>
- Covassin, L., Amigo, J. D., Suzuki, K., Teplyuk, V., Straubhaar, J., & Lawson, N. D. (2006). Global analysis of hematopoietic and vascular endothelial gene expression by tissue specific microarray profiling in zebrafish. *Developmental Biology*, *299*(2), 551–562.
<https://doi.org/10.1016/j.ydbio.2006.08.020>
- Coyoy, Angelica, Olguin-Albuerno, M., Martinez-Briseno, P., & Moran, J. (2013). Role of reactive oxygen species and NADPH-oxidase in the development of rat cerebellum. *Neurochemistry International*, *62*(7), 998–1011.
<https://doi.org/10.1016/j.neuint.2013.03.009>
- Coyoy, Angélica, Valencia, A., Guemez-Gamboa, A., & Morán, J. (2008). Role of NADPH oxidase in the apoptotic death of cultured cerebellar granule neurons. *Free Radical Biology and Medicine*, *45*(8), 1056–1064. <https://doi.org/10.1016/j.freeradbiomed.2008.06.027>
- Cross, A. R. (2000). p40phox participates in the activation of NADPH oxidase by increasing the affinity of p47phox for flavocytochrome b558. *Biochemical Journal*, *349*(1), 113–117.
<https://doi.org/10.1042/bj3490113>

- Cross, A. R., & Segal, A. W. (2004). The NADPH oxidase of professional phagocytes — prototype of the NOX electron transport chain systems. *Biochimica et Biophysica Acta*, *1657*(1), 1–22. <https://doi.org/10.1016/j.bbabbio.2004.03.008>
- Csányi, G., Feck, D. M., Ghoshal, P., Singla, B., Lin, H., Nagarajan, S., ... Pagano, P. J. (2017). CD47 and Nox1 mediate dynamic fluid-phase macropinocytosis of native LDL. *Antioxidants and Redox Signaling*, *26*(16), 886–901. <https://doi.org/10.1089/ars.2016.6834>
- Cunningham, C. L., Martinez-Cerdeno, V., & Noctor, S. C. (2013). Microglia regulate the number of neural precursor cells in the developing cerebral cortex. *The Journal of Neuroscience*, *33*(10), 4216–4233. <https://doi.org/10.1523/JNEUROSCI.3441-12.2013>
- Dahlqwtist, E., Magnusson, P. K. E., Pawitan, Y., & Sjölander, A. (2019). On the relationship between the heritability and the attributable fraction. *Human Genetics*, *138*(4), 425–435. <https://doi.org/10.1007/s00439-019-02006-8>
- Dalle-Donne, I., Giustarini, D., Rossi, R., Colombo, R., & Milzani, A. (2003). Reversible S-glutathionylation of Cys374 regulates actin filament formation by inducing structural changes in the actin molecule. *Free Radical Biology and Medicine*, *34*(1), 23–32. [https://doi.org/10.1016/S0891-5849\(02\)01182-6](https://doi.org/10.1016/S0891-5849(02)01182-6)
- Damiano, S., Fusco, R., Morano, A., de Mizio, M., Paternò, R., de Rosa, A., ... Avvedimento, E. V. (2012). Reactive oxygen species regulate the levels of dual oxidase (duox1-2) in human neuroblastoma cells. *PLoS ONE*, *7*(4), e34405. <https://doi.org/10.1371/journal.pone.0034405>
- Davalli, P., Mitic, T., Caporali, A., Lauriola, A., & D'Arca, D. (2016). ROS, cell senescence, and novel molecular mechanisms in aging and age-related diseases. *Oxidative Medicine and Cellular Longevity*, *2016*(3565127). <https://doi.org/10.1155/2016/3565127>
- De La Torre, J. R., Höpker, V. H., Ming, G. L., Poo, M. M., Tessier-Lavigne, M., Hemmati-Brivanlou, A., & Holt, C. E. (1997). Turning of retinal growth cones in a netrin-1 gradient mediated by the netrin receptor DCC. *Neuron*, *19*(6), 1211–1224. [https://doi.org/10.1016/S0896-6273\(00\)80413-4](https://doi.org/10.1016/S0896-6273(00)80413-4)
- Deiner, M. S., Kennedy, T. E., Fazeli, A., Serafini, T., Tessier-Lavigne, M., & Sretavan, D. W. (1997). Netrin-1 and DCC mediate axon guidance locally at the optic disc: Loss of function leads to optic nerve hypoplasia. *Neuron*, *19*(3), 575–589. [https://doi.org/10.1016/S0896-6273\(00\)80373-6](https://doi.org/10.1016/S0896-6273(00)80373-6)

- Del Bene, F., Ettwiller, L., Skowronska-Krawczyk, D., Baier, H., Matter, J. M., Birney, E., & Wittbrodt, J. (2007). In vivo validation of a computationally predicted conserved Ath5 target gene set. *PLoS Genetics*, 3(9), 1661–1671.
<https://doi.org/10.1371/journal.pgen.0030159>
- Dent, E. W., Gupton, S. L., & Gertler, F. B. (2011). The growth cone cytoskeleton in axon outgrowth and guidance. *Cold Spring Harbor Perspectives in Biology*, 3(3), a001800.
<https://doi.org/10.1101/cshperspect.a001800>
- Dickinson, B. C., & Chang, C. J. (2011). Chemistry and biology of reactive oxygen species in signaling or stress responses. *Nature Chemical Biology*, 7(8), 504–511.
<https://doi.org/10.1038/nchembio.607>
- Dickinson, B. C., Peltier, J., Stone, D., Schaffer, D. V., & Chang, C. J. (2011). Nox2 redox signaling maintains essential cell populations in the brain. *Nature Chemical Biology*, 7(2), 106–112. <https://doi.org/10.1038/nchembio.497>
- Dinauer, M. C., Orkin, S. H., Brown, R., Jesaitis, A. J., & Parkos, C. A. (1987). The glycoprotein encoded by the X-linked chronic granulomatous disease locus is a component of the neutrophil cytochrome b complex. *Nature*, 327, 717–720. <https://doi.org/10.1038/327717a0>
- Donkó, Á., Péterfi, Z., Sum, A., Leto, T., & Geiszt, M. (2005). Dual oxidases. *Philosophical Transactions of the Royal Society B: Biological Sciences*, 360(1464), 2301–2308.
<https://doi.org/10.1098/rstb.2005.1767>
- Dvorianchikova, G., Grant, J., Santos, A. R. C., Hernandez, E., & Ivanov, D. (2012). Neuronal NAD(P)H oxidases contribute to ROS production and mediate RGC death after ischemia. *Investigative Ophthalmology and Visual Science*, 53(6), 2823–2830.
<https://doi.org/10.1167/iovs.12-9526>
- Eble, J. A., & De Rezende, F. F. (2014). Redox-relevant aspects of the extracellular matrix and its cellular contacts via integrins. *Antioxidants and Redox Signaling*, 20(13), 1977–1993.
<https://doi.org/10.1089/ars.2013.5294>
- Erskine, L., & Herrera, E. (2007). The retinal ganglion cell axon's journey: Insights into molecular mechanisms of axon guidance. *Developmental Biology*, 308(1), 1–14.
<https://doi.org/10.1016/j.ydbio.2007.05.013>
- Erskine, L., & Herrera, E. (2014). Connecting the retina to the brain. *ASN Neuro*, 6(6), 1–26.
<https://doi.org/10.1177/1759091414562107>

- Eyrich, N. W., Potts, C. R., Robinson, M. H., Maximov, V., & Kenney, A. M. (2019). Reactive oxygen species signaling promotes hypoxia-inducible factor 1 α stabilization in sonic hedgehog-driven cerebellar progenitor cell proliferation. *Molecular and Cellular Biology*, 39(8), e00268-18. <https://doi.org/10.1128/MCB.00268-18>
- Fadool, J. M., & Dowling, J. E. (2008). Zebrafish: A model system for the study of eye genetics. *Progress in Retinal and Eye Research*, 27(1), 89–110. <https://doi.org/10.1016/j.preteyeres.2007.08.002>
- Flores, M. V., Crawford, K. C., Pullin, L. M., Hall, C. J., Crosier, K. E., & Crosier, P. S. (2010). Dual oxidase in the intestinal epithelium of zebrafish larvae has anti-bacterial properties. *Biochemical and Biophysical Research Communications*, 400(1), 164–168. <https://doi.org/10.1016/j.bbrc.2010.08.037>
- Forman, H. J., Maiorino, M., & Ursini, F. (2010). Signaling functions of reactive oxygen species. *Biochemistry*, 49(5), 835–842. <https://doi.org/10.1021/bi9020378>
- Forscher, P., Lin, C. H., & Thompson, C. (1992). Novel form of growth cone motility involving site-directed actin filament assembly. *Nature*, 357(6378), 515–518. <https://doi.org/10.1038/357515a0>
- Francis-Oliveira, J., Vilar Higa, G. S., Dati, L. M. M., Shieh, I. C., & De Pasquale, R. (2018). Metaplasticity in the visual cortex: crosstalk between visual experience and reactive oxygen species. *Journal of Neuroscience*, 38(25), 5649–5665. <https://doi.org/10.1523/JNEUROSCI.2617-17.2018>
- Fricke, C., Lee, J., Geiger-Rudolph, S., Bonhoeffer, F., & Chien, C. (2001). astray , a Zebrafish roundabout Homolog Required for Retinal Axon Guidance. *Science*, 292, 507–511.
- Fulton, D. J. R. (2009). Nox5 and the regulation of cellular function. *Antioxidants and Redox Signaling*, 11(10), 2443–2452. <https://doi.org/10.1089/ars.2009.2587>
- Gallo, G. (1998). Involvement of microtubules in the regulation of neuronal growth cone morphologic remodeling. *Journal of Neurobiology*, 35(2), 121–140. [https://doi.org/10.1002/\(SICI\)1097-4695\(199805\)35:2<121::AID-NEU1>3.0.CO;2-6](https://doi.org/10.1002/(SICI)1097-4695(199805)35:2<121::AID-NEU1>3.0.CO;2-6)
- Ganzen, L., Venkatraman, P., Pang, C. P., Leung, Y. F., & Zhang, M. (2017). Utilizing zebrafish visual behaviors in drug screening for retinal degeneration. *International Journal of Molecular Sciences*, 18(6), 1185. <https://doi.org/10.3390/ijms18061185>

- Gauron, C., Meda, F., Dupont, E., Albadri, S., Quenech'Du, N., Ipendey, E., ... Vríz, S. (2016). Hydrogen peroxide (H₂O₂) controls axon pathfinding during zebrafish development. *Developmental Biology*, 414(2), 133–141. <https://doi.org/10.1016/j.ydbio.2016.05.004>
- Geer, A. Van De, Nieto-Patlan, A., Kuhns, D. B., Tool, A. T. J., Arias, A. A., Bouaziz, M., ... Bustamante, J. (2018). Inherited p40phox deficiency differs from classic chronic granulomatous disease. *Journal of Clinical Investigation*, 128(9), 3957–3975. <https://doi.org/doi.org/10.1172/JCI97116>.
- Geiszt, M., Lekstrom, K., Brenner, S., Hewitt, S. M., Dana, R., Malech, H. L., & Leto, T. L. (2003). NAD(P)H oxidase 1, a product of differentiated colon epithelial cells, can partially replace glycoprotein 91phox in the regulated production of superoxide by phagocytes. *The Journal of Immunology*, 171(1), 299–306. <https://doi.org/10.4049/jimmunol.171.1.299>
- Geiszt, M., Lekstrom, K., Witta, J., & Leto, T. L. (2003). Proteins homologous to p47phox and p67phox support superoxide production by NAD(P)H oxidase 1 in colon epithelial cells. *Journal of Biological Chemistry*, 278(22), 20006–20012. <https://doi.org/10.1074/jbc.M301289200>
- Gerich, F. J., Funke, F., Hildebrandt, B., Faßhauer, M., & Müller, M. (2009). H₂O₂-mediated modulation of cytosolic signaling and organelle function in rat hippocampus. *Pflugers Archiv European Journal of Physiology*, 458(5), 937–952. <https://doi.org/10.1007/s00424-009-0672-0>
- Ghoshal, P., Singla, B., Lin, H., Feck, D. M., Cantu-Medellin, N., Kelley, E. E., ... Csányi, G. (2017). Nox2-mediated PI3K and cofilin activation confers alternate redox control of macrophage pinocytosis. *Antioxidants and Redox Signaling*, 26(16), 902–916. <https://doi.org/10.1089/ars.2016.6639>
- Giannoni, E., Buricchi, F., Raugei, G., Ramponi, G., & Chiarugi, P. (2005). Intracellular reactive oxygen species activate Src tyrosine kinase during cell adhesion and anchorage-dependent cell growth. *Molecular and Cellular Biology*, 25(15), 6391–6403. <https://doi.org/10.1128/mcb.25.15.6391-6403.2005>
- Giger, R. J., Hollis, E. R., & Tuszynski, M. H. (2010). Guidance molecules in axon regeneration. *Cold Spring Harbor Perspectives in Biology*, 2(7), a001867. <https://doi.org/10.1101/cshperspect.a001867>

- Giorgio, M., Trinei, M., Migliaccio, E., & Pelicci, P. G. (2007). Hydrogen peroxide: a metabolic by-product or a common mediator of ageing signals? *Nature Reviews Molecular Cell Biology*, *8*(9), 722–728. <https://doi.org/10.1038/nrm2240>
- Glass, M. J., Huang, J., Oselkin, M., Tarsitano, M. J., Wang, G., Iadecola, C., & Pickel, V. M. (2006). Subcellular localization of nicotinamide adenine dinucleotide phosphate oxidase subunits in neurons and astroglia of the rat medial nucleus tractus solitarius: Relationship with tyrosine hydroxylase immunoreactive neurons. *Neuroscience*, *143*(2), 547–564. <https://doi.org/10.1016/j.neuroscience.2006.08.051>
- Gomez-Nicola, D., Suzzi, S., Vargas-Caballero, M., Fransen, N. L., Al-Malki, H., Cebrian-Silla, A., ... Perry, V. H. (2014). Temporal dynamics of hippocampal neurogenesis in chronic neurodegeneration. *Brain: A Journal of Neurology*, *137*, 2312–2328. <https://doi.org/10.1093/brain/awu155>
- Gomez, T. M., & Letourneau, P. C. (2014). Actin dynamics in growth cone motility and navigation. *Journal of Neurochemistry*, *129*(2), 221–234. <https://doi.org/10.1111/jnc.12506>
- Gorin, Y., Ricono, J. M., Kim, N.-H., Bhandari, B., Choudhury, G. G., & Abboud, H. E. (2003). Nox4 mediates angiotensin II-induced activation of Akt/protein kinase B in mesangial cells. *American Journal of Physiology-Renal Physiology*, *285*(2), F219–F229. <https://doi.org/10.1152/ajprenal.00414.2002>
- Görlach, A., Bertram, K., Hudecova, S., & Krizanova, O. (2015). Calcium and ROS: a mutual interplay. *Redox Biology*, *6*, 260–271. <https://doi.org/10.1016/j.redox.2015.08.010>
- Grandvaux, N., Soucy-Faulkner, A., & Fink, K. (2007). Innate host defense: Nox and Duox on phox's tail. *Biochimie*, *89*(9), 1113–1122. <https://doi.org/10.1016/j.biochi.2007.04.008>
- Gregorian, C., Nakashima, J., Le Belle, J., Ohab, J., Kim, R., Liu, A., ... Wu, H. (2009). Pten deletion in adult neural stem/progenitor cells enhances constitutive neurogenesis. *The Journal of Neuroscience*, *29*(6), 1874–1886. <https://doi.org/10.1523/JNEUROSCI.3095-08.2009>
- Grintsevich, E. E., Ge, P., Sawaya, M. R., Yesilyurt, H. G., Terman, J. R., Zhou, Z. H., & Reisler, E. (2017). Catastrophic disassembly of actin filaments via Mical-mediated oxidation. *Nature Communications*, *8*(1), 2183. <https://doi.org/10.1038/s41467-017-02357-8>

- Grintsevich, E. E., Yesilyurt, H. G., Rich, S. K., Hung, R. J., Terman, J. R., & Reisler, E. (2016). F-actin dismantling through a redox-driven synergy between Mical and cofilin. *Nature Cell Biology*, *18*(8), 876–885. <https://doi.org/10.1038/ncb3390>
- Grogan, A., Reeves, E., Keep, N., Wientjes, F., Totty, N. F., Burlingame, A. L., ... Segal, A. W. (1997). Cytosolic phox proteins interact with and regulate the assembly of coronin in neutrophils. *Journal of Cell Science*, *110*(24), 3071–3081.
- Groszer, M., Erickson, R., Scripture-Adams, D. D., Dougherty, J. D., Belle, J. Le, Zack, J. A., ... Wu, H. (2006). PTEN negatively regulates neural stem cell self-renewal by modulating G0-G1 cell cycle entry. *PNAS*, *103*(1), 111–116. <https://doi.org/10.1073/pnas.0509939103>
- Gutscher, M., Sobotta, M. C., Wabnitz, G. H., Ballikaya, S., Meyer, A. J., Samstag, Y., & Dick, T. P. (2009). Proximity-based protein thiol oxidation by H₂O₂-scavenging peroxidases. *Journal of Biological Chemistry*, *284*(46), 31532–31540. <https://doi.org/10.1074/jbc.M109.059246>
- Hahn, M. E., Timme-Laragy, A. R., Karchner, S. I., & Stegeman, J. J. (2015). Nrf2 and Nrf2-related proteins in development and developmental toxicity: Insights from studies in zebrafish (*Danio rerio*). *Free Radical Biology and Medicine*, *88*, 275–289. <https://doi.org/10.1016/j.freeradbiomed.2015.06.022>
- Haigh, C. L., Tumpach, C., Collins, S. J., & Drew, S. C. (2016). A 2-substituted 8-hydroxyquinoline stimulates neural stem cell proliferation by modulating ROS signalling. *Cell Biochemistry and Biophysics*, *74*(3), 297–306. <https://doi.org/10.1007/s12013-016-0747-4>
- Halfter, W. (1996). Intraretinal grafting reveals growth requirements and guidance cues for optic axons in the developing avian retina. *Developmental Biology*, *177*(1), 160–177. <https://doi.org/10.1006/dbio.1996.0153>
- Han, C.-H., Freeman, J. L. R., Lee, T., Motalebi, S. A., & Lambeth, J. D. (1998). Regulation of the Neutrophil Respiratory Burst Oxidase Identification of an Activation Domain in p67phox. *The Journal of Biological Chemistry*, *273*(27), 16663–16668. <https://doi.org/10.1074/jbc.273.27.16663>

- Harrison, C. B., Selemidis, S., Guida, E., King, P. T., Sobey, C. G., & Drummond, G. R. (2012). NOX2 β : A novel splice variant of NOX2 that regulates NADPH Oxidase activity in macrophages. *PLoS ONE*, 7(10), e48326. <https://doi.org/10.1371/journal.pone.0048326>
- Haslund-Vinding, J., McBean, G., Jaquet, V., & Vilhardt, F. (2017). NADPH oxidases in oxidant production by microglia: activating receptors, pharmacology and association with disease. *British Journal of Pharmacology*, 174(12), 1733–1749. <https://doi.org/10.1111/bph.13425>
- He, J., & Jiang, B. H. (2016). Interplay Between Reactive Oxygen Species and MicroRNAs in Cancer. *Current Pharmacology Reports*, 2(2), 82–90. <https://doi.org/10.1007/s40495-016-0051-4>
- He, L., He, T., Farrar, S., Ji, L., Liu, T., & Ma, X. (2017). Antioxidants maintain cellular redox homeostasis by elimination of reactive oxygen species. *Cellular Physiology and Biochemistry*, 44(2), 532–553. <https://doi.org/10.1159/000485089>
- He, Y., Ren, Y., Wu, B., Decourt, B., Lee, A. C., Taylor, A., & Suter, D. M. (2015). Src and cortactin promote lamellipodia protrusion and filopodia formation and stability in growth cones. *Molecular Biology of the Cell*, 26(18), 3129–3371. <https://doi.org/10.1091/mbc.E15-03-0142>
- Heidari, Y., Shah, A. M., & Gove, C. (2004). NOX-2S is a new member of the NOX family of NADPH oxidases. *Gene*, 335(1–2), 133–140. <https://doi.org/10.1016/j.gene.2004.03.019>
- Hemmings, B. A., & Restuccia, D. F. (2012). PI3K-PKB/Akt pathway. *Cold Spring Harbor Perspectives in Biology*, 4(9), a011189. <https://doi.org/10.1101/cshperspect.a011189>
- Hervera, A., De Virgiliis, F., Palmisano, I., Zhou, L., Tantardini, E., Kong, G., ... Di Giovanni, S. (2018). Reactive oxygen species regulate axonal regeneration through the release of exosomal NADPH oxidase 2 complexes into injured axons. *Nature Cell Biology*, 20(3), 307–319. <https://doi.org/10.1038/s41556-018-0039-x>
- Hilenski, L. L., Clempus, R. E., Quinn, M. T., Lambeth, J. D., & Griendling, K. K. (2004). Distinct subcellular localizations of Nox1 and Nox4 in vascular smooth muscle cells. *Arteriosclerosis, Thrombosis, and Vascular Biology*, 24(4), 677–683. <https://doi.org/10.1161/01.ATV.0000112024.13727.2c>
- Hobbs, A.G., Zhou, B., Cox, A. D., & Campbell, S. L. (2014). Rho GTPases, oxidation, and cell redox control. *Small GTPases*, 5(2), e28579. <https://doi.org/10.4161/sgtp.28579>

- Hohn, D. C., & Lehrer, R. I. (1975). NADPH oxidase deficiency in X-linked chronic granulomatous disease. *Journal of Clinical Investigation*, *55*(4), 707–713.
<https://doi.org/10.1172/JCI107980>
- Holmström, K. M., & Finkel, T. (2014). Cellular mechanisms and physiological consequences of redox-dependent signalling. *Nature Reviews Molecular Cell Biology*, *15*(6), 411–421.
<https://doi.org/10.1038/nrm3801>
- Hsu, A. Y., Wang, D., Gurol, T., Zhou, W., Zhu, X., Lu, H. Y., & Deng, Q. (2017). Overexpression of microRNA-722 fine-tunes neutrophilic inflammation by inhibiting Rac2 in zebrafish. *Disease Models and Mechanisms*, *10*(11), 1323–1332.
<https://doi.org/10.1242/dmm.030791>
- Hsu, A. Y., Wang, D., Liu, S., Lu, J., Syahirah, R., Bennin, D. A., ... Denga, Q. (2019). Phenotypical microRNA screen reveals a noncanonical role of CDK2 in regulating neutrophil migration. *Proceedings of the National Academy of Sciences of the United States of America*, *116*(37), 18561–18570. <https://doi.org/10.1073/pnas.1905221116>
- Hu, M., & Easter, S. S. (1999). Retinal neurogenesis : The formation of the initial central patch of postmitotic cells. *Developmental Biology*, *207*, 309–321.
<https://doi.org/10.1006/dbio.1998.9031>
- Hu, Q., Khanna, P., Ee Wong, B. S., Heng, Z. S. L., Subhramanyam, C. S., Thanga, L. Z., ... Baeg, G. H. (2018). Oxidative stress promotes exit from the stem cell state and spontaneous neuronal differentiation. *Oncotarget*, *9*(3), 4223–4238.
<https://doi.org/10.18632/oncotarget.23786>
- Huang, Z. H., Wang, Y., Su, Z. Da, Geng, J. G., Chen, Y. Z., Yuan, X. B., & He, C. (2011). Slit-2 repels the migration of olfactory ensheathing cells by triggering Ca²⁺-dependent cofilin activation and RhoA inhibition. *Development*, *124*(3), 186–197.
<https://doi.org/10.1242/jcs.071357>
- Huberman, A. D., Wei, W., Elstrott, J., Stafford, B. K., Feller, M. B., & Barres, B. A. (2009). Genetic identification of an on-off direction- selective retinal ganglion cell subtype reveals a layer-specific subcortical map of posterior motion. *Neuron*, *62*(3), 327–334.
<https://doi.org/10.1016/j.neuron.2009.04.014>
- Hung, R.-J., Pak, C. W., & Terman, J. R. (2011). Direct redox regulation of F-actin. *Science*, *334*(6063), 1710–1713. <https://doi.org/10.1126/science.1211956>

- Hung, R. J., Yazdani, U., Yoon, J., Wu, H., Yang, T., Gupta, N., ... Terman, J. R. (2010). Mical links semaphorins to F-actin disassembly. *Nature*, *463*(7282), 823–827. <https://doi.org/10.1038/nature08724>
- Hur, E. M., Saijilafu, & Zhou, F. Q. (2012). Growing the growth cone: remodeling the cytoskeleton to promote axon regeneration. *Trends in Neurosciences*, *35*(3), 164–174. <https://doi.org/10.1016/j.tins.2011.11.002>
- Hutson, L. D., & Chien, C. (2002). Pathfinding and Error Correction by Retinal Axons : The Role of astray / robo2. *Neuron*, *33*, 205–217. [https://doi.org/10.1016/s0896-6273\(01\)00579-7](https://doi.org/10.1016/s0896-6273(01)00579-7)
- Ibi, M., Katsuyama, M., Fan, C., Iwata, K., Nishinaka, T., Yokoyama, T., & Yabe-Nishimura, C. (2006). NOX1/NADPH oxidase negatively regulates nerve growth factor-induced neurite outgrowth. *Free Radical Biology and Medicine*, *40*(10), 1785–1795. <https://doi.org/10.1016/j.freeradbiomed.2006.01.009>
- Infanger, D. W., Sharma, R. V., & Davisson, R. L. (2006). NADPH oxidases of the brain: distribution, regulation, and function. *Antioxidants & Redox Signaling*, *8*(9–10), 1583–1596. <https://doi.org/10.1089/ars.2006.8.1583>
- Jagnandan, D., Church, J. E., Banfi, B., Stuehr, D. J., Marrero, M. B., & Fulton, D. J. R. (2007). Novel mechanism of activation of NADPH oxidase 5: Calcium sensitization via phosphorylation. *Journal of Biological Chemistry*, *282*(9), 6494–6507. <https://doi.org/10.1074/jbc.M608966200>
- Janda, E., Boi, L., & Carta, A. R. (2018). Microglial phagocytosis and its regulation: a therapeutic target in parkinson's disease? *Frontiers in Molecular Neuroscience*, *11*(April), 144. <https://doi.org/10.3389/fnmol.2018.00144>
- Jao, L. E., Wentz, S. R., & Chen, W. (2013). Efficient multiplex biallelic zebrafish genome editing using a CRISPR nuclease system. *Proceedings of the National Academy of Sciences of the United States of America*, *110*(34), 13904–13909. <https://doi.org/10.1073/pnas.1308335110>
- Kamsler, A., & Segal, M. (2003). Hydrogen peroxide modulation of synaptic plasticity. *The Journal of Neuroscience*, *23*(1), 269–276. <https://doi.org/doi.org/10.1523/JNEUROSCI.23-01-00269.2003>

- Karlstrom, R. O., Trowe, T., Klostermann, S., Baier, H., Brand, M., Crawford, A. D., ... Bonhoeffer, F. (1996). Zebrafish mutations affecting retinotectal axon pathfinding. *Development*, *123*, 427–438.
- Kawahara, T., & Lambeth, J. D. (2007). Molecular evolution of Phox -related regulatory subunits for NADPH oxidase enzymes. *BMC Evolutionary Biology*, *7*(178), 178. <https://doi.org/10.1186/1471-2148-7-178>
- Kawahara, T., Quinn, M. T., & Lambeth, J. D. (2007). Molecular evolution of the reactive oxygen-generating NADPH oxidase (Nox/Duox) family of enzymes. *BMC Evolutionary Biology*, *7*(109), 109. <https://doi.org/10.1186/1471-2148-7-109>
- Kawakami, K., Asakawa, K., Hibi, M., Itoh, M., Muto, A., & Wada, H. (2016). Gal4 driver transgenic zebrafish: Powerful tools to study developmental biology, organogenesis, and neuroscience. In *Advances in Genetics* (Vol. 95). <https://doi.org/10.1016/bs.adgen.2016.04.002>
- Kawakami, Koichi, Takeda, H., Kawakami, N., Kobayashi, M., Matsuda, N., & Mishina, M. (2004). A transposon-mediated gene trap approach identifies developmentally regulated genes in zebrafish. *Dev Cell*, *7*(1), 133–144. <https://doi.org/10.1016/j.devcel.2004.06.005>
- Kawano, M., Miyamoto, K., Kaito, Y., Sumimoto, H., & Tamura, M. (2012). Noxa1 as a moderate activator of Nox2-based NADPH oxidase. *Archives of Biochemistry and Biophysics*, *519*(1), 1–7. <https://doi.org/10.1016/j.abb.2011.12.025>
- Kay, J. N., Finger-Baier, K. C., Roeser, T., Staub, W., & Baier, H. (2001). Retinal ganglion cell genesis requires lakritz, a zebrafish atonal homolog. *Neuron*, *30*(3), 725–736. [https://doi.org/10.1016/S0896-6273\(01\)00312-9](https://doi.org/10.1016/S0896-6273(01)00312-9)
- Kay, J. N., Link, B. A., & Baier, H. (2005). Staggered cell-intrinsic timing of ath5 expression underlies the wave of ganglion cell neurogenesis in the zebrafish retina. *Development*, *132*(11), 2573–2585. <https://doi.org/10.1242/dev.01831>
- Kemp, H. A., Carmany-Rampey, A., & Moens, C. (2009). Generating Chimeric Zebrafish Embryos by Transplantation. *Journal of Visualized Experiments*, (29), 1–5. <https://doi.org/10.3791/1394>

- Kemp, K., Hares, K., Mallam, E., Heesom, K. J., Scolding, N., & Wilkins, A. (2010). Mesenchymal stem cell-secreted superoxide dismutase promotes cerebellar neuronal survival. *Journal of Neurochemistry*, *114*(6), 1569–1580. <https://doi.org/10.1111/j.1471-4159.2009.06553.x>
- Kennedy, K. A. M., Ostrakhovitch, E. A., Sandiford, S. D. E., Dayarathna, T., Xie, X., Waese, E. Y. L., ... Li, S. S. C. (2010). Mammalian numb-interacting protein 1/dual oxidase maturation factor 1 directs neuronal fate in stem cells. *Journal of Biological Chemistry*, *285*(23), 17974–17985. <https://doi.org/10.1074/jbc.M109.084616>
- Kidd, T., Brose, K., Mitchell, K. J., Fetter, R. D., Tessier-Lavigne, M., Goodman, C. S., & Tear, G. (1998). Roundabout controls axon crossing of the CNS midline and defines a novel subfamily of evolutionarily conserved guidance receptors. *Cell*, *92*(2), 205–215. [https://doi.org/10.1016/S0092-8674\(00\)80915-0](https://doi.org/10.1016/S0092-8674(00)80915-0)
- Kim, J.-S., Huang, T. Y., & Bokoch, G. M. (2009). Reactive oxygen species regulate a slingshot-cofilin activation pathway. *Molecular Biology of the Cell*, *20*, 2650–2660. <https://doi.org/10.1091/mbc.E09-02-0131>
- Kimmel, C. B., Ballard, W. W., Kimmel, S. R., Ullmann, B., & Schilling, T. F. (1995). Stages of embryonic development of the zebrafish. *Developmental Dynamics*, *203*(3), 253–310. <https://doi.org/10.1002/aja.1002030302>
- Kishida, K. T., Hoeffler, C. A., Hu, D., Pao, M., Holland, S. M., & Klann, E. (2006). Synaptic plasticity deficits and mild memory impairments in mouse models of chronic granulomatous disease. *Molecular and Cellular Biology*, *26*(15), 5908–5920. <https://doi.org/10.1128/MCB.00269-06>
- Kishida, K. T., & Klann, E. (2007). Sources and targets of reactive oxygen species in synaptic plasticity and memory. *Antioxidants and Redox Signaling*, *9*(2), 233–244. <https://doi.org/10.1089/ars.2007.9.233>
- Kishida, K. T., Pao, M., Holland, S. M., & Klann, E. (2005). NADPH oxidase is required for NMDA receptor-dependent activation of ERK in hippocampal area CA1. *Journal of Neurochemistry*, *94*(2), 299–306. <https://doi.org/10.1111/j.1471-4159.2005.03189.x>
- Kita, E. M., Scott, E. K., & Goodhill, G. J. (2015). Topographic wiring of the retinotectal connection in zebrafish. *Developmental Neurobiology*, *75*(6), 542–556. <https://doi.org/10.1002/dneu.22256>

- Klamt, F., Zdanov, S., Levine, R. L., Parisera, A., Zhang, Y., Zhang, B., ... Shacter, E. (2009). Oxidant-induced apoptosis is mediated by oxidation of the actin-regulatory protein cofilin. *Nature Cell Biology*, *11*(10), 1241–1246. <https://doi.org/10.1038/ncb1968>
- Klemke, M., Wabnitz, G. H., Funke, F., Funk, B., Kirchgessner, H., & Samstag, Y. (2008). Oxidation of cofilin mediates T cell hyporesponsiveness under oxidative stress conditions. *Immunity*, *29*(3), 404–413. <https://doi.org/10.1016/j.immuni.2008.06.016>
- Knoefler, D., Thamsen, M., Koniczek, M., Niemuth, N. J., Diederich, A. K., & Jakob, U. (2012). Quantitative in vivo redox sensors uncover oxidative stress as an early event in life. *Molecular Cell*, *47*(5), 767–776. <https://doi.org/10.1016/j.molcel.2012.06.016>
- Kokovay, E., Wang, Y., Kusek, G., Wurster, R., Lederman, P., Lowry, N., ... Temple, S. (2012). VCAM1 is essential to maintain the structure of the SVZ niche and acts as an environmental sensor to regulate SVZ lineage progression. *Cell Stem Cell*, *11*(2), 220–230. <https://doi.org/10.1016/j.stem.2012.06.016>
- Konovalova, J., Gerasymchuk, D., Parkkinen, I., Chmielarz, P., & Domanskyi, A. (2019). Interplay between MicroRNAs and oxidative stress in neurodegenerative diseases. *International Journal of Molecular Sciences*, *20*(23), 6055. <https://doi.org/10.3390/ijms20236055>
- Kuhn, T. B. (2014). Oxygen radicals elicit paralysis and collapse of spinal cord neuron growth cones upon exposure to proinflammatory cytokines. *Biomed Research International*, *2014*(191767), 191767. <https://doi.org/10.1155/2014/191767>
- Kuiper, J. W. P., Sun, C., Magalhães, M. A. O., & Glogauer, M. (2011). Rac regulates PtdInsP3 signaling and the chemotactic compass through a redox-mediated feedback loop. *Blood*, *118*(23), 6164–6171. <https://doi.org/10.1182/blood-2010-09-310383>
- Kuribayashi, F., Nuno, H., Wakamatsu, K., Tsunawaki, S., Sato, K., Ito, T., & Sumimoto, H. (2002). The adaptor protein p40phox as a positive regulator of the superoxide-producing phagocyte oxidase. *EMBO Journal*, *21*(23), 6312–6320. <https://doi.org/10.1093/emboj/cdf642>
- Kuroda, J., Nakagawa, K., Yamasaki, T., Nakamura, K. I., Takeya, R., Kuribayashi, F., ... Sumimoto, H. (2005). The superoxide-producing NAD(P)H oxidase Nox4 in the nucleus of human vascular endothelial cells. *Genes to Cells*, *10*(12), 1139–1151. <https://doi.org/10.1111/j.1365-2443.2005.00907.x>

- Kwan, K. M., Fujimoto, E., Grabher, C., Mangum, B. D., Hardy, M. E., Campbell, D. S., ... Chien, C. Bin. (2007). The Tol2kit: A multisite gateway-based construction Kit for Tol2 transposon transgenesis constructs. *Developmental Dynamics*, 236(11), 3088–3099. <https://doi.org/10.1002/dvdy.21343>
- Lalucque, H., & Silar, P. (2003). NADPH oxidase: an enzyme for multicellularity? *Trends in Microbiology*, 11(1), 9–12. [https://doi.org/10.1016/S0966-842X\(02\)00007-0](https://doi.org/10.1016/S0966-842X(02)00007-0)
- Le Belle, J. E., Orozco, N. M., Paucar, A. A., Saxe, J. P., Mottahedeh, J., Pyle, A. D., ... Kornblum, H. I. (2011). Proliferative neural stem cells have high endogenous ROS levels that regulate self-renewal and neurogenesis in a PI3K/Akt-dependant manner. *Cell Stem Cell*, 8(1), 59–71. <https://doi.org/10.1016/j.stem.2010.11.028>
- Le Belle, J. E., Sperry, J., Ngo, A., Ghochani, Y., Laks, D. R., López-Aranda, M., ... Kornblum, H. I. (2014). Maternal inflammation contributes to brain overgrowth and autism-associated behaviors through altered redox signaling in stem and progenitor cells. *Stem Cell Reports*, 3(5), 725–734. <https://doi.org/10.1016/j.stemcr.2014.09.004>
- Lee, J.-E., Cho, K. E., Lee, K. E., Kim, J., & Bae, Y. S. (2014). Nox4-mediated cell signaling regulates differentiation and survival of neural crest stem cells. *Molecules and Cells*, 37(12), 907–911. <https://doi.org/10.14348/molcells.2014.0244>
- Lee, J. S., Ray, R., & Chien, C. Bin. (2001). Cloning and expression of three zebrafish roundabout homologs suggest roles in axon guidance and cell migration. *Developmental Dynamics*, 221(2), 216–230. <https://doi.org/10.1002/dvdy.1136>
- Lelli, A., Gervais, A., Colin, C., Cheret, C., Ruiz De Almodovar, C., Carmeliet, P., ... Mallat, M. (2013). The NADPH oxidase Nox2 regulates VEGFR1/CSF-1R-mediated microglial chemotaxis and promotes early postnatal infiltration of phagocytes in the subventricular zone of the mouse cerebral cortex. *Glia*, 61(9), 1542–1555. <https://doi.org/10.1002/glia.22540>
- Li, J., Cao, L., & Staiger, C. J. (2017). Capping protein modulates actin remodeling in response to reactive oxygen species during plant innate immunity. *Plant Physiology*, 173(2), 1125–1136. <https://doi.org/10.1104/pp.16.00992>
- Li, J. M., & Shah, A. M. (2002). Intracellular localization and preassembly of the NADPH oxidase complex in cultured endothelial cells. *Journal of Biological Chemistry*, 277(22), 19952–19960. <https://doi.org/10.1074/jbc.M110073200>

- Li, J. M., & Shah, A. M. (2003). ROS generation by nonphagocytic NADPH oxidase: Potential relevance in diabetic nephropathy. *Journal of the American Society of Nephrology*, *14*, 221–226. <https://doi.org/10.1097/01.asn.0000077406.67663.e7>
- Li, P., White, R. M., & Zon, L. I. (2011). Transplantation in zebrafish. In *Methods Cell Biol* (Third Edit, Vol. 105). <https://doi.org/10.1016/B978-0-12-381320-6.00017-5>
- Li, Q. F., & Tang, D. D. (2009). Role of p47phox in regulating Cdc42GAP, vimentin, and contraction in smooth muscle cells. *American Journal of Physiology - Cell Physiology*, *297*(6), 1424–1433. <https://doi.org/10.1152/ajpcell.00324.2009>
- Li, Z., Ptak, D., Zhang, L., Walls, E. K., Zhong, W., & Leung, Y. F. (2012). Phenylthiourea specifically reduces zebrafish eye size. *PLoS ONE*, *7*(6), e40132. <https://doi.org/10.1371/journal.pone.0040132>
- Lin, C. H., Espreafico, E. M., Mooseker, M. S., & Forscher, P. (1996). Myosin drives retrograde F-actin flow in neuronal growth cones. *Neuron*, *16*(4), 769–782. [https://doi.org/10.1016/S0896-6273\(00\)80097-5](https://doi.org/10.1016/S0896-6273(00)80097-5)
- Lin, Chi Hung, & Forscher, P. (1993). Cytoskeletal remodeling during growth cone-target interactions. *Journal of Cell Biology*, *121*(6), 1369–1383. <https://doi.org/10.1083/jcb.121.6.1369>
- Long, H., Sabatier, C., Ma, L., Plump, A., Yuan, W., Ornitz, D. M., ... Tessier-Lavigne, M. (2004). Conserved roles for Slit and Robo proteins in midline commissural axon guidance. *Neuron*, *42*(2), 213–223. [https://doi.org/10.1016/S0896-6273\(04\)00179-5](https://doi.org/10.1016/S0896-6273(04)00179-5)
- Lopes, L. R., Dagher, M. C., Gutierrez, A., Young, B., Bouin, A. P., Fuchs, A., & Babior, B. M. (2004). Phosphorylated p40phox As a negative regulator of NADPH oxidase. *Biochemistry*, *43*(12), 3723–3730. <https://doi.org/10.1021/bi035636s>
- Lowery, L. A., & Vactor, D. Van. (2009). The trip of the tip: understanding the growth cone machinery. *Nature Reviews Molecular Cell Biology*, *10*(5), 332–343. <https://doi.org/10.1038/nrm2679>
- Lucas, B., & Hardin, J. (2017). Mind the (sr)GAP – roles of Slit–Robo GAPs in neurons, brains and beyond. *Journal of Cell Science*, *130*(3), 3965–3974. <https://doi.org/10.1242/jcs.215392>
- Luxen, S., Noack, D., Frausto, M., Davanture, S., Torbett, B. E., & Knaus, U. G. (2009). Heterodimerization controls localization of Duox-DuoxA NADPH oxidases in airway cells. *Journal of Cell Science*, *122*(8), 1236–1247. <https://doi.org/10.1242/jcs.044123>

- Ma, M. W., Wang, J., Zhang, Q., Wang, R., Dhandapani, K. M., Vadlamudi, R. K., & Brann, D. W. (2017). NADPH oxidase in brain injury and neurodegenerative disorders. *Molecular Neurodegeneration*, *12*(7), 7. <https://doi.org/10.1186/s13024-017-0150-7>
- Ma, Y., Mi, Y. J., Dai, Y. K., Fu, H. L., Cui, D. X., & Jin, W. L. (2013). The inverse F-BAR domain protein srGAP2 acts through srGAP3 to modulate neuronal differentiation and neurite outgrowth of mouse neuroblastoma cells. *PLoS ONE*, *8*(3), e57865. <https://doi.org/10.1371/journal.pone.0057865>
- Mahler, J., & Driever, W. (2007). Expression of the zebrafish intermediate neurofilament Nestin in the developing nervous system and in neural proliferation zones at postembryonic stages. *BMC Developmental Biology*, *7*, 1–11. <https://doi.org/10.1186/1471-213X-7-89>
- Marengo, B., Nitti, M., Furfaro, A. L., Colla, R., Ciucis, C. De, Marinari, U. M., ... Domenicotti, C. (2016). Redox homeostasis and cellular antioxidant systems: Crucial players in cancer growth and therapy. *Oxidative Medicine and Cellular Longevity*, *2016*, 6235641. <https://doi.org/10.1155/2016/6235641>
- Marrali, G., Casale, F., Salamone, P., Fuda, G., Caorsi, C., Amoroso, A., ... Chiò, A. (2014). NADPH oxidase (Nox2) activity is a modifier of survival in ALS. *Journal of Neurology*, *261*(11), 2178–2183. <https://doi.org/10.1007/s00415-014-7470-0>
- Martinez-Morales, J. R., Del Bene, F., Nica, G., Hammerschmidt, M., Bovolenta, P., & Wittbrodt, J. (2005). Differentiation of the vertebrate retina is coordinated by an FGF signaling center. *Developmental Cell*, *8*(4), 565–574. <https://doi.org/10.1016/j.devcel.2005.01.022>
- Masai, I., Stemple, D. L., Okamoto, H., & Wilson, S. W. (2000). Midline signals regulate retinal neurogenesis in zebrafish. *Neuron*, *27*(2), 251–263. [https://doi.org/10.1016/S0896-6273\(00\)00034-9](https://doi.org/10.1016/S0896-6273(00)00034-9)
- Mason, F. M., Heimsath, E. G., Higgs, H. N., & Soderling, S. H. (2011). Bi-modal regulation of a formin by srGAP2. *Journal of Biological Chemistry*, *286*(8), 6577–6586. <https://doi.org/10.1074/jbc.M110.190397>

- Mazzonetto, P. C., Ariza, C. B., Ocanha, S. G., de Souza, T. A., Ko, G. M., Menck, C. F. M., ... Porcionatto, M. A. (2019). Mutation in NADPH oxidase 3 (NOX3) impairs SHH signaling and increases cerebellar neural stem/progenitor cell proliferation. *Biochimica et Biophysica Acta - Molecular Basis of Disease*, 1865(6), 1502–1515.
<https://doi.org/10.1016/j.bbadis.2019.02.022>
- Mcphail, L. C., Henson, P. M., & Johnston, R. B. (1981). Respiratory burst enzyme in human neutrophils. Evidence for multiple mechanisms of activation. *Journal of Clinical Investigation*, 67(3), 710–716. <https://doi.org/10.1172/JCI110087>
- Meda, F., Gauron, C., Rampon, C., Teillon, J., Volovitch, M., & Vríz, S. (2016). Nerves control redox levels in mature tissues through schwann cells and hedgehog signaling. *Antioxidants & Redox Signaling*, 24(6), 299–311. <https://doi.org/10.1089/ars.2015.6380>
- Meda, F., Rampon, C., Dupont, E., Gauron, C., Mourton, A., Queguiner, I., ... Vríz, S. (2018). Nerves, H₂O₂ and Shh: three players in the game of regeneration. *Seminars in Cell and Developmental Biology*, 80, 65–73. <https://doi.org/10.1016/j.semcdb.2017.08.015>
- Miller, E. W., Dickinson, B. C., & Chang, C. J. (2010). Aquaporin-3 mediates hydrogen peroxide uptake to regulate downstream intracellular signaling. *PNAS*, 107(36), 15681–15686. <https://doi.org/10.1073/pnas.1005776107>
- Miller, K. E., & Suter, D. M. (2018). An integrated cytoskeletal model of neurite outgrowth. *Frontiers in Cellular Neuroscience*, 12(447), 447. <https://doi.org/10.3389/fncel.2018.00447>
- Min, J. Y., Park, M. H., Park, M. K., Park, K. W., Lee, N. W., Kim, T., ... Lee, D. H. (2006). Staurosporin induces neurite outgrowth through ROS generation in HN33 hippocampal cell lines. *Journal of Neural Transmission*, 113(11), 1821–1826.
<https://doi.org/10.1007/s00702-006-0500-z>
- Mizuki, K., Kadomatsu, K., Hata, K., Ito, T., Fan, Q., Kage, Y., ... Sumimoto, H. (1998). Functional modules and expression of mouse p40phox and p67phox, SH3-domain-containing proteins involved in the phagocyte NADPH oxidase complex. *European Journal of Biochemistry*, 251, 573–582. <https://doi.org/10.1046/j.1432-1327.1998.2510573.x>
- Mofarrahi, M., Brandes, R. P., Gorchach, A., Hanze, J., Terada, L. S., Quinn, M. T., ... Hussain, S. N. A. (2008). Regulation of proliferation of skeletal muscle precursor cells by NADPH oxidase. *Antioxidants & Redox Signaling*, 10(3), 559–574.
<https://doi.org/10.1089/ars.2007.1792>

- Morand, S., Ueyama, T., Tsujibe, S., Saito, N., Korzeniowska, A., & Leto, T. L. (2009). Duox maturation factors form cell surface complexes with Duox affecting the specificity of reactive oxygen species generation. *The FASEB Journal*, *23*(4), 1205–1218.
<https://doi.org/10.1096/fj.08-120006>
- Morinaka, A., Yamada, M., Itofusa, R., Funato, Y., Yoshimura, Y., Nakamura, F., ... Miki, H. (2011). Thioredoxin mediates oxidation-dependent phosphorylation of CRMP2 and growth cone collapse. *Science Signaling*, *4*(170), ra26. <https://doi.org/10.1126/scisignal.2001127>
- Muller, B., Stahl, B., & Bonhoeffer, F. (1990). In vitro experiments on axonal guidance and growth-cone collapse. *Journal of Experimental Biology*, *153*, 29–46.
- Munnamalai, V., & Suter, D. M. (2009). Reactive oxygen species regulate F-actin dynamics in neuronal growth cones and neurite outgrowth. *Journal of Neurochemistry*, *108*(3), 644–661.
<https://doi.org/10.1111/j.1471-4159.2008.05787.x>
- Munnamalai, V., Weaver, C. J., Weisheit, C. E., Venkatraman, P., Agim, Z. S., Quinn, M. T., & Suter, D. M. (2014). Bidirectional interactions between Nox2-type NADPH oxidase and the F-actin cytoskeleton in neuronal growth cones. *Journal of Neurochemistry*, *130*(4), 526–540. <https://doi.org/10.1111/jnc.12734>
- Narumiya, S., Tanji, M., & Ishizaki, T. (2009). Rho signaling, ROCK and mDia1, in transformation, metastasis and invasion. *Cancer and Metastasis Reviews*, *28*(1–2), 65–76.
<https://doi.org/10.1007/s10555-008-9170-7>
- Nathan, C., & Cunningham-Bussel, A. (2013). Beyond oxidative stress: an immunologist's guide to reactive oxygen species. *Nature Reviews Immunology*, *13*(5), 349–361.
<https://doi.org/10.1038/nri3423>
- Nayernia, Z., Colaianna, M., Robledinos-Antón, N., Gutzwiller, E., Sloan-Béna, F., Stathaki, E., ... Krause, K. H. (2017). Decreased neural precursor cell pool in NADPH oxidase 2-deficiency: from mouse brain to neural differentiation of patient derived iPSC. *Redox Biology*, *13*(April), 82–93. <https://doi.org/10.1016/j.redox.2017.04.026>
- Nayernia, Z., Jaquet, V., & Krause, K.-H. (2014). New insights on NOX enzymes in the central nervous system. *Antioxidants & Redox Signaling*, *20*(17), 2815–2837.
<https://doi.org/10.1089/ars.2013.5703>

- Neuhaus-Follini, A., & Bashaw, G. J. (2015). Crossing the embryonic midline: Molecular mechanisms regulating axon responsiveness at an intermediate target. *Wiley Interdisciplinary Reviews: Developmental Biology*, 4(4), 377–389.
<https://doi.org/10.1002/wdev.185>
- Neumann, C. J., & Nusslein-Volhard, C. (2000). Patterning of the zebrafish retina by a wave of sonic Hedgehog activity. *Science*, 289(5487), 2137–2139.
<https://doi.org/10.1126/science.289.5487.2137>
- Nguyen, T., Nioi, P., & Pickett, C. B. (2009). The Nrf2-antioxidant response element signaling pathway and its activation by oxidative stress. *Journal of Biological Chemistry*, 284(20), 13291–13295. <https://doi.org/10.1074/jbc.R900010200>
- Niethammer, P., Grabher, C., Look, A. T., & Mitchison, T. J. (2009). A tissue-scale gradient of hydrogen peroxide mediates rapid wound detection in zebrafish. *Nature*, 459(7249), 996–999. <https://doi.org/10.1038/nature08119>
- Nimmual, A. S., Taylor, L. J., & Bar-Sagi, D. (2003). Redox-dependent downregulation of Rho by Rac. *Nature Cell Biology*, 5(3), 236–241. <https://doi.org/10.1038/ncb938>
- Nisimoto, Y., Motalebi, S., Han, C. H., & Lambeth, J. D. (1999). The p67(phox) activation domain regulates electron flow from NADPH to flavin in flavocytochrome b558. *Journal of Biological Chemistry*, 274(33), 22999–23005. <https://doi.org/10.1074/jbc.274.33.22999>
- Nitti, M., Furfaro, A. L., Cevasco, C., Traverso, N., Marinari, U. M., Pronzato, M. A., & Domenicotti, C. (2010). PKC delta and NADPH oxidase in retinoic acid-induced neuroblastoma cell differentiation. *Cellular Signalling*, 22(5), 828–835.
<https://doi.org/10.1016/j.cellsig.2010.01.007>
- Nitti, M., Furfaro, A. L., Traverso, N., Odetti, P., Storage, D., Cottalasso, D., ... Domenicotti, C. (2007). PKC delta and NADPH oxidase in AGE-induced neuronal death. *Neuroscience Letters*, 416(3), 261–265. <https://doi.org/10.1016/j.neulet.2007.02.013>
- Olguín-Albuerne, M., & Morán, J. (2015). ROS produced by NOX2 control in vitro development of cerebellar granule neurons development. *ASN Neuro*, 7(2), 1759091415578712.
<https://doi.org/10.1177/1759091415578712>
- Omotade, O. F., Pollitt, S. L., & Zheng, J. Q. (2017). Actin-based growth cone motility and guidance. *Molecular and Cellular Neuroscience*, 84, 4–10.
<https://doi.org/10.1016/j.mcn.2017.03.001>

- Oster, S. F., Bodeker, M. O., He, F., & Sretavan, D. W. (2003). Invariant Sema5A inhibition serves an ensheathing function during optic nerve development. *Development*, *130*(4), 775–784. <https://doi.org/10.1242/dev.00299>
- Oster, S. F., Deiner, M., Birgbauer, E., & Sretavan, D. W. (2004). Ganglion cell axon pathfinding in the retina and optic nerve. *Seminars in Cell and Developmental Biology*, *15*(1), 125–136. <https://doi.org/10.1016/j.semcdb.2003.09.006>
- Ostrakhovitch, E. A., & Semenikhin, O. A. (2011). p53-mediated regulation of neuronal differentiation via regulation of dual oxidase maturation factor 1. *Neuroscience Letters*, *494*(1), 80–85. <https://doi.org/10.1016/j.neulet.2011.02.061>
- Oury, T. D., Card, J. P., & Klann, E. (1999). Localization of extracellular superoxide dismutase in adult mouse brain. *Brain Research*, *850*(1–2), 96–103. [https://doi.org/10.1016/S0006-8993\(99\)02103-4](https://doi.org/10.1016/S0006-8993(99)02103-4)
- Paffenholz, R., Bergstrom, R. A., Pasutto, F., Wabnitz, P., Munroe, R. J., Jagla, W., ... Bergstrom, D. E. (2004). Vestibular defects in head-tilt mice result from mutations in *Nox3*, encoding an NADPH oxidase. *Genes and Development*, *18*(5), 486–491. <https://doi.org/10.1101/gad.1172504>
- Pao, M., Wiggs, E. A., Anastacio, M. M., Hyun, J., DeCarlo, E. S., Miller, J. T., ... Holland, S. M. (2004). Cognitive function in patients with chronic granulomatous disease: a preliminary report. *Psychosomatics*, *45*(3), 230–234. <https://doi.org/10.1176/appi.psy.45.3.230>
- Park, L., Zhou, P., Pitstick, R., Capone, C., Anrather, J., Norris, E. H., ... Iadecola, C. (2008). *Nox2*-derived radicals contribute to neurovascular and behavioral dysfunction in mice overexpressing the amyloid precursor protein. *PNAS*, *105*(4), 1347–1352. <https://doi.org/10.1073/pnas.0711568105>
- Perez Estrada, C., Covacu, R., Sankavaram, S. R., Svensson, M., & Brundin, L. (2014). Oxidative stress increases neurogenesis and oligodendrogenesis in adult neural progenitor cells. *Stem Cells and Development*, *23*(19), 2311–2327. <https://doi.org/10.1089/scd.2013.0452>
- Peterson, S. M., & Freeman, J. L. (2009). RNA isolation from embryonic zebrafish and cDNA synthesis for gene expression analysis. *Journal of Visualized Experiments*, *30*. <https://doi.org/10.3791/1470>

- Picker, A., & Brand, M. (2005). Fgf signals from a novel signaling center determine axial patterning of the prospective neural retina. *Development*, *132*(22), 4951–4962. <https://doi.org/10.1242/dev.02071>
- Piper, M., Anderson, R., Dwivedy, A., Weinl, C., Van Horck, F., Leung, K. M., ... Holt, C. (2006). Signaling mechanisms underlying Slit2-induced collapse of *Xenopus* retinal growth cones. *Neuron*, *49*(2), 215–228. <https://doi.org/10.1016/j.neuron.2005.12.008>
- Pittman, A. J., Law, M. Y., & Chien, C. Bin. (2008). Pathfinding in a large vertebrate axon tract: Isotypic interactions guide retinotectal axons at multiple choice points. *Development*, *135*(17), 2865–2871. <https://doi.org/10.1242/dev.025049>
- Plachez, C., Andrews, W., Liapi, A., Knoell, B., Drescher, U., Mankoo, B., ... Sundaresan, V. (2008). Robos are required for the correct targeting of retinal ganglion cell axons in the visual pathway of the brain. *Molecular and Cellular Neuroscience*, *37*(4), 719–730. <https://doi.org/10.1016/j.mcn.2007.12.017>
- Plump, A. S., Erskine, L., Sabatier, C., Brose, K., Epstein, C. J., Goodman, C. S., ... Tessier-Lavigne, M. (2002). Slit1 and Slit2 cooperate to prevent premature midline crossing of retinal axons in the mouse visual system. *Neuron*, *33*(2), 219–232. [https://doi.org/10.1016/S0896-6273\(01\)00586-4](https://doi.org/10.1016/S0896-6273(01)00586-4)
- Pollock, J. D., Williams, D. A., Gifford, M. A. C., Li, L. L., Du, X., Fisherman, J., ... Dinauer, M. C. (1995). Mouse model of X-linked chronic granulomatous disease, an inherited defect in phagocyte superoxide production. *Nature Genetics*, *9*, 202–209. <https://doi.org/10.1038/ng0295-202>
- Rada, B., & Leto, T. L. (2008). Oxidative innate immune defenses by Nox/Duox family NADPH Oxidases. *Contributions to Microbiology*, *15*, 164–187. <https://doi.org/10.1159/000136357>
- Raftopoulou, M., & Hall, A. (2004). Cell migration: Rho GTPases lead the way. *Developmental Biology*, *265*(1), 23–32. <https://doi.org/10.1016/j.ydbio.2003.06.003>
- Rama Rao, K. V., Iring, S., Younger, D., Kuriakose, M., Skotak, M., Alay, E., ... Chandra, N. (2018). A single primary blast-induced traumatic brain injury in a rodent model causes cell-type dependent increase in nicotinamide adenine dinucleotide phosphate oxidase isoforms in vulnerable brain regions. *Journal of Neurotrauma*, *35*(17), 2077–2090. <https://doi.org/10.1089/neu.2017.5358>

- Rao, X., Huang, X., Zhou, Z., & Lin, X. (2013). An improvement of the $2^{-(\Delta\Delta CT)}$ method for quantitative real-time polymerase chain reaction data analysis. *Biostatistics, Bioinformatics and Biomathematics*, 3(3), 71–85.
- Ravelli, K. G., Santos, G. D., dos Santos, N. B., Munhoz, C. D., Azzi-Nogueira, D., Campos, A. C., ... Hernandez, M. S. (2019). Nox2-dependent neuroinflammation in an EAE model of multiple sclerosis. *Translational Neuroscience*, 10, 1–9. <https://doi.org/10.1515/tnsci-2019-0001>
- Reczek, C. R., & Chandel, N. S. (2015). ROS-dependent signal transduction. *Current Opinion in Cell Biology*, 33, 8–13. <https://doi.org/10.1016/j.ceb.2014.09.010>
- Ren, Y., He, Y., Brown, S., Zbornik, E., Mlodzianoski, M. J., Ma, D., ... Suter, D. M. (2019). A single tyrosine phosphorylation site in cortactin is important for filopodia formation in neuronal growth cones. *Molecular Biology of the Cell*, 30(15), 1781–1877. <https://doi.org/10.1091/mbc.e18-04-0202>
- Rieger, S., & Sagasti, A. (2011). Hydrogen peroxide promotes injury-induced peripheral sensory axon regeneration in the zebrafish skin. *PLoS Biology*, 9(5), e1000621. <https://doi.org/10.1371/journal.pbio.1000621>
- Rigutto, S., Hoste, C., Grasberger, H., Milenkovic, M., Communi, D., Dumont, J. E., ... de Deken, X. (2009). Activation of dual oxidases Duox1 and Duox2: differential regulation mediated by cAMP-dependent protein kinase and protein kinase C-dependent phosphorylation. *Journal of Biological Chemistry*, 284(11), 6725–6734. <https://doi.org/10.1074/jbc.M806893200>
- Robles, E., Filosa, A., & Baier, H. (2013). Precise lamination of retinal axons generates multiple parallel input pathways in the tectum. *Journal of Neuroscience*, 33(11), 5027–5039. <https://doi.org/10.1523/JNEUROSCI.4990-12.2013>
- Robles, E., Laurell, E., & Baier, H. (2014). The retinal projectome reveals brain-area-specific visual representations generated by ganglion cell diversity. *Current Biology*, 24(18), 2085–2096. <https://doi.org/10.1016/j.cub.2014.07.080>
- Rola, R., Zou, Y., Huang, T. T., Fishman, K., Baure, J., Rosi, S., ... Fike, J. R. (2007). Lack of extracellular superoxide dismutase (EC-SOD) in the microenvironment impacts radiation-induced changes in neurogenesis. *Free Radical Biology and Medicine*, 42(8), 1133–1145. <https://doi.org/10.1016/j.freeradbiomed.2007.01.020>

- Rolas, L., Boussif, A., Weiss, E., Lettéron, P., Haddad, O., El-Benna, J., ... Périanin, A. (2018). NADPH oxidase depletion in neutrophils from patients with cirrhosis and restoration via toll-like receptor 7/8 activation. *Gut*, *67*(8), 1505–1516. <https://doi.org/10.1136/gutjnl-2016-313443>
- Rossi, A., Kontarakis, Z., Gerri, C., Nolte, H., Hölper, S., Krüger, M., & Stainier, D. Y. R. (2015). Genetic compensation induced by deleterious mutations but not gene knockdowns. *Nature*, *524*(7564), 230–233. <https://doi.org/10.1038/nature14580>
- Ryder, L. S., Dagdas, Y. F., Mentlak, T. A., Kershaw, M. J., Thornton, C. R., Schuster, M., ... Talbot, N. J. (2013). NADPH oxidases regulate septin-mediated cytoskeletal remodeling during plant infection by the rice blast fungus. *PNAS*, *110*(8), 3179–3184. <https://doi.org/10.1073/pnas.1217470110>
- Sakai, J. A., & Halloran, M. C. (2006). Semaphorin 3d guides laterality of retinal ganglion cell projections in zebrafish. *Development*, *133*(6), 1035–1044. <https://doi.org/10.1242/dev.02272>
- Sakai, J., Li, J., Subramanian, K. K., Mondal, S., Bajrami, B., Hattori, H., ... Luo, H. R. (2012). Reactive oxygen species-induced actin glutathionylation controls actin dynamics in neutrophils. *Immunity*, *37*(6), 1037–1049. <https://doi.org/10.1016/j.immuni.2012.08.017>
- Sant, K. E., Hansen, J. M., Williams, L. M., Tran, N. L., Goldstone, J. V., Stegeman, J. J., ... Timme-Laragy, A. (2017). The role of Nrf1 and Nrf2 in the regulation of glutathione and redox dynamics in the developing zebrafish embryo. *Redox Biology*, *13*, 207–218. <https://doi.org/10.1016/j.redox.2017.05.023>
- Scherz-Shouval, R., Shvets, E., Fass, E., Shorer, H., Gil, L., & Elazar, Z. (2007). Reactive oxygen species are essential for autophagy and specifically regulate the activity of Atg4. *EMBO Journal*, *26*(7), 1749–1760. <https://doi.org/10.1038/sj.emboj.7601623>
- Schiavone, S., Neri, M., Trabace, L., & Turillazzi, E. (2017). The NADPH oxidase NOX2 mediates loss of parvalbumin interneurons in traumatic brain injury: human autoptic immunohistochemical evidence. *Scientific Reports*, *7*(1), 8752. <https://doi.org/10.1038/s41598-017-09202-4>

- Schröder, K., Zhang, M., Benkhoff, S., Mieth, A., Pliquett, R., Kosowski, J., ... Brandes, R. P. (2012). Nox4 is a protective reactive oxygen species generating vascular NADPH oxidase. *Circulation Research*, *110*(9), 1217–1225.
<https://doi.org/10.1161/CIRCRESAHA.112.267054>
- Seeger, M., Tear, G., Ferres-Marco, D., & Goodman, C. S. (1993). Mutations affecting growth cone guidance in drosophila: Genes necessary for guidance toward or away from the midline. *Neuron*, *10*(3), 409–426. [https://doi.org/10.1016/0896-6273\(93\)90330-T](https://doi.org/10.1016/0896-6273(93)90330-T)
- Serrander, L., Cartier, L., Bedard, K., Banfi, B., Lardy, B., Plastre, O., ... Krause, K.-H. (2007). Nox4 activity is determined by mRNA levels and reveals a unique pattern of ROS generation. *Biochemical Journal*, *406*(1), 105–114. <https://doi.org/10.1042/bj20061903>
- Serrander, L., Jaquet, V., Bedard, K., Plastre, O., Hartley, O., Arnaudeau, S., ... Krause, K. H. (2007). Nox5 is expressed at the plasma membrane and generates superoxide in response to protein kinase C activation. *Biochimie*, *89*(9), 1159–1167.
<https://doi.org/10.1016/j.biochi.2007.05.004>
- Serrano, F., Kolluri, N. S., Wientjes, F. B., Card, J. P., & Klann, E. (2003). NADPH oxidase immunoreactivity in the mouse brain. *Brain Research*, *988*(1–2), 193–198.
[https://doi.org/10.1016/S0006-8993\(03\)03364-X](https://doi.org/10.1016/S0006-8993(03)03364-X)
- Sham, D., Wesley, U. V., Hristova, M., & van der Vliet, A. (2013). ATP-mediated transactivation of the epidermal growth factor receptor in airway epithelial cells involves DUOX1-dependent oxidation of Src and ADAM17. *PLoS ONE*, *8*(1), e54391.
<https://doi.org/10.1371/journal.pone.0054391>
- Shanmugasundaram, K., Nayak, B. K., Friedrichs, W. E., Kaushik, D., Rodriguez, R., & Block, K. (2017). NOX4 functions as a mitochondrial energetic sensor coupling cancer metabolic reprogramming to drug resistance. *Nature Communications*, *8*(1), 997.
<https://doi.org/10.1038/s41467-017-01106-1>
- Shao, D., Segal, A. W., & Dekker, L. V. (2010). Subcellular localisation of the p40phox component of NADPH oxidase involves direct interactions between the Phox homology domain and F-actin. *International Journal of Biochemistry and Cell Biology*, *42*(10), 1736–1743. <https://doi.org/10.1016/j.biocel.2010.07.009>

- Sharma, N., & Nehru, B. (2016). Apocyanin, a microglial NADPH oxidase inhibitor prevents dopaminergic neuronal degeneration in lipopolysaccharide-induced parkinson's disease model. *Molecular Neurobiology*, *53*(5), 3326–3337. <https://doi.org/10.1007/s12035-015-9267-2>
- Shiose, A., Kuroda, J., Tsuruya, K., Hirai, M., Hirakata, H., Naitoi, S., ... Sumimoto, H. (2001). A novel superoxide-producing NAD(P)H oxidase in kidney. *Journal of Biological Chemistry*, *276*(2), 1417–1423. <https://doi.org/10.1074/jbc.M007597200>
- Siebold, C., Berrow, N., Walter, T. S., Harlos, K., Owens, R. J., Stuart, D. I., ... Jones, E. Y. (2005). High-resolution structure of the catalytic region of MICAL (molecule interacting with CasL), a multidomain flavoenzyme-signaling molecule. *Proceedings of the National Academy of Sciences*, *102*(46), 16836–16841. <https://doi.org/10.1073/pnas.0504997102>
- Sirokmány, G., Donkó, Á., & Geiszt, M. (2016). Nox/Duox family of NADPH oxidases: lessons from knockout mouse models. *Trends in Pharmacological Sciences*, *37*(4), 318–327. <https://doi.org/10.1016/j.tips.2016.01.006>
- Small, E. M., Sutherland, L. B., Rajagopalan, K. N., Wang, S., & Olson, E. N. (2010). MicroRNA-218 regulates vascular patterning by modulation of slit-robo signaling. *Circulation Research*, *107*(11), 1336–1344. <https://doi.org/10.1161/CIRCRESAHA.110.227926>
- Somanna, N. K., Valente, A. J., Krenz, M., Fay, W. P., Delafontaine, P., & Chandrasekar, B. (2016). The Nox1/4 dual inhibitor GKT137831 or Nox4 knockdown inhibits angiotensin-II-induced adult mouse cardiac fibroblast proliferation and migration. AT1 physically associates with Nox4. *Journal of Cellular Physiology*, *231*(5), 1130–1141. <https://doi.org/10.1002/jcp.25210>
- Sorce, S., & Krause, K.-H. (2009). NOX enzymes in the central nervous system: from signaling to disease. *Antioxidants & Redox Signaling*, *11*(10), 2481–2504. <https://doi.org/10.1089/ARS.2009.2578>
- Souren, M., Martinez-Morales, J. R., Makri, P., Wittbrodt, B., & Wittbrodt, J. (2009). A global survey identifies novel upstream components of the Ath5 neurogenic network. *Genome Biology*, *10*(9), 1–16. <https://doi.org/10.1186/gb-2009-10-9-r92>
- Sretavan, D. W., & Reichardt, L. F. (1993). Time-lapse video analysis of retinal ganglion cell axon pathfinding at the mammalian optic chiasm: growth cone guidance using intrinsic chiasm cues. *Neuron*, *10*(4), 761–777. [https://doi.org/10.1016/0896-6273\(93\)90176-R](https://doi.org/10.1016/0896-6273(93)90176-R)

- Stein, E., & Tessier-Lavigne, M. (2001). Hierarchical organization of guidance receptors: Silencing of netrin attraction by slit through a Robo/DCC receptor complex. *Science*, 291(5510), 1928–1938. <https://doi.org/10.1126/science.1058445>
- Stenkamp, D. L. (2015). Development of the Vertebrate Eye and Retina. In *Molecular Biology of Eye Disease* (1st ed., Vol. 134). <https://doi.org/10.1016/bs.pmbts.2015.06.006>
- Stuermer, C. A. O. (1988). Retinotopic organization of the developing retinotectal projection in the zebrafish embryo. *Journal of Neuroscience*, 8(12), 4513–4530. <https://doi.org/10.1523/jneurosci.08-12-04513.1988>
- Sucharov, J., Ray, K., Brooks, E. P., & Nichols, J. T. (2019). Selective breeding modifies mef2ca mutant incomplete penetrance by tuning the opposing Notch pathway. *PLoS Genetics*, 15(12), e1008507. <https://doi.org/10.1371/journal.pgen.1008507>
- Suh, C. Il, Stull, N. D., Xing, J. L., Tian, W., Price, M. O., Grinstein, S., ... Dinauer, M. C. (2006). The phosphoinositide-binding protein p40phox activates the NADPH oxidase during FcγIIA receptor-induced phagocytosis. *Journal of Experimental Medicine*, 203(8), 1915–1925. <https://doi.org/10.1084/jem.20052085>
- Sumimoto, H. (2008). Structure, regulation and evolution of Nox-family NADPH oxidases that produce reactive oxygen species. *FEBS Journal*, 275(13), 3249–3277. <https://doi.org/10.1111/j.1742-4658.2008.06488.x>
- Suter, D. M. (2011). *Live Cell Imaging of Neuronal Growth Cone Motility and Guidance In Vitro*. https://doi.org/10.1007/978-1-61779-207-6_6
- Suter, D. M., & Forscher, P. (1998). An emerging link between cytoskeletal dynamics and cell adhesion molecules in growth cone guidance. *Current Opinion in Neurobiology*, 8(1), 106–116. [https://doi.org/10.1016/S0959-4388\(98\)80014-7](https://doi.org/10.1016/S0959-4388(98)80014-7)
- Suzukawa, K., Miura, K., Mitsushita, J., Resau, J., Hirose, K., Crystal, R., & Kamata, T. (2000a). Nerve growth factor-induced neuronal differentiation requires generation of Rac1-regulated reactive oxygen species. *Journal of Biological Chemistry*, 275(18), 13175–13178. <https://doi.org/10.1074/jbc.275.18.13175>
- Suzukawa, K., Miura, K., Mitsushita, J., Resau, J., Hirose, K., Crystal, R., & Kamata, T. (2000b). Nerve growth factor-induced neuronal differentiation requires generation of Rac1-regulated reactive oxygen species. *Journal of Biological Chemistry*, 275(18), 13175–13178. <https://doi.org/10.1074/jbc.275.18.13175>

- Takac, I., Schröder, K., Zhang, L., Lardy, B., Anilkumar, N., Lambeth, J. D., ... Brandes, R. P. (2011). The E-loop is involved in hydrogen peroxide formation by the NADPH oxidase Nox4. *Journal of Biological Chemistry*, 286(15), 13304–13313.
<https://doi.org/10.1074/jbc.M110.192138>
- Tamura, M., Kanno, M., & Endo, Y. (2000). Deactivation of neutrophil NADPH oxidase by actin-depolymerizing agents in a cell-free system. *Biochemical Journal*, 349(1), 369–375.
<https://doi.org/10.1042/bj3490369>
- Tanaka, E., & Sabry, J. (1995). Making the connection: cytoskeletal rearrangements during growth cone guidance. *Cell*, 83(2), 171–176. [https://doi.org/10.1016/0092-8674\(95\)90158-2](https://doi.org/10.1016/0092-8674(95)90158-2)
- Taniyama, Y., & Griendling, K. K. (2003). Reactive oxygen species in the vasculature: molecular and cellular mechanisms. *Hypertension*, 42(6), 1075–1081.
<https://doi.org/10.1161/01.HYP.0000100443.09293.4F>
- Taulet, N., Delorme-Walker, V. D., & DerMardirossian, C. (2012). Reactive oxygen species regulate protrusion efficiency by controlling actin dynamics. *PLoS ONE*, 7(8), e41342.
<https://doi.org/10.1371/journal.pone.0041342>
- Tejada-Simon, M. V., Serrano, F., Villasana, L. E., Kanterewicz, B. I., Wu, G. Y., Quinn, M. T., & Klann, E. (2005). Synaptic localization of a functional NADPH oxidase in the mouse hippocampus. *Molecular and Cellular Neuroscience*, 29(1), 97–106.
<https://doi.org/10.1016/j.mcn.2005.01.007>
- Terzi, A., & Suter, D. M. (2020). The role of NADPH oxidases in neuronal development. *Free Radical Biology and Medicine*, 154, 33–47.
<https://doi.org/10.1016/j.freeradbiomed.2020.04.027>
- Tessier-lavigne, M., & Goodman, C. S. (1996). The molecular biology of axon guidance. *Science*, 274(5290), 1123–1133. <https://doi.org/10.1126/science.274.5290.1123>
- Thompson, H., Barker, D., Camand, O., & Erskine, L. (2006). Slits contribute to the guidance of retinal ganglion cell axons in the mammalian optic tract. *Developmental Biology*, 296(2), 476–484. <https://doi.org/10.1016/j.ydbio.2006.06.017>
- Thompson, H., Camand, O., Barker, D., & Erskine, L. (2006). Slit proteins regulate distinct aspects of retinal ganglion cell axon guidance within dorsal and ventral retina. *Journal of Neuroscience*, 26(31), 8082–8091. <https://doi.org/10.1523/JNEUROSCI.1342-06.2006>

- Timme-Laragy, A. R., Goldstone, J. V., Imhoff, B. R., Stegeman, J. J., Hahn, M. E., & Hansen, J. M. (2013). Glutathione redox dynamics and expression of glutathione-related genes in the developing embryo. *Free Radical Biology and Medicine*, *65*, 89–101.
<https://doi.org/10.1016/j.freeradbiomed.2013.06.011>
- Topchiy, E., Panzhinskiy, E., Griffin, W. S. T., Barger, S. W., Das, M., & Zawada, W. M. (2013). Nox4-generated superoxide drives angiotensin II-induced neural stem cell proliferation. *Developmental Neuroscience*, *35*(4), 293–305.
<https://doi.org/10.1159/000350502>
- Torreillas, G., Boyano-Adanez, M. D. C., Medina, J., Parra, T., Griera, M., Lopez-Ongil, S., ... Rodriguez-Puyol, D. (2001). The role of hydrogen peroxide in the contractile response to angiotensin II. *Molecular Pharmacology*, *59*(1), 104–112.
<https://doi.org/10.1124/mol.59.1.104>
- Touyz, R. M., Yao, G., Quinn, M. T., Pagano, P. J., & Schiffrin, E. L. (2005). p47phox associates with the cytoskeleton through cortactin in human vascular smooth muscle cells role in NAD(P)H oxidase regulation by angiotensin II. *Arteriosclerosis, Thrombosis, and Vascular Biology*, *25*(3), 512–518. <https://doi.org/10.1161/01.ATV.0000154141.66879.98>
- Truong, T. H., & Carroll, K. S. (2013). Redox regulation of protein kinases. *Critical Reviews in Biochemistry and Molecular Biology*, *48*(4), 332–356.
<https://doi.org/10.3109/10409238.2013.790873>
- Tsatmali, M., Walcott, E. C., & Crossin, K. L. (2005). Newborn neurons acquire high levels of reactive oxygen species and increased mitochondrial proteins upon differentiation from progenitors. *Brain Research*, *1040*(1–2), 137–150.
<https://doi.org/10.1016/j.brainres.2005.01.087>
- Tsatmali, M., Walcott, E. C., Makarenkova, H., & Crossin, K. L. (2006). Reactive oxygen species modulate the differentiation of neurons in clonal cortical cultures. *Molecular and Cellular Neuroscience*, *33*(4), 345–357. <https://doi.org/10.1016/j.mcn.2006.08.005>
- Tsunawaki, S., & Yoshikawa, K. (2000). Relationships of p40phox with p67phox in the activation and expression of the human respiratory burst NADPH oxidase. *Journal of Biochemistry*, *128*, 777–783. <https://doi.org/10.1093/oxfordjournals.jbchem.a022815>
- Turpaev, K. T. (2002). Reactive oxygen species and regulation of gene expression. *Biochemistry*, *67*(3), 281–292. <https://doi.org/10.1023/a:1014819832003>

- Ueno, N., Takeya, R., Miyano, K., Kikuchi, H., & Sumimoto, H. (2005). The NADPH oxidase Nox3 constitutively produces superoxide in a p22 phox-dependent manner: its regulation by oxidase organizers and activators. *Journal of Biological Chemistry*, *280*(24), 23328–23339. <https://doi.org/10.1074/jbc.M414548200>
- Ueyama, T., Geiszt, M., & Leto, T. L. (2006). Involvement of Rac1 in activation of multicomponent Nox1- and Nox3- based NADPH oxidases. *Molecular and Cellular Biology*, *26*(6), 2160–2174. <https://doi.org/10.1128/MCB.26.6.2160-2174.2006>
- Ueyama, T., Nakakita, J., Nakamura, T., Kobayashi, T., Kobayashi, T., Son, J., ... Saito, N. (2011). Cooperation of p40phox with p47phox for Nox2-based NADPH oxidase activation during Fcγ receptor (FcγR)-mediated phagocytosis: mechanism for acquisition of p40 phox phosphatidylinositol 3-phosphate (PI(3)P) binding. *Journal of Biological Chemistry*, *286*(47), 40693–40705. <https://doi.org/10.1074/jbc.M111.237289>
- Usatyuk, P. V., Romer, L. H., He, D., Parinandi, N. L., Kleinberg, M. E., Zhan, S., ... Natarajan, V. (2007). Regulation of hyperoxia-induced NADPH oxidase activation in human lung endothelial cells by the actin cytoskeleton and cortactin. *Journal of Biological Chemistry*, *282*(32), 23284–23295. <https://doi.org/10.1074/jbc.M700535200>
- Ushio-Fukai, M. (2009). Compartmentalization of redox signaling through NADPH oxidase-derived ROS. *Antioxidants and Redox Signaling*, *11*(6), 1289–1299. <https://doi.org/10.1089/ars.2008.2333>
- Valek, L., Häußler, A., Dröse, S., Eaton, P., Schröder, K., & Tegeder, I. (2017). Redox-guided axonal regrowth requires cyclic GMP dependent protein kinase 1: implication for neuropathic pain. *Redox Biology*, *11*, 176–191. <https://doi.org/10.1016/j.redox.2016.12.004>
- Vallet, P., Charnay, Y., Steger, K., Ogier-Denis, E., Kovari, E., Herrmann, F., ... Szanto, I. (2005). Neuronal expression of the NADPH oxidase NOX4, and its regulation in mouse experimental brain ischemia. *Neuroscience*, *132*(2), 233–238. <https://doi.org/10.1016/j.neuroscience.2004.12.038>
- Van Buul, J. D., Fernandez-Borja, M., & Hordijk, P. L. (2005). Expression and localization of Nox2 and Nox4 in primary human endothelial cells. *Antioxidants & Redox Signaling*, *7*, 308–317. <https://doi.org/10.1089/ars.2005.7.308>

- Wang, X., Wang, Z., Yao, Y., Li, J., Zhang, X., Li, C., ... Ding, Z. (2011). Essential role of ERK activation in neurite outgrowth induced by α -lipoic acid. *Biochimica et Biophysica Acta*, *1813*(5), 827–838. <https://doi.org/10.1016/j.bbamer.2011.01.027>
- Wang, Yaping, Dakubo, G. D., Thurig, S., Mazerolle, C. J., & Wallace, V. A. (2005). Retinal ganglion cell-derived sonic hedgehog locally controls proliferation and the timing of RGC development in the embryonic mouse retina. *Development*, *132*(22), 5103–5113. <https://doi.org/10.1242/dev.02096>
- Wang, Ying, Branicky, R., Noë, A., & Hekimi, S. (2018). Superoxide dismutases: dual roles in controlling ROS damage and regulating ROS signaling. *Journal of Cell Biology*, *217*(6), 1915–1928. <https://doi.org/10.1083/jcb.201708007>
- Weaver, C. J., Leung, Y. F., & Suter, D. M. (2016). Expression dynamics of NADPH oxidases during early zebrafish development. *Journal of Comparative Neurology*, *524*(10), 2130–2141. <https://doi.org/10.1002/cne.23938>
- Weaver, C. J., Terzi, A., Roeder, H., Gurol, T., Deng, Q., Leung, Y. F., & Suter, D. M. (2018). *nox2/cybb* deficiency affects zebrafish retinotectal connectivity. *Journal of Neuroscience*, *38*(26), 5854–5871. <https://doi.org/10.1523/JNEUROSCI.1483-16.2018>
- Weinberg, F., Ramnath, N., & Nagrath, D. (2019). Reactive oxygen species in the tumor microenvironment: an overview. *Cancers*, *11*(8), E1191. <https://doi.org/10.3390/cancers11081191>
- Westerfield, M. (2000). *The zebrafish book. A guide for the laboratory use of zebrafish (Danio rerio)* (4th ed.). Eugene, OR: Univ. of Oregon Press.
- Westerfield, Monte, Zon, L. I., & Detrich III, H. W. (2009). *Essential zebrafish methods: Cell and developmental biology* (1st ed.; Monte Westerfield, L. I. Zon, & H. W. Detrich III, eds.). Academic Press.
- Wientjes, F. B., Hsuan, J. J., Totty, N. F., & Segal, A. W. (1993). p40(phox), a third cytosolic component of the activation complex of the NADPH oxidase to contain src homology 3 domains. *Biochemical Journal*, *296*(3), 557–561. <https://doi.org/10.1042/bj2960557>
- Wientjes, Frans B., Panayotou, G., Reeves, E., & Segal, A. W. (1996). Interactions between cytosolic components of the NADPH oxidase: p40phox interacts with both p67phox and p47phox. *Biochemical Journal*, *317*(3), 919–924. <https://doi.org/10.1042/bj3170919>

- Wientjes, Frans B., Reeves, E. P., Soskic, V., Furthmayr, H., & Segal, A. W. (2001). The NADPH oxidase components p47phox and p40phox bind to moesin through their PX domain. *Biochemical and Biophysical Research Communications*, *289*(2), 382–388. <https://doi.org/10.1006/bbrc.2001.5982>
- Wilkinson, R. N., Elworthy, S., Ingham, P. W., & van Eeden, F. J. M. (2013). A method for high-throughput PCR-based genotyping of larval zebrafish tail biopsies. *BioTechniques*, *55*(6), 314–316. <https://doi.org/10.2144/000114116>
- Wilson, C., & González-Billault, C. (2015). Regulation of cytoskeletal dynamics by redox signaling and oxidative stress: implications for neuronal development and trafficking. *Frontiers in Cellular Neuroscience*, *9*(381), 381. <https://doi.org/10.3389/fncel.2015.00381>
- Wilson, C., Muñoz-Palma, E., & González-Billault, C. (2018). From birth to death: a role for reactive oxygen species in neuronal development. *Seminars in Cell and Developmental Biology*, *80*, 43–49. <https://doi.org/10.1016/j.semcdb.2017.09.012>
- Wilson, C., Muñoz-Palma, E., Henríquez, D. R., Palmisano, I., Núñez, M. T., Di Giovanni, S., & González-Billault, C. (2016). A feed-forward mechanism involving the NOX complex and RyR-mediated Ca²⁺ release during axonal specification. *Journal of Neuroscience*, *36*(43), 11107–11119. <https://doi.org/10.1523/JNEUROSCI.1455-16.2016>
- Wilson, C., Nunez, M. T., & González-Billault, C. (2015). Contribution of NADPH oxidase to the establishment of hippocampal neuronal polarity in culture. *Journal of Cell Science*, *128*(16), 2989–2995. <https://doi.org/10.1242/jcs.168567>
- Wilson, C., Terman, J. R., González-Billault, C., & Ahmed, G. (2016). Actin filaments—A target for redox regulation. *Cytoskeleton*, *73*(10), 577–595. <https://doi.org/10.1002/cm.21315>
- Wong, K., Park, H. T., Wu, J. Y., & Rao, Y. (2002). Slit proteins : molecular guidance cues for cells ranging from neurons to leukocytes. *Current Opinion in Genetics and Development*, *12*, 583–591.
- Wu, D., Berangere Re, D., Nagai, M., Ischiropoulos, H., & Przedborski, S. (2006). The inflammatory NADPH oxidase enzyme modulates motor neuron degeneration in amyotrophic lateral sclerosis mice. *PNAS*, *103*(32), 12132–12137. <https://doi.org/10.1073/pnas.0603670103>

- Xiao, T., & Baier, H. (2007). Lamina-specific axonal projections in the zebrafish tectum require the type IV collagen Dragnet. *Nature Neuroscience*, *10*(12), 1529–1537.
<https://doi.org/10.1038/nn2002>
- Xiao, T., Roeser, T., Staub, W., & Baier, H. (2005). A GFP-based genetic screen reveals mutations that disrupt the architecture of the zebrafish retinotectal projection. *Development*, *132*, 2955–2967. <https://doi.org/10.1242/dev.01861>
- Xiao, T., Staub, W., Robles, E., Gosse, N. J., Cole, G. J., & Baier, H. (2011). Assembly of lamina-specific neuronal connections by slit bound to type IV collagen. *Cell*, *146*(1), 164–176. <https://doi.org/10.1016/j.cell.2011.06.016>
- Xing, L., Quist, T. S., Stevenson, T. J., Dahlem, T. J., & Bonkowsky, J. L. (2014). Rapid and efficient zebrafish genotyping using PCR with high-resolution melt analysis. *Journal of Visualized Experiments*, *84*(84), e51138. <https://doi.org/10.3791/51138>
- Xu, Q., Huff, L. P., Fujii, M., & Griendling, K. K. (2017). Redox regulation of the actin cytoskeleton and its role in the vascular system. *Free Radical Biology and Medicine*, *109*(December 2016), 84–107. <https://doi.org/10.1016/j.freeradbiomed.2017.03.004>
- Yan, Y., Wei, C., Zhang, W., Cheng, H., & Liu, J. (2006). Crosstalk between calcium and reactive oxygen species signaling. *Acta Pharmacologica Sinica*, *27*(7), 821–826.
<https://doi.org/10.1111/j.1745-7254.2006.00390.x>
- Yang, T., Huang, H., Shao, Q., Yee, S., Majumder, T., & Liu, G. (2018). miR-92 suppresses Robo1 translation to modulate slit sensitivity in commissural axon guidance. *Cell Reports*, *24*(10), 2694–2708.e6. <https://doi.org/10.1016/j.celrep.2018.08.021>
- Ye, X., Qiu, Y., Gao, Y., Wan, D., & Zhu, H. (2019). A subtle network mediating axon guidance: intrinsic dynamic structure of growth cone, attractive and repulsive molecular cues, and the intermediate role of signaling pathways. *Neural Plasticity*, *2019*, 1719829. <https://doi.org/10.1155/2019/1719829>
- Yoneyama, M., Kawada, K., Gotoh, Y., Shiba, T., & Ogita, K. (2010). Endogenous reactive oxygen species are essential for proliferation of neural stem/progenitor cells. *Neurochemistry International*, *56*(6–7), 740–746.
<https://doi.org/10.1016/j.neuint.2009.11.018>

- Yoo, S. K., Freisinger, C. M., LeBert, D. C., & Huttenlocher, A. (2012). Early redox, Src family kinase, and calcium signaling integrate wound responses and tissue regeneration in zebrafish. *Journal of Cell Biology*, *199*(2), 225–234. <https://doi.org/10.1083/jcb.201203154>
- Yoo, S. K., Starnes, T. W., Deng, Q., & Huttenlocher, A. (2011). Lyn is a redox sensor that mediates leukocyte wound attraction in vivo. *Nature*, *480*(7375), 109–112. <https://doi.org/10.1038/nature10632>
- Yoshii, A., & Constantine-Paton, M. (2010). Postsynaptic BDNF-TrkB signaling in synapse maturation, plasticity, and disease. *Developmental Neurobiology*, *70*(5), 304–322. <https://doi.org/10.1002/dneu.20765>
- Yoshikawa, Y., Ago, T., Kuroda, J., Wakisaka, Y., Tachibana, M., Komori, M., ... Kitazono, T. (2019). Nox4 promotes neural stem/precursor cell proliferation and neurogenesis in the hippocampus and restores memory function following trimethyltin-induced injury. *Neuroscience*, *398*, 193–205. <https://doi.org/10.1016/j.neuroscience.2018.11.046>
- Yu, J. S. L., & Cui, W. (2016). Proliferation, survival and metabolism: the role of PI3K / AKT / mTOR signalling in pluripotency and cell fate determination. *Development*, *143*(17), 3050–3060. <https://doi.org/10.1242/dev.137075>
- Zawada, W. M., Banninger, G. P., Thornton, J., Marriott, B., Cantu, D., Rachubinski, A. L., ... Jones, S. M. (2011). Generation of reactive oxygen species in 1-methyl-4-phenylpyridinium (MPP+) treated dopaminergic neurons occurs as an NADPH oxidase-dependent two-wave cascade. *Journal of Neuroinflammation*, *8*, 129. <https://doi.org/10.1186/1742-2094-8-129>
- Zhang, C., Gao, J., Zhang, H., Sun, L., & Peng, G. (2012). Robo2-Slit and Dcc-netrin1 coordinate neuron axonal pathfinding within the embryonic axon tracts. *Journal of Neuroscience*, *32*(36), 12589–12602. <https://doi.org/10.1523/JNEUROSCI.6518-11.2012>
- Zhang, X., & Forscher, P. (2009). Rac1 Modulates Stimulus-evoked Ca²⁺ Release in Neuronal Growth Cones via Parallel Effects on Microtubule / Endoplasmic Reticulum Dynamics and Reactive Oxygen Species Production. *Molecular Biology of the Cell*, *20*(16), 3700–3712. <https://doi.org/10.1091/mbc.e08-07-0730>
- Zhang, X. M., & Yang, X. J. (2001). Regulation of retinal ganglion cell production by Sonic hedgehog. *Development*, *128*(6), 943–957.

- Zhou, F. Q., & Cohan, C. S. (2001). Growth cone collapse through coincident loss of actin bundles and leading edge actin without actin depolymerization. *Journal of Cell Biology*, *153*(5), 1071–1083. <https://doi.org/10.1083/jcb.153.5.1071>
- Zhou, W., Cao, L., Jeffries, J., Zhu, X., Staiger, C. J., & Deng, Q. (2018). Neutrophil-specific knockout demonstrates a role for mitochondria in regulating neutrophil motility in zebrafish. *Disease Models & Mechanisms*, *11*(3), dmm.033027. <https://doi.org/10.1242/dmm.033027>
- Zhu, X., Xu, Y., Yu, S., Lu, L., Ding, M., Cheng, J., ... Tian, Y. (2014). An efficient genotyping method for genome-modified animals and human cells generated with CRISPR/Cas9 system. *Scientific Reports*, *4*, 6420. <https://doi.org/10.1038/srep06420>
- Zimmerman, M. C., Takapoo, M., Jagadeesha, D. K., Stanic, B., Banfi, B., Bhalla, R. C., & Miller, F. J. (2011). Activation of NADPH oxidase 1 increases intracellular calcium and migration of smooth muscle cells. *Hypertension*, *58*(3), 446–453. <https://doi.org/10.1161/HYPERTENSIONAHA.111.177006>
- Zou, Y., Corniola, R., Leu, D., Khan, A., Sahbaie, P., Chakraborti, A., ... Huang, T. T. (2012). Extracellular superoxide dismutase is important for hippocampal neurogenesis and preservation of cognitive functions after irradiation. *Proceedings of the National Academy of Sciences of the United States of America*, *109*(52), 21522–21527. <https://doi.org/10.1073/pnas.1216913110>

PUBLICATIONS

Terzi, A.*, Roeder, H.*, Weaver, C.J., Suter, D.M., “Neuronal NADPH oxidase 2 regulates growth cone guidance downstream of slit2/robo2” (*submitted*).

Terzi, A., Suter, D.M., “The role of NADPH oxidases in neuronal development” *Free Radical Biology and Medicine* 154 (2020) 33-47. doi: 10.1016/j.freeradbiomed.2020.04.027.

Weaver, C.J., **Terzi, A.**, Roeder, H., Gurol T.M., Deng, Q., Leung, Y.F., Suter, D.M., “nox2/cybb deficiency affects zebrafish retinotectal connectivity” *Journal of Neuroscience* 38(26) (2018) 5854–5871. doi: 10.1523/JNEUROSCI.1483-16.2018.